BINARY-DIFFUSION COEFFICIENTS FOR LIQUIDS

by: ABBAS • ALIZADEH

BSc.Tech; MSc; DIC

Department of Chemical Engineering and Chemical Technology

IMPERIAL COLLEGE

University of London

December 1981

A thesis submitted for the degree of Doctor of Philosophy
of the University of London

T O :

The man who once told me

"We come and go with sufferings,
and in between, experience a few
real happy moments.
Nothing we have remains, but our
knowledge, ideas and thoughts.
Them, can never be lost or taken
away from us,
and them, what better than
to leave behind".

M.H. ALIZADEH ESQ. - my father

A B S T R A C T

In view of the scarcity of reliable thermophysical property data, in particular, of liquid-phase diffusion coefficients, this thesis describes the design, construction and use of an apparatus which enables the measurement of the binary diffusion coefficients of liquids with an accuracy of ±1%. A complete analysis of the theory of the instrument based upon the phenomenon of Taylor dispersion is presented. An instrument has been designed such that it operates very nearly in accordance with the simplest mathematical description of the dispersion of a solute pulse in a fluid in laminar flow within a long, straight circular cross-section tube. The small departures of the instrument from its ideal model are evaluated as corrections which include the effects of non-zero volumes of the injected pulse and the concentration monitor, the coiling of the diffusion tube, its non-uniformity and non-circularity of the cross-section and the variation of the fluid properties with composition. Owing to the instrument design and under the selected experimental conditions, the effect of such corrections are found to be either negligible or less than one percent. Experimental results are persented which confirm that the instrument does indeed operate in accordance with the theory of it.

Experimental data for the binary diffusion coefficients of three binary liquid mixtures, n-hexane + n-heptane, n-hexane + n-octane and n-heptane + n-octane, of various compositions in the temperature range 20°C to 70°C and at a pressure of 1 bar are reported. The accuracy and precision of these measurements are estimated to be ±1% and ±0.5% respectively. The experimental data have been used to assess the validity of the theoretical descriptions of diffusion in liquid mixtures, as well as testing several estimation procedures, which are in current use.

ACKNOWLEDGEMENTS

The author is forever indebted and grateful to his supervisor, Dr. W.A. Wakeham for his continuous encouragement, excellent counsel and guidance during the course of this work.

The author wishes to express his sincere gratitude to his previous supervisor Professor D.L. Trimm (U.N.S.W., Australia) who, together with Dr. Hall and Mr. W. Watkins (ESSO Research Centre, Abingdon) have been a great help in the early stages of the present work. The industrial scholarship awarded to the author by ESSO Research Centre at Abingdon in order to cover the equipment expenditure is gratefully appreciated.

Special thanks are due to the author's laboratory colleagues, Drs. J. Menashe and V. Vesovic, and, in particular, Professor C.A. Nieto de Castro (IST, Lisbon) whose friendship and continuous assistance and guidance in fruitful discussions are deeply appreciated.

The author extends his thanks to Messrs. W.D. Geal, R. Wood and M.J. Dix who have helped in the construction of the equipment; to Mr. S. Ranson, the Technical Director of SPECAC for his assistance in modifying the injection valve; to Miss M. McNeile for her skillful typing of this thesis; to Mr. I. Drummond of Analytical Services, and to Miss P. Browett and Mrs. C. Fletcher, the two excellent and most helpful Departmental Librarians.

Finally, the author wishes to express his deepest gratitude and appreciation to his parents for their care and concern, trust and encouragement, as well as their moral and financial support, not only during the course of this work, but also throughout the author's education. Without them it would have been impossible to carry out this work.

C O N T E N T S

INTRODUCTION

The transport properties of fluids associated with the transfer of mass, momentum and heat are the diffusion coefficient, viscosity and thermal conductivity. An accurate knowledge of these quantities is required to improve the existing statistical mechanical theories of fluids (Sections 1.2 and 1.3; [1, 2]) whilst being highly significant for process plant design [3-6]. In the absence of an exact theory the transport properties of many fluids are estimated by methods which are based upon simple models (Sections 1.2 and 1.3; [7-9]) and hence the generated data are necessarily burdened with large uncertainties which could affect the overall technical design of equipment and increase the capital cost of items of plant. Investigators have shown [3, 4] that such expenditure would be considerably reduced by more reliable estimation procedures based on accurate experimental data for transport properties.

The process of molecular diffusion in liquids, reviewed extensively by several workers [10-13], is often the rate limiting factor in chemical engineering operations involving mass transfer such as absorption, liquid-liquid extraction [14] and heterogeneous chemical reactions [15-17]. In addition, it is the combined effect of molecular diffusion and advection that give rise to the longitudinal dispersion of material flowing through a circular tube, a phenomenon known as the Taylor dispersion (Section 1.4.4). In general, longitudinal dispersion is of theoretical and considerable practical importance and arises frequently in industrial processes. It is common practice to use a single pipeline to convey different materials over long distances by introducing them consecutively. Since it is not generally economical to clean the

line after each operation, it is desirable to know the extent of mixing and how much contaminated material must be rejected. In tubular chemical reactors the mixing of reactants and products, caused by diffusion and advection, usually has an adverse effect on the degree of conversion and hence a larger reactor is required than would be the case if no dispersion took place. Furthermore kinetic studies interpreted on the assumption of plug flow in the absence of diffusion may lead to erroneous reaction mechanism.

The primary application of diffusion coefficients in chemical engineering calculations is in the Schmidt number, ν/D, which is generally used to correlate mass transfer properties. More directly, mass transfer equations (Fick's equations) may be integrated to solve such practical problems as the rate of diffusion and the local concentration of water diffusing into hydrocarbons in a storage tank. The equations are used in reaction rate calculations for which the rate of diffusion to a catalyst is important. Hence, accurate values of diffusion coefficients are required not only for their primary direct application in the field of mass transfer, but also for the molecular theories of liquid behaviour. Unfortunately, accurate values of diffusion coefficients are scarce [18-21] and most of the available diffusivity data, particularly in the liquid phase, carry uncertainties of high order (10-50%; [22]). Consequently, the correlations that are developed from such data necessarily reflect these uncertainties. It is therefore regrettable that there have been few reliable, systematic studies of molecular diffusion coefficients in the liquid phase. There are three main reasons, well documented, for this lack of measurements [9, 11, 18, 20]. Firstly, the fact that the liquid phase diffusion is a slow process, thus requiring experiments of several days' duration to obtain a single datum.

Secondly, the experimental methods for diffusion coefficient measurements either depart significantly from their principle ideal models, or, thirdly, they are somewhat limited in the range of thermodynamic states to which they may be applied.

In the last few years, new methods for the measurement of diffusion coefficients in the liquid phase have been developed [18, 21, 23-26]. Amongst them, the Taylor dispersion technique has recently received a new stimulus owing to its relative simplicity and wide range of application as well as the relatively short duration of the measurements [21, 23, 27-29]. The method has been unjustly neglected [30], but the development of sensitive detectors, such as the refractive index detector for liquid chromatography, and of computer techniques has created the conditions for fast and accurate measurements of the diffusion coefficients for liquids by this technique.

The objective of the work undertaken for this thesis has been to develop the apparatus and, where necessary, the theory of the Taylor dispersion technique, so as to enable the accurate measurement of binary diffusion coefficients for liquids at elevated temperatures and atmospheric pressure. It is hoped that the measurements reported here, as well as those which could be obtained for other liquid systems from this apparatus, will be used both to examine liquid phase diffusivity theories which have been developed or will be developed in future and also for direct application in predicting the diffusion coefficients for liquids.

The first chapter of this thesis begins with the basic concepts and definitions in the isothermal molecular transport of mass which are essential in defining the binary diffusion, and diffusion coefficients, of fluids. This is followed by a description of the simple models for

diffusion in liquids, namely the hydrodynamic, kinetic and van der Waals models, which establishes the need for the development of a satisfactory theory of the liquid structure and hence a theory of the liquid phase diffusion that can precisely describe this transport phenomenon. The statistical mechanical and computer simulation studies which seem very promising in the development of theories of the liquid-state are then briefly discussed. The last section of the chapter is dedicated to a review of the experimental methods fo measuring binary diffusion coefficients for liquids, revealing the advantages of the "Taylor dispersion technique" whose precision has been made comparable with that of the other methods.

In the second chapter, a more complete treatment of the theory of "Taylor dispersion technique" for accurate liquid diffusivity measurements is provided so as to obtain a set of working equations for an instrument operating on this principle. It will be shown that by means of these equations, the accuracy of the results of measurements with this method can be assessed and made comparable with that of other techniques. In the subsequent chapter, the apparatus design, the experimental procedure and the performance of the equipment are described. Chapter Four contains the results of the measurements for binary mixtures of n-hexane, n-heptane and n-octane liquids in the temperature range 20°C - 70°C.

Finally, the discussion of the experimental results and the conclusions drawn from this work are included in Chapter Five.

CHAPTER 1

ISOTHERMAL DIFFUSION AND DIFFUSION COEFFICIENTS

1.1 BASIC CONCEPTS AND DEFINITIONS

1.1.1 Isothermal Diffusion

Diffusion of mass under isothermal and isobaric conditions is the dissipation of a concentration (Section 1.1.2), or chemical potential (Section 1.1.8), gradient by molecular transport without overall mass flow. For example, consider an isothermal system of two fluid phases α and β (solvents) in which a substance i, whose chemical potential is $\dot{\mu}_i$, is distributed. The transport of substance i from phase β to phase α takes place by molecular diffusion according to the equation

$$[\dot{\mu}_{i\alpha} - \dot{\mu}_{i\beta}]\, dN_{i\beta} \leq 0 \qquad (1.1)$$

derived by Denbeigh [31], where $dN_{i\beta}$ is the number of moles of substance i which pass from phase β into phase α. From equation (1.1) it follows that the sign of $[\dot{\mu}_{i\alpha} - \dot{\mu}_{i\beta}]$ is opposite to that of $dN_{i\beta}$. Consequently, if $dN_{i\beta}$ is a positive transfer from β to α, then the chemical potential of substance i must be less in the phase α than in β. At equilibrium, there is no difference in the chemical potential of i in the two phases so that $\dot{\mu}_{i\alpha} = \dot{\mu}_{i\beta}$. Differences of chemical potential may thus be regarded as the origin of all processes of diffusion. Strictly speaking, it is erroneous to regard diffusion as necessarily taking place in the direction of decreasing concentration [31]. However, in physical situations where there is no discontinuity of the medium, the direction of decreasing chemical potential usually coincides with that of decreasing concentration. In this case, in a homogeneous material system consisting of two or more components, a chemical substance is transported from regions where its concentration is higher towards those of

lower concentration or - in non-ideal mixtures - of lower activity. The diffusion rate of the substance (known as the flux of the substance) is considered to be proportional to either its concentration gradient, by the experimentalists, or, by the theoreticians, to its gradient of chemical potential which is the driving force of diffusion.

The diffusion defined above occurs in a single-phase fluid mixture and is usually referred to as Fickian, ordinary or isothermal diffusion. It is thus distinguished from thermal diffusion which is due to a temperature gradient, or pressure diffusion due to a pressure gradient, or from forced diffusion caused by an external force such as that of an electric field which leads to "mass conductivity" by ionic migration [17, 32]. Isothermal diffusion is a macroscopic concept and an irreversible process. Thus it can either be described through irreversible thermodynamics (i.e. in terms of dissipation of chemical potential gradient) or by Fick's law (i.e. in terms of dissipation of concentration gradient). The significance of each description is established in the following sections.

1.1.2 Diffusion Coefficient

The diffusion coefficient, or diffusivity, is the proportionality factor between the diffusion rate and the concentration gradient causing diffusion and is generally defined by Fick's first law [13a, 17, 33, 34]

$$\vec{J}_i = -D_i \nabla c_i = -D_i c_T \nabla x_i \qquad (1.2)$$

Here we have written $\vec{J}_i$ = molar flux of the i^{th} component in the mixture, i.e. moles of i diffusing across a unit cross-section perpendicular to the direction of the current. D_i = the ordinary diffusion coefficient of the i^{th} component whose concentration gradient, in the mixture of concentration c_T, is ∇c_i and whose mole fraction is x_i.

The negative sign in equation (1.2) indicates that the material is transported in the direction of decreasing concentration. In practice, it is important to consider the changes of concentration with respect to time at a given point of the system due to diffusion. The description of the rate of change of concentration, based on equation (1.2) and for a constant diffusion coefficient, is given by Fick's second law [13b, 17]

$$\frac{\partial c_i}{\partial t} = D_i \nabla^2 c_i = D_i c_T \nabla^2 x_i \qquad (1.3)$$

When the diffusion coefficient depends upon the concentration [13b, 33, 35], equation (1.3) becomes

$$\frac{\partial c_i}{\partial t} = \nabla \cdot (D_i \nabla c_i) \qquad (1.4)$$

1.1.3 Unidirectional Diffusion

Although under real conditions, substances usually diffuse in all directions by virtue of their concentration gradients, the essential features of the transport phenomenon can satisfactorily be revealed by considering the mass transport taking place in one direction. In this case, the diffusion process becomes unidirectional and hence simpler to analyse. This is desirable for experimentalists who often aim at one-dimensional changes of concentration in the design of equipment to measure diffusion rates or diffusion coefficients. Thus the diffusion equations (1.2) - (1.4) are written in unidirectional form as

$$\vec{J}_i = -D_i \frac{\partial c_i}{\partial z} = -D_i c_T \frac{\partial x_i}{\partial z} \qquad (1.5)$$

$$\frac{\partial c_i}{\partial t} = D_i \frac{\partial^2 c_i}{\partial z^2} = D_i c_T \frac{\partial^2 x_i}{\partial z^2} \qquad (1.6)$$

$$\frac{\partial c_i}{\partial t} = \frac{\partial}{\partial z}\left(D_i \frac{\partial c_i}{\partial z}\right) \qquad (1.7)$$

The diffusion flow has also been described by the mass and molar fluxes relative to the mass-average velocity $\bar{v}$, or relative to the molar-average velocity $\bar{v}^*$ by Bird et al. [17]

$$\vec{n}_{ir} = \rho_i(\bar{v}_i - \bar{v}) = \rho_i v_i \quad \text{mass flux} \qquad (1.8)$$

$$\vec{N}_{ir} = c_i(\bar{v}_i - \bar{v}) = c_i v_i \quad \text{molar flux} \qquad (1.9)$$

$$\vec{j}_{ir} = \rho_i(\bar{v}_i - \bar{v}^*) = \rho_i v_i^* \quad \text{mass flux} \qquad (1.10)$$

$$\vec{J}_{ir} = c_i(\bar{v}_i - \bar{v}^*) = c_i v_i^* \quad \text{molar flux} \qquad (1.11)$$

where

$$\bar{v}_i = \left(\frac{\sum_{i=1}^{k} v_i}{\sum_{i=1}^{k} n_i} \right)_{\delta V}, \quad \bar{v} = \frac{\sum_{i=1}^{k} \rho_i v_i}{\sum_{i=1}^{k} \rho_i} \quad \text{and} \quad \bar{v}^* = \frac{\sum_{i=1}^{k} c_i v_i}{\sum_{i=1}^{k} c_i}$$

for a mixture of k species in which component i is diffusing with a velocity v_i. In equations (1.8)-(1.11), fluxes refer to "flow systems" where the diffusion velocity of species i is given with respect to $\bar{v}$ or $\bar{v}^*$ and not with respect to "stationary" (i.e. whole fluid at rest macroscopically) coordinate axes in which case

$$\vec{j}_i = \vec{n}_i = \rho_i \bar{v}_i \quad \text{mass flux} \qquad (1.10b)$$

$$\vec{J}_i = \vec{N}_i = c_i \bar{v}_i \quad \text{molar flux} \qquad (1.11b)$$

It must be emphasized that the flux definition is not complete until both units and reference frame [13, 17, 35], i.e. the location of that unit cross-section at which the transport rate of material is referred to as the flux, have been given.

1.1.4 Binary Systems

Limiting the isothermal diffusion process to two-component solutions (by the word "solution" we mean a single-phase gaseous or liquid mixture), linear diffusion should be described by two simultaneously valid

equations, regarding the flow of the two components in opposite directions:

$$\vec{J}_1 = -D_1 \frac{\partial c_1}{\partial z} \tag{1.12}$$

$$\vec{J}_2 = -D_2 \frac{\partial c_2}{\partial z} \tag{1.13}$$

where the subscripts 1 and 2 in the flux, concentration and diffusion coefficient refer to the first and second component respectively.

The discussion of diffusion is simplest, hence very important to the experimentalist, when the reference plane is defined so as to make the two diffusion coefficients identical with each other [13, 35-37]. This can be achieved by referring the diffusion flow to that plane where the change in volume due to the two-directional mass flow crossing the plane compensate each other, i.e. across this plane there is no 'transport of volume'. If the partial molar volumes of the two components are $\dot{V}_1$ and $\dot{V}_2$ and $\vec{J}_1^V$ and $\vec{J}_2^V$ are the fluxes measured with respect to the 'volume frame of reference', we have:

$$\vec{J}_1^V \dot{V}_1 + \vec{J}_2^V \dot{V}_2 = 0 \tag{1.14}$$

Introducing the fluxes from equations (1.12) and (1.13) and denoting the diffusion coefficients related to this reference frame by D_1^V and D_2^V, we obtain:

$$D_1^V \dot{V}_1 \frac{\partial c_1}{\partial z} + D_2^V \dot{V}_2 \frac{\partial c_2}{\partial z} = 0 \tag{1.15}$$

1.1.5 Binary Diffusion Coefficient

According to the definition of the molar volume:

$$\dot{V}_1 c_1 + \dot{V}_2 c_2 = 1 \tag{1.16}$$

and

$$c_1 \delta \dot{V}_1 + c_2 \delta \dot{V}_2 = 0 \tag{1.17}$$

It therefore follows that:

$$\dot{V}_1 \delta c_1 + \dot{V}_2 \delta c_2 = 0 \qquad (1.18)$$

Taking this into account, it follows from equation (1.15), that the two diffusion coefficients must be equal

$$D_1^v = D_2^v = D_{12} \qquad (1.19)$$

and thus the subscripts and superscripts in (1.19) may be deleted since a binary system may be described by a single "mutual-", "inter-" or "binary-" diffusion coefficient D_{12}. This is often practically equal to the diffusion coefficient determined experimentally by performing a diffusion process in which two dilute solutions of different concentration diffuse towards each other through an initially sharp horizontal boundary [13a].

1.1.6 Binary-, Self-, and Tracer-Diffusion Coefficients

As indicated earlier, the diffusion coefficient D_{12} is termed mutual or binary diffusion coefficient and refers to the diffusion of one constituent in a binary system. A similar coefficient, D_{1m}, would imply the diffusivity of component 1 in a mixture [17, 36-38]. Experiments indicate that Fick's first law is not always sufficient to describe the solute flows in multicomponent systems. Hence, more generalized diffusion equations have been developed by Onsager [11b], Kirkwood and Dunlop *et al*, [36-39]. Their analyses led to equations and correlations involving various diffusivities, namely binary-, self- and tracer-diffusion coefficients.

Tracer-diffusion coefficients (also referred to as intra-diffusion coefficients) relate to the diffusion of a labelled component within a homogeneous mixture. That is, the component present in traces in the solution

has a concentration gradient, while the concentration gradient of all the other components of high concentration in comparison with the former is zero. In general, the tracer-diffusion coefficient of a pure liquid is obtained by adding a small number of radioactively-labelled molecules of the same substance and allowing them to diffuse into a sample with a lower concentration of the labelled species. If the molarity of the labelled species at any point is c_i^*, then it follows from equation (1.6) that the tracer-diffusion coefficient D^* is defined

$$\frac{\partial c_i^*}{\partial t} = D_i^* \cdot \frac{\partial^2 c_i^*}{\partial z^2} \qquad (1.20)$$

similarly, the diffusion of labelled molecules or of ions in a solution of the same, unlabelled, species can be followed and a tracer-diffusion coefficient, defined by equation (1.20), measured. The smaller the difference in properties between the labelled and unlabelled species the closer the experimental tracer-diffusivity approximates to the true self-diffusion coefficient [13]. Like binary-diffusion coefficient (D_{12}), tracer-diffusivity (D^*) can depend on the concentration [6, 13a, 32].

The tracer-diffusivity in a pure fluid represents the closest practical approach to the measurement of the self-diffusivity of the fluid. The self-diffusion coefficient is the transport property characteristic of the hypothetical process in which molecules of one species diffuse through themselves (i.e. interdiffusion of identical molecules). Evidently, this quantity can never be measured experimentally. Consequently it has sometimes been assumed that the tracer-diffusion coefficient is identical with the self-diffuion coefficient. Such an assumption is not justified and gives rise to the so-called isotope effect which describes the dependence of the tracer-diffusivity on the particular

isotope used for its measurement [32, 40-42]. Tracer-, and self-diffusion coefficients may also be defined for mixtures of fluids. In a binary mixture, there are two tracer-, and two self-diffusion coefficients, one each for the two species. The two tracer-diffusion coefficients correspond to measurements of the diffusion of one labelled species in the mixture.

The various diffusion coefficients described above are shown by Fig. 1.1 which refers to the experimental results for n-octane (1)/ n-dodecane (2) at 60°C, due to Van Geet et al. [39].

Fig. 1.1 - Binary-, self-, and tracer-diffusion coefficients D_{12}, D_{22} and D_2^* respectively

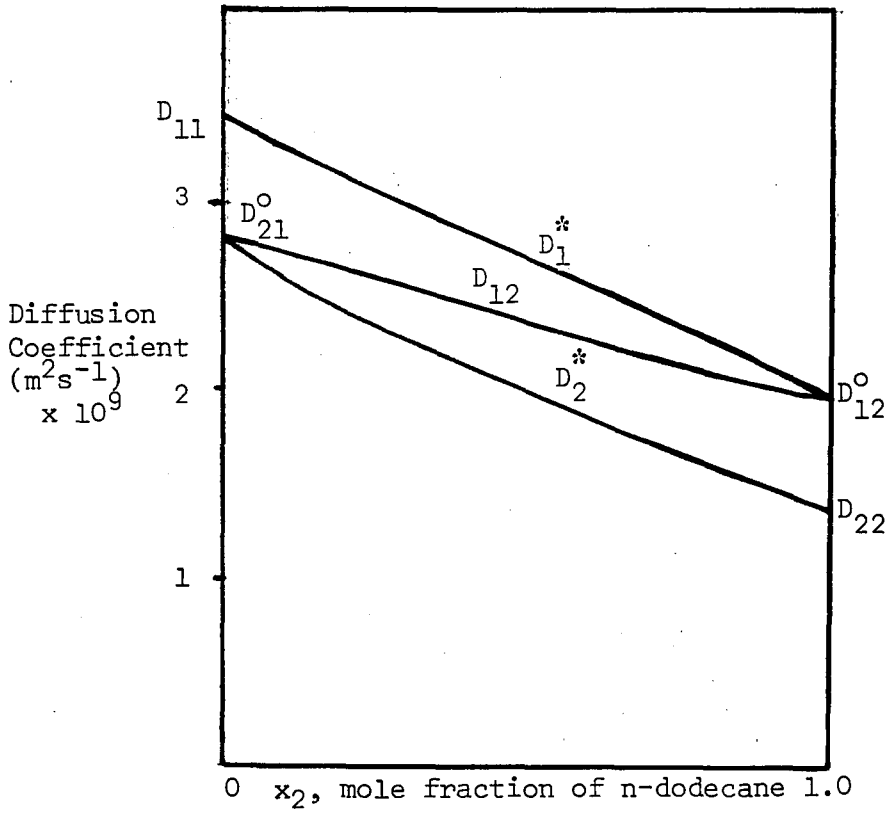

In this case, the binary diffusion coefficient, D_{12}, decreases as the mixture becomes richer in n-dodecane (2). As $x_2 \to 1.0$, $D_{12} = D_{21} \to D_{12}^\circ$ the limiting diffusion coefficient (or intrinsic diffusivity D_1^i) when the mixture essentially consists of n-dodecane, i.e. n-octane (1)

molecules diffusing through almost pure n-dodecane. Similarly, D_{21}^{o} is the diffusivity of n-dodecane in essentially pure n-octane. It is useful to note that as $x_2 \rightarrow 0$, i.e. $x_1 \rightarrow 1.0$, the intra-diffusion coefficient (D_2^*) tends to the limiting inter-diffusion coefficient (D_{21}^{o}). When $x_2 \rightarrow 1.0$, $D_2^* \rightarrow D_{22}$, i.e. the tracer diffusion coefficient tends to the self-diffusion coefficient of pure n-dodecane.

1.1.7 Chemical Potential Driving Force

The 'driving force' of diffusion is the chemical potential gradient $\nabla\dot{\mu}_i$. However, the changes in chemical potential are determined by the changes in concentration in ideal mixtures

$$(\dot{\mu}_i)_{T,P}^{mix} - (\dot{\mu}_i)_{T,P}^{\Theta} = \Delta\dot{\mu}_i = RT \ln x_i \qquad (1.20a)$$

But, for real mixtures, the changes in activity a_i must be applied

$$(\dot{\mu}_i)_{T,P}^{mix} - (\dot{\mu}_i)_{T,P}^{\Theta} = \Delta\dot{\mu}_i = RT \ln a_i = RT \ln \gamma_i^* x_i \qquad (1.21)$$

where γ_i^* is the activity coefficient of the i^{th} component at a given point in the mixture. In real mixtures, the activity coefficient depends on the nature and concentration of all of the components. In multi-component systems, it can occur that the direction of the activity gradient of a component does not coincide with that of its concentration gradient and so the component will diffuse from regions of lower concentration towards those of higher ones. This often happens in the course of diffusion through an interface of different phases in heterogeneous systems, since the requirement of equilibrium between different phases containing a given substance is its identical activity (or identical $\dot{\mu}$). Thus, solutes often diffuse through interfaces towards points of higher concentration and an example of this is the diffusion

of iodine, at the interface of chloroform and water, into the chloroform solution of higher concentration. In this respect, there is apparently an essential difference between diffusion and heat conduction although they are rather similar in a phenomenological sense. Thermal energy is always transported in the direction of decreasing temperature, and this applies to its transport through interfaces too. In each case the requirement for equilibrium is the identical temperature at every point of the system. As for diffusion, the concentrations are usually different at the two sides of the interface even after reaching the equilibrium state.

In diffusion, the gradient of chemical potential and not that of concentration is the analogue of temperature gradient in heat conduction. However, since there is no instrument which directly measures the chemical potential or the absolute value of activity, attention is focussed upon concentration gradients for all practical purposes.

In binary systems where the chemical potential is related to activity by equation (1.21), all modern theories of diffusion [1] lead to an activity-corrected diffusion coefficient $\mathfrak{D}_{12}$:

$$\mathfrak{D}_{12} = \frac{D_{12}}{\left[(\partial \ln a_1)/(\partial \ln x_1)\right]_{T,P}} \tag{1.22}$$

where $\mathfrak{D}_{12}$ is often less sensitive to composition than D_{12} [6].

1.1.8 The Phenomenological Equation of Diffusion in Irreversible Thermodynamics

Because of the irreversibility of the transport phenomena, their relationships cannot be deduced from classical thermodynamics which only deals with equilibria and reversible processes. The thermodynamics of irreversible processes has shown a marked development, initiated by Onsager, De Groot and Prigogine [11b, 13, 43], in the last fifty years. It is now well-known that the rate of entropy production of component i,

ds_i/dt, arising from irreversible processes within a system can be written in the form of a sum of products of generalized fluxes $\vec{J}_i$ with generalized forces X_i giving rise to flows [26]

$$\Phi \equiv T \frac{ds_i}{dt} = \Sigma_i \vec{J}_i X_i \qquad (1.23)$$

Here Φ represents the dissipation function [13a].

According to the phenomenological laws of Fourier (for heat conduction), Ohm (for electrical conduction) and Fick (for diffusion), the correlation between the fluxes ($\vec{J}_i$) of heat, electricity or mass and the forces (X_i) giving rise to them is linear. This is shown experimentally to be true when a system is close to equilibrium, otherwise the correlation is a power series in X_i. The linear relationship is basically the so-called Onsager linear law (verified by the Bearman-Kirkwood statistical mechanical theory of transport process [44, 45]), given by the phenomenological equation

$$\vec{J}_i = L_i^* X_i \qquad (1.24)$$

where it is assumed that X_i is the only force acting on the i^{th} component to cause the flow $\vec{J}_i$. In this equation, L_i^* is the phenomenological coefficient of flow [13]. In an isothermal non-electrolytic system, the thermodynamic force X_i resulting in diffusion of the i^{th} component is the gradient of chemical potential [11b, 43a].

Hence equation (1.24) becomes:

$$X_i = -\nabla \dot{\mu}_i \qquad (1.25)$$

$$(i = 1, 2, 3 \ldots)$$

$$\vec{J}_i = -L_i^* \nabla \dot{\mu}_i \qquad (1.26)$$

Equations (1.23) and (1.26) clearly indicate that the rate of entropy production of species i depends on the dissipation of the chemical

potential gradient of i. The comparison of equation (1.26) with (1.2) shows that the diffusion flux $\vec{J}_i$ can be related to either the dissipation of a concentration, or chemical, potential gradient.

In general, if several other thermodynamic forces X_k, ... X_n (e.g. gradients of temperature, electrical charge, etc.) simultaneously influence the i^{th} component of a thermodynamic system, then the transport of i due to its chemical potential gradient would be affected by such forces, referred to as the "cross-effects" [13], and its flux will be given by

$$\vec{J}_i = \sum_{k=1}^{n} L^*_{ik} X_k \tag{1.27}$$

The phenomenological coefficients of the cross-effects are "symmetrical" according to the Onasger reciprocity theory [13]

$$L^*_{ik} = L^*_{ki} \tag{1.28}$$

This theory can be easily understood by a simple example. Consider a binary solution in which there is temperature and composition variations. The fluxes $\vec{J}_m$ of mass flow and $\vec{J}_h$ of heat flow are determined by the chemical potential gradient X_m and the temperature gradient X_θ simultaneously.

$$\vec{J}_m = L^*_{mm} X_m + L^*_{mh} X_h \qquad \text{mass} \tag{1.29}$$

$$\vec{J}_h = L^*_{hh} X_h + L^*_{hm} X_m \qquad \text{heat} \tag{1.30}$$

where L^*_{mm} and L^*_{hh} are the phenomenological coefficients corresponding to the effect of chemical potential gradient on mass transport in diffusion and that of temperature gradient on heat transport, respectively. Of the cross-effects, L^*_{mh} is the phenomenological coefficient corresponding to the effect of the temperature gradient on mass transport,

while L^*_{hm} refers to that of the chemical potential gradient on heat transfer. Now according to the Onsager reciprocity theory (equation (1.28), confirmed experimentally [46])

$$L^*_{mh} = L^*_{hm} \tag{1.31}$$

It has been shown [13] that for the isobaric and isothermal binary mixture of a non-electrolyte consisting of species 1 and 2, we obtain

$$\vec{J}_1 = -L^*_{11}(\nabla \dot{\mu}_1 - \nabla \dot{\mu}_2)_{T,P} = \frac{-L^*_{11}}{W_2} \nabla \dot{\mu}_1 \tag{1.32}$$

and

$$\vec{J}_2 = -L^*_{22}(\nabla \dot{\mu}_2 - \nabla \dot{\mu}_1)_{T,P} = \frac{-L^*_{22}}{W_1} \nabla \dot{\mu}_2 \tag{1.33}$$

where W denotes the weight fraction of the diffusing species, and $\vec{J}_1 + \vec{J}_2 = 0$ so that $L^*_{11} = L^*_{22}$. Equations (1.32) and (1.33) are the phenomenological equations of diffusion of species 1 and 2. From equation (1.32) and equation (1.12) for the unidirectional isothermal diffusion, it can easily be deduced that the relation between the ordinary diffusion coefficient and the phenomenological one is given by

$$D_{12} = \frac{RT\, L^*_{11}}{\rho_{12} W_2 x_1} \cdot \frac{(M_1 x_1 + M_2 x_2)^2}{M_1^2 M_2} \qquad \text{for ideal mixtures} \tag{1.34}$$

and

$$D_{12} = \frac{RT\, L^*_{11}}{\rho_{12} W_2 x_1} \cdot \frac{(M_1 x_1 + M_2 x_2)}{M_1^2 M_2} \left[1 + \frac{\partial \ln \gamma_1^*}{\partial \ln x_1}\right] \qquad \text{for non-ideal mixtures} \tag{1.35}$$

The phenomenological coefficients cannot be measured and their calculation relies entirely on the knowledge of the diffusivity data. Thus analysis of the diffusion process by irreversible thermodynamics does not provide any means of calculating the diffusion coefficients and hence it is still of little practical value. However, its fruitful application in the study of the cross-effects in transport processes cannot be ignored [13, 26, 32].

1.2 MODELS FOR DIFFUSION IN LIQUIDS

In principle, the theory of statistical mechanics of liquids [47] should enable any process in liquids, including the transport processes, to be described in terms of the motion and properties of the atoms and molecules which make up the liquid. But in practice, this approach has so far not been developed to the point where the diffusion coefficient may be calculated for a real fluid without further approximations. Frequently these approximations take the form of a model of the liquid and the motion of its molecules. Recently it has become possible to assess the validity of some of these models of liquids by means of molecular dynamics simulations and they have often been found to be unsatisfactory [48]. Nevertheless, the approximate theories are often all that is available for the calculation and correlation of diffusion coefficients of liquids so that there is little doubt that they will be in common use for some time to come. In some cases, the approximate theories yield relationships between diffusion coefficients and the properties of a system with considerable value for estimation purposes. For these reasons we consider here first the approximate models of diffusion in liquids and postpone a discussion of the current state of the rigorous statistical mechanical theory until later.

In general, the models for diffusion in liquids can be classified into three groups:

(1) Hydrodynamic models - based on the Stokes-Einstein analysis.

(2) Kinetic models - due to Eyring and other investigators.

(3) The van der Waals model.

1.2.1 The Hydrodynamic Model for Diffusion

The hydrodynamic model of diffusion [1a, 13a, 32, 45] considers the liquid as a continuum in which the transport of a component is determined by the resultant of the driving force and the frictional resistance force acting upon it. As mentioned in our earlier discussions, the gradient of chemical potential is the driving force. (In old theories, due to Sutherland and Einstein [49, 50], the gradient of osmotic pressure was considered as the driving force). If species 1 dissolves in liquid 2 and an ideal mixture is formed on dissolving, then from equation (1.20a), we have

$$\frac{\partial \dot{\mu}_1}{\partial z} = RT \frac{\partial \ \ell n \ c_1}{\partial z} = \left(\frac{RT}{c_1}\right) \frac{\partial c_1}{\partial z} \qquad (1.36)$$

where $\partial \dot{\mu}_1 / \partial z$ is the chemical potential gradient of the solute (the measure of the driving force of diffusion) in the z direction. If f_s is the frictional force of resistance of the solute per molecule (i.e. Nf_s per mole), the average velocity of one-dimensional diffusion is

$$\bar{v}_1 = -\left(\frac{RT}{Nf_s}\right) \frac{\partial \ \ell n \ c_1}{\partial z} = -\left(\frac{KT}{f_s}\right) \frac{\partial \ \ell n \ c_1}{\partial z} \qquad (1.37)$$

According to hydrodynamic considerations and from equations (1.5) and (1.11b), the binary diffusion coefficient D_{12} is therefore given by

$$D_{12} = \frac{KT}{f_s} = \mathcal{M} KT \qquad (1.38)$$

where $\mathcal{M}$ is the mobility of the solute particles (i.e. their velocity gained as a result of unit force). This is the so-called "Nernst-Einstein equation" [17]. The most difficult, and still not reliably solved, problem which arises in the hydrodynamic theory is the calculation of the frictional resistance from other properties of solutions. This is due to our inadequate knowledge of the liquid structure. Con-

sequently, the diffusion coefficient calculated from other properties of a solution is not accurate since the assumptions applied in evaluating f_s are only approximate and of limited validity. An early assumption, which can still be applied in several cases and provides the framework for several useful prediction methods for calculating D_{12}, was suggested by Stokes [13a, 17] in 1850. He showed that the frictional resistance acting on a spherical body which is moving in a continuum (not true for liquids since they consist of discrete molecules) is given by

$$f_s = 6\pi r_1 \eta_2 \frac{1 + \frac{2\eta_2}{\beta r_1}}{1 + \frac{3\eta_2}{\beta r_1}} \tag{1.39}$$

where η_2 is the solvent viscosity, r_1 is the spherical solute radius and β is the sliding frictional coefficient. It has been shown by Sutherland [49] that for the diffusion of large spherically symmetrical molecules in a solvent with small molecules $\beta = \infty$ so that from equations (1.38) and (1.39) we obtain the well-known Stokes-Einstein equation

$$D_{12} = \frac{KT}{6\pi \eta_2 r_1} \text{ for } f_s = 6\pi \eta_2 r_1 \tag{1.40}$$

In the course of diffusion of small molecules in a solvent consisting of similar (e.g. in self-diffusion) or larger molecules $\beta \simeq 0$, so that

$$D_{12} = \frac{KT}{4\pi \eta_2 r_1} \text{ for } f_s = 4\pi \eta_2 r_1 \tag{1.41}$$

A "Stokes'law radius" can be calculated for a solute molecule from its measured binary diffusion coefficient, especially if the solution is dilute in which case the error in viscosity value is minimized [51, 52]. It has been suggested [51] that for non-spherical (macro-) molecules, it is necessary to introduce three frictional coefficients f_1, f_2, and f_3 and that

$$D_{12} = \frac{KT}{3}\left(\frac{1}{f_1} + \frac{1}{f_2} + \frac{1}{f_3}\right) \tag{1.42}$$

If the particles are rotational ellipsoids $f_2 = f_3$. Experimental determination of the diffusion coefficient of non-solvated large molecules of rotational ellipsoidal shape, leads to the empirical frictional coefficient f_e (related to the actual conditions) to be calculated from equation (1.38):

$$\frac{1}{f_e} = \frac{1}{3}\left(\frac{1}{f_1} + \frac{1}{f_2}\right) \tag{1.43}$$

The frictional ratio f_e/f_s, where f_s is the Stokes frictional resistance, deviates from unity if the molecule is solvated or non-spherical [13a].

Although various methods of calculating diffusion coefficients lead to different numerical factors in the equation of frictional resistance, it can be established that the frictional resistance is approximately proportional to viscosity. Thus

$$D_{12} = \frac{RT}{Nf_s} = \frac{KT}{\alpha'\eta} \tag{1.44}$$

where $f_s = \alpha'\eta$, α' being a parameter with a dimension of length and approximately independent of concentration. This equation is consistent with an early general observation that the product $D\eta$ changes much less with composition than D itself. It has been shown that [44] from the hydrodynamic treatment of Bearman [53], several relationships for the binary diffusion coefficients of a two-component liquid can be deduced if suitable assumptions are applied for the frictional coefficients.

The preceding analyses have been employed as the basis for the development of many empirical relations between diffusion coefficient and viscosity. Of course, these relationships have little theoretical foundation, but are sometimes useful for estimation purposes. For example,

in the case of very dilute solutions ($x_2 \rightarrow 1.0$) it can be supposed that

$$D_{12}^{o} = \frac{KT}{\eta_2 \alpha'} \tag{1.45}$$

It is well known that, under comparable conditions, the higher the molecular weight of the diffusing species, the lower its diffusion coefficient. In solutions of various substances of molecular weight M_1, the following equation has been proved to hold in several cases [54-56]

$$D_{12}\eta_2 M_1^{\frac{1}{2} \text{ or } 1/3} \simeq \text{constant} \tag{1.46}$$

The correlation between the binary diffusion coefficient and the viscosity of a non-ideal solution has been shown to take different forms depending on the type and concentration of the solution [44, 57-61]

$$D_{12}^{c} = \frac{\eta_2}{\eta_{12}} B_1^{c} D_{12} \qquad \text{dilute solutions of real electrolytes and non-electrolytes} \tag{1.47}$$

where
$$B_1^{c} = \left[1 + \frac{\partial \ell n \gamma_1^{*}}{\partial \ell n c_1}\right]_{T,P} = \left[1 + c_1 \left(\frac{\partial \ell n \gamma_1^{*}}{\partial c_1}\right)\right]_{T,P} \tag{1.48}$$

and
$$D_{12}^{c} = \eta_{12}^{-1} \left(\frac{\partial \ell n x_1 \gamma_1^{*}}{\partial \ell n x_1}\right)_{T,P} \left(x_1 \eta_1 D_{21}^{o} + x_2 \eta_2 D_{12}^{o}\right) \qquad \text{solutions of real electrolytes and non-electrolytes} \tag{1.49}$$

where D_{12}^{c} is the concentration dependent diffusion coefficient, with D_{21}^{o} and D_{12}^{o} representing the limiting diffusivity values at x_1 and x_2 approaching unity, respectively. Thus for ideal solutions of non-electrolytes, in which case $\gamma^{*} = (a/x) \rightarrow 1.0$, the above equations simplify to the form

$$D_{12}^{c} = \frac{\eta_2}{\eta_{12}} D_{12} \tag{1.50}$$

and
$$D_{12}^{c} = \eta_{12}^{-1} \left(x_1 \eta_1 D_{21}^{o} + x_2 \eta_2 D_{12}^{o}\right) \tag{1.51}$$

where η_1, η_2 and η_{12} in all the above equations denote the viscosities of the pure solute, pure solvent and the solution respectively. A number of similar correlations have been recorded in the literature [6, 13a, 44]. However, the experimental results of Van Geet et al. ([39]; n-ocante/n-dodecane mixture) and King et al. ([62]; glycol/water mixture) can provide a way of determining the validity of any such correlations. According to their empirical findings

$$D_{12}^{c} = x_1 D_{21}^{o} + x_2 D_{12}^{o} \qquad \text{Van Geet et al.} \quad (1.52)$$

$$\left(\frac{D_{12}\eta_{12}}{T}\right) \neq f(T) \qquad \text{King et al.} \quad (1.53)$$
$$= f(c)$$

Equation (1.52) has been varified empirically by a number of investigators [58, 124].

1.2.2 Kinetic Models of Diffusion

Although certain relationships have been revealed by various treatments of the hydrodynamic model of diffusion, none of the analyses provide a deeper understanding of the molecular mechanism of the phenomenon. This is because they regard the liquid as a continuum and neglect its molecular structure. The kinetic statistical models, such as that of Eyring et al. [63-65] assume a molecular mechanism of diffusion. The particular model of molecular motion embodied in the Eyring theory has recently been shown to be incorrect [48, 66]. Nevertheless, its widespread use makes it necessary to discuss it and many of its qualitative predictions are in reasonably good agreement with experimental observations [62]. The theory is based upon a relatively simple model of the liquid state (i.e. spherically symmetric, monatomic, molecules such as those of liquefied rare gases and alkali metals) and leads to the derivation of an expression for the diffusion coefficient by applying the theory of

absolute reaction rates. It assumes that the diffusion can be described in a similar fashion to the rate processes of mono-molecular reactions, involving a temporary configuration of the species which can be considered as an intermediate activated state. The mechanism of diffusion is, in many respects, similar to that of viscous flow, except that unlike molecules are involved in the former process. In solution, diffusion requires the slipping of the solute and solvent molecules past one another. In the course of their movement, solute molecules should cross the potential barrier (free enthalpy barrier) separating two adjacent equilibrium positions in the liquid structure. If λ^* is the distance between the two equilibrium positions, then the molecules cover this distance in each jump in the direction of decreasing concentration. Because the standard free enthalpy of ideal solutions is identical in all equilibrium positions occupied by the diffusing molecules, then, assuming a symmetrical energy barrier, the free enthalpy of activation of the process in the direction of decreasing concentration must be identical to that in the opposite direction. In other words, the forward (diffusional) and backward (thermal) rates of molecular transport are equal. Consequently, the specific rate constants of the process in the two directions are equal to each other ($k_f = k_b = k$). It can easily be shown [32] that the actual rate of one-dimensional diffusion (i.e. the resultant velocity of the solute molecules) is given by

$$\bar{v} = \bar{v}_f - \bar{v}_b = -N\lambda^{*2}k\frac{dc}{dz} \qquad (1.54)$$

$$= -DN\frac{dc}{dz} \quad \text{according to Fick's law}$$

and hence by comparison

$$D = \lambda^{*2}k \qquad (1.55)$$

When the Eyring's theory of viscosity is applicable (e.g. in the case of self-diffusion), then $\lambda^{*2}k \simeq KT/\lambda^{*}\eta$ [13a, 32,63] and we have

$$D \simeq \frac{KT}{\lambda^{*}\eta} \tag{1.56}$$

Thus, the expression for the diffusion coefficient given by Eyring does not differ from that of Stokes-Einstein (equation (1.40)), except for the term $1/\lambda^{*}$, which replaces the frictional coefficient $6\pi r_1$. It must be noted that the Eyring and Stokes relationships are not, in fact, comparable. The latter is based on the assumption that the solvent molecules are small in comparison with those of the solute (i.e. diffusing molecules move in a continuum) and hence the laws of classical hydrodynamics are applicable at least in approximation. On the other hand, the Eyring theory is based on the supposition that the solute and solvent molecules are of the same order of magnitude in size and the movement of both has been considered during the process of diffusion.

The mechanism of diffusion given above can hardly be valid for the diffusion of large species in a solvent consisting of small molecules. In this case, we cannot assume that the rate determining step will be the jump of the solute molecule from one equilibrium position to the adjacent one because this requires a large amount of energy. It is more probable that the small solvent molecules jump (rate-determining step) and cause the large solute molecules to be displaced in the opposite direction in order to occupy the empty spaces left by the solvent molecules. The results of a detailed investigation of this mechanism of diffusion and the one described previously are given elsewhere [67]. However, on the basis of the theory of absolute reaction rates [63, 64], several equations have been derived for the calculation of the diffusion coefficient when at least two kinds of molecules (those of solute and the solvent) participate in diffusion. Examples of such equations, whose applications are limited include those for ideal and non-ideal

binary solutions [32, 68]

$$D = \frac{\lambda^{*2}}{v_f^{1/3}} \left(\frac{KT}{2\pi m}\right)^{\frac{1}{2}} \exp\left[-\frac{\Delta H_{evap}}{nRT}\right] \quad \text{ideal solution} \qquad (1.57)$$

where v_f is the liquid-free volume [68] and $m = m_1 m_2 / m_1 + m_2$ is the reduced mass of two types of molecules,

$$D|_{solute} = \frac{\lambda^*|_{[73,\ 75]}}{\eta|_{solution}} \cdot \left(\frac{\partial\ \ell n\ a}{\partial\ \ell n\ x}\right)_{solute}$$

or

$$\frac{D\eta}{\left(\frac{\partial\ \ell n\ a}{\partial\ \ell n\ x}\right)} = \lambda^* KT \qquad (1.58)$$

This equation is in good agreement with the experimental results for the chloroform-ether mixture [32] as shown in Fig. 1.2.

Fig. 1.2 - Variation of $D\eta$ and $D\eta/(\partial\ \ell n\ a/\partial\ \ell n\ x)$ with concentration in chloroform-ether mixture

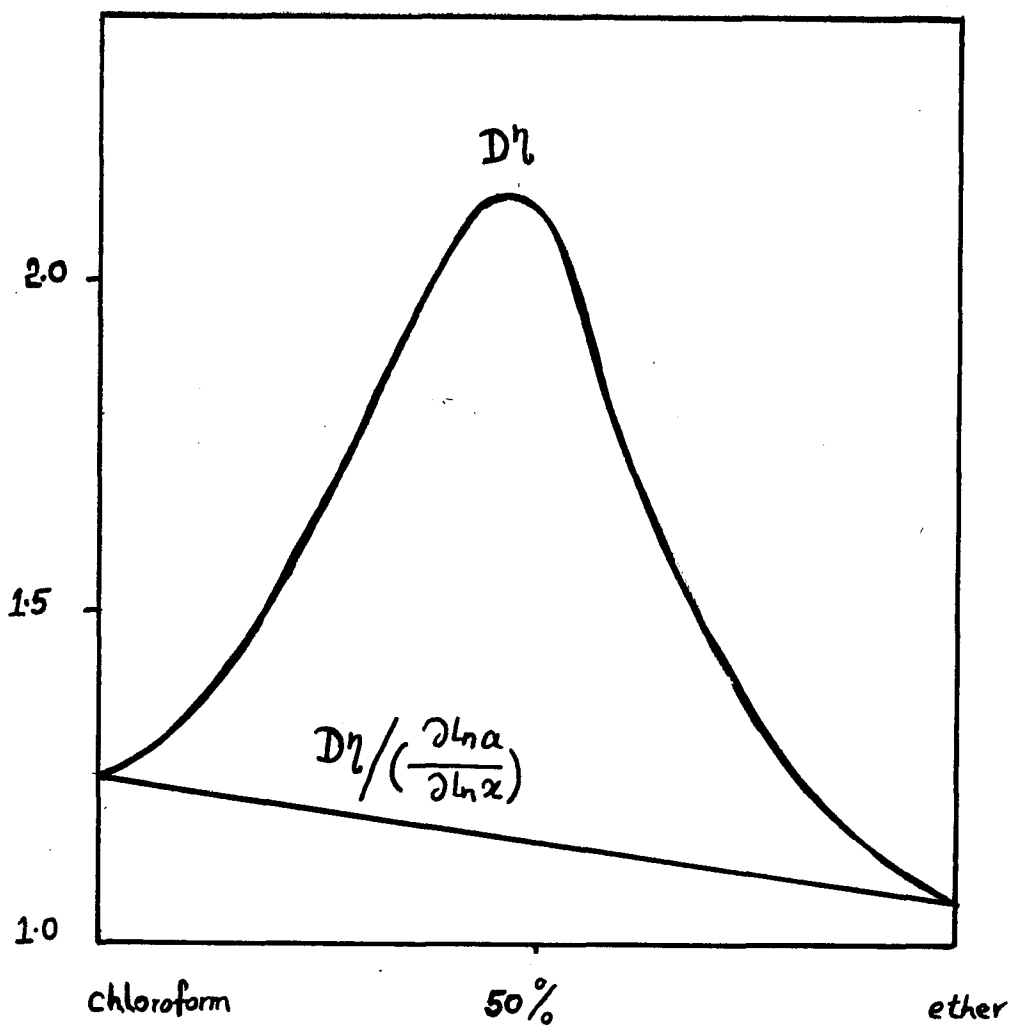

Thus, according to equation (1.58), the product $D\eta$ has a maximum in agreement with the experimental data. Similar results have been obtained for other mixtures whose activities could be determined by measuring the partial vapour pressures proportional to the activities.

In view of the fact that the Eyring theory has now been discredited [48, 66], it is not surprising that marked deviations can be observed between the calculated and measured values of some properties such as the diffusion coefficient [32, 48, 66]. This is because the theory in its details is based on very simple assumptions, and more or less, reliable conclusions could be drawn from it only for the main features of diffusion. The theory has been extended and modified to eliminate its deficiencies by several workers [e.g. 69]. In addition, several other molecular theories such as the theory of transfer diffusion [70], (based on the assumption that diffusion is due to a molecular exchange of reactions as well as migration to lower concentration regions), Panchenkov theory [71], (based on van der Waals/Maxwell analyses - a molecule will diffuse (a) if it has gained sufficient kinetic energy to break the van der Waals bonds with its neighbours (b) if adjacent molecules are sufficiently far apart for the diffusing molecule to pass between them), Frenkel *et al.* theory [72], (the onset of diffusion is considered to be the rotational and vibrational motion due to collisions in a liquid containing dipole molecules) and the theory of Jensen *et al.* [73], (based on time-dependent correlation functions, the diffusion coefficient and viscosity are correlated through such functions) have been proposed. Unfortunately, all such attempts have failed to produce a satisfactory theory of diffusion.

1.2.3 The van der Waals' Model

Although the van der Waals' model has proved to be of great value for calculation of density dependence of self-diffusion coefficients, it has not so far been of great value to the description of the temperature and concentration dependence of binary diffusion coefficients.

Computer simulation studies by the method of molecular dynamics (Section 1.3.4) have now discredited the Eyring activation energy model for diffusion in liquids. The studies also reveal that the effect of the attractive part of the intermolecular potential energy function is far less significant than is postulated in the Brownian motion approximation (Section 1.3.2). Indeed, they prove that the van der Waals' model is a better approximation even under ordinary liquid conditions. The findings of this model and molecular dynamics simulations are often similar and very valuable in the study of the transport properites and hence attaching a significant importance upon the model and the results described here, even though they are limited to pure fluids. In fact, it will be seen later on that recent efforts, based on molecular dynamics simulations, to extend the rough hard sphere theory for pure fluids to binary systems depend on the transport property data for the pure fluids.

The van der Waals' model of a fluid considers the molecules to have an intermolecular potential made up of a hard core surrounded by a weak, long-range attractive component [74, 75]. For a system of such molecules, the well-known van der Waals' equation of state is rigorously obeyed [76]. For real fluids the intermolecular potential does possess a steep repulsive wall, although not infinitely steep, and the range of the attractive forces is large relative to the intermolecular spacing at densities higher than the critical density. Furthermore, the attrac-

tive potential may be considered weak relative to the kinetic energy whenever the temperature is greater than the well-depth (or ≈ 0.7 times the critical temperature). As a result for relatively high temperatures and densities, real fluids obey the van der Waals' equation of state quite well [6], provided that the core size is allowed to decrease as the temperature increases to reflect the finite steepness of the repulsive wall of the potential [77].

From the point of view of the transport properties of dense fluids, the van der Waals' model is consistent with the findings of molecular dynamics simulations (see Section 1.3.4) in that the molecules move very nearly in straight lines between hard core collisions; because at high densities the attractive potential forms a uniform surface [78]. The description of the van der Waals' model indicates that it should be most accurate at high densities and high temperatures, i.e. at the very dense gas region. But it has also been successfully applied to liquids, and even extended to lower densities where perturbation theory may be used to account for the increasing influence of attractive forces [79]. Under conditions of high density and temperature, the van der Waals' model allows the transport properties of monatomic fluids to be described by the Enskog smooth rigid sphere theory which has been treated in detail by Chapman *et al.* [80]. Basically, the assumption is made that the fluid consists of hard spheres and behaves like a low-density hard sphere (Boltzmann analysis) system except that all events occur at a faster rate due to the higher rate of collision [81, 82]. The transport coefficients for the dense fluid may thus be written in terms of their dilute gas values. For example, the ratio of the self-diffusion coefficient D_E, valid at high number density n^*, to that at low density n^*_o, denoted by D_o, is given by [48]

$$\frac{n^* D_E}{n^*_o D_o} = g(\sigma_p) \tag{1.59}$$

where $g(\sigma_p)$ is the radial distribution function [1b,c,d] at contact for spheres of diameter σ_p and depends on the co-volume b. In order to employ equation (1.59) for the calculation of the diffusion coefficients it is necessary only to find $g(\sigma_p)$ and a suitable value for the co-volume b. In the original application of this method b was obtained by fitting the PVT data for the noble gases to the van der Waals' equation of state and $g(\sigma_p)$ was taken from the results of computer simulations [74]. It was found that the calculated high density transport coefficients differed by less than 10% from the experimental values.

However, the Enskog theory neglects all correlations of molecular velocities in the evaluation of the transport coefficients (e.g. the Enskog expression for dense fluid diffusion based on the molecular chaos approximation). Because the computer simulations indicate their existence and the van der Waals' model allows them, an improved calculation of the transport properties is possible when they are included [78]. Molecular dynamics simulations, of the type described in Section 1.3.4, have been employed to deduce the corrections to the Enskog theory which arises from velocity correlations for smooth hard spheres [79]. For instance, the correction for self-diffusivity, in the form of ratios of the exact hard sphere result to the Enskog result, may be written as

$$\frac{n^* D}{n^*_o D_o} = \frac{D_E}{D_o} \cdot \frac{D_{MD}}{D_E} \tag{1.60}$$

D_o is related to the number density n^*_o at temperature T by

$$D_o = \left(\frac{3}{8n^*_o}\sigma_p^2\right)\left(\frac{KT}{\pi m}\right)^{\frac{1}{2}} \tag{1.61}$$

where m is the mass per molecule. It has been found that the correction is largest for self-diffusivity and it amounts to an increase of about 35% at densities 1.5 to 2 times the critical density, but to a decrease of about 40% as solidification is approached. On the other hand,

thermal conductivity corrections show a weak dependency upon the density, never exceeding 10%.

Dymond [83, 84] has considered a number of ways of applying the corrected Enskog theory to the calculation and correlation of the transport properties of dense gases and liquids. An equation for $g(\sigma_p)$ is adopted which provides a good representation of the pair distribution function for hard spheres from computer simulations which has been given by Carnahan and Starling [85]

$$g(\sigma_p) = (1 - \frac{\psi}{2})(1 - \psi)^{-3} \tag{1.62}$$

Here $\psi = b/4\overset{\bullet}{V}$; $\overset{\bullet}{V}$ is the independent variable molar volume and $b = (2\pi n^*/3)\sigma_p^3$ is the co-volume. The results for $g(\sigma_p)$ may be combined with the molecular dynamics results for D_{MD}/D_E by means of the definition

$$D^+ = (\frac{\overset{\bullet}{V}}{\overset{\bullet}{V}_o}) \frac{1}{g(\sigma_p)} \left(\frac{D_{MD}}{D_E}\right) \tag{1.63}$$

to yield an equation for the self-diffusion coefficient for the hard sphere fluid. Dymond [83a,b] has given two equations which represent the volume dependence of D^+ obtained from the computer simulations of hard spheres

$$D^+ = 1.27 \left[\frac{\overset{\bullet}{V}}{\overset{\bullet}{V}_o} - 1.384\right] \quad ; \quad 1.5 \leq \frac{\overset{\bullet}{V}}{\overset{\bullet}{V}_o} \leq 2.5 \tag{1.64}$$

$$D^+ = 2.379 \left[(\frac{\overset{\bullet}{V}}{\overset{\bullet}{V}_o})^{2/3} - 1.256\right] \quad ; \quad 1.6 \leq \frac{\overset{\bullet}{V}}{\overset{\bullet}{V}_o} \leq 6.6 \tag{1.65}$$

The low volume (high density) limit of these correlations is imposed by the fact that a rigid sphere fluid becomes meta stable at higher densities. For a real fluid the high density limit corresponds to approximately 3 times the critical density (ρ_c) and the low density limit to 0.8 times ρ_c. Equations (1.64) and (1.65) may be used to

represent the density dependence of the self-diffusion coefficients of real monatomic fluids under the conditions for which the van der Waals' model is applicable, (i.e. $T > 0.7\ T_c$, high density) in both gaseous and liquid phase. From equations (1.64) and (1.61) we find

$$D = 0.4763 \frac{(KT/\pi m)^{1/2}}{(2n^*)^{1/3} \dot{V}_o^{2/3}} \left[\dot{V} - 1.384\ \dot{V}_o\right] \text{ for } 1.5 \leq \frac{\dot{V}}{\dot{V}_o} \leq 2.5 \tag{1.66}$$

Thus the self-diffusivity of a real dense fluid is predicted to be a linear function of $\dot{V}$ over the specified density range along an isotherm. Over the larger density range of equation (1.65) which is representative of dense gaseous regions we can define

$$D^x = \frac{1}{g(\sigma_p)} \left(\frac{D_{MD}}{D_E}\right) \left(\frac{\dot{V}}{\dot{V}_o}\right)^{2/3} = f(\dot{V}/\dot{V}_o) \tag{1.67}$$

D^x may also be calculated from experimental data along an isotherm, since

$$D^x_{expt} = \frac{8D}{3\dot{V}^{1/3}} (2n^*)^{1/3} \left(\frac{\pi m}{KT}\right)^{\frac{1}{2}} \tag{1.68}$$

It follows that it should be possible to superimpose a plot of D^x_{expt} vs log $\dot{V}$ upon a plot of D^x_{theo} vs log $(\dot{V}/\dot{V}_o)$ merely by a shift along the log $\dot{V}$ axis. It has been shown by Dymond et al. [48] that the available experimental data on transport properties for several fluids conform extremely well to the above equations and those similarly obtained for viscosity and thermal conductivity ($\sim$ 5%). It is therefore possible to use the equations not only as correlations but also for the calculation of the transport of fluids for conditions other than those for which they were measured.

The van der Waals' model and the Enskog theory are strictly restricted to a consideration of monatomic species, or at the least, those interacting through spherically symmetric intermolecular potentials. Chandler [86] has extended the study to include dense fluids consisting of rough

hard spheres, model for a system in which there is translational-internal energy coupling through non-spherically symmetrical force fields. He has shown that [86b] for a rough hard sphere fluid at densities greater than twice the critical density

$$D_{RHS} \simeq A\, D_{SHS} \tag{1.69}$$

where A represents a translational-rotational coupling factor less than unity which is assumed to be independent of temperature and density. Thus for the non-spherically symmetric molecules equation (1.66) is expected to reform to

$$D = \frac{0.4763A}{\dot{V}_o^{2/3}(2n)^{1/3}}\left(\frac{KT}{\pi m}\right)^{\frac{1}{2}} (\dot{V} - 1.384\, \dot{V}_o) \tag{1.70}$$

so that A and V_o may be determined from experimental data.

The rough hard sphere theory of Chandler [79] and Dymond [78, 83c] for pure fluids have been extended to binary mixtures by Anderson *et al.* [87] and Bertucci *et al.* [88]. It has been assumed that the kinetic diffusion coefficient D_{12}^{Kin} of a real two-component fluid is given by [89]

$$D_{12}^{Kin} = D_E^{Kin}\, A\, F(\phi, \frac{m_1}{m_2}, \frac{\sigma_1}{\sigma_2}, x_1) \tag{1.71}$$

where D_E^{Kin} is the kinetic binary diffusion coefficient derived by Enskog for a mixture of hard spheres at the same temperature as the real fluid and function F depends on the packing factor ϕ, the appropriate mass and molecular diameter ratios and the mole fraction of the solvent. Calado and Castro [89] have shown that it is possible to obtain the values of the translational-rotational coupling factor A and the hard core volumes from the viscosity and self-diffusion data.

1.3 THE RIGOROUS THEORY OF THE TRANSPORT PROPERTIES OF DENSE FLUIDS

From the macroscopic point of view the transport properties of a fluid are those coefficients which give a measure of its tendency to produce entropy when perturbed from an equilibrium state [13, 32]. From the microscopic point of view the entropy production, and hence the values of the transport coefficients, are a manifestation of the motion of the molecules which make up the fluid as well as the exchange of energy and momentum among them. For this reason the transport coefficients are closely related to molecular motion, to the mechanism of molecular encounters and thereby to the intermolecular force field. The rigorous molecular theory of fluids seeks to establish the formal connection between these microscopic events and the observable transport coefficients. First, such a connection enables a knowledge of the details of molecular encounters to be employed to evaluate the transport coefficients. Secondly, a precise knowledge of the transport coefficients from experiment can be applied to the verification of the molecular theory itself and of hypotheses and statements made about the intermolecular potential. Finally, the molecular theory may reveal relationships among different transport coefficients or between transport coefficients and the parameters of the thermodynamic state of the fluid [44, 45, 53, 90] which considerably reduce the experimental effort required to determine all of the coefficients over a wide range of states.

So far, one of the most successful theories of this kind has been the well-known kinetic theory of gases [91-94] which has its origins in the works of Bernoulli, Clausius, Maxwell and Boltzmann [95]. The simplest fluid and that for which the kinetic theory is most secure is a dilute gas composed of identical, monatomic molecules interacting through a

spherically-symmetric force field and obeying the laws of classical mechanics. In view of the difficulties which surround the theory even in this simple case, it is not surprising that as the system becomes progressively more complicated, either by virtue of increasing complexity of the molecules or increasing density, its theoretical description becomes less secure. For dense gases and liquids, the formal theory is not yet fully developed and their treatment has proved to be exceedingly difficult. Thus, although a formal statistical mechanical theory for the transport coefficients exists [92, 93], its implementation for calculations for real fluids has only been accomplished by means of approximations. These approximations are based on still further models of molecular motion whose physical basis is uncertain.

1.3.1 Statistical Mechanical Theory

The most complete statistical mechanical description of the behaviour of a fluid is given by the Liouville equation [1b,c,d, 91]. This equation describes the evolution of the N-particle distribution function $\tilde{f}_{N_p}$ in the 6N-dimensional phase space for a fluid of N_p particles. The changes in this distribution function occur because of free molecular motion and interactions among all N_p particles. The Liouville equation is based upon classical mechanics and is therefore reversible in time. This means that if at some instant of time the velocities of all the particles in the system were reversed, then the particles would retrace their trajectories in phase space so that all earlier states of the system in phase space would be recovered.

According to the usual statistical mechanical hypothesis the value of any macroscopic quantity, $\tilde{\alpha}$, for a fluid is given by the average of the corresponding microscopic quantity $\tilde{\alpha}(\Gamma N_p)$ over the relevant phase space

$$\tilde{\alpha}(\underline{r}, t) = \int \tilde{\alpha}(\Gamma_{N_p}) \tilde{f}_{N_p}(\Gamma_{N_p}; t) d\Gamma_{N_p} \qquad (1.72)$$

where Γ_{N_p} represents a point in 6N-dimensional phase space. With the aid of the Liouville equation it is then possible to obtain the equations of change for any quantity $\tilde{\alpha}(\underline{r}, t)$, such as the mass, momentum and energy, in terms of integrals over the N-particle distribution function [91]. These equations represent the statistical mechanical analogues of the equations of motion for the fluid in terms of the N-particle distribution function. Thus if $\tilde{f}_{N_p}$ the distribution function were known, the equations of motion could be evaluated and the coefficients of the gradients of the macroscopic variables identified with the transport coefficients and expressed in terms of the microscopic properties of the molecules of the fluid.

There are two difficulties encountered in carrying out this programme. First, a kinetic theory must be established for the function $\tilde{f}_{N_p}$ which involves, in principle, the solution of a dynamic problem involving N_p particles (the so-called "many-body problem"). Secondly, because the Liouville equation is reversible it is necessary to somehow introduce irreversibility into the theory in order that it agrees with practical experience. In the case of dilute gas the first difficulty is overcome by simply the rarity of many-body events, whereas the irreversibility is introduced by the molecular chaos assumption [1d, 95]. But for dense fluids neither of these difficulties has been fully resolved so that it has been necessary to develop approximate theories [93, 96]. Generally such theories employ a contracted description of the fluid in terms of the single-particle and two-particle distribution functions. The introduction of irreversibility into the theory is then accomplished by a statistical assumption concerning the lack of correlation in molecular motion on some macroscopic time scale. In the particular case of the

dilute gas the appropriate time scale is the duration of a single collision, t_{col}, but in a dense fluid it may be significantly larger.

1.3.2 The Rice-Allnat Theory

The Rice-Allnat theory [91-94] is based upon a model of the fluid for which it is possible to discern two microscopic time scales. In the first instance, the theory is applied to spherically symmetric monatomic species interacting through pairwise additive intermolecular pair potentials. The model replaces the true intermolecular pair potential by a rigid repulsive core of diameter σ_p surrounded by an arbitrary attractive potential. In the dense fluid state, the attractive potential is assumed to contribute to a weak fluctuating background force acting on the particles. The first time scale of the theory is then associated with the large momentum and energy transfer which occurs when the hard cores of two molecules interact. The second time scale corresponds to the frequent, but small, energy and momentum transfers which occur during the Brownian-type motion caused by the weak attractive force field. The hard core collisions are supposed to occur in a time short enough that no more than binary encounters of this kind need be considered.

The first essential simplification that results from this model is that the hard core collisions may be treated in the same way as for the dilute gas. That is, the Brownian motion between such collisions is supposed to randomize the velocities of the particles following one hard sphere collision so that they are uncorrelated before the next. Thus the changes in the single particle distribution function, $\tilde{f}_1$, which occur because of hard sphere collisions may be represented by the collision term of the original Boltzmann equation [1e, 95]. The changes in the single-particle distribution function caused by the Brownian motion are then treated in an additive fashion. Thus the changes in $\tilde{f}_1$ by

virtue of collision are written as [91]

$$\left(\frac{\partial \tilde{f}_1}{\partial t}\right)_{coll} = \left(\frac{\partial \tilde{f}_1}{\partial t}\right)_{CE} + \left(\frac{\partial \tilde{f}_1}{\partial t}\right)_{FP} \tag{1.73}$$

where the first term is the Chapman-Enskog collision term of the dilute gas and the second, Fokker-Planck term describes the effects of the Brownian motion [1c, 91]. The separation of the two components in this equation enables a solution to be obtained for $\tilde{f}_1$ (and also for $\tilde{f}_2$) which can be used in the statistical mechanical equations of motion to obtain explicit equations for transport coefficients. The simplest example of this is the self-diffusion coefficient [92]

$$D = \frac{KT}{f_H + f_B} \tag{1.74}$$

where $f_H = \frac{8}{3} n^* \sigma_p^2 g(\sigma_p)(\pi m KT)^{\frac{1}{2}}$ is an effective friction coefficient for the hard sphere interactions and f_B is a friction coefficient for the Brownian motion. If the Brownian motion is neglected, equation (1.74) reduces to the Enskog result for a dilute gas of hard spheres undergoing uncorrelated collisions. In the more general case, the determination of f_B requires a calculation based on molecular statistical dynamics for which a further model must be introduced. Of all the models suggested for this purpose none is satisfactory [91, 92a].

The model of molecular motion upon which the Rice-Allnat theory is based has been challenged by the results of molecular dynamics simulations of liquids (Section 1.3.4; [66, 92, 97, 98]). In these calculations, the classical equations of motion for an assembly of N_p particles are solved numerically so that it is possible to follow the motion of individual molecules and groups of molecules in the simulated liquid. These computer simulations show that the soft and hard collisions occur in roughly equal proportions [66] and hence there is not a large majority

of soft collisions as implied by the Rice-Allnat model. Calculations of transport coefficients of liquefied noble gases based on this model have generally been in poor agreement with experimental results [91, 92]. It has not yet been established whether this is due to incorrect modelling of the molecular motion or poor radial distribution functions and intermolecular potentials for the liquid.

1.3.3 Method of Time Correlation Functions

An alternative method of formulating the transport coefficients of dense fluids is provided by the fluctuation dispersion theorem [1b, 43a]. This theorem relates a correlation function for spontaneous fluctuations in a system in stationary state to the dissipation (or, in thermodynamics terms, entropy production) of the system under the influence of time dependent driving forces. If the time dependent driving forces are the concentration (chemical potential in thermodynamics terms), flow velocity or temperature, it is possible to express the corresponding transport coefficients in terms of auto-correlation functions of microscopic fluxes [1b, d]. Thus the self-diffusion coefficient of a fluid is written in terms of the velocity auto-correlation function as [99, 100]

$$D = \frac{1}{3}\int_0^\infty \langle \underline{v}_i(0) \cdot \underline{v}_i(\tau)\rangle d\tau \qquad (1.75)$$

where $\underline{v}_i(0)$ and $\underline{v}_i(\tau)$ are the velocities of the molecule i at time zero and some later time τ, respectively. The angle brackets denote an ensemble average of the quantity, using an N-particle distribution function for the unperturbed system.

The expression of the transport coefficients in terms of time correlation functions does not immediately represent an advance over other formulations. This is because in order to evaluate such functions it is neces-

sary to find the time dependence of the microscopic variables involved, which in turn, requires a solution of the Liouville equation that does not exist. Nevertheless, the correlation function formulation does have two advantages which have proved of great value in the development of the theories of dense fluids. First, it can provide a method for the description of phenomena in liquids such as absorption and scattering of electromagnetic radiation which yield information about the details of molecular motion [99]. Secondly, it enables the calculation of the transport coefficients of a hypothetical dense fluid by means of a molecular dynamics simulation on a computer.

1.3.4 The Technique of Molecular Dynamics Simulation

Molecular dynamics simulation is a computational technique whereby the positions and velocities of N_p particles contained in a cell are followed over a period of time by the numerical solution of Newton's laws of motion. Thus it readily allows the study of time dependent phenomena such as diffusion (a transport process tackled by non-equilibrium thermodynamics [13]).

Evidently, for even a small number of particles ($N_p \simeq 100$) over even quite a short time, the computational effort required to carry out such a programme is enormous [1b, c]. Consequently, it was not until the advent of fast digital computers that such calculations became feasible [100, 101a]. Since their introduction, molecular dynamics simulations have given considerable insight into the nature of molecular motion and brought to light novel effects not previously considered. Although such techniques have occasionally been misused, there seems no doubt that they will have a large part to play in the development of theories of the fluid state in the future.

In the basic molecular dynamics method [1b, c, 92b, c] a three-dimensional cell is established in the computer which contains N_p molecules with specified positions and velocities so that the total energy (i.e. kinetic + potential) is defined. The form of the potential energy of interaction between the molecules is specified by the investigator. Usually it is chosen to be of a relatively simple form and assumed to be pairwise additive, although neither condition is necessary. In order to minimize surface effects and to simulate more closely the properties of an infinite system, a periodic boundary condition is almost invariably imposed. The way in which the boundary condition works in a two-dimensional system is illustrated in Fig. 1.3.

Fig. 1.3 - Periodic boundary conditions used in MDS

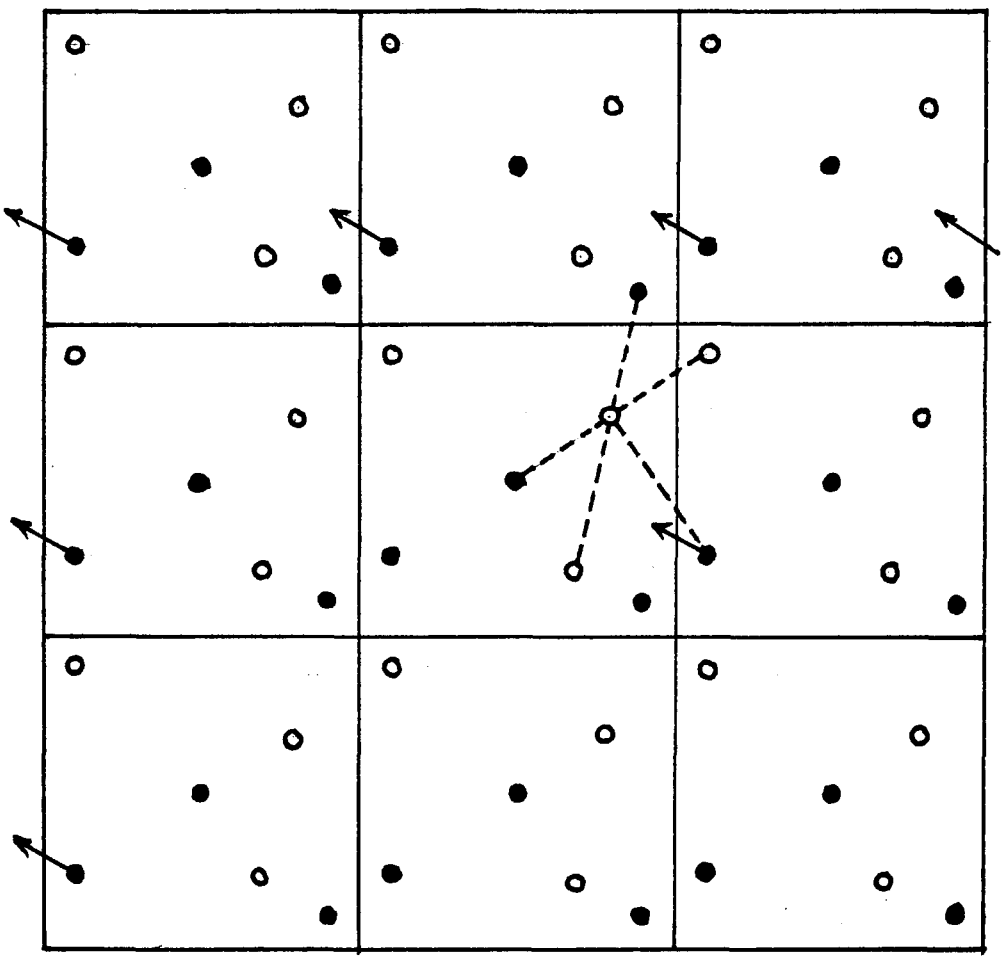

"The Assembly"

The molecules of interest lie in the central cell of the "assembly", and this basic unit is surrounded on all sides by periodically repeating replicas of itself, each image cell containing N_p molecules in the same relative position. When a molecule enters or leaves through one face of the basic cell, the move is balanced by an image of that particle leaving or entering a neighbouring cell through the opposite face. It is often advantageous to choose N_p and the shape of the cells in such a way that the periodic boundary generates a perfect lattice appropriate to the physical system under study when the particles are arranged in a suitably ordered manner. For example, in the case of liquid argon a cubic lattice with $N_p = 4n^3$ (n being an integer) is chosen since it crystallizes in a face-centred cubic lattice. This explains the use of samples containing N_p = 4, 32, 108, 500, ... etc. particles.

The positions and velocities of the molecules are then followed from the initial state by numerical integration of the equations of motion for all of the molecules. The integration time step, t_{int}, is chosen to be small compared with the time between molecular collisions and the entire process is followed for several thousands of such steps (e.g. liquid argon, $t_{int} \simeq 10^{-14}$ s and 10^3 - 10^5 steps). For each step, the force on any molecule is evaluated as the resultant of the forces due to all other molecules (Kirkwood's hypothesis; [1d]). In this calculation, the distance between any pair of molecules i and j in the cell is compared with that between i and all images of j in the surrounding cells. The force between the pair is then evaluated for the shortest distance encountered. As mentioned earlier if, during the course of integration of the equations of motion, one molecule moves through the wall of the central cell, a molecule enters through the opposite face of the cell to maintain the total number of the molecules in the cell

constant. By means of these periodic boundary conditions, the central cell simulates just part of a larger volume of gas [101].

The molecular dynamics method represents the behaviour of the molecules of a fluid with the microscopic properties specified by the investigator. It is therefore possible to determine the motion of the molecules in the fluid essentially exactly and to calculate the transport properties of the fluid from the time correlation function. For this reason a molecular dynamics simulation is sometimes thought of as a "quasi-experimental technique" for determination of the properties of a hypothetical fluid. Of course, if the intermolecular potential selected were exactly that of a real fluid, the method should yield the observable properties of the real fluid. Thus, in principle, the simulation method provides a means whereby intermolecular potentials proposed for a fluid may be examined, although the computational effort necessary often inhibits the systematic investigation required [92b].

There are a number of difficulties which arise in "computer experiments" such as molecular dynamics simulations. The most obvious one being the fact that by microscopic standards the size of sample which can be studied economically is extremely small ($N_{pmax} \simeq 10^3$). There is no general solution to the problem of choosing a small periodic system whose properties are truly representative of the macroscopic system which the model is designed to simulate. Only in a number of cases the N_p dependence of properties of periodic systems is known exactly [102]. But in general, it is true to say that the bulk properties are weakly dependent on size for $N_p \geq 100$ and such errors as exist are for the most part no larger than the inevitable statistical errors. An exception must be made for critical point phenomena because the large scale density fluctuations which characterize the critical region are suppressed by the use of a periodic boun-

dary condition. Another difficulty which is particularly severe for small systems is the so-called quasi-ergodic problem [103]. By this is meant that the system may become locked for an extended period of time in a small region of phase space. Eventually, escape may be possible, but it would require calculations of unreasonable length. Near the melting temperature (i.e. near the transition from solid to liquid state at the triple point), for example, an initial lattice type arrangement of particles will generally persist for a very long time unless the density is some ten percent below the melting density of the model. In situations such as this, it is clear that the system may remain in a metastable state indefinitely and care is needed if fallacious results are to be avoided. Generally speaking, it is not possible to say what time must elapse before a system evolving from some arbitrary chosen initial conditions reaches the region of phase space which is of interest. This can be judged only in an empirical way and much can be learned by carefully monitoring the calculated bulk properties of the system and the way these fluctuate in the course of a calculation.

Among the early results from molecular dynamics studies of dense fluids was the clear demonstration of the breakdown of the "molecular chaos" assumption of the dilute gas [92b, 100, 101b]. It was found that at high densities there is a higher than random probability that a molecule will have its direction of travel reversed by being scattered back by the surrounding particles. This has the effect that the self-diffusion coefficient of the fluid is smaller than the value predicted on the basis of uncorrelated motions. At moderate densities a positive type of correlated motion was observed extending over as many as ten mean free times, contributing to an enhanced diffusion coefficient. Some of these observations raised fundamental issues concerning the relationship

between statistical mechanics and continuum hydrodynamics which are discussed elsewhere [98, 101b]. Here we describe some of the applications of the results of molecular dynamics simulations which have led to the establishment of reliable correlation procedures for the transport properties of fluids.

One important application of molecular dynamics results has been the assessment of the validity of statistical mechanical theories and the models which they employ. First, the details of the molecular motion obtained from a molecular dynamics calculation enable simple models of it to be examined. Secondly, the calculations provide "experimental data" for the transport coefficient of a gas whose intermolecular potential energy function is known. Thus, when statistical mechanical theories are applied to the evaluation of the transport coefficients for the same fluid, one source of discrepancy in the comparison is removed leaving only the theory itself.

It is the first type of test which has cast doubt on the activation energy theory of liquid transport (e.g. Eyring's model, Section 1.2) as well as upon the Rice-Allnat theory (Section 1.3.2). In the activation energy theory (Section 1.2; [63]) a molecule is envisaged to make a large number of oscillations about an equilibrium position in a cell formed by its immediate neighbours, with occasional, but large jumps to a new equilibrium position. An examination of the mean free path distribution in a molecular dynamics simulation indicates that, as it has already been pointed out, this is not a significant contribution to molecular motion in liquids [104]. Instead, the computer simulations indicate that the motion of the molecules is close to that of van der Waals' model of a fluid in which the molecules travel essentially unperturbed between a succession of hard-core collisions [74]. The same behaviour represents

the opposite extreme from that of the Rice-Allnat hypothesis [91, 92, 105]. The reason is that the van der Waals' model allows correlated hard-core collisions, whereas the Rice-Allnat theory contains completely uncorrelated hard-core collision by virtue of the Brownian motion assumption. Reality must lie somewhere between these two extremes and the quantitative consequences of the difference in the two models may not be large. Nevertheless, the similarity of the molecular dynamics results to those of the van der Waals' model has encouraged the development of the successful method of correlating the transport properties of liquids based upon it (Section 1.2.3).

Thus it seems certain that such computer simulation techniques will be increasingly used in the development of the liquid-state theories.

1.4 EXPERIMENTAL METHODS OF MEASURING BINARY DIFFUSION COEFFICIENTS FOR LIQUIDS

Accurate measurement of the binary diffusion coefficients has proved a formidable task facing the experimentalist [13a]. Even small changes in temperature, or a minute alteration of the flow patterns by the induced pulsating and secondary flows, or a slight mechanical vibration transmitted to the diffusion cell can all cause a much more rapid mixing of the diffusing substance than the diffusion process itself. Consequently, a large number of techniques of measuring the diffusivities have been discarded. Moreover, methods based on principles that deviate seriously from the reality, for instance, one which assumes a "diffusion constant" completely independent of concentration or ignores the possible importance of the frame of reference, have led to erroneous results and hence become obsolete. With reference to the excellent reviews given by Tyrrell *et al.*

[13a, 24, 26] and Dunlop et al. [37], here we describe the methods which are most widely used for measurements of binary diffusion coefficients for liquid mixtures of two non-reacting components. Such methods may conveniently be grouped into five categories, depending on the nature of the diffusion process occurring:

(1) Free Diffusion - Optical Interferometric Methods (Gouy/Rayleigh).

(2) Steady State or Stationary Diffusion - The Diaphragm Cell Technique (Northrop and Anson).

(3) Restricted Diffusion - The Conductance Method (Harned).

(4) Dynamic Diffusion - The Taylor Dispersion Technique.

(5) Other Important Methods.

1.4.1. Free Diffusion Methods

In experiments of this kind a diffusion boundary, which is initially sharp, is formed between two solutions or a solution and the pure solvent within a vertical diffusion cell. The boundary is horizontal and the denser medium lies below it. Mutual diffusion takes place across the boundary and the region over which the concentration changes occur becomes more extensive with time. In the early stages, the concentrations at each end of the diffusion cell will retain their initial values and the observation period is confined to this phase during which the diffusion process can be described as free diffusion.

Changes in concentration of a solution are reflected in refractive index changes and the most sensitive methods of following these are based upon optical interference phenomena and fall into two broad classes:

(a) Those methods, based on Gouy interferometry, which effectively measure refractive index gradients as a function of time and of distance from the initial diffusion boundary;

(b) Those, based on Rayleigh's interferometric method, which effectively measure refractive index, relative to some constant reference medium, as a function of cell position and time.

Almost all the methods for studying transport as described in Sections 1.1.2 - 1.1.6 employ the optical technique (a) or (b) to yield time-dependent patterns that can be photographed and then analyzed to yield the binary diffusion coefficients.

(a) Gouy Interference Method

When a beam of light is passed through the diffusion cell it is bent through an angle proportional to the refractive index gradient in the cell. The angular deflection will therefore be a function of the height at which the light beam passes through the cell, and will vary with time. Measurements of the deflection of the beam give the refractive index gradient in the cell as a function of cell height and time. As well as being deflected by different amounts at different levels in the cell, the exit beam is not uniform in phase. Thus for a symmetrical diffusion boundary it is possible to produce time-dependent patterns of horizontal interference fringes (known as Gouy fringes) from which the diffusion coefficients can be deduced. Atlhough in 1880 Gouy [106] predicted that the interference fringes might be useful for studying diffusion, 75 years elapsed before Longworth [107] published a photograph of a Gouy fringe pattern and suggested that a quantitative treatment of the phenomenon would probably lead to greater precision in the measurement of diffusion coefficients.

In 1947 Longsworth [107] reported some preliminary tests of the wave optical theory of the Gouy interference method provided by Kegeles and Gosting [108] in a companion paper. Two years later, Morris and Gosting et al. [109, 110] described the construction of a Gouy diffusiometer of

high sensitivity and reported some experimental results (on sucrose solutions and by using green light from an Hg lamp) with the apparatus, and refined [110] the original wave optical treatment [108]. At a later stage, Gosting and Onsager [111] published a more general theoretical treatment of the entire method. Since the appearance of these important developments, the Gouy diffusiometer has been much improved to measure the binary diffusion coefficients with a high precision (∿ 0.2%). Although the optical system itself is quite elementary, the refined wave optical theory of the Gouy interference method is quite complex.

Figure 1.4 is a schematic diagram of the single-lens Gouy diffusiometer apparatus. A monochromatic light source is used to illuminate the horizontal source slit S, which is focussed by means of the lens L onto the photographic plate P. A mercury vapour lamp with a condenser lens and an optical filter provides illumination of sufficient intensity to give reasonably short exposure times. The diffusion cell C is placed between the lens and the photographic plate and with the windows of the cell at right angles to the optic axis of the system.

Fig. 1.4 - Optical system due to Gosting for the single-lens Gouy diffusiometer [37]

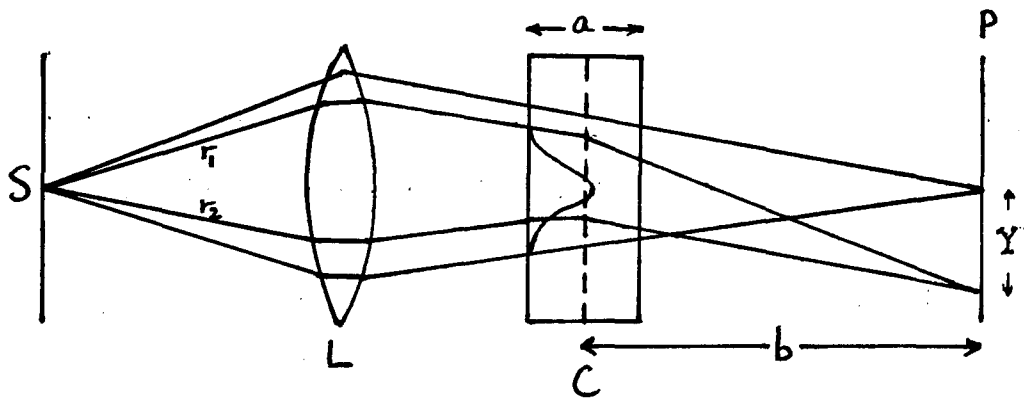

In performing a diffusion experiment, a sharp boundary is formed between two solutions of different concentrations and the solutions are then

allowed to mix. Light passing through regions of the diffusion cell where there is refractive index gradient is deflected downward and then focussed by the lens at a position below the optic axis on the photographic plate. Light passing through regions of constant composition, above and below the boundary region, remains in focus on the optic axis to give an intense undeviated image of the source slit. The light rays passing through the boundary are deflected downward a distance Y according to the relation [37]

$$Y = \acute{a}b \frac{dn_D}{dz} \tag{1.76}$$

Here $\acute{a}$ is the cell thickness parallel to the optic axis and b is the optical lever arm for the convergent light equal to $\Sigma \frac{\ell_i}{n_{Di}}$ where ℓ_i is the distance along the optic axis in each medium i of refractive index n_{Di} relative to air as unity. Interference fringes occur at the photographic plate because two light rays, r_1 and r_2, say, which originate at the light source and then co-focus at the photographic plate, follow different optical paths both in the diffusion cell and in the air before reaching the plate.

Calculation of the binary diffusion coefficient D_{12}

The solute distribution in a free diffusion experiment in which D_{12} is independent of concentration and a solution of concentration C_B diffuses upwards into another solution of concentration C_T, is obtained by solving Fick's second law, i.e. equation (1.6) which is the unidirectional form of equation (1.3), subject to the initial conditions for $t = 0$,

$$C = C_T \text{ for } z < 0,$$

$$C = C_B \text{ for } z > 0,$$

and for the boundary conditions for $t > 0$,

$$C \to C_T \text{ as } z \to -\infty,$$

$$C \to C_B \text{ as } z \to +\infty.$$

According to Dunlop *et al.* [37] the solution yields both the concentration gradient distribution

$$\frac{\partial C}{\partial z} = \frac{\Delta C}{2\sqrt{\pi D_{12}}} \exp\left(\frac{-z^2}{4D_{12}t}\right) \tag{1.77}$$

and the concentration distribution

$$C = \overline{C} + \frac{\Delta C}{2} \cdot \frac{2}{\sqrt{\pi}} \int_0^{z/2\sqrt{D_{12}t}} \exp(-z^2)dz \tag{1.78}$$

where $\Delta C = C_B - C_T$ and $\overline{C} = (C_B + C_T)/2$. In many systems the refractive index n_D is a linear function of C over the concentration range used in an experiment. From the results of Dunlop and Fugita [37, 112]

$$n_D = n_D(\overline{C}) + \left(\frac{\partial n_D}{\partial C}\right)_{T,P,\overline{C}} (C - \overline{C}) \tag{1.79}$$

Thus equations (1.77) and (1.78) may be combined with (1.79) to give

$$n_D = n_D(\overline{C}) + \frac{\Delta n_D}{2} \cdot \frac{2}{\sqrt{\pi}} \int_0^{z/2\sqrt{D_{12}t}} \exp(-z^2)dz \tag{1.80}$$

and

$$\frac{\partial n_D}{\partial z} = \left(\frac{\Delta n_D}{2\sqrt{\pi D_{12}t}}\right) \exp\left(-\frac{z^2}{4D_{12}t}\right) \tag{1.81}$$

where Δn_D is the total difference in refractive index across the initial boundary. At this point it is convenient to introduce an important experimental quantity Q defined by

$$Q_{ra} \equiv \frac{(\Delta n_D)^2}{4\pi t \left(\frac{\partial n_D}{\partial z}\right)^2_{max}} \tag{1.82}$$

which is known as the reduced height-area ratio and used to calculate binary diffusion coefficients from the experimental data obtainable with a particular optical system. Of course, for the binary systems

considered here, i.e. when D_{12} is constant and n_D is a linear function of C, we have

$$Q_{ra} = D_{12} \tag{1.83}$$

Systems in which D_{12} depends on concentration and n_D is not a linear function of C are also discussed in the literature [37, 112].

Two other experimental quantities are also required in order to calculate D_{12}. They are the maximum displacement of light predicted by ray optics C_t defined by

$$C_t \equiv (Y_i)_{max} = \acute{a}b \left(\frac{dn_D}{dz}\right)_{max} \tag{1.84}$$

and the total number of interference fringes j in the Gouy patterns

$$j = \frac{\acute{a}\,\Delta n_D}{\lambda} \tag{1.85}$$

where λ is the wavelength of the monochromatic light. The quantities j (seldom an integer) and C_t are determined by methods described in the literature [13a, 37].

Equations (1.82)-(1.85) may now be used to obtain the value of D_{12}

$$D_{12} = \frac{(j\,\lambda\,b)^2}{4\pi t\,C_t} \tag{1.86}$$

The advanced Gouy interferometric technique has permitted the determination of D_{12} with a precision of 0.1-0.2% [42, 112-115].

(b) Rayleigh Interference Method

It is also possible to devise interferometric methods which measure the differences in refractive index in corresponding planes of two similar cells, one of which contains a diffusion boundary and the other a homogeneous liquid (integral fringe methods). Thus several optical systems have been used to produce interference fringes with a shape that is pro-

portional to the refractive index distribution in a diffusion cell. Data obtained from photographs of these Rayleigh or integral fringes may be analyzed to give binary diffusion coefficients with a precision of about 0.1% [37].

Recently a group of optical methods based on the Rayleigh interference phenomenon have become important. The exact arrangement of the optical components vary to some extent, but Fig. 1.5 shows one suitable arrangement.

Fig. 1.5 - Plan view of optical system for Rayleigh fringes [13a]

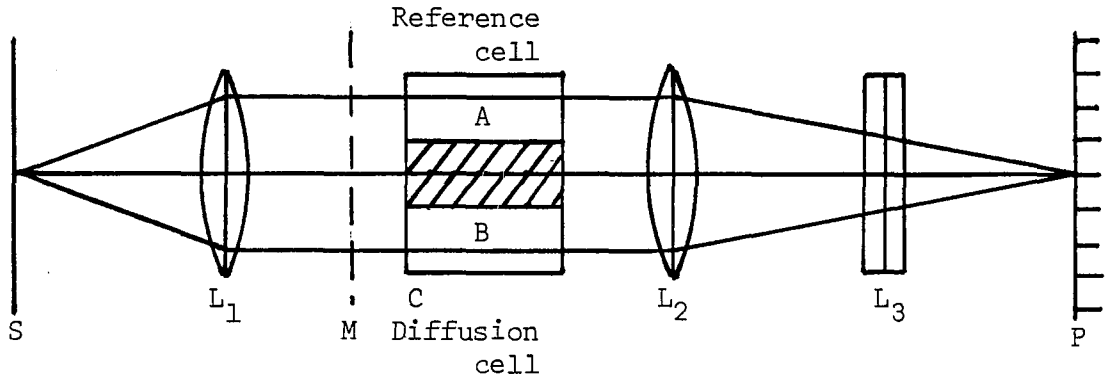

Monochromatic light from theilluminated vertical source slit S is focussed and rendered parallel by the lens L_1. This passes through a vertical double slit M and then through the double diffusion cell C (consisting of two identical cells A and B). The second convex lens L_2 images S in a horizontal plane at P while the cylindrical lens L_3 is used to focus the double cell at the photographic plate P. When cells A and B both contain liquids with the same refractive index, the charcteristics of the interference pattern at P are solely determined by the double slit. This pattern is produced by the superposition of the diffraction envelopes generated by the slits. In this way, equally-spaced interference fringes are produced within the defraction envelope. When one cell (say B) contains a refractive index gradient and the other (A) the solvent

or the reference solution, the interference fringes conjugate to B move sideways within the stationary diffraction envelope and horizontal fringe displacements (corresponding to each level in the diffusion boundary) are observed. The displacement of a given fringe is proportional to the refractive index difference between the liquids in A and B. The distance between adjacent fringes of the pattern is directly proportional to the wavelength of the light and inversely proportional to the distance d between the centers of the two slits in mask M. Also the width of the diffraction envelope w is directly proportional to the wavelength of the light, but inversely proportional to the width of the double slit. Hence the number of interference fringes in the pattern is determined by d/w.

Evaluation of binary diffusion coefficients

Here we outline a method reported by Creeth [116] for obtaining differential diffusion coefficients from photographs of Rayleigh integral fringes for binary systems in which both D_{12} and differential refractive increments are independent of concentration. In this case we can write

$$\tilde{\phi}(z^*) = \frac{2k_n j}{j} \tag{1.87}$$

where k_n is the number of any fringe maximum, j is the total number of fringes corresponding to the difference in refractive index across the diffusion boundary, and $\tilde{\phi}$ is the probability integral which has been tabulated [37]. These tables may be used to evaluate z^* from the $\tilde{\phi}(z^*)$ values computed by equation (1.87). For ideal binary systems

$$z^* = \frac{z}{2\sqrt{D_{12}t}} \tag{1.88}$$

and thus, if this equation is written for the k_n^{th} and $(j-k_n)^{th}$ fringes, the diffusion coefficient may be obtained from the relation

$$D_{12} = \frac{[(X_{j-k_n} - X_{k_n})/2z^*]^2}{4M^2t} \qquad (1.89)$$

where X_{k_n} is the comparator reading for the k_n^{th} fringe, X_{j-k_n} that of the $(j-k)_n^{th}$ fringe and M is the magnification factor. Like Gouy's interference method, the Rayleigh interference technique has been studied extensively and its modifications have led to a less complicated operation and better performance [13a, 26, 37]. For instance, similar fringes can be produced in the Mach-Zehnder interferometer (with widespread applications in various fields of engineering research; [13a, 117]) in which the integral fringe patterns coincident with the real image of the diffusion cell are produced (unlike Rayleigh's interferometer). This has many advnatges when it becomes necessary to investigate the possible causes for abnormal fringe patterns encountered in a particular experiment [26]. The Mach-Zehnder interferometer has been modified by Babb et al. [117] and employed to measure binary diffusion coefficients of organic liquids (e.g. ethanol/benzene mixtures) to within ±1% accuracy. Gosting and his associates have developed (1973) a versatile diffusiometer (Rayleigh/Gouy fringe method) with a precision of 0.03% [118]. Other important optical techniques, such as the shearing interference method (utilizing a monochromatic light beam polarized in the direction of transport, a birefringent crystal and Savart plates), have been developed and their details are well-documented in the literature [13a, 37, 119a]. It is important to record that the development of LASER light sources has made an impact on the integral fringe methods of class (b), yielding the diffusion coefficients with an uncertainty of about ±1% [120], though their use improves the sharpness of all fringe patterns. Moreover, since phase-coherent light can be obtained from both ends of a laser tube, the construction of Mach-Zehnder type interferometers can also be

greatly simplified [121, 122]. Perhaps the greatest achievement provided by laser sources has been the development of a relatively simple and cheap technique namely that of holographic interferometry which, unlike the previous methods, can be applied to very dilute solutions [26, 124, 125]. In general, it must be realized that in order to enhance the precision of the diffusivity measurements the resolution of the optical method used must be increased and the influence of the concentration dependence decreased. This is the fundamental difficulty of the limitation of the optical resolution [119].

1.4.2 Steady-State Diffusion - The Diaphragm-Cell Technique

The diaphragm-cell technique is one of the relatively simple and most widely used methods for obtaining differential diffusion coefficients for liquid systems of two and three components [37; Ch. 4, refs. 179-215]. First devised in 1928 by Northrop and Anson [126] it was developed more than twenty years later into a precision method, mainly by Stokes [127, 128], and it has proved particularly useful for the measurement of intradiffusion coefficients [129]. All the experimental details of this technique can easily be found in a number of publications [7, 13a, 127, 130]. In one of the simpler and more popular designs, a porous diaphragm (glass, stainless steel or nylon) is used in a glass cell to separate two solutions of different concentrations. Both solutions are mechanically stirred so that, if the less dense (top) solution is separated from the denser (bottom) solution by a horizontal diaphgram of essentially constant thickness, then all concentration gradients are in the diaphragm. Hence if it is assumed that the diaphragm is in a steady-state, then there would be no accumulation of material in the diaphragm during the time that transport by diffusion is taking place. Thus at a particular time the flux $\vec{J}_i$ of each component across any plane parallel to the horizontal

direction is independent of diaphragm thickness ℓ. But due to the solute conservation in the cell, each $\vec{J}_i$ is time-dependent so that in the following treatment for obtaining the differential diffusion coefficients, based essentially on the works of Barnes [131], Gordon [132] and Stokes [127], it is convenient to write $\vec{J}_i(t)$.

Let the positive direction of z coordinate be in upward direction and consider the changes in solute concentration taking place in the bottom and top cell compartments of volume V_B and V_T, respectively. In the bottom compartment

$$\frac{dC_B}{dt} = -\vec{J}(t)\,\frac{A_p}{V_B} \tag{1.90}$$

and in the top compartment

$$\frac{dC_T}{dt} = \vec{J}(t)\,\frac{A_p}{V_T} \tag{1.91}$$

where C_B and C_T are the solute concentrations in the bottom and top compartments and A_p is the effective cross-section of the pores in the diaphragm. Combining these two relations and denoting $(C_B - C_T)$ by ΔC we obtain

$$\frac{d(\Delta C)}{dt} = -\vec{J}(t)A_p\left(\frac{1}{V_B} + \frac{1}{V_T}\right) \tag{1.92}$$

It is convenient to define the average value of the differential diffusion coefficient D_{12} over the concentration range C_B to C_T by the time-dependent integral diffusion coefficient, $\overline{D}(t)$, using equation (1.13)

$$\overline{D}(t) \equiv \frac{1}{\Delta C}\int_{C_T}^{C_B} D_{12}\,dC = -\frac{1}{\Delta C}\int_{z=0}^{\ell} D_{12}\left(\frac{\partial C}{\partial z}\right)dz = \frac{\ell\vec{J}(t)}{\Delta C} \tag{1.93}$$

Thus combining this equation with (1.92)

$$\frac{d\,\ell n(\Delta C)}{dt} = \frac{-A_p}{\ell}\left(\frac{1}{V_B} + \frac{1}{V_T}\right)\overline{D}(t) = -\beta_C\overline{D}(t) \tag{1.94}$$

where β_C (typically 0.07 - 0.2; [133]) is the cell constant. Integrating

this equation over the experimental duration t yields

$$\ell n \frac{\Delta C^{o}}{\Delta C^{t}} = \beta_{c} \int_{0}^{t} \overline{D}(t)dt \qquad (1.95)$$

and

$$\overline{D} = \frac{1}{\beta_{c} t} \ell n \frac{\Delta C^{o}}{\Delta C^{t}} \qquad (1.96)$$

where $\overline{D} = (1/t)\int_{0}^{t} \overline{D}(t)dt$ is the time average of the diffusion coefficient $\overline{D}(t)$ and ΔC^{o} and ΔC^{t} are the initial and final concentration differences of the solute, each for the top and bottom compartments. For the special case that the diffusion coefficient is independent of concentration, equation (1.96) obviously gives the differential diffusion coefficient directly, If $V_B = V_T$ and $\overline{D} \neq f(C)$, then $\overline{D}$ is the differential diffusion coefficient at the average concentration of the two compartments. Equation (1.96) may also be used to obtain intradiffusion coefficients, when composition of the system is essentially identical in both sides of the diaphragm cell. If, however, $\overline{D} = f(C)$, Gordon [132] has shown that (to approximately 0.02%)

$$\overline{D} = \frac{1}{\Delta C} \int_{\overline{C}_T}^{\overline{C}_B} D_{12} dC \qquad (1.97)$$

where

$$\overline{C}_B = \frac{C_B^{o} + C_B^{t}}{2}, \quad \overline{C}_T = \frac{C_T^{o} + C_T^{t}}{2} \text{ and } \overline{\Delta C} = \overline{C}_B - \overline{C}_T \qquad (1.98)$$

In order to compute differential diffusion coefficients at particular concentrations from the integral values, an analytical expression with arbitrary coefficients is usually assumed for D_{12} [$D_{12} = f(C)$], and these coefficients determined from the measured values of $\overline{D}$, $\overline{C}_B$ and $\overline{C}_T$ by, for example, a least-squares procedure.

Since the development of the diaphragm cell by Stokes, many changes have been proposed in the materials used for the diaphragm [128, 134, 135] in the cell geometry [39, 135-138] and stirring method [39, 133], and in the

methods of analysing concentration changes [139-141]. Nevertheless, none of the changes or modifications have so far made a significant improvement either in the accuracy of the diaphragm-cell technique (∿ 1-2% within its feasibility) or in solving the major problems associated with it, such as the cell calibration and the long experimental duration (many hours or even several days) that is required for a single evaluation of the diffusion coefficient with sufficient accuracy [30, 39, 130, 133-145].

1.4.3 Restricted Diffusion - The Conductance Method

If a free diffusion experiment with a binary system is permitted to proceed until the solute concentration changes at both ends of the cell (i.e. $z = 0$ and $z = \ell$), then equation (1.78) is no longer a valid solution for Fick's second law (equation (1.6)) which must now be solved subject to the new boundary conditions

$$\left(\frac{\partial C}{\partial z}\right)_t = 0 \text{ at } z = 0, \ell \qquad (1.99)$$

According to Crank [35, 146] and Carslaw et al. [146], the required solution for the time variation of the solute concentration C at each position z in the cell is given by the Fourier series

$$C = A_o^i + \sum_{n=1}^{\infty} A_n^i \exp\left(-\frac{n^2\pi^2 D_{12}}{\ell^2} t\right) \cos\frac{n\pi z}{\ell} \qquad (1.100)$$

where A_o^i and A_n^i are constants. This relation is best utilized as first suggested by Onsager [11b] and for large values of t,

$$F(C) \equiv \ell n \left[C\left(\frac{\ell}{6}\right) - C\left(\frac{5\ell}{6}\right)\right] = \text{const.} - \frac{\pi^2 D_{12} t}{\ell^2} \qquad (1.101)$$

so that the differential diffusion coefficient D_{12} is obtained from this relation by determining the variation with time of the difference function F(C). This equation has been used by Harned et al. [147], who have constructed suitable cells, to develop a method for measuring differential

diffusion coefficients for dilute binary electrolyte solutions [13a, 37]. At large values of t the function F(C) was found to be directly proportional to the same function of the reciprocal resistance of the electrolyte solution. Thus determination of the absolute values of the electrolyte concentrations were unnecessary. Using the literature data, it was verified that for dilute KCℓ solutions negligible error is introduced by assuming the difference in concentration to be proportional to the difference in reciprocal resistance, a relationship which subsequently has been applied to many other systems. Hence in this method, the reciprocal resistances at the two fixed positions in the cell are determined as a function of time (≡ F(C) as f(t)), and the diffusion coefficient is obtained as previously described. An experiment may take over a week to yield a single diffusion coefficient with a precision of about 0.3%.

1.4.4 Taylor Dispersion Technique

This is a flow method ideally based on the study of the dispersion of a delta function pulse of a solution, injected at time zero into a stream of liquid flowing in a laminar regime through a long straight tube with a uniform circular cross-section. The technique is also referred to as the "chromatographic method" and has been described in detail elsewhere (Chapter 2 and [18, 21, 23, 24]).

In 1953, Taylor [148] first showed that the injected pulse is dispersed (as observed initially by Griffiths in 1911; [24]) by the combined action of the laminar velocity profile and molecular diffusion (essentially in radial direction). Hence after an initial transient period (t_a) the injected material is distributed normally about an origin moving at the mean velcoity (U_o) of the stream. Physically, the reasoning can

be followed in Fig. 1.6.

Fig. 1.6 - Illustration of the solute dispersion in laminar flow

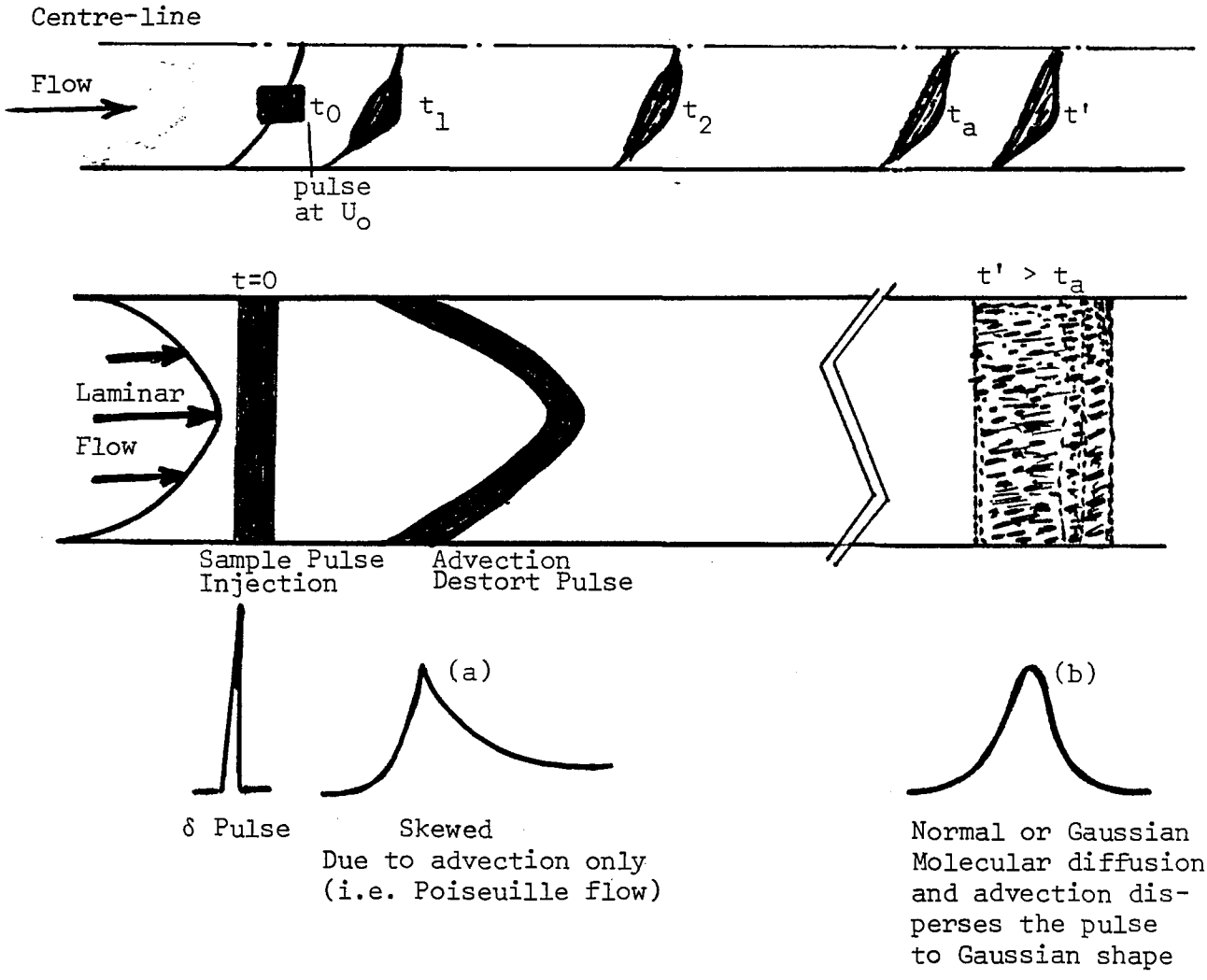

If we assume the absence of molecular difusion then the solute molecules remain in their streamline throughout their residence in the tube, and would be carried out intact at the mean velocity U_o (i.e. the solute progress would be described by $\partial C/\partial t = U_o \nabla C$). Consequently, the solute cloud is dispersed as an ever-sharpening and thinning parabola as it moves along the tube. Then the solute concentration distribution curve, obtained from a concentration detector placed at the end of the tube

(Chapters 2 and 3), will be highly skewed as shown by Fig. 1.6(a). However, this assumption of no molecular diffusivity is far from reality in liquids and cannot be verified experimentally. The experimentally observed shape of the curve is almost Gaussian as shown by Fig. 1.6(b). This is because the solute molecules at the tip of the parabola (i.e. at the centre line) diffuse towards the tube wall into a streamline of lower velocity, while those near the wall (parabola tail) diffuse towards the centre line into a higher streamline velocity. This phenomenon minimizes the stretching of the parabola through a recirculating motion of the solute cloud, as if stirred by a molecular stirrer, with a speed that depends on the molecular difusivity, flow rate and tube diameter.

If the cross-section averaged concentration of the injected material is observed as a function of time at some distance (L) downstream from the point of injection, the moelcular diffusion coefficient can be obtained from the moments of the eluted solute distribution (see Chapter 2 and [18, 21, 23, 28] for binary-, self-, and intra-diffusion coefficient measurements). It is important to note that the theoretical analysis of the dispersion process given originally by Taylor [148], and later more exactly by Aris [149], was not intended to form the foundation of a technique for diffusivity measurements, but rather to predict solute dispersion in pipelines. Consequently, the use of this theoretical description of the dispersion process without modification for the particular application of diffusivity measurements has, in the past, been justified on the basis of empirical observations. Such procedures inevitably degrade the accuracy of the experimental data obtained, and for this reason: the method has been termed one of moderate accuracy [24]. In Chapter 2 we provide a more complete treatment of the theory of the Taylor dispersion technique for diffusivity measurements in order

to obtain a set of working equations for an instrument operating on this principle. In turn, these equations permit us to assess the accuracy of the results of measurements with this method, and to show that it can be made comparable with that of other techniques. Measurements of the binary diffusion coefficients reported in Chapter 4 support this contention.

Most of the reliable diffusivity data for liquids have been obtained through the use of highly sophisticated but relatively expensive and painfully slow experimental techniques, usually involving the use of free or porous diaphragm diffusion cells. One of the difficulties encountered in a free diffusion technique is in establishing an initially sharp boundary between the pure solvent and the solution. Maintaining an undisturbed medium (minimizing vibration) throughout the experiment has also been a major problem. Although the porous diaphragm diffusion cell method minimizes most of the problems that arise in a free diffusion method, it has some drawbacks of its own. Since it requires a porous membrane, with some resistance to the transport of the solute, the technique does not yield diffusion coefficients directly and needs to be calibrated with a known standard. Other problems related to the use of the porous diaphragm such as adsorption of solute on the surface of the porous membrane, bulk streaming and semi-permeability due to improper selection of diaphragm porosity can also occur. The method cannot easily be employed as a continuous observation type and requires a relatively long period of time (two or more days) to complete a single diffusion measurement. All of these problems are reduced if diffusion experiments are conducted by the Taylor dispersion technique.

In addition to being relatively fast (a few hours at the most to complete the measurement), the Taylor dispersion technique requires only microgram

sized samples instead of the gram amounts needed by the free or steady-state diffusion methods. It is also versatile (gaseous/liquid mixtures; [23, 27, 28]) and easily adaptable to extremes of temperature and pressure (high pressure increases solubility which in turn makes the detection of the dispersion peak easier). Nevertheless, it is true that measurements with the highest precision are obtained by optical methods, but they cannot be employed over a wide temperature range because it is only near room temperature that sufficient temperature stability and uniformity can be maintained. Thus the Taylor dispersion method represents a reasonable compromise between the precision and the extent of the temperature range which can be investigated for a system.

When the technique is fully refined (see Chapters 2 and 3) it enables the measurement of diffusion coefficients with an accuracy of ±1%. It is an absolute method and hence does not involve the uncertainties associated with calibration using systems of known diffusivity, which is inherent in the porous disc (or frit [151]) and diaphragm cell methods [37]. Furthermore, when the technique is applied to gas/liquid mixtures it does not require precise solubility data as is the case in absorption methods [7, 8] and accurate chemical analysis of the liquid phase is unnecessary.

1.4.5 Other Important Methods

The methods described above are the only ones which have yielded a large body of data over a wide range of conditions with high precision. There are a number of methods which have been employed with some success to particular types of liquid systems such as polymers in liquids. However, for mixtures of simple liquids used techniques have not yet been developed to the point where accurate measurements can be made. Such techniques include the n.m.r. Spin-Echo (observing the effect of diffusion on the

decay of n.m.r. signals; precision ∿2-5%) and the Light Scattering methods ("light-beating spectroscopy", central to photon correlation spectroscopy, or "line broadening" - precision ∿1-4%) which have been described in the literature [24, 26, 152, 153].

CHAPTER 2

THE THEORY OF THE EXPERIMENTAL METHOD

2. Introduction

The need for accurate measurements of the transport properties of fluids and, in particular, the diffusion coefficient in mixtures was emphasized in the introduction of this thesis. As has been indicated, and illustrated in Chapter 1, the lack of accurate experimental data for diffusion coefficients in liquids arises from a combination of the inherent slowness of the diffusion process and the failure to develop reliable theories of some techniques for their measurement [7-9,11,18-20,30]. The Taylor dispersion technique [Ch. 1, Section 1.4.4] employed for the measurements described in this thesis offers the opportunity for rapid diffusion coefficient measurements which may also be made accurately, provided a suitable theory of the method is available. The present chapter is dedicated to providing this theory in the form of a set of working equations combined with a full set of corrections.

2.1 The Principle of the Experimental Method

We consider first the simplest mathematical model of an instrument to measure liquid phase diffusivities using Taylor dispersion. This mathematical model refers to an idealized experiment, which cannot be realized in practice. Nevertheless, it will be shown that a practical instrument can be designed such that its departures from the ideal are small and so that they may be evaluated with the aid of a proper analysis.

Figure 2.1 shows the ideal experimental arrangement and defines the geometry of the apparatus. For generality, we consider a homogeneous liquid mixture of species 1 and 2 flowing in laminar flow through an

infinitely long, isothermal, straight tube of uniform, circular cross-section, radius R_o, with impermeable walls. We denote the molar concentrations of the species in the flowing mixture by C_{1f} and C_{2f} respectively. The mean velocity of the liquid mixture in the tube is denoted by U_o. At time t = 0, a sample of liquid mixture of the same two components but of a different composition is introduced into the tube by injection as a "δ pulse" at z = 0.

Fig. 2.1 - The ideal Taylor dispersion experiment δ pulse dispersed by the combined effects of the laminar velocity profile and molecular diffusion

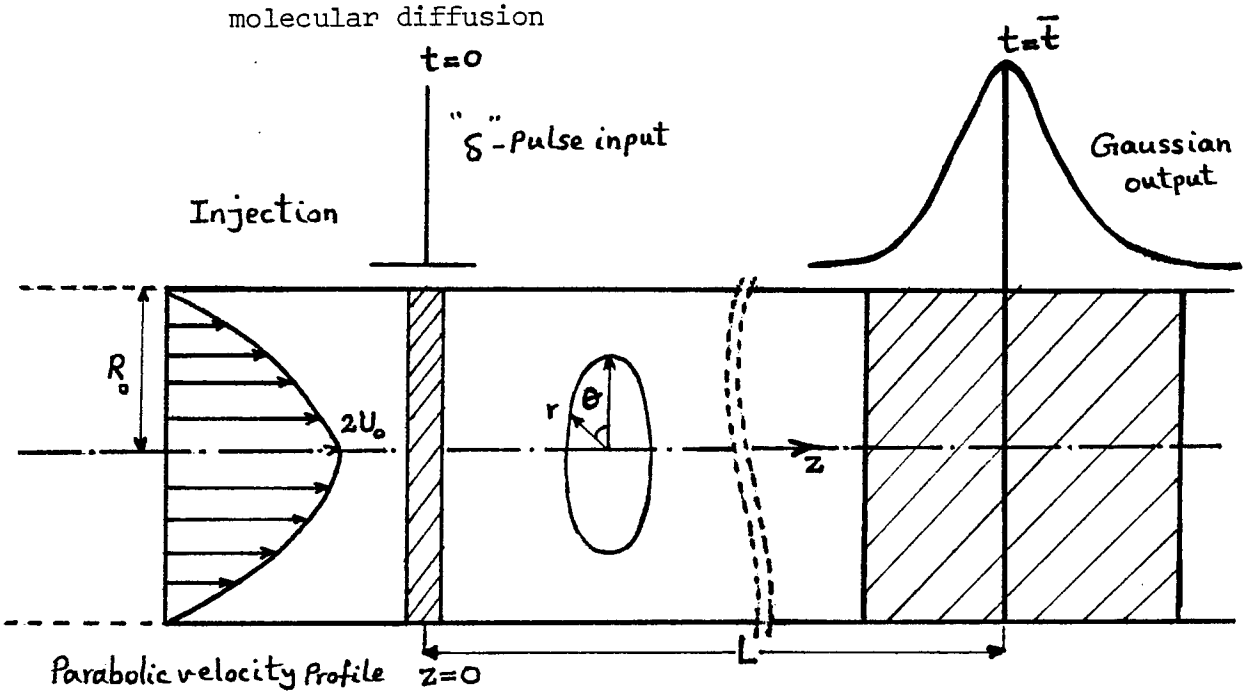

The molar concentrations of the two components in the sample are C_{1i} and C_{2i} respectively and its mass density is supposed to be the same as that of the flowing stream. The sample fills the cross-section of the tube at z = 0 completely, it is of uniform composition over this cross-section and is supposed to extend infinitesimally in the axial direction. Therefore the only perturbation of the flowing stream arises from the change in the concentration of component 1 at z = 0 which may be represented by a delta-function, δ(z), which is normalized so that

$$\pi R_o^2 \int_{-\infty}^{\infty} \delta(z)[C_{1i} - C_{1f}]dz = N_1 \qquad (2.1)$$

where $\delta(z) = 0$ for $z \neq 0$, and N_1 represents the number of moles of component 1 in excess of those present in the same volume of the flowing stream.

The concentration gradient established by the introduction of this sample, together with the action of the parabolic velocity profile of laminar flow results in dispersion of the pulse. The process of molecular diffusion involved is clearly that of mutual or interdiffusion and, in the present analysis, the appropriate diffusion coefficient, D_{12}, is supposed to be independent of the composition of the liquid mixture.

If we denote the perturbation to the flowing stream composition caused by the pulse by $\Delta C_1(r, \theta, z, t)$, then the differential equation for ΔC_1, describing the dispersion, is

$$\frac{1}{D_{12}} \frac{\partial(\Delta C_1)}{\partial t} = \nabla^2(\Delta C_1) - \frac{2U_o}{D_{12}} \left[1 - 2\left(\frac{r}{R_o}\right)^2\right] \frac{\partial(\Delta C_1)}{\partial z} \qquad (2.2)$$

and the conditions for its solutions are, at $t = 0$,

$$\Delta C_1(r, \theta, 0, 0) = \delta(z)(C_{1i} - C_{1f}) \quad , \qquad (2.3)$$

$$\delta(z) = 0 \text{ for } z = 0$$

and

$$\frac{\partial(\Delta C_1)}{\partial r} = 0 \text{ at } r = R_o \text{ for all } t \qquad (2.4)$$

together with sufficient conditions on ΔC_1 for $z = \pm\infty$.

In his original analysis, Taylor [148] introduced an approximation concerning the relative magnitudes of axial and radial dispersion so as to render the solution of equation (2.2) practicable. But in this work we prefer to follow the analysis of Aris [149], and to seek solutions for various spatial moments of the concentration distribution, since these turn out to be sufficient for the analysis of the experiment.

We define the p^{th} spatial moment of the concentration distribution at a radial position r about an origin moving with the mean velocity of the flow by the equation

$$c_p(r, \theta, t) = R_o^{p+1} \int_{-\infty}^{\infty} \zeta^p \, \Delta C_1(\zeta, r, \theta, t) d\zeta \tag{2.5}$$

with

$$\zeta = (z - U_o t)/R_o \tag{2.6}$$

denoting a dimensionless axial coordinate with respect to the moving origin. The moments of the distribution, averaged over a cross-section of the tube, are then defined by the equation

$$m_p = \frac{1}{\pi R_o^2} \int_0^{2\pi} \int_0^{R_o} r c_p(r, \theta, t) dr \, d\theta \tag{2.7}$$

and the normalized moments by

$$\mu_p^* = \frac{m_p}{m_o} \tag{2.8}$$

Following the work of Aris [149] two sets of differential equations for c_p and m_p can then be derived from equation (2.1) which read

$$\frac{1}{D_{12}} \frac{\partial c_p}{\partial t} = \frac{1}{r} \frac{\partial}{\partial r} \left(r \frac{\partial c_p}{\partial r} \right) + \frac{1}{r^2} \frac{\partial^2 c_p}{\partial \theta^2} + p(p-1) c_{p-2} + \frac{U_o}{D_{12}} p \left(1 - 2\left(\frac{r}{R_o}\right)^2 \right) c_{p-1} \tag{2.9}$$

$$\text{and} \quad \frac{1}{D_{12}} \frac{dm_p}{dt} = p(p-1) m_{p-2} + \frac{pU_o}{\pi R_o^2 D_{12}} \int_0^{2\pi} d\theta \int_0^{R_o} r \left(1 - 2\left(\frac{r}{R_o}\right)^2 \right) c_{p-1} dr \tag{2.10}$$

For the conditions of this analysis, sufficient conditions on the beahviour of ΔC_1 at $\zeta = \pm\infty$ are ensured by the fact that the sample introduced occupies a finite volume of the tube.

The solutions of equations (2.9) and (2.10) for the present boundary conditions have been given by Aris [149]. For the zeroth moment averaged over a cross-section, i.e. p = 0 in equation (2.10), we obtain

$$m_o = \text{constant or } \mu_o^* = 1 \tag{2.11}$$

which merely states that the total quantity of the injection sample is constant. Furthermore,

$$m_1 = 0 = \mu_1^* \tag{2.12}$$

which expresses the fact that the mean of the distribution, averaged over a cross-section, travels in the tube with the mean velocity of the flow. The solution of equation (2.9) for period 2π in θ and with the boundary conditions

$$c_p(r, \theta, 0) = c_{p0}(r, \theta) \tag{2.13}$$

$$\frac{\partial c_p}{\partial r} = 0 \text{ at } r = R_o \tag{2.14}$$

gives the mean of the distribution, as a function of radial position in the tube as

$$c_1 = -\tfrac{1}{4}\frac{U_o R_o^2}{D_{12}}\left\{\frac{1}{3} + \left(\frac{r}{R_o}\right)^2 - \tfrac{1}{2}\left(\frac{r}{R_o}\right)^4\right\} + \frac{8U_o R_o^2}{D_{12}} \sum_{n=1}^{\infty} \alpha_{on}^{-4} \frac{J_o(\alpha_{on}\cdot\frac{r}{R_o})}{J_o(\alpha_{on})} \exp\left[-\frac{D_{12}\alpha_{on}^2 t}{R_o^2}\right] \tag{2.15}$$

with α_{on} representing the n^{th} zero of $dJ_o(z)/dz$, where J_o is the zeroth-order Bessel function of the first kind. It is useful to record that the original expressions for c_1 and m_1 given by Aris were found to be incorrect in the sign as indicated by Tillman [149*]

The cross-section averaaged second moment, μ_2^*, may also be derived, and is given by the expression

$$\mu_2^* = 2\left[D_{12} + \frac{R_o^2 U_o^2}{48 D_{12}}\right]t - 128\left(\frac{R_o^4 U_o^4}{D_{12}}\right)\sum_{n=1}^{\infty} \alpha_{on}^{-8}\left[1 - \exp\left(-\left(\frac{D_{12}\alpha_{on}^2}{R_o^2}\right)t\right)\right] \tag{2.16}$$

It has been shown by Aris that the longitudinal distribution of concentration approaches that of a normal distribution as $t \to \infty$. The expression for the skewness of the cross-section averaged distribution is

$$Sk = \frac{(\mu_3^*)^2}{(\mu_2^*)^3} \tag{2.17}$$

which is given asymptotically by the relation

$$Sk = \frac{49U_o^6R_o^8}{2^{20}D_{12}^7\left(1 + \frac{U_o^2 R_o^2}{48D_{12}^2}\right)^3 t} \tag{2.18}$$

indicating that the approach to normality occurs as t^{-1}.

Equations (2.12) and (2.16) yield the fundamental working equations for the analysis of the ideal experiment. It is clear that the exponential transient term in equation (2.16) can be made to decay arbitrarily rapidly by the choice of suitable conditions. Thus for

$$\frac{D_{12}}{R_o^2} t > 0.6 \tag{2.19}$$

the transient term contributes less than 0.01% to the second term of equation (2.16). Hence if condition (2.19) is satisfied, equation (2.16) may be written as

$$\mu_2^* = 2\left(D_{12} + \frac{R_o^2U_o^2}{48D_{12}}\right)t - \frac{128\ R_o^4U_o^2}{D_{12}^2}\left[\frac{1}{(3.8317)^8} + \frac{1}{(7.0156)^8} + \ldots\right] \tag{2.20}$$

Because the mean velocity of the flow can be chosen independently of the time t, we note that if

$$U_o > 700\left(\frac{D_{12}}{R_o}\right) \tag{2.21}$$

then equation (2.20) reduces to the form

$$\mu_2^* = \left(\frac{R_o^2U_o^2}{24D_{12}}\right)t - \frac{128K_cR_o^4U_o^2}{D_{12}^2} \tag{2.22}$$

with an associated error of less than 0.01% which we regard as negligible. In this equation, we have written

$$K_c = \sum_{n=2}^{\infty} \alpha_{on}^{-8} = 2.1701 \ldots \times 10^{-5} \tag{2.23}$$

for convenience. Condition (2.21) is easily satisfied for measurements in liquids while maintaining the fluid flow in the laminar regime.

Equation (2.22) could evidently form the fundamental working equation for the ideal experiment, since the binary diffusion coefficient D_{12} could be derived from experimental measurements of the second moment, μ_2^*, with the aid of it. For later use, it is more convenient to employ a limiting form of this equation. Since the duration, t, of the measurement may be chosen arbitrarily, the time-independent term in equation (2.22) may be made negligible (less than 0.01%) by choosing

$$\left(\frac{D_{12}}{R_o^2}\right) t > 700 \tag{2.24}$$

This selection automatically ensures that the transient term in equation (2.16) is even smaller than that corresponding to condition (2.19). In this case, equation (2.22) reduces to the very simple form

$$\mu_2^* = \left(\frac{R_o^2 U_o^2}{24 D_{12}}\right) t = \mu_{2s}^* \tag{2.25}$$

where the subcript s implies that conditions (2.21) and (2.24) are satisfied in the experiment. Furthermore, by virtue of equation (2.12), the fluid mean velocity U_o may be determined from the first moment of the distribution with respect to the fixed origin z = 0. Denoting the first moment by $\bar{z}$, it follows that

$$U_o = \frac{\bar{z}}{t} \tag{2.26}$$

so that the final working equation for the ideal diffusion experiment becomes

$$D_{12} = \frac{R_o^2 - 2\bar{z}^2}{24 \mu_{2s}^* t} \tag{2.27}$$

Hence a diffusion coefficient determination may be performed by measuring just the first and second spatial moments of the cross-section averaged concentration distribution of the injected sample, after flowing for a time t through a tube of known radius.

If condition (2.24) is not satisfied, the second moment required in equation (2.27) can still be derived from the measured moment, μ_2^*, by application of the correction $\delta\mu_2^*$ in the form

$$\mu_{2s}^* = \mu_2^* + \delta\mu_2^* \tag{2.28}$$

where

$$\delta\mu_2^* = \frac{128 K R_o^4 U_o^2}{D_{12}^2} \tag{2.29}$$

Provided that

$$\left(\frac{D_{12}}{R_o^2}\right) t > 20 \tag{2.30}$$

the correction $\delta\mu_2^*$ amounts to no more than 0.3% (0.06% under selected conditions for the measurements of this work) of μ_2^*, and so may be calculated with sufficient accuracy using an estimate for D_{12}.

Finally, in this section, we record for future use that if conditions (2.21) and (2.22) are satisfied, then the absolute skewness of the spatial distribution is less than 5×10^{-8}, so that for all practical purposes the distribution may be regarded as normal. Furthermore, it follows that the Taylor dispersion process under the conditions specified may be equally well-described by the one-dimensional differential equation [148, 149].

$$E \frac{\partial^2(\Delta C_{1m})}{\partial z^2} - U_o \frac{\partial(\Delta C_{1m})}{\partial z} = \frac{\partial(\Delta C_{1m})}{\partial t} \tag{2.31}$$

where E is an effective diffusivity given by

$$E = \frac{R_o^2 U_o^2}{48 D_{12}} \tag{2.32}$$

and ΔC_{1m} is the concentration perturbation averaged over a cross-section. This one-dimensional representation is equivalent to the process of plug flow plus axial diffusion with a diffusivity E. The moments of the solution of equation (2.31) are identical to those for the solution of the full diffusion equation under the above conditions.

2.2 Practical Considerations

The ideal experimental method outlined in the previous section is not practicable for measurements of diffusion coefficients. Furthermore, even if it were, it would not be possible to construct an apparatus which excactly conforms with the ideal. In order to perform such measurements using the same principle, it is therefore necessary to make changes to the experimental method and to examine the ways in which a practical instrument departs from the ideal. Such departures may be classified under four headings:

1. Concentration Distribution Determination.
2. Sample Introduction.
3. Diffusion Tube Geometry.
4. Concentration Dependent Fluid Properties.

We shall examine each of these in turn in the following sections and, where it is appropriate, express the effect of the departure from the ideal instrument as a small correction to the ideal working equations. In some cases, it will be possible to render the corrections negligible by proper design. In other cases, the correction can only be made small by design, but then it can be estimated with sufficient accuracy to make the contribution to the overall uncertainty in the diffusion coefficient measurements negligible.

In the following sections of this chapter, we examine the consequences of the above considerations for the design of an apparatus and the working equations for the analysis of the experimental data. In this examination, we shall presume that all the corrections due to the non-ideal model are small, so that they may all be treated as first-order perturbations. In this case, we may further assume that the interaction between any two or more of these first-order effects is negligible so that

each perturbation can be treated independently. The conditions under which such assumptions are valid will, of course, emerge from the analysis and form the basis of the design criteria.

2.3 Concentration Distribution Determination

2.3.1 Temporal moments

It is much more convenient experimentally to observe the concentration distribution at a particular cross-section in the tube as a function of time, rather than to observe it at one instant of time as a function of axial position. Therefore we consider the diffusion process described earlier in the ideal apparatus again, but now we suppose that we can determine the cross-section averaged perturbation of the concentration of component 1, denoted by ΔC_{1m}, at an axial position $z = L$, in an infinitesimally small length of the diffusion tube. Then, in order to relate the temporal moments of the distribution observed in this way to the spatial moments of the previous section, we use the result derived there that the spatial distribution is essentially normal. For such distribution we can write [148]

$$\Delta C_{1m} = \frac{N_1}{(2\pi^3 \mu_2^*)^{\frac{1}{2}} R_o^2} \exp^{-\left[\frac{(z-U_o t)^2}{2\mu_2^*}\right]} \qquad (2.33)$$

For an observation carried out in the cross-section at the axial position $z = L$, we define

$$\tau = \frac{U_o t}{L}$$

and

$$\zeta = \frac{\mu_2^*}{2U_o L t}$$

Equation (2.33) can then be rewritten as

$$\Delta C_{Im} = \frac{N_1}{2\pi R_o^2 L} (\pi \zeta \tau)^{-\frac{1}{2}} \exp^{-\left[\frac{(1-\tau)^2}{4 \zeta \tau}\right]} \qquad (2.34)$$

The normalized temporal moments of this distribution, for a measurement carried out in the idealized apparatus, $(\mu_p)_{id}$, are then defined by the equation

$$(\mu_p)_{id} = \frac{(\frac{L}{U_o})^p \int_0^\infty \tau^p \, \Delta C_{lm} \, d\tau}{\int_0^\infty \Delta C_{lm} \, d\tau} \tag{2.35}$$

In general, the quantity ζ is time-dependent, due to the definition of μ_2^* in equation (2.22), and the analytic evaluation of equation (2.35) is impossible. Consequently, we seek approximate solutions for the temporal moments. Because the time-dependent part of ζ is generally small (less than 0.6% if condition (2.30) is satisfied), these approximations will prove sufficiently accurate.

2.3.2 Zeroth-order approximation

If both conditions (2.21) and (2.22) are satisfied, then with negligible error,

$$\zeta = \zeta_o = \frac{\mu_{2s}^*}{2U_oLt} = \frac{R_o^2U_o}{48LD_{12}} \tag{2.36}$$

which is time-independent. The evaluation of the first raw temporal moment, $(\mu_1')_{id} \equiv \bar{t}_{id}$, leads to the result of Pratt and Wakeham [23]

$$\bar{t}_{id} = \frac{L}{U_o}(1 + 2\zeta_o) \tag{2.37}$$

Under the same conditions, the second raw temporal moment, $(\mu_2')_{id}$, has been evaluated by Levenspiel and Smith [155] as

$$(\mu_2')_{id} = \left(\frac{L}{U_o}\right)^2 (1 + 6\zeta_o + 12\zeta_o^2) \tag{2.38}$$

so that the temporal variance of the distribution, denoted by σ_{id}^2, may be written

$$\sigma_{id}^2 = (\mu_2')_{id} - \left[(\mu_1')_{id}\right]^2 = \left(\frac{L}{U_o}\right)^2 (8\zeta_o^2 + 2\zeta_o) \tag{2.39a}$$

$$= \left[\frac{8\zeta_o^2 + 2\zeta_o}{(1 + 2\zeta_o)^2}\right](\bar{t}_{id})^2 \qquad (2.39b)$$

Here the subscript (id) denotes that the various moments refer to measurements in the ideal diffusion apparatus of the previous section. Equation (2.39) can be solved exactly for ζ_o to yield

$$\zeta_o = \frac{2\sigma_{id}^2 - \bar{t}_{id}^2 + \left[\bar{t}_{id}^4 + 4\bar{t}_{id}^2\sigma_{id}^2\right]^{\frac{1}{2}}}{(8\bar{t}_{id}^2 - 4\sigma_{id}^2)} \qquad (2.40)$$

Finally, from equations (2.37) and (2.25), we note that

$$D_{12} = \left(\frac{1 + 2\zeta_o}{\zeta_o}\right)\frac{R_o^2}{48\bar{t}_{id}} \qquad (2.41)$$

so that using equation (2.40) in (2.41), we obtain the final working equation for the experiment in the form

$$D_{12} = \frac{R_o^2}{24\bar{t}_{id}}\left\{\frac{\left[1 + \frac{4\sigma_{id}^2}{\bar{t}_{id}^2}\right]^{\frac{1}{2}} + 3}{\left[\left(1 + \frac{4\sigma_{id}^2}{\bar{t}_{id}^2}\right)^{\frac{1}{2}} + \frac{2\sigma_{id}^2}{\bar{t}_{id}^2} - 1\right]}\right\} \qquad (2.42)$$

With this equation the diffusion coefficient can be determined from measurements of the first two temporal moments of the concentration distribution at a particular cross-section of the tube.

2.3.3 First-order approximation

If condition (2.21) is satisfied, but the measurement time, t, is such that condition (2.24) is not satisfied, it is still possible to obtain an analytic working equation provided that condition (2.30) on the diffusion time is met. In this case we can write

$$\zeta = \zeta_1 = \zeta_o + \delta\zeta$$

where

$$\delta\zeta = \frac{-64KR_c^4U_o}{D_{12}^2 Lt}$$

The major contribution to the integrals in equation (2.35) arises from near $\tau = 1$. Thus we may employ a quasi-steady state approximation to evaluate the small correction $\delta\zeta$, i.e. we evaluate $\delta\zeta$ at $t = \frac{L}{U_o}$,

$$\delta\zeta = -\frac{64 K R_c^4 U_o^2}{D_{12}^2 L^2}$$

and so $\delta\zeta$ within this approximation can be treated as time-independent. If now the procedures of the zeroth-order analysis are carried through again, using ζ_1 in place of ζ_o, the final working equation becomes

$$D_{12} = \frac{R_o^2}{24\bar{t}_{id}} \left\{ \frac{\left[1 + \frac{4\sigma_{id}^2}{\bar{t}_{id}^2}\right]^{\frac{1}{2}} + 3}{\left[1 + \frac{4\sigma_{id}^2}{\bar{t}_{id}^2}\right]^{\frac{1}{2}} + \frac{2\sigma_{id}^2}{\bar{t}_{id}^2} - 1} \right\} \left[\tfrac{1}{2} + \tfrac{1}{2}(1 - \delta_a)^{\frac{1}{2}}\right] \quad (2.43)$$

where

$$\delta_a = (768)^2 K_c \zeta_o$$

Again, the working equation relates the diffusion coefficient to the first two temporal moments of the distribution observed in the diffusion tube. Provided that condition (2.30) is satisfied, the term δ_a contributes at most 0.6% to the measured diffusion coefficient, so that the foregoing analysis for its estimation is sufficiently accurate. Hence equation (2.43) constitutes the fundamental working equation for the evaluation of diffusion coefficients from temporal moment measurements in this work. Finally, we note that if $D_{12}t/R_o^2 \geq 20$, (c.f. $D_{12}t/R_o^2 \geq 50/(3.8)^2$ an empirical result obtained by Pratt and Wakeham [18] in order to satisfy Taylor/Aris criterion), so that condition (2.30) is satisfied, then

$$\zeta_o \leq 10^{-3} \quad (2.44)$$

and hence from equations (2.25) and (2.38) we can write (with an error of no more than 0.2%)

$$\zeta_o = \frac{R_o^2}{48 D_{12} t} \tag{2.45}$$

This equation and condition (2.44) will only be used as a design criterion and constraint later on. For the condition $\zeta_o < 10^{-3}$, equations (2.39) and (2.41) may be linearized with respect to ζ_o as it has been done by other workers [23]. In this case, the approximate working equation (with an error of less than 1%) which is found useful later, becomes

$$D_{12} = \frac{R_o^2 \bar{t}_{id}}{24 \sigma_{id}^2} \tag{2.46}$$

2.3.4 The concentration monitor

The preceding analysis were based upon the assumption that the average concentration in a cross-section of the diffusion tube could be determined at a particular axial position. In practice, such a measurement is not possible and some average concentration in a finite length of the tube must be determiend instead. There are two ways in which this may be accomplished, both of them being considered in the following sections.

2.3.5 A section of the diffusion tube

Figure 2.2 represents a schematic diagram of the concentration monitor as a section of the diffusion tube. In this concentration monitor, we assume that it is possible to determine the average perturbation to the concentration of the flowing stream in a small length δL of the tube itself, beginning at $z = L$. We denote this average concentration perturbation by $\overline{\Delta C_1}$, defined by the equation

$$\overline{\Delta C_1}(L, t) = \frac{1}{\pi R_o^2 \delta L} \int_L^{L+\delta L} \int_0^{R_o} \int_0^{2\pi} \Delta C_1(r, \theta, z, t) d\theta \; r \, dr \, dz \tag{2.47}$$

A composition monitor of this type can be used when one of the components of the perturbing pulse is radioactive [28,150]. The detector would then consist of a test section of the diffusion tube within the field of view of a suitable activity monitor which would define the length δL observed.

Fig. 2.2 - The concentration monitor as a finite length of the diffusion tube

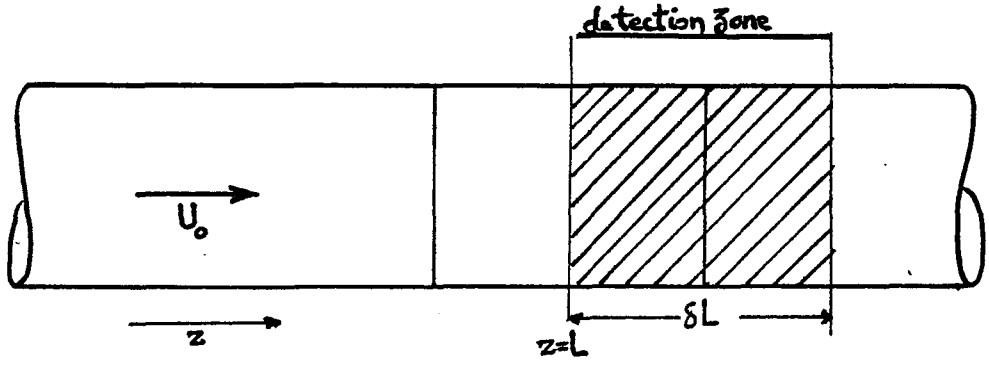

This might be employed for measurements of self-diffusion coefficients of liquids. Clearly, because of the non-zero volume of the detector the temporal moments of $\overline{\Delta C_1}$ will not be identical to those of ΔC_{1m}. Introducing again the cross-section averaged composition perturbation ΔC_{1m}, equation (2.47) can be written in the form

$$\overline{\Delta C_1}\,(L,\,t) \;=\; \frac{1}{\delta L}\int_{L}^{L+\delta L} \Delta C_{1m}\, dz$$

Assuming that all of our previous conditions are satisfied in the experiment, then we can use equation (2.33) for ΔC_{1m} so that $\overline{\Delta C_1}(L,\,t)$ becomes

$$\Delta C_1 \;=\; \frac{N_1}{(2\pi^3 \mu^*_{2s})^{\frac{1}{2}} R_o^2 \delta L}\int_{L}^{L+\delta L} \exp\left[-\frac{(z-U_o t)^2}{2\mu^*_{2s}}\right] dz \qquad (2.48)$$

setting $\mu^*_2 = \mu^*_{2s}$ for the present purposes. Evaluating the integral in equation (2.48), we obtain

$$\overline{\Delta C_1} \;=\; \frac{N_1}{2\pi R_o^2 \delta L}\left\{\operatorname{erf}\left[\frac{(1-\tau)}{(4\zeta_o\tau)^{\frac{1}{2}}} + \frac{\delta L/L}{(4\zeta_o\tau)^{\frac{1}{2}}}\right] - \operatorname{erf}\left[\frac{(1-\tau)}{(4\zeta_o\tau)^{\frac{1}{2}}}\right]\right\} \qquad (2.49)$$

with τ and ζ_o being defined earlier in Section 2.3.1.

According to the approach outlined earlier in Section 2.2, we can now suppose that $\delta L/L$ is small; in particular that

$$\frac{\delta L}{L} << (4\zeta_o\tau)^{\frac{1}{2}}$$

In this case the error function in equation (2.49) may be expanded by a Taylor series in the form

$$\overline{\Delta C_1}(L, t) = \frac{N_1}{2\pi R_o^2 L}(\pi\zeta_o\tau)^{-\frac{1}{2}}\exp\left[-\frac{(1-\tau)^2}{4\zeta_o\tau}\right]\left\{1 - \frac{(1-\tau)}{4\zeta_o\tau}\left(\frac{\delta L}{L}\right) + \frac{1}{3(4\zeta_o\tau)}\left[\frac{2(1-\tau)^2}{(4\zeta_o\tau)} - 1\right]\left(\frac{\delta L}{L}\right)^2 + \ldots\right\} \quad (2.50)$$

This result allows the computation of the normalized temporal moments of the distribution $\overline{\Delta C_1}(L, t)$, defined in the standard manner. After some laborious algebra, it can be shown that the first moment is given by

$$\bar{t} = \frac{L}{U_o}\left(1 + 2\zeta_o + \frac{\delta L}{L}\right) = \bar{t}_{expt} = \bar{t}_{id} + \frac{L}{U_o}\left(\frac{\delta L}{L}\right) \quad (2.51)$$

and the variance by

$$\sigma^2 = \left(\frac{L}{U_o}\right)^2\left[2\zeta_o + 8\zeta_o^2 + \zeta_o\left(\frac{\delta L}{L}\right) + \frac{1}{12}\left(\frac{\delta L}{L}\right)^2\right] = \sigma_{id}^2 + \left(\frac{L}{U_o}\right)^2\left[\zeta_o\left(\frac{\delta L}{L}\right) + \frac{1}{12}\left(\frac{\delta L}{L}\right)^2\right] \quad (2.52)$$

correct to the order of $\left(\frac{\delta L}{L}\right)^2$. We use suffix (expt) to denote the measured or experimental moments.

Comparison of equations (2.51) and (2.52) with those for the ideal moments, equations (2.37) and (2.39), reveals the form of a correction to be applied to each measured moment to recover the ideal moments. Thus

$$\bar{t}_{id} = \bar{t}_{expt} - \delta\bar{t}_o \quad (2.53)$$

and

$$\sigma_{id}^2 = \sigma_{expt}^2 - \delta\sigma_o^2 \quad (2.54)$$

Here

$$\delta\bar{t}_o = \frac{\delta L}{2U_o} \quad (2.55)$$

and

$$\delta\sigma_o^2 = \delta L\left[\frac{R_o^2}{48D_{12}U_o} + \frac{\delta L}{12U_o^2}\right] \quad (2.56)$$

Therefore both corrections may be calculated from a knowledge of the mean velocity of the flow and an estimate of the diffusion coefficient. For the purpose of design, we may assume that $U_o = L/\bar{t}_{id}$ and $D_{12}t/R_o^2 \geq 20$ (i.e. $\zeta_o \leq 10^{-3}$). With these approximations we find

$$\frac{\delta\bar{t}_o}{\bar{t}_{id}} \leq \frac{\delta L}{2L}$$

and

$$\frac{\delta\sigma_o^2}{\sigma_{id}^2} \leq \frac{\delta L}{L}\left[\frac{1}{2} + 40\,\frac{\delta L}{L}\right]$$

so that for $\delta L/L \leq 0.01$, the corrections to either moment become $\leq 0.9\%$ indicating that the method proposed for their estimation must be satisfactory.

2.3.6 A small volume at the tube exit

The most commonly used concentration monitor consists of a small sampling volume V_d, placed at the exit of the diffusion tube. The concentration of the effluent from the tube in this volume is usually measured with a refractive index detector [18,19,23,27,30] an instrument which has been employed in the measurements reported in this thesis. The differences between the moments observed with this type of detector and the ideal ones are difficult to analyse because the flow pattern and geometry of the sample volume are not well known. Consequently, we examine two extreme cases to set bounds on the effect and to provide guidance for the design of an instrument.

First we consider that within the sample volume the dispersion process proceeds unaltered and that the refractive index detector determines the average concentration of the dispersing material within it. In this case, the analysis is identical to that given above, and, in terms of the detector volume, the corrections to the moments are

$$\delta\bar{t}_{1a} = \frac{L}{U_o}\left(\frac{V_d}{2\pi R_o^2 L}\right) \tag{2.57}$$

and

$$\delta\sigma_{1a}^2 = \left(\frac{L}{U_o}\right)^2\left[\zeta_o\left(\frac{V_d}{\pi R_o^2 L}\right) + \frac{1}{12}\left(\frac{V_d}{\pi R_o^2 L}\right)^2\right] \tag{2.58}$$

An alternative model of the detector is one that behaves as a perfectly mixed volume in which the composition is uniform. This model, which is probably closer to reality, is illustrated schematically in Fig. 2.3 below.

Fig. 2.3 - The concentration monitor as a perfectly mixed volume, V_d, at the exit of the diffusion tube

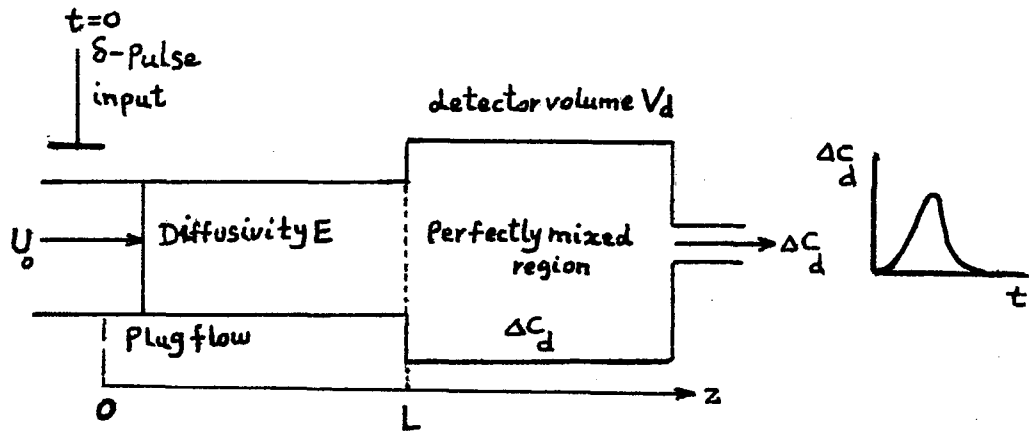

The presence of the perfectly mixed region implies that there exists now a boundary condition for the diffusion equation at the exit from the diffusion tube, and not at infinity, as described previously.

In order to analyse this problem, we first make use of the result given earlier. That is the description of Taylor's dispersion process, for the present condition $D_{12}t/R_o^2 \geq 20$, by means of the one-dimensional diffusion equation (2.31) to a very good approximation. For the model of the diffusion tube and detector shown in Fig. 2.3 above, the boundary conditions for the solution of this equation are:

at $z = 0$

$$\Delta C_{1m} = \delta(z)(C_{1i} - C_{1f}) \tag{2.59}$$

and at $z = L$

$$V_d \frac{\partial(\Delta C_d)}{\partial t} = -\pi R_o^2 E\left(\frac{\partial \Delta C_{1m}}{\partial z}\right)$$

where ΔC_d is the perturbation to the concentration in the detector volume. The second boundary condition implies that the concentration at the exit from the diffusion tube is identical with that in the entire detector volume.

The transfer function for this process has been given by Yano and Aratani [154] and reads

$$H(s) = \frac{2\beta \exp\left[(1/2\zeta_o)(1-\beta)\right]}{\left(\frac{2\alpha Ls}{U_o}\right)\left(1-\exp^{-}(\beta/\zeta_o)\right) + (1+\beta) - (1-\beta)\exp^{-}(\beta/\zeta_o)} \qquad (2.60)$$

where $$\beta = \left[1 + \frac{4\zeta_o Ls}{U_o}\right]^{\frac{1}{2}}$$

and $$\alpha = \frac{V_d}{\pi R_o^2 L} = \frac{\text{Detector Volume}}{\text{Diffusion Tube Volume, } V_t}$$

In addition, s is the Laplace transform variable conjugate to the time t. The transfer function H(s) can be used to derive the temporal moments of the concentration perturbation ΔC_d for a δ-pulse input by means of the standard relation [155, 156]

$$\mu_p' = \lim_{s\to 0} (-1)^p \frac{d^p H(s)}{ds^p} \qquad (2.61)$$

For the first moment we find

$$\mu_1' = \bar{t} = \frac{L}{U_o}\left\{1 - \zeta_o\left[1 - e^{-1/\zeta_o}\right] + \alpha\left(1 - e^{-1/\zeta_o}\right)\right\} = \bar{t}_{expt} \qquad (2.62)$$

and for the variance

$$\sigma^2 = \mu_2' - (\mu_1')^2 = \left(\frac{L}{U_o}\right)^2\left\{2\zeta_o(1+2e^{-1/\zeta_o}) + \zeta_o^2(-5+4e^{-1/\zeta_o}+e^{-2/\zeta_o}) + \left(\frac{V_d}{\pi R_o^2 L}\right)^2\left[1-2e^{-1/\zeta_o}+2e^{-2/\zeta_o}\right] + \frac{V_d}{\pi R_o^2 L}\left[2\zeta_o(1-e^{-2/\zeta_o})-4e^{-1/\zeta_o}\right]\right\} = \sigma^2_{expt} \qquad (2.63)$$

The choice of $\zeta_o \leq 10^{-3}$ for diffusion coefficient measurements implies

that the exponential terms in equations (2.62) and (2.63) are entirely negligible, and we obtain simply

$$\bar{t}_{expt} = \frac{L}{U_o}\left[1 - \zeta_o + \frac{V_d}{\pi R_o^2 L}\right] = \bar{t}_{id} + \frac{L}{U_o}\left[\frac{V_d}{\pi R_o^2 L} - 3\zeta_o\right] \qquad (2.64)$$

and

$$\sigma^2_{expt} = \left(\frac{L}{U_o}\right)^2\left[(2\zeta_o - 5\zeta_o^2) + \left(\frac{V_d}{\pi R_o^2 L}\right)^2 + 2\zeta_o^2\left(\frac{V_d}{\pi R_o^2 L}\right)^2\right] = \bar{t}_{id} + \left(\frac{L}{U_o}\right)^2 \left[\left(\frac{V_d}{\pi R_o^2 L}\right)^2 + 2\zeta_o\left(\frac{V_d}{\pi R_o^2 L}\right) - 13\zeta_o^2\right] \qquad (2.65)$$

The corrections to be applied to the experimental moments observed with this detector in order to recover those of the ideal experiment can then be obtained by comparison with equations (2.37) and (2.39a). That is,

$$\bar{t}_{id} = \bar{t}_{expt} - \delta\bar{t}_{1b}$$

and

$$\sigma^2_{id} = \sigma^2_{expt} - \delta\sigma^2_{1b}$$

where

$$\delta\bar{t}_{1b} = \frac{L}{U_o}\left(\frac{V_d}{\pi R_o^2 L} - 3\zeta_o\right) \qquad (2.66)$$

and

$$\delta\sigma^2_{1b} = \left(\frac{L}{U_o}\right)^2\left\{\left(\frac{V_d}{\pi R_o^2 L}\right)^2 + 2\zeta_o\left(\frac{V_d}{\pi R_o^2 L}\right) - 13\zeta_o^2\right\} \qquad (2.67)$$

In both of these corrections, the last terms arise from the modifications of the diffusion process caused by the perfectly mixed region, whereas the remaining terms are due to the non-zero volume of the detector. These latter terms are naturally somewhat larger than those for an unmixed detector of the same volume given in equations (2.57) and (2.58). In a practical instrument, if it is known which type of model detector represents the reality most closely, then the appropriate corrections given above should be applied. However, it is most likely that a practical detector will have a behaviour intermediate between these two extremes.

Therefore, it is best to design the instrument so that the corrections evaluated for either model are negligible. Irrespective of the possible external constraints dictating the detector volume V_d, the relative errors due to all the corrections can be made arbitrarily small by the selection of the length of the diffusion tube, L, for a fixed fluid velocity and diffusivity.

2.4 Sample Introduction

So far, we have been concerned with the evaluation of the temporal moments of the concentration distribution based upon a delta function injection of a sample at z = 0, which is uniform across the diffusion tube cross-section. In this section, we recognize that it is impossible to provide such a δ-function pulse in practice, and suggest an alternative. It is relatively straightforward to introduce an approximately rectangular pulse of a sample into the tube at z = 0, which is uniform across the diffusion tube cross-section.

Therefore, we now consider the temporal moments of the concentration distribution detected in a cross-section at an axial distance z = L, as a result of an exactly rectangular pulse input. For this input, the original boundary conditions of equation (2.3) at z = 0 is modified to read

$$\Delta C_1(r, \theta, 0, t) = (C_{1i} - C_{1f}) \qquad 0 \leq t \leq t_i$$

$$\Delta C_1(r, \theta, 0, t) = 0 \text{ otherwise} \qquad (2.68)$$

The injection time t_i is equal to $V_i/\pi R_o^2 U_o$, where V_i is the volume of the sample injected. Instead of solving the complete Taylor dispersion problem subject to this new boundary condition, it is much simpler to use the approximation that the dispersion process can be described by the one-dimensional equation (2.31) as the effect of rectangular pulse

injection is expected to be small. In this case, the problem is a standard one and its solution is obtained by the transfer function method described in Section 2.3.6. The results for the first raw moment and the variance observed at a fixed cross-section in the tube are [154]

$$\bar{t}_{expt} = \frac{L}{U_o}(1 + 2\zeta_o) + \frac{t_i}{2} = \bar{t}_{id} + \frac{t_i}{2} \qquad (2.69)$$

$$= \frac{L}{U_o}\left(1 + 2\zeta_o + \frac{V_i}{2\pi R_o^2 L}\right)$$

and

$$\sigma^2_{expt} = \left(\frac{L}{U_o}\right)^2\left[2\zeta_o + 8\zeta_o^2 + \frac{t_i^2}{12}\right] = \sigma^2_{id} + \frac{t_i^2}{12} \qquad (2.70)$$

$$= \left(\frac{L}{U_o}\right)^2\left[2\zeta_o + 8\zeta_o^2 + \frac{1}{12}\left(\frac{V_i}{\pi R_o^2 L}\right)^2\right]$$

Thus

$$\bar{t}_{id} = \bar{t}_{expt} - \delta\bar{t}_2$$

$$\sigma^2_{id} = \sigma^2_{expt} - \delta\sigma^2$$

with

$$\delta\bar{t}_2 = \tfrac{1}{2}\left(\frac{L}{U_o}\right)\left(\frac{V_i}{\pi R_o^2 L}\right) \qquad (2.71)$$

$$\delta\sigma_2^2 = \frac{1}{12}\left(\frac{L}{U_o}\right)^2\left(\frac{V_i}{\pi R_o^2 L}\right)^2 \qquad (2.72)$$

As for the non-zero volume of the detector, the corrections are made smaller by increasing the diffusion tube volume for a fixed injection volume. Provided that the corrections can be made sufficiently small, departures from a true rectangular pulse will have an insignificant effect upon the observed moments.

2.5 Diffusion Tube Geometry

The analysis of the ideal experiment presumes that the diffusion tube is straight, and of uniform, circular cross-section. We have already

established in Sections 2.3.4 and 2.4 that in order to minimise the corrections arising from the concentration distribution and sample introduction, the tube must be as long as possible for a fixed mean velocity of the flow. Since there is a practical lower limit to the flow velocity that can be held constant, a tube of about 10 m long is required [18,23]. Such a tube cannot be conveniently maintained at a constant temperature if it is straight. So it is wound in the form of a helix as described in the proceeding chapter. Furthermore, in order to satisfy condition (2.30), it is necessary to use a tube with very small internal diameter (about one millimetre; [18,23]). Consequently, the uniformity of the bore in manufacture becomes difficult to achieve and the exact circularity of the cross-section cannot be assured. Finally, it is often necessary to connect the diffusion tube to the refractometer by coupling the former with a short connecting tube of a different bore (see Chapter 3, Section 3.2.2).

In this section, we consider the implications of each of these effects for the first and second spatial moments of the concentration distribution in the diffusion tube, and hence for the diffusion coefficient measurements.

2.5.1 Helical diffusion tube

In Chapter 3, we describe how the diffusion tube of internal radius R_o is wound into a helical coil of radius R_c. In this case, the varying path lengths traversed by the fluid at different radial positions in the tube and the secondary flows present in the main flow contribute to the dispersion process. This topic has been extensively studied [18,23,29,157-164] in view of its significance in physiological problems [165] and in many engineering applications. Consequently, it is sufficient for the present purpose to make use of these earlier studies. Basically, it

has been shown that two competing mechanisms exist in curved tubes. Curvature increases the variation in residence time across the flow in comparison with the straight tube and this in turn enhances the dispersion. On the other hand, the secondary flows create a transverse mixing which diminish the process of dispersion. The results of Nunge, Lin and Gill [160] demonstrate that the relative importance of these two effects change with the Reynolds number. As the Reynolds number is increased, the dispersion is first enhanced, but diminishes later on.

However, none of the studies of the tube curvature effects [18, 157-164, 166] provides a description of the dispersion process in a closed form. Nevertheless, within the range of conditions of interest here (i.e. $De^2.Sc \leq 20$; $D_{12}t/R_o^2 > 20$), all the treatments lead to essentially identical results. Also, the approximate nature of the analyses implies that it is satisfactory to employ the results to establish conditions under which the tube curvature effects become negligible [29, 167]. This is more prudent than to use the results to obtain corrections to spatial moments observed in a curved tube in order to correct the moments to those for a straight tube. For this purpose, we employ the results of Nunge, Lin and Gill [160] to examine the fractional difference between the spatial variance of the concentration distribution in a curved tube and that in a straight tube for the same mean velocity.

Among the parameters that characterize the dispersion process in helical tubes, we consider

The Radius Ratio $$\omega = \frac{R_c}{R_o} \tag{2.73}$$

The Reynolds Number $$Re = \frac{2R_o U_o}{\nu} \tag{2.74}$$

The Schmidt Number $$Sc = \frac{\nu}{D_{12}} \tag{2.75}$$

and the Dean Number $$De = Re.\omega^{-\frac{1}{2}} \tag{2.76}$$

Because of the assumptions of the theoretical analysis, the first moments are necessarily identical. The second spatial moment difference may be written as

$$\Delta = \frac{\mu^*_{2s} - \mu^*_{2c}}{\mu^*_{2s}} = f(Re, Sc, \omega) \equiv \frac{\sigma^2_s - \sigma^2_c}{\sigma^2_s} \tag{2.77}$$

where μ^*_{2s}, defined by equation (2.25), and μ^*_{2c} are the second spatial moments for the straight and curved tubes respectively. For the purpose of this work, and with sufficient accuracy [23a, 160],

$$f(Re, Sc, \omega) = 192\omega^{-\frac{1}{2}}\left\{\frac{4Re^4}{576^2 \times 160}\left[\frac{-2569}{15,840}Sc^2 + \frac{109}{43,200}\right] + \frac{2Re^2}{576 \times 144}\left[\frac{31}{60}Sc - \frac{25497}{13440}\right] + \frac{419}{196 \times 120} + \frac{1}{4}\left[\frac{1}{Re^2.Sc^2} + \frac{1}{192}\right]\right\} \tag{2.78}$$

For the range of values of ω of interest here, $100 \leq \omega \leq 500$, the function $f(Re, Sc, \omega)$ is essentially dependent upon the single dimensionless group $[De^2.Sc]$ as indicated by Janssen [161]. Consequently, in Fig. 3.9 in Chapter 3 we make use of this fact to provide a convenient representation of the behaviour of $f(Re, Sc, \omega)$ for the apparatus design and operation. The plot, represented here by Fig. 2.4, indicates that for any value of ω in the prescribed range, a choice of conditions such that

$$De^2.Sc \leq 20 \tag{2.79}$$

with

$$100 \leq \omega \leq 500 \tag{2.80}$$

will ensure that coiling of the diffusion tube has an effect on the second central moment (i.e. variance) of the distribution no greater than ±0.05%. It must be emphasized, however, that it will still be essential to examine the effect of the diffusion tube curvature on the second moment experimentally for a particular instrument. This is

easily accomplished, because the Dean number for the flow can be altered by using different flow velocities. When the effect of diffusion tube curvature is insignificant, the observed diffusion coefficients must be independent of the flow velocity within the precision of their measurements.

Fig. 2.4 - The effects of tube coiling on the spatial variance of the concentration distribution for $100 \leq \omega \leq 500$

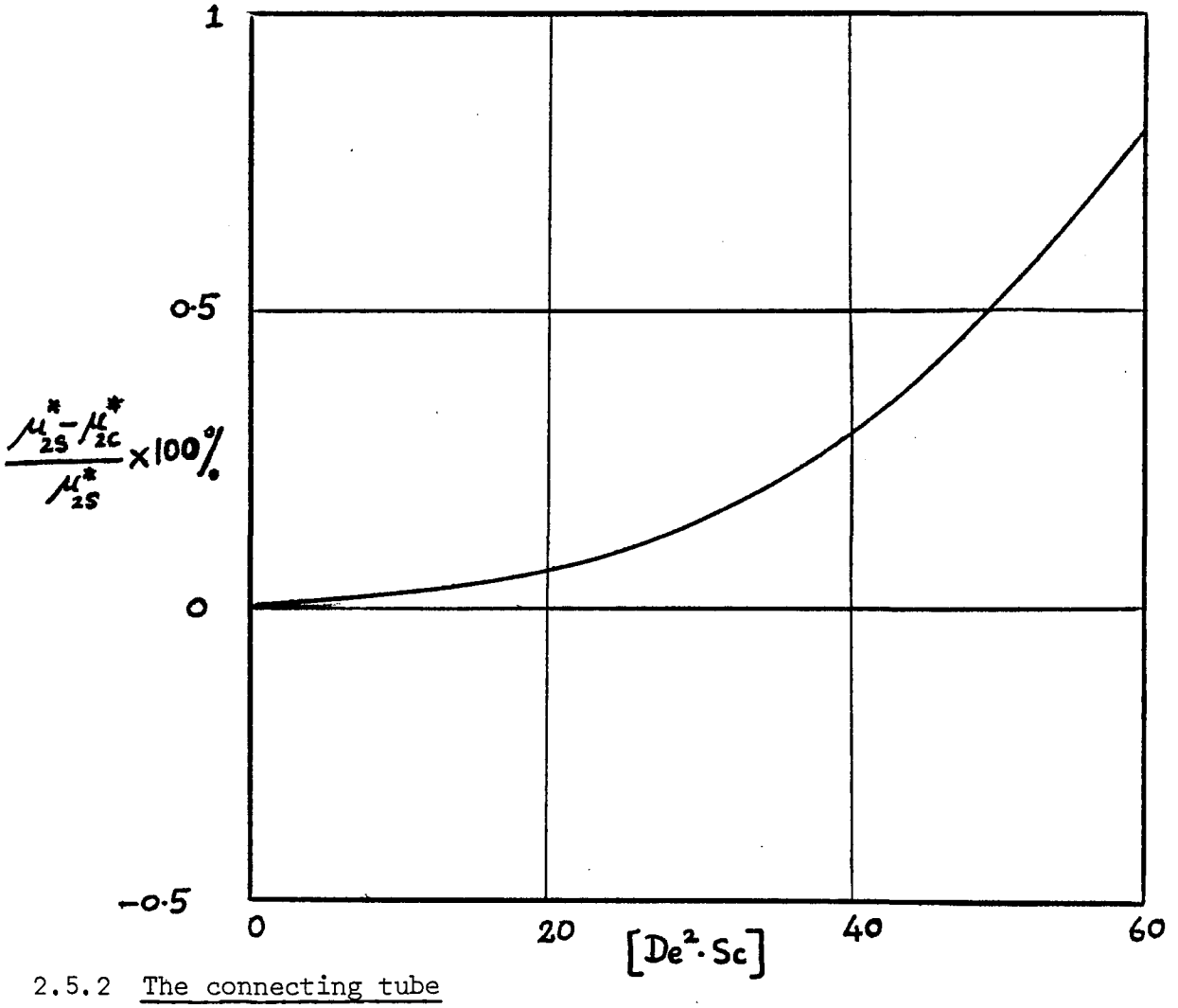

2.5.2 The connecting tube

In this section, we consider the effect of adding a short length of connecting tube of a different diameter to the exit of the diffusion tube. Again we employ an approximate treatment which is justified by the small magnitude of the effect to be considered. We suppose the connecting tube, with an internal radius r_c, to be joined to the diffusion tube as shown by Fig. 2.5 so that the junction occurs at $z' = 0$.

Fig. 2.5 - The connecting tube between the diffusion tube and the refractometer

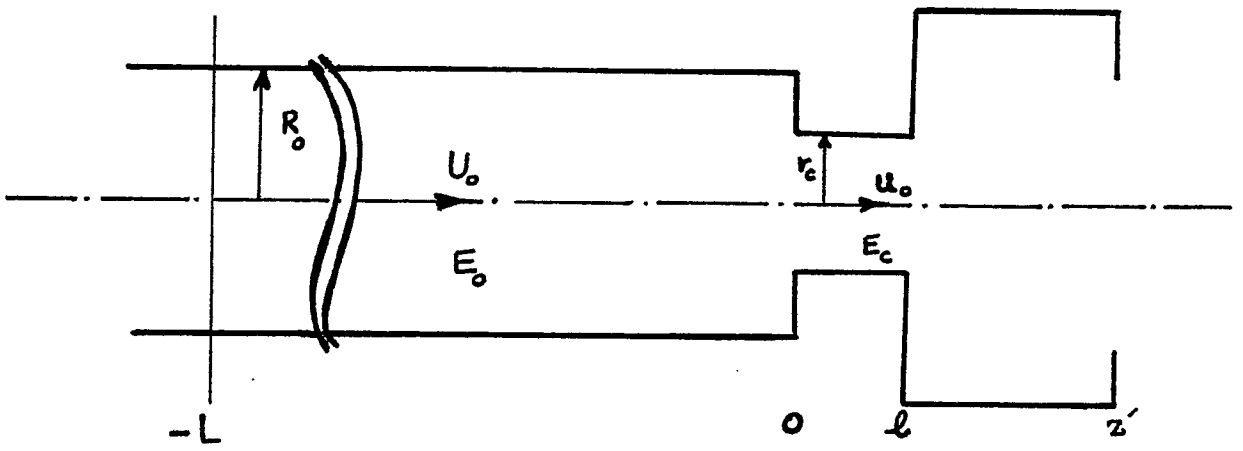

We assume that there is a sharp transition in the flow pattern in the tube from the fully-developed profile of laminar flow in the diffusion tube to that fully-developed profile characteristic of the connecting tube. From the continuity equation we have

$$R_o^2 U_o = r_c^2 u_o$$

where u_o is the mean flow velocity in the connecting tube. It is further assumed that the diffusion tube and the connecting tube extend to infinity in either direction about $z' = 0$, and that the concentration distribution resulting mainly from dispersion in the diffusion tube is observed as a cross-section average at $z' = \ell$. In order to obtain the concentration distribution observed at $z' = \ell$, as a result of a sample injection into the diffusion tube, again we use the Taylor approximation. That is, in each tube the diffusion process may be described by the one-dimensional equation (2.31). Hence we ignore any transient effects in the entrance region to the connecting tube. In particular, we define the effective diffusion coefficient E_c by

$$E_c = \frac{r_c^2 u_o^2}{48 D_{12}}$$

which is analogous to that defined for the diffusion tube in equation (2.32). With these approximations, we first obtain the moments observed at $z' = \ell$ in response to a δ-pulse injected at $z' = 0$, and in this calculation dispersion is allowed both upstream and downstream of $z' = 0$. Here we adapt the analysis given by Van der Laan [168] who has solved a very similar problem. The first raw moment $\bar{t}_c$ and the variance σ_c^2 of the distribution are given by

$$\bar{t}_c = \frac{\ell}{U_o}\left[1 + \zeta_c\left(1 + \frac{r_c^2}{R_o^2}\right)\right] = \frac{L}{U_o}\left(\frac{r_c}{R_o}\right)^2\left[\frac{\ell}{L} + \zeta_o\left(1 + \frac{r_c^2}{R_o^2}\right)\right] \quad (2.81)$$

and

$$\sigma_c^2 = \left(\frac{\ell}{U_o}\right)^2\left\{2\zeta_c + \zeta_c^2\frac{r_c^2}{R_o^2}\left(\frac{3r_c^2}{R_o^2} + 2\right)\right\} = \left(\frac{L}{U_o}\right)^2\left(\frac{r_c}{R_o}\right)^4\left[2\zeta_o\frac{\ell}{L} + \zeta_o^2\frac{r_c^2}{R_o^2}\left(\frac{3r_c^2}{R_o^2} + 2\right)\right] \quad (2.82)$$

where

$$\zeta_c = \frac{r_c^2 u_o}{48 D_{12} \ell} = \zeta_o \frac{L}{\ell} \quad (2.83)$$

It can be easily varified (from the definition of the raw moments as in equation (2.61)) that: "the first raw moment and the variance of the response of any input function are just the moments of the response to a δ-pulse added to the appropriate moment of the input function". Hence we suppose that the input to the connecting tube is now provided by the concentration distribution resulting from Taylor's dispersion in the diffusion tube, with the moments $\bar{t}_{id}$ and σ_{id}^2 given by equations (2.37) and (2.39a). In this case, the moments observed at $z' = \ell$ as a result of a δ-pulse injection at $z' = -L$ are

$$(\mu_1')_{expt} = \bar{t}_{id} + \bar{t}_c = \bar{t}_{id} + \delta\bar{t}_3$$

and

$$(\sigma^2)_{expt} = \sigma_{id}^2 + \sigma_c^2 = \sigma_{id}^2 + \delta\sigma_3^2$$

Hence the equations for the ideal moments read

$$\bar{t}_{id} = (\mu_1')_{id} = (\mu_1')_{expt} - \delta\bar{t}_3 = \bar{t}_{expt} - \delta\bar{t}_3 \quad (2.84)$$

and $$\sigma_{id}^2 = \sigma_{expt}^2 - \sigma_c^2 = \sigma_{expt}^2 - \delta\sigma_3^2 \qquad (2.85)$$

where $\delta\bar{t}_3 = \bar{t}_c$ and $\delta\sigma_3^2 = \sigma_c^2$ can be obtained from equations (2.82) and (2.83). Equations (2.82)-(2.85) may be used to show that the fractional corrections to the observed moments are given to a good approximation by the results

$$\frac{\delta\bar{t}_3}{\bar{t}_{id}} = \left(\frac{r_c}{R_o}\right)^2 \left[\frac{\ell}{L} + \zeta_o\left(1 + \frac{r_c^2}{R_o^2}\right)\right] \qquad (2.86)$$

and

$$\frac{\delta\sigma_3^2}{\sigma_{id}^2} = \left(\frac{r_c}{R_o}\right)^4 \left[\frac{\ell}{L} + \frac{3}{2}\zeta_o\left(\frac{r_c}{R_o}\right)^4 + \zeta_o\left(\frac{r_c}{R_o}\right)^2\right] \qquad (2.87)$$

Because ζ_o itself is inversely proportional to L, it is evident that reducing both the length and radius of the connecting tube decreases the magnitude of the correction. For example, for a radius ratio $\frac{r_c}{R_o} = \frac{1}{4}$, even if $\frac{\ell}{L} = 0.04$, the correction to the first moment is less than 0.3% and that to the variance less than 1.6×10^{-2}%.

2.5.3 Non-uniform diffusion tube

A solution of the diffusion equation for steady flow in a straight tube of circular cross-section, whose area varies in an arbitrary fashion along the axis of the tube, is not practical. Consequently, we consider a simple model of the possible non-unifromities in the cross-sectional area of the tube that has the benefit of relative simplicity and incorporates some of the features of the non-uniformities likely to be present in real tubes. Figure 2.6 contains a sketch of this model.

Fig. 2.6 - The model of the non-uniform diffusion tube.

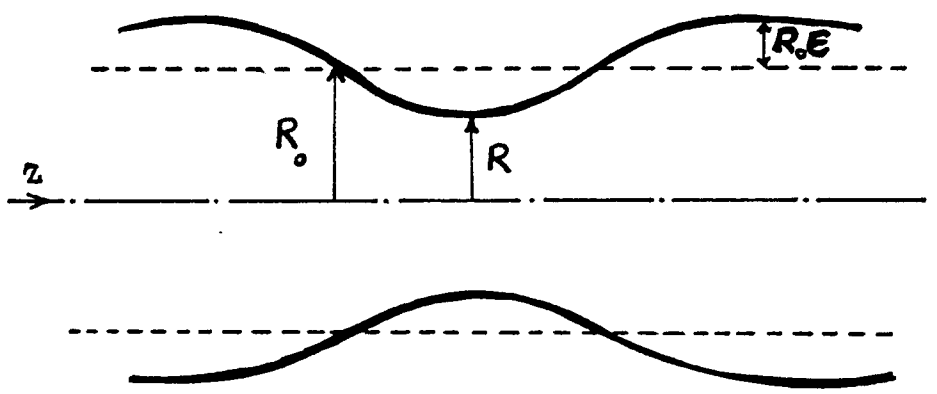

The radius of the cross-section of the tube is assumed to vary sinusoidally according to the equation

$$R(z) = R_o \left(1 + \varepsilon \sin \frac{2\pi z}{\lambda}\right) \tag{2.88}$$

We presume that the amplitude of the oscillations is small,

$$\varepsilon << 1$$

the wavelength is large compared to the radius,

$$\lambda >> R$$

but it is much smaller than the tube length L.

$$\lambda << L$$

In line with our earlier arguments, we seek to analyse the diffusion process in this non-uniform tube in an approximate manner. So our aim is to obtain the moments of the concentration distribution in the tube as a perturbation to those in a uniform tube with a constant radius R_o for the same volumetric flow rate. Accordingly, we restrict our discussion to flows for which the lubrication approximation is valid, i.e. $Re\left|\frac{dR}{dz}\right| << 1$. These flows are usually employed for the measurements in order to ensure laminar flow and satisfaction of condition (2.30). In this case, the Navier-Stokes equations reduce to the form [169]

$$\frac{\partial P}{\partial r} = \eta\left\{\frac{\partial}{\partial r}\left(\frac{1}{r}\frac{\partial}{\partial r}(rU_r)\right) + \frac{\partial^2 U_r}{\partial z^2}\right\}$$

$$\frac{\partial P}{\partial z} = \eta\left\{\frac{1}{r}\frac{\partial}{\partial r}\left(r\frac{\partial U_z}{\partial r}\right) + \frac{\partial^2 U_z}{\partial z^2}\right\}$$

and

$$\frac{\partial U_z}{\partial z} + \frac{1}{r}\frac{\partial}{\partial r}(rU_r) = 0$$

where cylindrical symmetry has been used and U_z and U_r represent the axial

and radial components of the fluid velocity respectively. Since $\partial^2 U_z/\partial z^2 < \partial^2 U_z/\partial r^2$ by a factor of order $(R_o/\lambda)^2$, we may neglect the former term completely for the conditions specified above. In this case we easily obtain the solutions for the two velocity components, correct to order $\varepsilon R_o/\lambda$, as

$$U_z\,(r,\,z) \;=\; \frac{2Q}{\pi R^2}\left[1 - \left(\frac{r}{R}\right)^2\right] \tag{2.89}$$

and

$$U_r\,(r,\,z) \;=\; \frac{4QR_o\varepsilon}{\lambda R^2}\cos\left(\frac{2\pi z}{\lambda}\right)\left[\left(\frac{r}{R}\right) - \left(\frac{r}{R}\right)^3\right] \tag{2.90}$$

where Q is the constant volumetric flow rate through the tube.

Anticipating that the concentration distribution in the tube is cylindrically symmetric, as it was for the uniform tube, the diffusion equation now takes the form

$$\frac{1}{D_{12}}\frac{\partial(\Delta C_1)}{\partial t} \;=\; \frac{1}{r}\frac{\partial}{\partial r}\left(r\frac{\partial \Delta C_1}{\partial r}\right) + \frac{\partial^2(\Delta C_1)}{\partial z^2} - U_z\frac{\partial \Delta C_1}{\partial z} - U_r\frac{\partial \Delta C_1}{\partial r} \tag{2.91}$$

The boundary conditions are, at $t = 0$,

$$\Delta C_1(r,\,0,\,0) \;=\; \delta(z)(C_{1i} - C_{1f})$$

and

$$\frac{\partial(\Delta C_1)}{\partial \nu} \;=\; 0 \text{ at } r \;=\; R(z) \text{ for all } t \tag{2.92}$$

where $\partial/\partial\nu$ indicates differentiation along the normal with respect to the tube wall. We now write the velocity components and the concentration distribution for the non-uniform tube as perturbations to those for the uniform tube, so that

$$U_z(r,\,z) \;=\; U_o(r) + \varepsilon U_z' \tag{2.93}$$

$$U_r(r,\,z) \;=\; \varepsilon U_r' \tag{2.94}$$

and

$$\Delta C_1 \;=\; \Delta C_1^o + \varepsilon c' \tag{2.95}$$

where the subscript or superscript 'o' denotes the concentration distri-

bution in the uniform tube. Expansion of equations (2.89) and (2.90) then shows that

$$U_z' = -4U_o \sin\left(\frac{2\pi z}{\lambda}\right)\left[1 - 2\left(\frac{r}{R_o}\right)^2\right] \tag{2.96}$$

and

$$U_r' = -\frac{4U_o R_o}{\lambda}\cos\left(\frac{2\pi z}{\lambda}\right)\left[\frac{r}{R_o} - \left(\frac{r}{R_o}\right)^3\right] \tag{2.97}$$

where U_o is the mean flow velocity in the uniform tube. For the conditions of interest, the contribution of axial molecular diffusion to the dispersion process is considered negligible as before. Consequently, following Taylor [148] we neglect the term $\partial^2(\Delta C_1)/\partial z^2$ in equation (2.91). Making use of the fact, to a very good approximation [148, 23a], that $\partial(\Delta C_1)/\partial z$ is independent of r. Hence the diffusion equation (2.91) for a uniform tube (i.e. to zeroth order in ε) is just that given by Taylor [148]. The temporal moments of the solution of this equation, averaged over a cross-section, are therefore the ideal moments given by equations (2.37) and (2.39a). To obtain the moments of the solution to first order in ε, we employ equations (2.93)-(2.95) in the diffusion equation (2.91). Again we neglect the longitudinal molecular diffusion term. Collecting terms of ε, we find the following equation for the concentration distribution perturbation c' in the non-uniform tube:

$$\frac{\partial c'}{\partial t} + U_o(r)\frac{\partial c'}{\partial z} + U_z'(r)\frac{\partial(\Delta C_1^o)}{\partial z} + U_r'\frac{\partial(\Delta C_1^o)}{\partial r} = D_{12}\left[\frac{1}{r}\frac{\partial}{\partial r}\left(r\frac{\partial c'}{\partial r}\right)\right] \tag{2.98}$$

To the same order in ε, the boundary condition of no molecular flux through the tube wall can be shown to be equivalent to

$$\frac{\partial(\Delta C_1)}{\partial r} = 0 \tag{2.99}$$

This is because the curvature of the wall, to first order, depends linearly on the product of ε with R_o/λ. But R_o/λ itself is presumed small so that the curvature is essentially only a second-order effect.

Now because $\partial(\Delta C_1^o)/\partial r$ is small and $U_r'/U_z' \simeq O(R_o/\lambda)$ then $U_r' \partial(\Delta C_1^o)/\partial r \ll U_z' \partial(\Delta C_1^o)/\partial z$. This justifies the neglect of the first of these terms in diffusion equation (2.98) for the concentration distribution perturbation c'. Averaging equation (2.98) over a cross-section of the tube, and making use of boundary condition (2.99), we obtain

$$\frac{\partial c_m'}{\partial t} + \overline{\left(U_z' \frac{\partial(\Delta C_1^o)}{\partial z} \right)} + \overline{U_o(r) \frac{\partial c'}{\partial z}} = 0 \qquad (2.100)$$

where subscript 'm' denotes a concentration averaged over a cross-section. In order to evaluate the remaining cross-section averages, again we make use of the Taylor approximation [148] that $\partial(\Delta C_1^o)/\partial z$ is indistinguishable from $(\partial \Delta C_{1m}^o/\partial z)$, where ΔC_{1m}^o is the cross-section averaged concentration in the uniform tube. The same approximation is made for $\partial c'/\partial z$ so that we obtain the final differential equation as

$$\frac{\partial c_m'}{\partial t} + \bar{U}_z' \left(\frac{\partial \Delta C_{1m}}{\partial z} \right) + U_o \left(\frac{\partial c_m'}{\partial z} \right) = 0 \qquad (2.101)$$

Here, $\bar{v}_o$ is the mean velocity in the diffusion tube, and $\bar{U}'(z)$ is the first-order perturbation to it in the non-uniform tube. Averaging the equation (2.89) over a cross-section yields

$$\bar{U}_z' = -2\bar{v}_o \sin \frac{2\pi z}{\lambda} \qquad (2.102)$$

which is identical to the result found by Thorsness [170].

Now taking Laplace transform of equation (2.101), we obtain

$$\frac{d\hat{c}_m'}{dz} + \left(\frac{\bar{U}_z'}{U_o} \right) \frac{d(\Delta C_{1m}^o)}{dz} + \left(\frac{s}{U_o} \right) \hat{c}_m' = 0 \qquad (2.103)$$

It now follows from equation (2.95) and the definition of the temporal moments of a distribution that, to first order in ε, the raw moments in the non-uniform tube are related to those in the uniform tube by the expression

$$\left(\mu_p'\right)_{nu} = \left[\mu_p'\right]_{id} + \delta\mu_{p4}' \tag{2.104}$$

where $\delta\mu_{p4}'$ is proportional to ε and represents the perturbation to the ideal moments of the uniform tube. Using the results [156] that

$$\delta\mu_{p4}' = \lim_{s\to 0} (-1)^p \frac{d^p c_m'}{ds^p}$$

and

$$\left(\mu_p'\right)_{id} = \lim_{s\to 0} (-1)^p \frac{d^p(\Delta c_{1m}^o)}{ds^p}$$

we can employ equation (2.103) to construct differential equations for the perturbation to each moment. Differentiating equation (2.103) once with respect to s, reversing the order of differentiation, and taking the limit as $s \to 0$, we obtain for the first moment

$$\frac{1}{\varepsilon}\frac{d}{dz}(\delta\mu_{1,4}') + \left(\frac{\bar{U}_z'}{\bar{U}_o}\right)\frac{d}{dz}(\bar{t}_{id}) = 0 \tag{2.105}$$

and after two differentiations of equation (2.103), we obtain in the limit $s \to 0$,

$$\frac{1}{\varepsilon}\frac{d}{dz}(\delta\mu_{2,4}') + \left(\frac{\bar{U}_z'}{\bar{U}_o}\right)\frac{d}{dz}(\mu_2')_{id} - \frac{2}{\bar{v}_o\varepsilon}\delta\mu_{1,4}' = 0 \tag{2.106}$$

Equation (2.105) is readily integrated using equation (2.102) for $\bar{u}_z'$ and equation (2.37) for t_{id} to yield the perturbation to the first moment at $z = L$ as

$$\delta\mu_{1,4}' = \frac{\varepsilon\lambda}{\pi\bar{v}_o}\left[1 - \cos\left(\frac{2\pi L}{\lambda}\right)\right] \tag{2.107}$$

where the boundary conditions reveal that $\delta\mu_{1,4}' = 0$ at $z = 0$, a fact which we have used. Equation (2.106) can be integrated using equation (2.38) for $(\mu_2')_{id}$ to yield at $z = L$

$$\delta\mu_{2,4}' = \varepsilon\left(\frac{2\lambda L}{\pi\bar{v}_o^2} + \frac{R_o^2\lambda}{8\pi D_{12}\bar{v}_o}\right)\left[1 - \cos\left(\frac{2\pi L}{\lambda}\right)\right] \tag{2.108}$$

The first temporal raw moment observed in the non-uniform tube is therefore

$$(\mu_1')_{nu} = \frac{L}{U_o}(1 + 2\zeta_o)\left[1 + \frac{\varepsilon\lambda(1-\cos\frac{2\pi L}{\lambda})}{\pi L(1 + 2\zeta_o)}\right] \qquad (2.109)$$

and this result together with equations (2.104) and (2.108), and the definition of the variance $(\sigma^2)_{nu} = (\mu_2')_{nu} - (\mu_1')^2_{nu}$, can be used to determine this central moment to first-order in ε as

$$(\sigma^2)_{nu} = \left(\frac{L}{U_o}\right)^2\left[8\zeta_o^2 + 2\zeta_o\right]\left\{1 + \frac{\varepsilon\lambda(1-\cos\frac{2\pi L}{\lambda})}{\pi L(1 + 4\zeta_o)}\right\} \qquad (2.110)$$

so that

$$\delta\sigma_4^2 = \frac{2\varepsilon\lambda\zeta_o L}{\pi U_o^2}\left[1 - \cos\left(\frac{2\pi L}{\lambda}\right)\right] \qquad (2.111)$$

From equations (2.109) and (2.110) it is clear that under practical conditions, $\zeta_o << 1$, the correction to both moments is of order $\varepsilon\frac{\lambda}{L}$. Because $\varepsilon << 1$ and $\frac{\lambda}{L} << 1$ for the most likely practical situations, the corrections to both moments are small. For example, if the non-uniformity of the tube bore is 1% and $\frac{\lambda}{L} \simeq 0.1$ then the correction to neither moment exceeds 0.06%. It was shown earlier that, to a very good approximation, equation (2.46) may be used to determine the value of D_{12}. For the non-uniform tube, this equation becomes

$$D_{12} = \frac{R_o^2(\mu_1')_{nu}}{24(\sigma^2)_{nu}} = \frac{R_o^2\bar{t}_{id}}{24\sigma^2_{id}} \qquad (2.112)$$

by virtue of smallness of ζ_o. That is, to first order in ε, the effect of the non-uniformity of the diffusion tube bore upon the moments of the concentration distribution in the evaluation of the diffusion coefficients only occurs in small terms ($\sim$ 1%) in the complete working equation (2.43). Furthermore, these effects are themselves very small under the conditions of interest in this work. Hence the overall contribution of non-uniformity to the evaluation of the diffusion coefficient from the observed moments is negligible. A final point of significance arising from the non-uniformity of the diffusion tube concerns the determination

of its internal radius R_o. It can easily be shown that for the present model of the non-uniform tube, the volume of the tube to first-order in ε is given by

$$V_t = A_o L\left\{1 + \frac{\varepsilon\lambda}{\pi L}\left[1 - \cos\left(\frac{2\pi L}{\lambda}\right)\right]\right\} \qquad (2.113)$$

where $A_o = \pi R_o^2$, is the tube cross-section area which can be determined from a measurement of the tube volume and its length. The maximum error in the value of R_o^2 calculated in this way is of the order of $\varepsilon\frac{\lambda}{L}$, which in practice can be made negligible by selection of tubing of a suitable quality (see Section 3.2.1).

2.5.4 Non-circular cross-section

As in the case of the preceding section, we consider the effects of the non-circular cross-section of the tube by means of a particular model. We assume that the tube has an elliptical cross-section with major and minor semi-axes a_1 and a_2 respectively. The eccentricity e is given by

$$e = \left[1 - \left(\frac{a_2}{a_1}\right)^2\right]^{\frac{1}{2}} \qquad (2.114)$$

Taylor dispersion in such a tube has been studied by Aris [149]. From his work it can be shown that in such a situation the simplified working equation (2.46) for circular tubes must be replaced by the equation

$$D_{12} = \frac{f(e)a_1^2\mu_{1e}'}{24\sigma_e^2} \qquad (2.115)$$

where μ_{1e}' and σ_e^2 are the first raw temporal moment and the variance observed in the elliptical tube respectively, and

$$f(e) = \frac{24 - 24e^2 + 5e^4}{24 - 12e^2} \qquad (2.116)$$

In practice, it is not convenient to determine the ellipticity of a tube or the semi-axes directly. But it is possible to measure the tube volume and its length so as to determine its cross-sectional area A_e where

$$A_e = \pi a_1 a_2 = \pi a_1^2 (1 - e^2)^{\frac{1}{2}} \tag{2.117}$$

Therefore we consider the result of evaluating the diffusion coefficient from experimentally determined moments μ'_{1e} and σ_e^2 in an elliptical tube by means of the equation

$$D_{12}^e = \frac{A_e \mu'_{1e}}{24\pi \sigma_e^2} \tag{2.118}$$

The ratio of the diffusion coefficient calculated for the elliptical tube, D_{12}^e, to true value, D_{12}, is

$$\frac{D_{12}^e}{D_{12}} = \frac{A}{\pi a_1^2 f(e)} = \frac{(1 - e^2)^{\frac{1}{2}}}{f(e)} \tag{2.119}$$

Expanding the ratio in powers of the eccentricity, e, we find that

$$\frac{D_{12}^e}{D_{12}} = 1 - \frac{14}{24} e^4 + \ldots \tag{2.120}$$

which indicates that for small eccentricities, we can equate D_{12}^e to D_{12} without introducing any significant error. Numerical evaluation of the ratio $\frac{D_{12}}{D_{12}^e}$ through equation (2.120) shows that when $e = 0.2$ ($\frac{a_2}{a_1} = 0.98$) the ratio departs only by 0.01% from unity. Therefore, as long as the tube cross-sectional area is determined experimentally, we can use equation (2.118) to interpret the experimental data even if the diffusion tube has an elliptical cross-section.

2.6 Concentration-Dependent Fluid Properties

In all of our analyses so far, we have assumed that the properties of the fluid mixtures involved are independent of composition. In this section, we examine the consequences of the fact that both the diffusion coefficient to be measured and the mixture density depend upon composition. Because the injected sample is necessarily of a different composition from

that of the flowing stream, the density of the mixture will vary from point to point in the diffusion tube. This may possibly cause natural convective flows. Besides, the composition dependence of D_{12} implies that we should re-examine our solution of the diffusion equation for this case.

2.6.1 Concentration-dependent diffusion coefficient

Because it is not possible to solve the dispersion equation (2.2) for the case when D_{12} is a function of C_1, we consider instead an approximate analysis based upon that originally given by Taylor [148]. That is, we again recognise that to a very good approximation, under the present conditions of interest, the dispersion process may be described by a one-dimensional diffusion equation. An equation which describes the evolution of the cross-section averaged composition which is characterized by the effective diffusivity

$$E = \frac{R_o^2 U_o^2}{48 D_{12}(C_1)} \tag{2.121}$$

which is now supposed a function of C_1, is proposed. Following Taylor [148] we can then write the diffusion equation in the form

$$\frac{\partial(\Delta C'_{1m})}{\partial t} = \frac{\partial}{\partial \xi}\left(E \frac{\partial(\Delta C'_{1m})}{\partial \xi} \right) \tag{2.122}$$

where ξ is the axial distance with respect to the moving origin defined by equation (2.6). The initial condition for the solution is the injection of a δ-function pulse at $z = 0$ at time $t = 0$.

Suppose that the composition dependency of D_{12} can, over a suitably small composition range, be represented by the equation

$$D^c_{12}(\Delta C_{1m}) = D_{12}(1 - x\, \Delta C_{1m}) \tag{2.123}$$

where D_{12} is the diffusion coefficient at the composition of the flowing

stream. Thus we have

$$E(\Delta C_{1m}) = E^{o}(1 + x\,\Delta C_{1m}) \tag{2.124}$$

where E^{o} is the effective diffusivity at the composition of the flowing stream. A perturbation solution of equation (2.122) with E given by equation (2.124) has been given by Hopkins [171]. The first-order perturbation solution reads

$$\Delta C'_{1m}(x, t) = \Delta C^{o}_{1m}\left\{1 + \frac{N_1 x}{4\pi^{3/2}(E^{o}t)^{\frac{1}{2}}}\left[\frac{\xi\sqrt{\pi}}{2(E^{o}t)^{\frac{1}{2}}}\,\mathrm{erf}\left(\frac{\xi}{2(E^{o}t)^{\frac{1}{2}}}\right) - \exp^{-}\left(\frac{\xi^2}{4E^{o}t}\right)\right]\right\} \tag{2.125}$$

Here, ΔC^{o}_{1m} is the solution when $E = E^{o}$ is a constant, i.e.

$$\Delta C^{o}_{1m} = \frac{N_1}{(2\pi^{3/2}(E_o t)^{\frac{1}{2}}R_o^2}\exp^{-}\left(\frac{\xi^2}{4E^{o}t}\right) \tag{2.126}$$

where N_1, as defined by equation (2.1), represents the number of moles of species 1 in the injected sample in excess of those present in the same volume of the flowing stream. The first and second spatial moments of this perturbed distribution can readily be evaluated with respect to the moving origin to lead to the results that

$$\mu_1^{*c} = 0$$

and

$$\mu_2^{*c} = 2E^{o}t\left[1 + \frac{1 + N_1 x\left(\frac{5}{16} - \frac{1}{8\sqrt{\pi}}\right)}{\pi R_o^2(2E^{o}t)^{\frac{1}{2}}}\right] \tag{2.127}$$

which can be written as

$$\mu_2^{*c} = 2E(C_{1r})t \tag{2.128}$$

where

$$E(C_{1r}) = E^{o}\left[1 + x\,\frac{N_1(\frac{5}{16} - \frac{1}{8\sqrt{\pi}})}{\pi R_o^2(2E^{o}t)^{\frac{1}{2}}}\right] \tag{2.129}$$

so that $E(C_{lr})$ is the value of E at a composition

$$C_{lr} = C_{lf} + \frac{N_1(\frac{5}{16} - \frac{1}{8\sqrt{\pi}})}{\pi R_o^2 (2E^o t)^{\frac{1}{2}}} \tag{2.130}$$

From equations (2.121), definition of E, and (2.128) we have

$$\mu_2^{*c} = \frac{R_o^2 U_o^2 t}{24 D_{12}(C_{lr})} \tag{2.131}$$

which has exactly the same form as that of the working equation (2.25) derived for the case of constant diffusivity. Hence we conclude that if we employ equation (2.25) or its equivalent in terms of temporal moments (equation (2.43)), the diffusion coefficient obtained should be referred to the composition C_{lr} given by equation (2.130) and not to the flowing stream composition. But because modern composition monitors, such as the refractive index detector, are extremely sensitive to composition changes, N_1 can usually be made very small. In this case, the departure of the reference composition from that of the flowing will be insignificant.

2.6.2 Concentration-dependent density

We now consider the consequences of the fact that the density of the liquid sample mixture injected into the flowing stream necessarily differs from that of the flowing stream. Assuming that the concentration differences are small, the density ρ at any point in the tube may be considered to be a linear function of the concentration. So we can write

$$\rho = \rho_f(1 + \gamma \Delta C_1) \tag{2.132}$$

where ρ_f is the flowing stream density. The occurence of density differences in the diffusion tube introduces two new effects in the dispersion process. First, the longitudinal density gradients lead to longitudinal pressure gradients which modify the velocity distribution in the flow. Second, due to radial density gradients, buoyancy forces are

induced which drive a secondary flow. An exact analysis of the equations of fluid mechanics which govern this situation is not available. But Erdogan and Chatwin [158] give an approximate treatment based upon the assumption of small density changes. Their analysis is restricted to the region where the Taylor dispersion process becomes one-dimensional. Under these conditions, they found that the evolution of the cross-section averaged concentration in the tube was controlled by the equation

$$\frac{\partial \Delta C_{1m}}{\partial t} = \frac{R_o^2 U_o^2}{48 D_{12}} \frac{\partial}{\partial \xi} \left[\frac{\partial C_{1m}}{\partial \xi} - \phi' Q_2 \left(\frac{\partial \Delta C_{1m}}{\partial \xi} \right)^3 \right] \tag{2.133}$$

Here Q_2 depends on the Peclet number, Pe, where

$$Pe = \frac{R_o U_o}{D_{12}} \tag{2.134}$$

and the Schmidt number defined by equation (2.75)

$$Q_2 = -\left(\frac{1}{2880}\right)^2 \left[\frac{-2569}{8448} Pe^2 . Sc^2 + \frac{19,797}{197,120} Pe^2 + \frac{10,425}{56} Sc + 60,480 \frac{Sc^2}{Pe^2} \right] \tag{2.135}$$

The parameter ϕ' is defined in terms of the coefficient γ by the equation

$$\phi' = \left[\frac{\gamma g R_o^4 \rho^2}{\eta^2} \right]^2 \tag{2.136}$$

where g is the acceleration due to gravity and η is the fluid viscosity.

Approximate solutions of equation (2.133), based on one-dimensional Taylor dispersion, have been obtained by Barton [172] and Smith [173]. They have used the results to derive expressions for the spatial variance of the concentration distribution. Smith's expression reads

$$\mu_2^{*\rho} = \frac{R_o^2 U_o^2}{24 D_{12}} t + \sigma_{IT}^2 + \frac{12 Q_2 \phi' D_{12}}{\pi^3 R_o^6 U_o^2 3^{3/2} t} \tag{2.137}$$

where σ_{IT}^2 is the variance at the end of a transient period when the asymptotic solution becomes valid. This transient region has never been analysed and hence equation (2.137), which is itself approximate, cannot

be used to provide the corrections to the observed moments. Also it does not give any guidance as to when buoyancy effects may be neglected. However, it does provide means of deciding whether or not buoyancy effects are significant in particular measurements. That is, if we use equation (2.27), the working equation for the ideal experiment, to determine the diffusion coefficients from experimentally measured spatial moments under significant buoyancy effects, then equation (2.137) shows that the resulting apparent diffusion coefficient $(D_{12}^a)_\rho$, will differ from its true value D_{12},

$$(D_{12}^a)_\rho = D_{12}\left[1 + \frac{24\sigma_{IT}^2 D_{12}}{R_o^2 U_o^2 t} + \frac{288 Q_2 D_{12}^2 N_1^2}{\pi^3 R_o^8 U_o^2 3^{3/2} t^2}\right]^{-1} \qquad (2.138)$$

Therefore, the apparent diffusion coefficient would depend upon the flow velocity U_o, time of measurement t, the excess number of moles N_1, injection and the magnitude of the initial concentration perturbation. On the other hand, if such dependencies are absent in the measurements, it implies that the experimental data are free from errors due to buoyancy effects. In order to ensure that the buoyancy effects are eliminated from our experiments, we must carry out measurements over a wide range of flow velocities and injection concentrations. Because buoyancy effects are minimized as the difference between the injection and flowing stream concentrations diminish, we must always use injection samples with concentrations as near as possible to that of the flowing stream.

2.7 Summary of the Theoretical Analysis

The foregoing analysis has shown how, under the appropriate conditions, it is possible to design an apparatus to measure liquid phase diffusion coefficients that departs only in small respects from its ideal model. Some of the departures from the ideal can be rendered so small as to be

negligible. Other effects, although not negligible, may be made suitably small by the design so that corrections may be applied to account for them with confidence. We conclude this chapter by summarizing the results for the convenience in the design and use of such an apparatus.

Among the effects that can be rendered negligible are those which arise from the coiling of the diffusion tube and non-uniformity. In order to eliminate coiling effects, conditions must be chosen such that

$$\left[De^2.Sc\right] \lesssim 20$$

and that

$$100 \lesssim \omega = \left(\frac{R_c}{R_o}\right) \lesssim 500$$

The non-uniformities of the diffusion tube bore are insignificant provided that the amplitude of the radius fluctuations, εR_o, and the length scale of their fluctuations are such that

$$\varepsilon \frac{\lambda}{L} < 10^{-3}$$

In view of both non-uniformities of the cross-section and its possible non-circularity, the effective cross-sectional area of the tube, A_o, should be determined by measuring its length and volume. This measurement then renders effects due to any ellipticity in the cross-section negligible, provided that

$$e = \left[1 - \left(\frac{a_2}{a_1}\right)^2\right]^{\frac{1}{2}} \lesssim 0.2$$

Buoyancy effects have not been accounted for exactly in the discussion, although an experimental method of checking and eliminating their contribution to the dispersion process has been proposed.

In addition, provided that conditions are chosen to satisfy the requirements of laminar flow,

$$Re = \frac{2R_o U_o}{\nu} < 2000$$

and the additional constraints

$$\left(\frac{D_{12}}{R_o^2}\right) t \geqslant 20$$

in which case

$$\zeta_o = \left(\frac{R_o^2}{48D_{12}}\right) t^{-1} \leqslant 10^{-3}$$

and

$$\left(\frac{R_o}{D_{12}}\right) U_o \geqslant 700$$

the working equation for the determination of the diffusion coefficient is

$$D_{12} = \frac{A_o}{24\pi \bar{t}_{id}} \left\{ \frac{\left[1 + \frac{4\sigma_{id}^2}{\bar{t}_{id}^2}\right]^{\frac{1}{2}} + 3}{\left[1 + \frac{4\sigma_{id}^2}{\bar{t}_{id}^2}\right]^{\frac{1}{2}} + 2\left(\frac{\sigma_{id}^2}{\bar{t}_{id}^2}\right) - 1} \right\} \left[\tfrac{1}{2} + \tfrac{1}{2}(1 - \delta_a)^{\frac{1}{2}}\right]$$

where

$$\delta_a = (768)^2 K_c \zeta_o$$

$$K_c = 2.1701 \ldots \times 10^{-5}$$

and

$$\zeta_o = \frac{2\sigma_{id}^2 - \bar{t}_{id}^2 + (\bar{t}_{id}^4 - 4\bar{t}_{id}^2\sigma_{id}^2)^{\frac{1}{2}}}{8\bar{t}_{id}^2 - 4\sigma_{id}^2}$$

In these expressions, $\bar{t}_{id}$ and σ_{id}^2 are the temporal first raw moment and the variance (equal to second central moment) in an ideal experiment. They may be obtained from measurements of the same moments in a real experiment, $\bar{t}_{expt}$ and σ_{expt}^2, by application of the equations

$$\bar{t}_{id} = \bar{t}_{expt} - \sum_n \delta\bar{t}_n$$

and

$$\sigma_{id}^2 = \sigma_{expt}^2 - \sum_n \delta\sigma_n^2$$

where $\delta\bar{t}_n$ and $\delta\sigma_n^2$ are small corrections due to the departures from the ideal, and for the present, they include

1. The corrections due to the Refractive Index Detector used to monitor the concentration distribution at the exit of the diffusion tube

$$\delta\bar{t}_1 = \left(\frac{L}{U_o}\right)\left[\left(\frac{V_d}{\pi R_o^2 L}\right) - 3\zeta_o\right]$$

$$\delta\sigma_1^2 = \left(\frac{L}{U_o}\right)^2\left[\left(\frac{V_d}{\pi R_o^2 L}\right)^2 + 2\zeta_o\left(\frac{V_d}{\pi R_o^2 L}\right) - 13\zeta_o^2\right]$$

2. The corrections due to the Sample Introduction by Rectangular Pulse Injection

$$\delta\bar{t}_2 = \tfrac{1}{2}\left(\frac{L}{U_o}\right)\left(\frac{V_i}{\pi R_o^2 L}\right)$$

$$\delta\sigma_2^2 = \frac{1}{12}\left(\frac{L}{U_o}\right)^2\left(\frac{V_i}{\pi R_o^2 L}\right)^2$$

3. The corrections due to the Connecting Tube between the diffusion tube and the refractive index detector

$$\delta\bar{t}_3 = \left(\frac{L}{U_o}\right)\left(\frac{r_c}{R_o}\right)^2\left[\left(\frac{\ell}{L}\right) + \zeta_o\left(1 + \frac{r_c^2}{R_o^2}\right)\right]$$

$$\delta\sigma_3^2 = \left(\frac{L}{U_o}\right)^2\left(\frac{r_c}{R_o}\right)^4\left[2\zeta_o\left(\frac{\ell}{L}\right) + \zeta_o^2\left(\frac{r_c}{R_o}\right)^2\left(\frac{3r_c^2}{R_o^2} + 2\right)\right]$$

In addition, the molar concentration of species 1 in the mixture to which the measured diffusion coefficient refers is C_{1r}, given by the equation

$$C_{1r} = C_{1f} + \delta C_1$$

where δC_1 is a further correction to the flowing stream concentration C_{1f} and may be obtained from

$$\delta C_1 = \frac{N_1\left(\frac{5}{16} - \frac{1}{8\sqrt{\pi}}\right)}{\pi R_o^2\left(2\zeta_o U_o L\bar{t}_{id}\right)^{\frac{1}{2}}}$$

for an extra number of moles, N_1, of species 1 injected.

Finally, it is important to record that the use of a laboratory metering pump [174] may appear to be a convenient choice for maintaining the constant flow rates through the diffusion tube. But such metering pumps can result in severe short time pulsations which could affect the laminar dispersion significantly. It has been found [167] that the effective diffusion coefficient under pulsating flow conditions could be higher, equal to, or less than, that for non-pulsating flow, depending on the experimental conditions. Therefore, the use of a gravity feed supply (see Section 3.4) to maintain the constant fluid flow rates through the diffusion tube will eliminate any errors introduced into the measurements due to this effect.

It will be shown in the proceeding chapter how the sometimes conflicting conditions for a suitable design can all be satisfied in a practical apparatus. It will also be verified that the residual systematic errors in the application of the Taylor Dispersion Method have been reduced to a level below that of the random errors of measurement.

CHAPTER 3

APPARATUS AND EXPERIMENTAL PROCEDURE

3. Introduction

The theoretical analysis of the previous chapter has been employed for the design and operation of the equipment used in this work. The instrument has been designed to operate in a wide temperature range, 10 - 200°C, at atmospheric pressure. The general features of the apparatus and the experimental procedure adopted are described below and subsequently individual items are discussed in more detail.

3.1 Apparatus Design

The function of the apparatus design was to determine the conditions of the experiment and dimensions of the instrument so that the departures from ideality, mentioned in the preceding chapters, contribute as little as possible to the measured diffusion coefficients. The geometric, mechanical, thermal and electrical characteristics of the equipment were therefore selected following a careful design study based upon the previous theoretical analysis. As a result of this study, an instrument has been designed which satisfies all the necessary conditions arising from the theory of the method and whose precision is one of ±0.5%. To attain this precision, all of the corrections for the first moment and the variance of a distribution have been constrained to be less than ±0.6% of the ideal moments. Because these corrections may be estimated to within ±5%, the residual uncertainty arising from each correction is therefore no more than ±0.03%. The design of the instrument together with the theory of its operation, ensure that systematic errors are negligible. Including errors in the measurement of the geometry of the diffusion tube, the accuracy of the diffusion coefficient is estimated to be one of ±1.0%.

Figure 3.1 shows a schematic diagram of the diffusion equipment whose flow diagram, Fig. 3.2, is presented later.

The diffusion tube, 1, whose length is 13.219 metres is made from 0.8198 millimetre internal diameter stainless steel tubing (Phase Separations, Ltd.) wound on a copper former, 2, by means of four equidistant copper pillars and embedded in lead, 3, to provide thermal stability. The tube is carefully wound round the pillars such that a smooth coil is obtained without any indentations or sharp corners. A modified liquid chromatograph injection valve, 4, Figs. 3.4-3.7, (Analytical Accessories, Ltd.) and the tube are contained in a copper isothermal enclosure, Fig. 3.8, fitted with $\frac{1}{4}$-inch I.D. bifilar copper pipes, 5, for the circulation of a heating fluid. An ultra thermostat circulating bath (Lauda - model NB-S 15/12 with universal relay unit R2 electronics) is employed for this purpose. The outer surface of the block with pipes is coated with a thick layer of lead, it is then jacketed by a highly insulating material, 2.5 inches thick (ICI). Thermal equilibrium is reached throughout the block after several hours of circulation of the heat exchange fluid. The temperature of the diffusion tube is measured with the aid of four iron-constantan thermocouples, 6, inserted into the lead support through the four equidistant copper pillars. An extra thermocouple measures the temperature of the injection valve to ensure that it is at the same temperature as the diffusion tube. All thermocouple junctions are electrically insulated by 'shellac' coating so as to prevent metal-to-metal contact. The temperature stability and uniformity is approximately $\pm 0.05\ ^{o}K$ over a period of several hours.

The fluid flow through the diffusion tube is maintained by a gravity feed, 7, from a reservoir, 7', which is designed and arranged so that the liquid level change during the course of a single measurement is negligible, hence the flow velocity remains constant during a particular

run (Section 3.4). The liquid flows from the reservoir, 7, to the injection valve through a preheater, 8, fourteen turns of tubing identical to the diffusion tube wound on a copper rod, to ensure thermal equilibrium before injection of the solute sample, 10. The effluent from the diffusion tube is fed to a differential refractometer, 9, (Waters Associates Inc.) employed for the detection of the eluted distribution. More details about the design or specifications of various parts of the equipment and its operation and performance are contained in the following sections.

3.2 The Diffusion Tube

The diffusion tube is the most important part of the equipment and therefore requires special consideration both in the selection of the material, and in the selection of its dimensions.

3.2.1 Material of the tube

The material from which the tube is constructed must be inert so as to ensure that chemisorption and physisorption of the species do not occur, even though the liquid alkanes used are saturated hydrocarbons and inert themselves. A relatively high thermal conductivity is essential for the rapid and efficient transfer of heat to the liquids flowing through it, without any phsyical or chemical deformation of the tube at high temperatures. The theory of the method indicates that a smooth, straight tube of several metres with circular cross-section is required. However, for reasons of practicality, such a long tube must be coiled in a helix of as large as possible radius with negligible variation of cross-section along its entire length.

In order to meet all the requirements mentioned above, drawn 316 stainless steel tubing was chosen (Phase Separations Ltd.).

Fig. 3.1 - Schematic diagram of the diffusion equipment

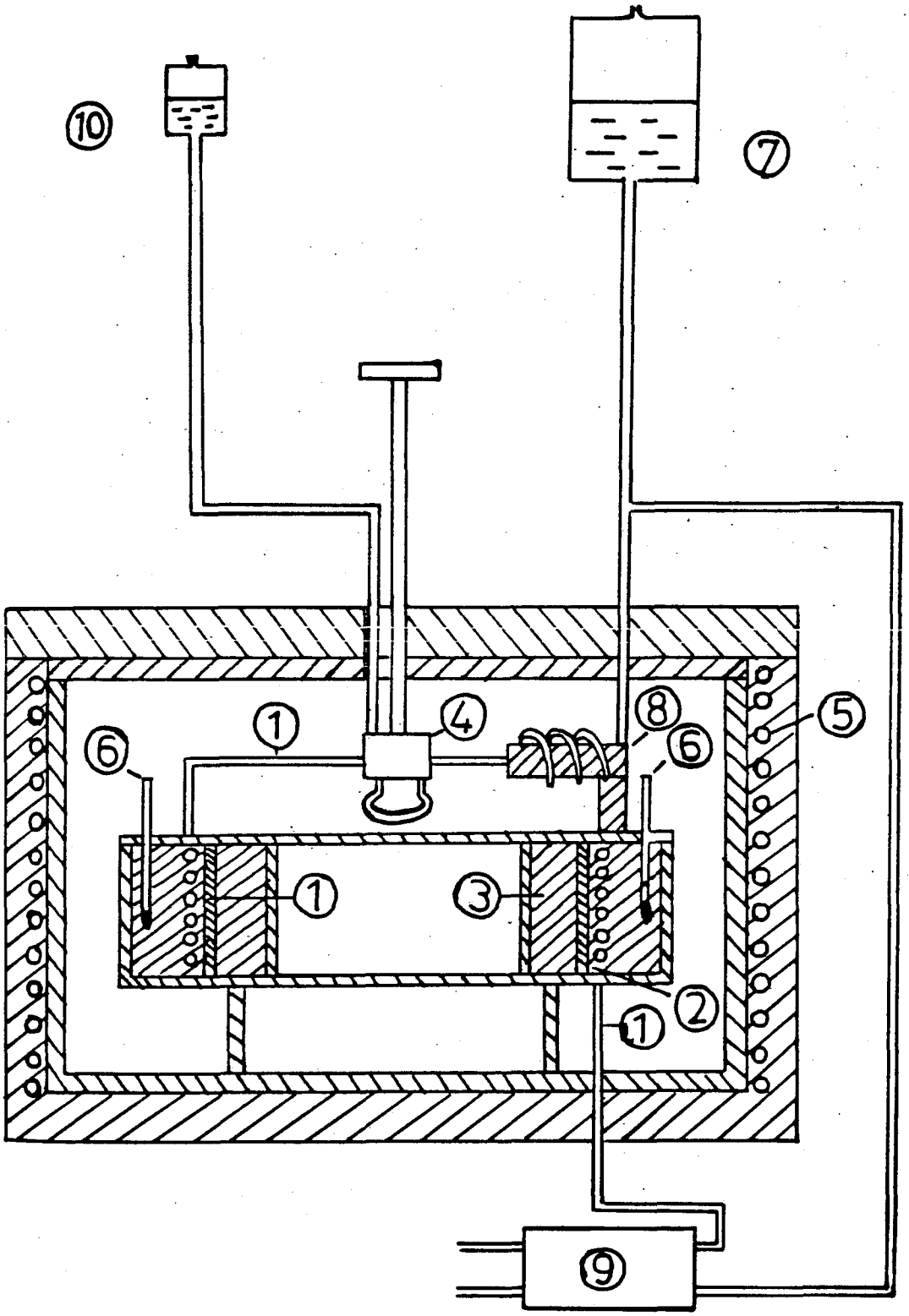

Fig. 3.2 - Flow diagram of the diffusion experiment

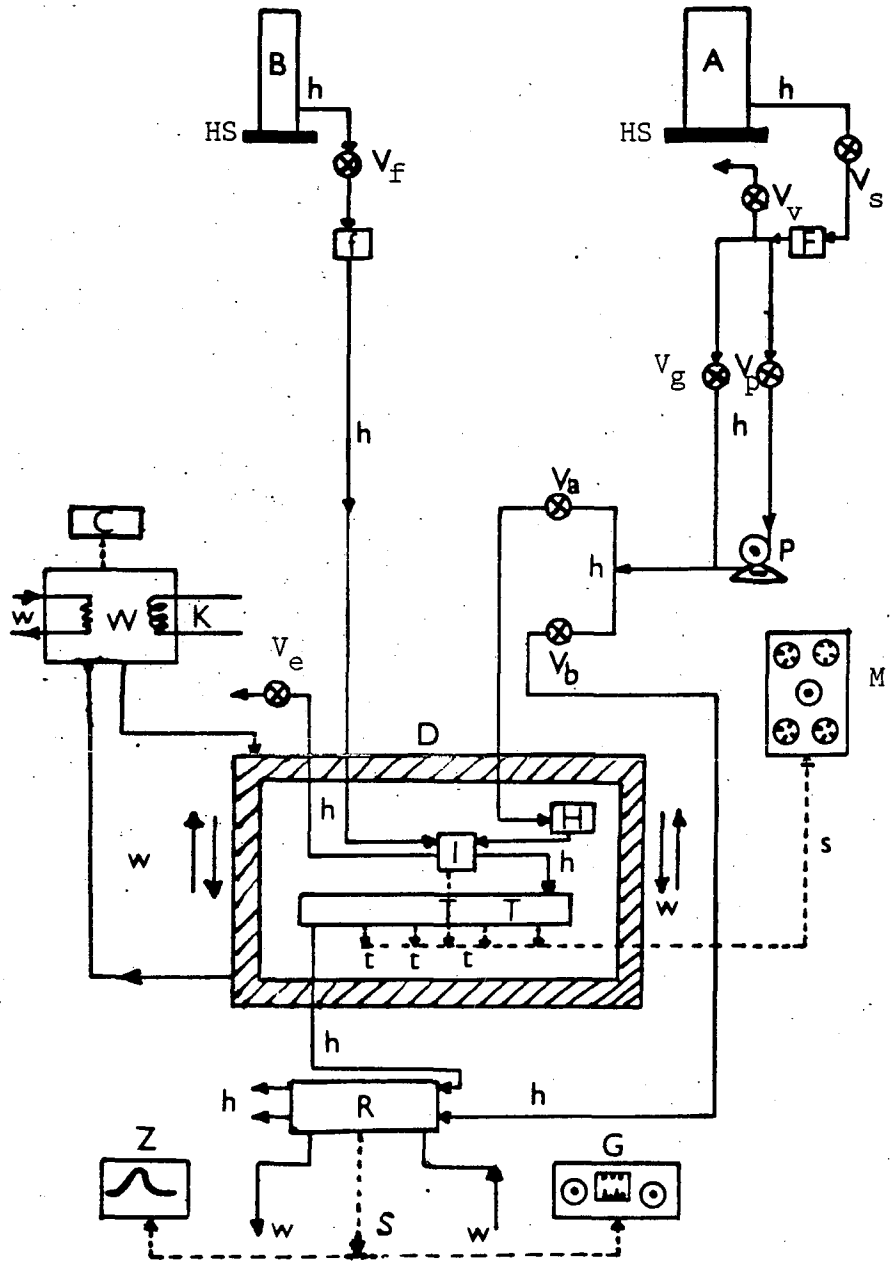

Fig. 3.3 - Schematic diagram of the injection value operation

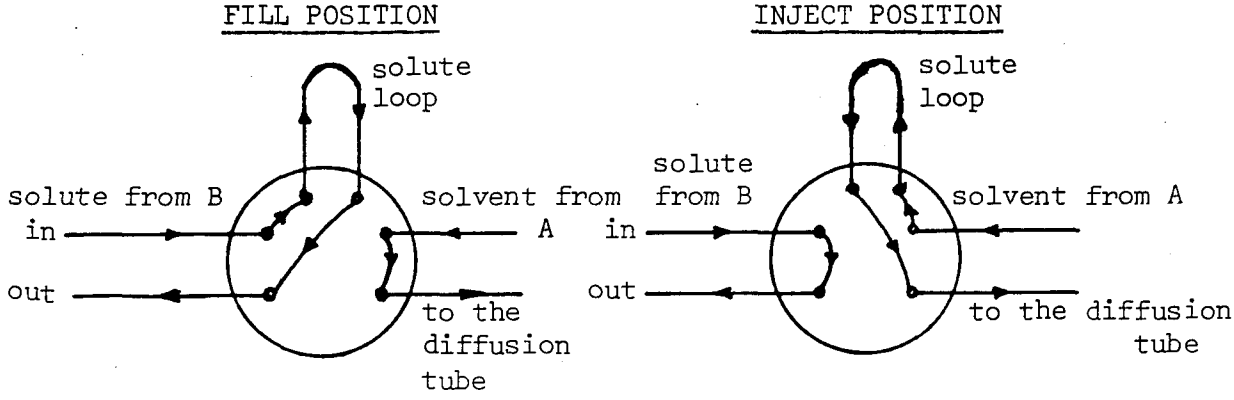

Description of Symbols of Fig. 3.2

A	solvent reservoir
B	solute reservoir
C	temperature control unit
D	the diffusion block
G	high precision potentiameter
H	the preheater
h	liquid hydrocarbon (n-alkane)
I	the injection valve
K	heating coils
M	the digital voltmeter and data logger
R	the refractometer
S	signal from the refractometer
s	signal from the thermocouples
T	the diffusion tube
V	miniature control valve
W	circulating bath (thermostatically-controlled)
w	cooling water
Z	chart recorder

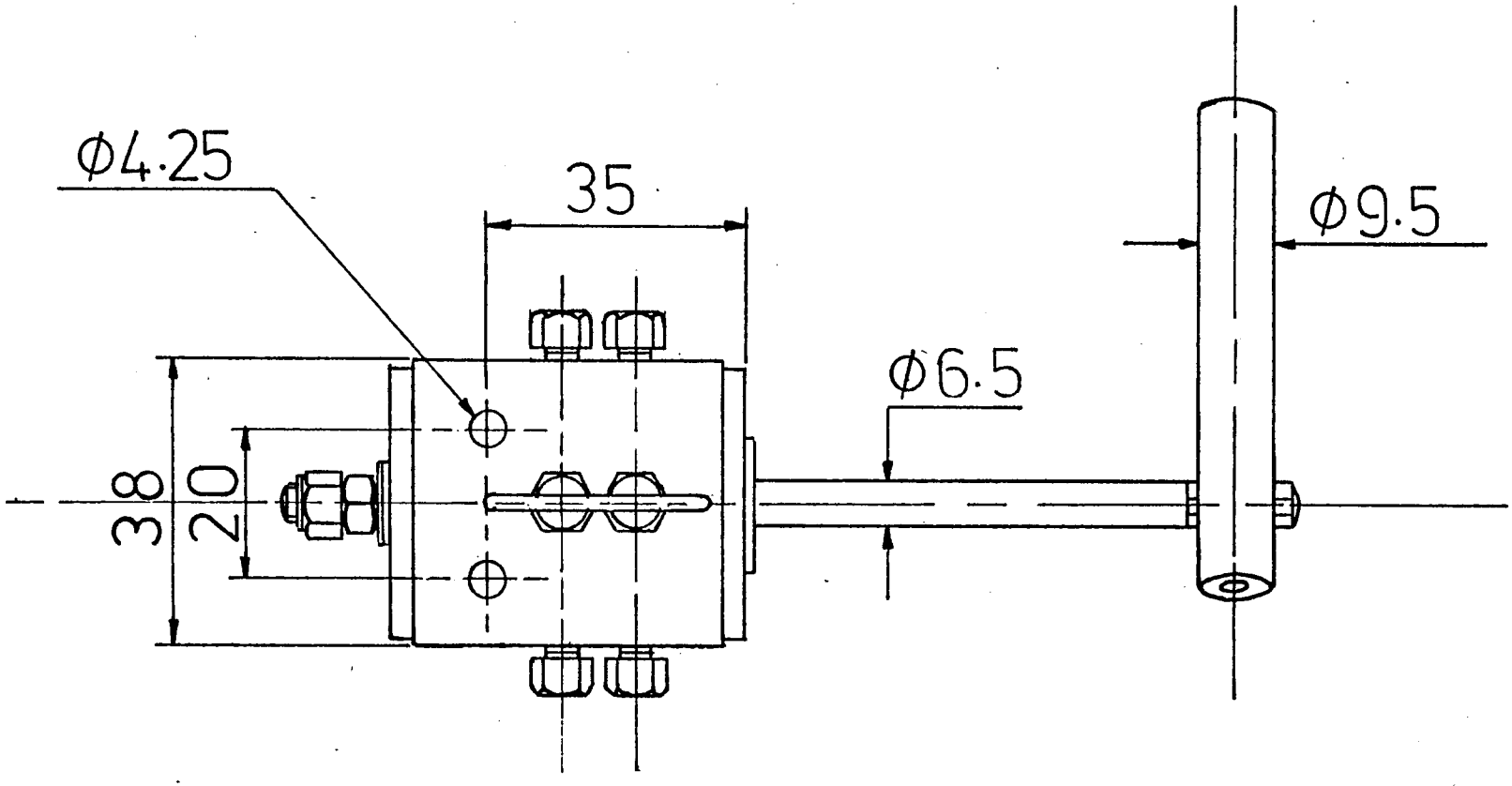

Fig. 3.4 - The injection valve
(all dimensions to scale in mm)

Fig. 3.5 - Rotation of the shaft through 90° for injection

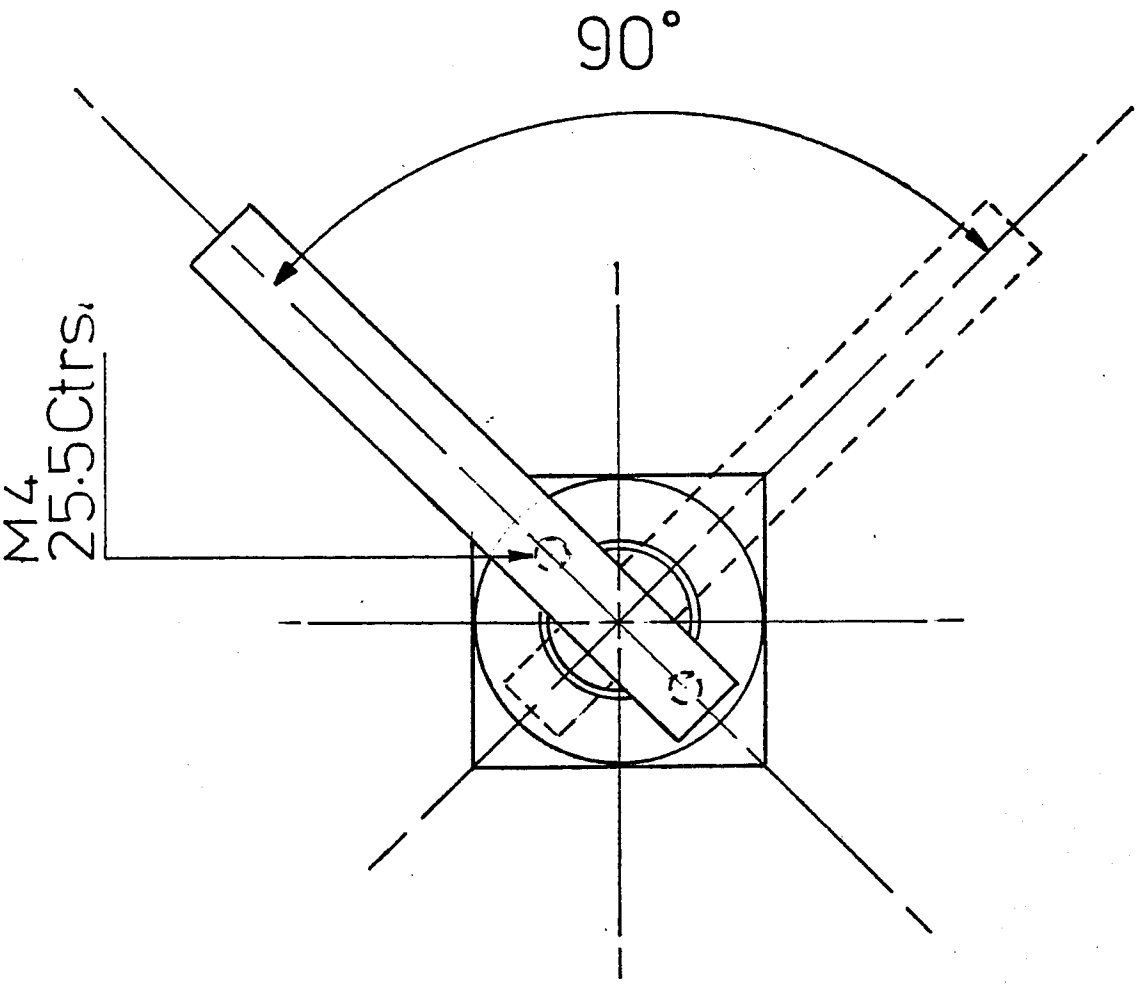

Fig. 3.6 - The injection valve with the sample loop

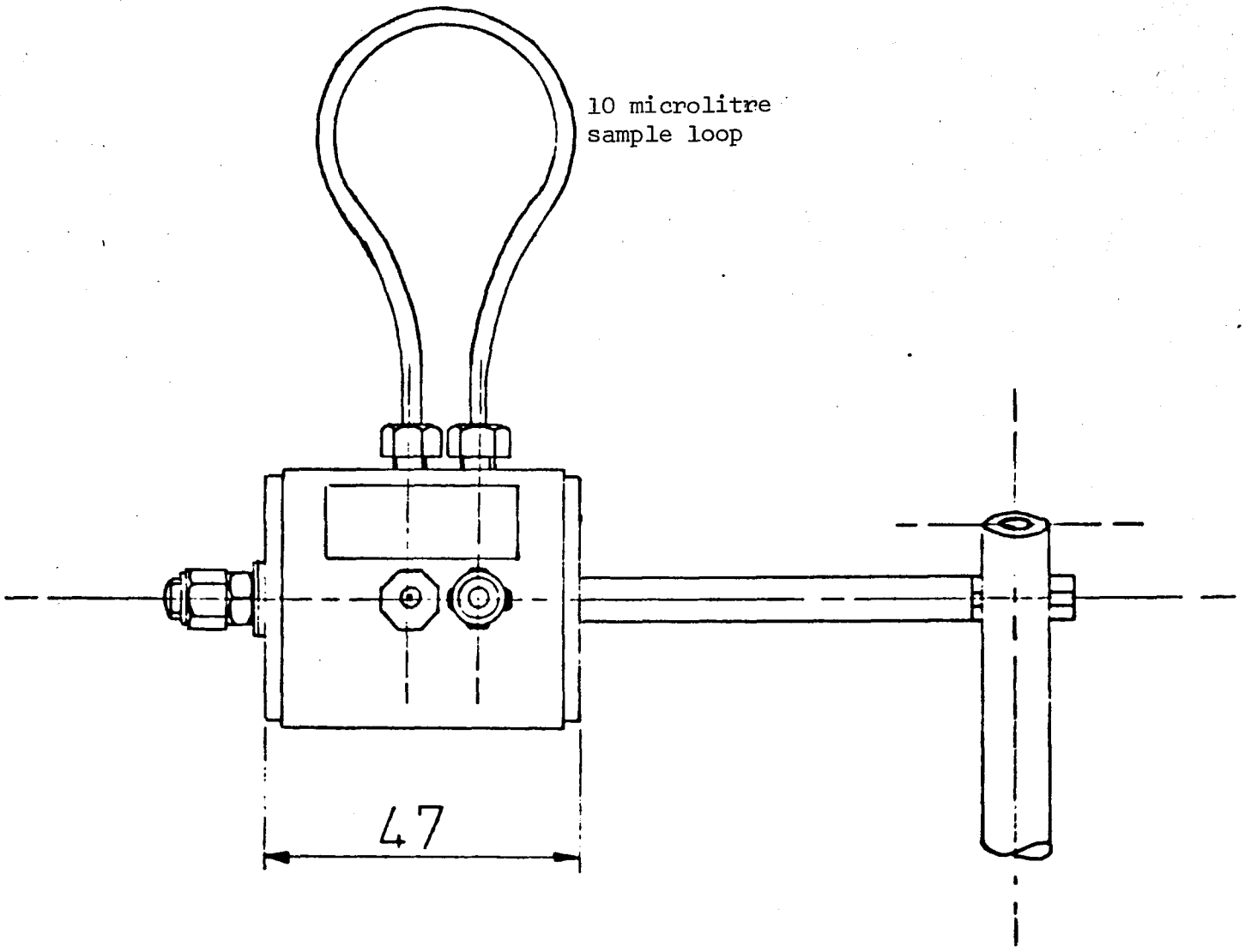

Fig. 3.7 - The conical rotor

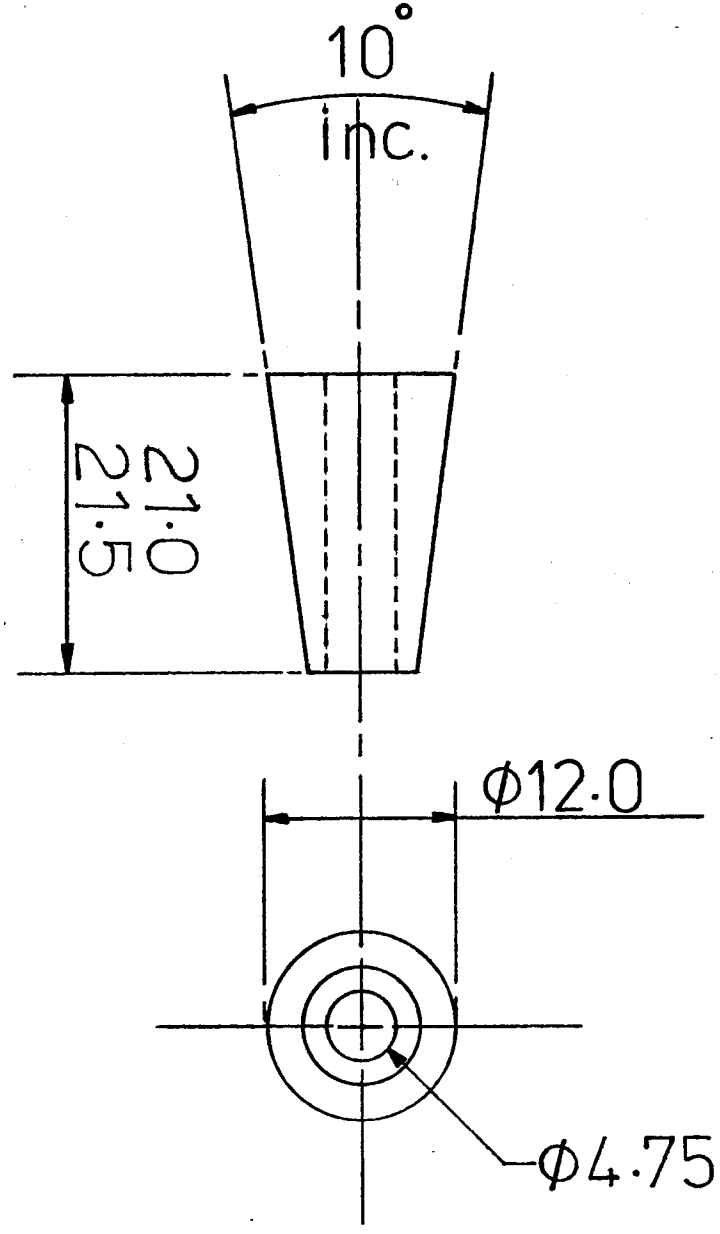

Fig. 3.8 - The isothermal diffusion block
(all dimensions in inches - not to scale)

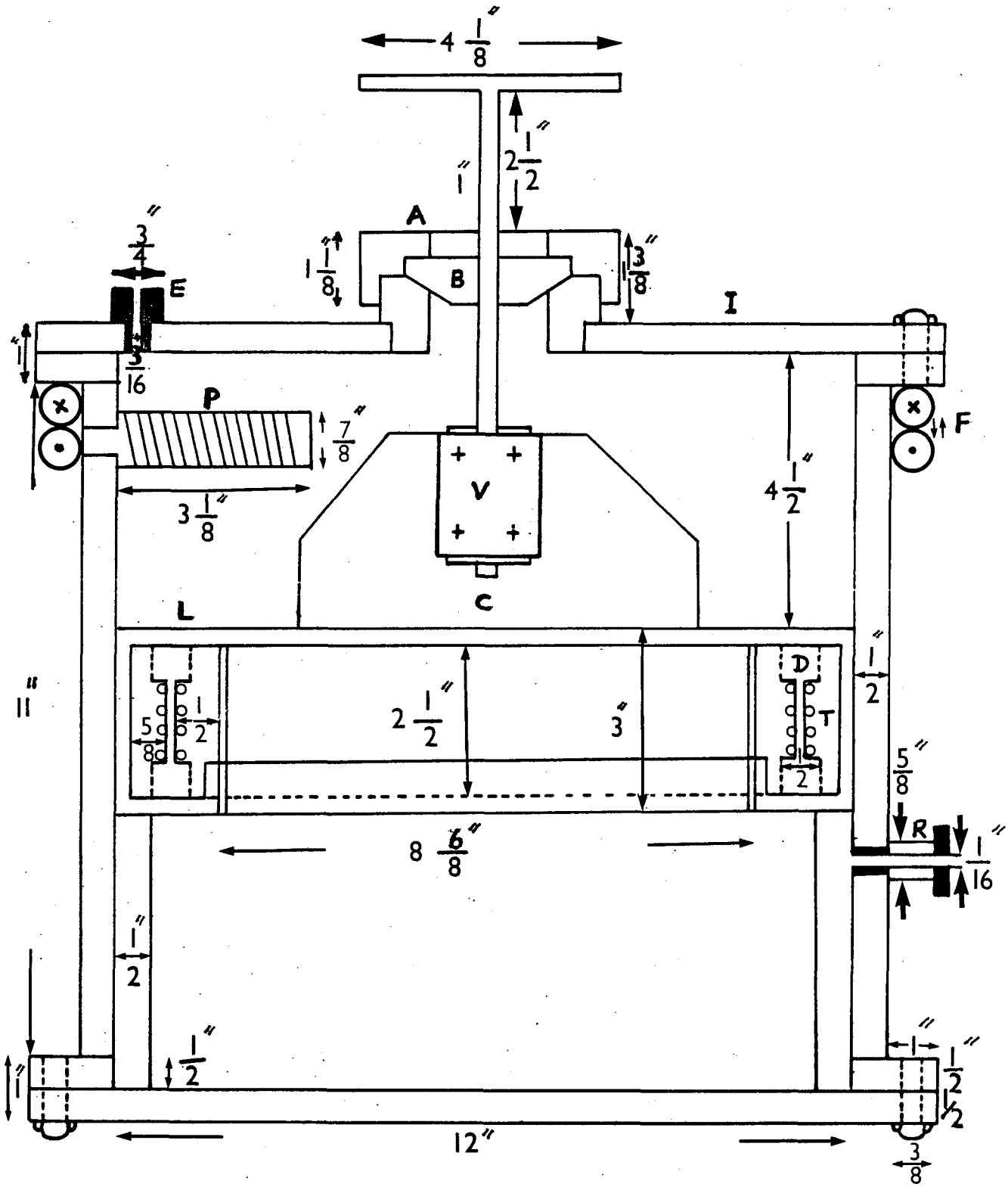

Description of Symbols of Fig. 3.8

A	copper screw cap
B	Teflon conical seal
C	copper bracket
D	copper pillar
E	port for solvent and solute tubes and thermocouples
F	bifilar copper tubes for heat exchange
I	copper block isothermal enclosure
L	diffusion tube assembly
P′	solvent preheater
R	diffusion tube exit port
T	diffusion tube
V	injection valve

3.2.2 Design study for optimum geometry of the diffusion tube

As indicated earlier, the object of the design study is to choose operating conditions such that the departures of the real apparatus from the ideal are either rendered negligible or small and amenable to calculation. Considering the theoretical analysis in Chapter 2, various criteria must be applied to the mathematical model for diffusion, i.e. to the working equation (2.46) in order to ascertain the appropriate conditions for operation. Because various requirements are often conflicting, it is necessary to search for the optimum dimensions of the diffusion tube subject to these constraints. The important constraints are:

(1) Time of measurement

(a) Immediately following the injection of a pulse of material into the flowing stream, there is a period of transient behaviour as shown by eqns (2.15-16). The time 't_a', which must elapse before the transient contributes a negligible amount to the final eluted concentration profile is given by Taylor/Aris criterion [18, 148, 149]

$$\bar{t}_a \geq \frac{10R_o^2}{D_{12}}$$

or

$$\zeta_o = \frac{R_o^2}{48D_{12}} \left(\equiv \frac{1}{t}\right) \leq 10^{-3}$$

This criterion satisfies condition (2.19) which makes the transient terms of eqns (2.15-16) unimportant. Thus, in order to operate in a region where the initial transient diffusion process is negligible, i.e. Taylor's region, the time of measurement should exceed the value '$\bar{t}_a$' which is a lower time limit in a given diffusion tube with a fixed diffusivity.

(b) On the other hand, for reasons of experimental convenience, and to achieve the necessary temperature stability, a measurement time should not be allowed to exceed four hours (14 Ks).

It has already been mentioned that the diffusion tube is several metres long. Thus it cannot be kept straight and thermostatted satisfactorily and must be coiled. This coiling is a cause of secondary dispersion effects [21, 29, 158, 160], but these can be kept within the desired limits by an appropriate choice of flow velocity. The diffusion peak must be attained within a few hours so that the measurement may be performed in a reasonable time. These latter points are significant, but cannot be allowed to dictate the design since, in principle, the tube coiling may be made of any necessary radius to render secondary dispersion negligible and the experiment duration can, if necessary, be extended.

(2) Reynolds Number 'Re' of the flow

In order to ensure that the flow velocity profile in the diffusion tube is parabolic as required for the laminar flow, conditions must be chosen to satisfy this requirement, i.e.

$$Re = \frac{2R_o U_o}{\nu} < 2000$$

(3) Dean's Number 'De' of the flow

The Dean's Number of the flow for the diffusion experiment is defined as

$$De = Re \cdot \left(\frac{R_o}{R_c}\right)^{\frac{1}{2}}$$

In order to eliminate the coiling effects, conditions must be chosen so that

$$[De^2.Sc] \leqslant 20$$

and that

$$100 \leqslant \left(\frac{R_c}{R_o}\right) \leqslant 500$$

Thus it is desirable to work with a Reynolds Number which is as low as possible. The results of the design calculations in Section 3.2.5 show that a suitable criterion is

$$Re \leqslant 6$$

(4) Magnitude of the corrections of the experimental moments

The ideal moments of the solute distribution are determined by correcting the experimental moments as shown in the previous Chapter. The relative corrections to the first moment are due to the injection volume V_i, the detector volume V_d, and the connecting tube volume V_o. They become insignificant if

$$\frac{V_i}{2\pi R_o^2 L} \leq 0.01$$

$$\frac{V_d}{\pi R_o^2 L} \leq 0.01$$

$$\frac{V_c}{\pi R_o^2 L} \leq 0.01$$

The corrections to the second and higher moments depend upon the square and greater powers of those for the first moment. Consequently, the corrections to these higher moments become negligible (less than 0.01%) when the corrections to the first moments are less than ±1% and ζ_o is less than 10^{-3}.

As explained in the previous Chapter, it is only possible to connect the diffusion tube to the refractometer by coupling the former with a connecting tube. This is a 316-stainless steel tube of 0.2 mm nominal internal diameter and 35 cm long, coupled with the diffusion tube by means of a zero dead-volume union. It is fixed to the refractometer and connected to the entrance of the sample cell internally which makes it difficult to handle. Corrections due to this effect will not introduce significant error if

$$\left(\frac{r_c}{R_o}\right)^2\left(\frac{\ell}{L}\right) = \frac{\pi r_c^2 \ell}{\pi R_o^2 L} = \frac{V_c}{\pi R_o^2 L} \leq 0.01$$

for $r_c = 10^{-4}$ m, $\ell = 0.35$ m and $\zeta_o \leq 10^{-2}$.

It can be seen that for $(\frac{r_c}{R_o})$ being one quarter, the error is less than 0.5% even if the ratio $\frac{\ell}{L}$ is as high as 7%. When $\frac{\ell}{L}$ is around 3.5% (L is around 10 metres) the error becomes less than 0.2%.

(5) Pressure drop 'ΔP' across the diffusion tube

The pressure drop across the diffusion tube [157, 175] is an additional parameter which must be evaluated for the conditions of the design. It cannot be used as a primary criterion of design since whatever pressure is required by the optimum design will have to be supplied. This pressure is the liquid head required to maintain the laminar flow and depends upon the ratio $\frac{L}{R_o^2}$ which must be taken into account for all practical purposes. The pressure drop required will constitute a primary constraint upon the design only if it is larger than can be withstood by available tubing materials.

Considering the above design criteria, it is evident that they conflict. Criteria (1)-(3) dictate that the tube radius must be as small as possible, whilst criteria (4) and (5) contradict this by requiring that it must be as large as possible. At the same time, the lower and upper limits of the measurement times in criterion (1), and of the ratio $\frac{R_c}{R_o}$ in criterion (3) bound the design parameters. Criteria (4) and (5) are themselves contradictory as far as the tube length is concerned, since it must be as long as possible for one, but as short as possible for the other.

However, the following sections show how all these conflicting conditions can be satisfied by proper design of an instrument which very nearly conforms to its ideal model.

3.2.3 Summary of the final design criteria and constraints

We may summarize the various primary design criteria and constraints before proceeding to the design itself. We require that:

$$\frac{10R_o^2}{D_{12}} \leqslant \bar{t} = \frac{L}{U_o} \leqslant 14\ Ks$$

$$\text{i.e. } \zeta_o = \frac{2\sigma_{id}^2 - \bar{t}_{id}^2 + \left[\bar{t}_{id}^4 + 4\bar{t}_{id}^2\sigma_{id}^2\right]^{\frac{1}{2}}}{(8\bar{t}_{id}^2 - 4\sigma_{id}^2)} = \frac{R_o^2}{48D_{12}}\left(\frac{1}{\bar{t}_{id}}\right) \leqslant 10^{-3}$$

$$Re = \frac{2R_oU_o}{\nu} \leqslant 6$$

$$\left[De^2.Sc\right] \leqslant 20$$

$$100 \leqslant \left(\frac{R_c}{R_o}\right) \leqslant 500$$

$$\frac{V_i}{2\pi R_o^2 L} \leqslant 0.01$$

$$\frac{V_d}{\pi R_o^2 L} \leqslant 0.01$$

$$\frac{V_c}{\pi R_o^2 L} \leqslant 0.01$$

$$\delta C_1 = \frac{N_1\left(\frac{5}{16} - \frac{1}{8\sqrt{\pi}}\right)}{\pi R_o^2(2\zeta_o U_o L t_{id})^{\frac{1}{2}}} \leqslant 10^{-3} \quad \text{(see Sections 2.6.1 and 2.7)}$$

3.2.4 The design calculations

For the purposes of the design, we have chosen ranges of values for most of the parameters of the diffusion tube and calculated for each set of conditions the Reynolds number, Re, the dimensionless group, $\left[De^2.Sc\right]$ and the corresponding coil effect on the second central moments of the distribution, the constant ζ_o, the minimum length and the pressure drop for the tube and the magnitude of each correction. Some parameters are known whilst others have been arbitrarily fixed at typical or reasonable values. The ranges of parameters employed are as follows:

Parameter	Range or value known or selected	Reference
D_{12}	$7 \times 10^{-10} - 7 \times 10^{-9}$ m^2 s^{-1}	6, 22, 39, 113, 144, 151, 176, 177
η	0.215 - 0.620 mN s m^{-2}	6, 22, 113, 144, 151, 177
ρ	620 - 850 kg m^{-3}	6, 22, 113, 144, 151, 171

Parameter	Range or value known or selected	Reference
ν	$3.5 \times 10^{-7} - 7.3 \times 10^{-7}$ m^2 s^{-1}	-
Sc	50 - 1000	-
L	1 - 26 m	-
$V_i = V_d$	10^{-8} m^3 = 10 μℓ	Analytical Acc. Co.
ℓ	0.35 m	Waters Ass. Inc.
r_c	1.143×10^{-4} m	Waters Ass. Inc.
R_o	$2 \times 10^{-4} - 1.2 \times 10^{-3}$ m	-

The range of densities, viscosities or the diffusion coefficients chosen spans that to be expected for the n-alkane binary mixtures in the liquid phase. The latter range covers a variety of other interesting and important systems [6,18,23,28,32,150,178,179], but if vastly different mixtures are to be studied then a new range of optimum conditions would have to be chosen. The changes of viscosities or densities of the fluids due to temperature or composition have been considered during the study, but they are relatively small and hence with little effects on the design.

3.2.5 The results of the design calculations

Figures 3.9 and 3.10 contain plots of the second central moments of deviation $\left(\frac{\sigma_s^2-\sigma_c^2}{\sigma_s^2}\right)$ due to tube coiling vs the dimensionless group $[De^2.Sc]$, and the Reynolds number $(Re^2 \leqslant 20\ (\frac{D}{\nu})(\frac{R_c}{R_o}))$ vs the ratio of the coil radius to that of the tube $\frac{R_c}{R_o}$ respectively. They reveal that for the expected range of diffusion coefficients, i.e. $7 \times 10^{-10} - 7 \times 10^{-9}$ m^2 s^{-1}, and for a suitable ratio of the radii, i.e. $\frac{R_c}{R_o} = 325$, constraints (2) and (3) are always satisfied when the Reynolds number is less than six. In order to ensure that the instrument operates in the Taylor/Aris asymptotic region, $\zeta_o = \frac{R_o^2}{48D_{12}}(\frac{1}{\bar{t}}) \leqslant 10^{-3}$ according to criterion (1a), the minimum time of measurement was determined by plotting ζ_o vs $\bar{t}$ for various tube

radii (2×10^{-4} - 1.2×10^{-3} m) as shown by Figs. 3.11 and 3.12. From these two Figures it is clear that the tube with a radius greater than 6×10^{-4} m would inevitably result in measurement times in excess of 14 Ks disobeying constraint (1b). Figure 3.13 contains the result of similar calculations for an average tube radius of 4×10^{-4} m covering the whole diffusivity range. The minimum time of measurement for each case corresponds to a minimum length of the diffusion tube which was then calculated. The result is presented by Fig. 3.14 which, together with the two previous Figures, give the possible range of the tube radii as 1.5×10^{-4} m $\lesssim R_o \lesssim 6 \times 10^{-4}$ m.

A plot of the total corrections, as in constraint (4), against the tube radius for three tube lengths of 6 m, 13 m and 20 m is contained in Fig. 3.15. It indicates that the corrections become less than 1% for the shortest tube only if $R_o \gtrsim 4 \times 10^{-4}$ m, whilst the longer tubes introduce corrections of less than ±0.5% for the same radius. The difference of the corrections for the latter tubes become insignificant (less than 0.05%) for $R_o \gtrsim 4 \times 10^{-4}$ m and so the shorter tube (13 m) is a better choice. Finally, Fig. 3.16, referring to constraint (5), contains the result of calculations of the pressure drop across various tubes, i.e. L = 6 m, 13 m and 20 m, R_o = 0.2 mm, 0.4 mm and 0.6 mm, at various times of measurement and for the most viscous fluid mixture ($D_{12} = 7 \times 10^{-10}$ m^2 s^{-1}, $\nu = 7.3 \times 10^{-7}$ m^2 s^{-1}) considered in this work. It is evident from this plot that for measurement times in the range 2.5 - 14 Ks, and for the two tubes whose dimensions are L = 20 m, R_o = 0.6 mm and L = 13 m, R_o = 0.4 mm, the maximum pressure drop required is 0.23 m of the liquid which is easily achieved. Due to the material cost and convenience ($R_c = 325\ R_o$), the smaller tube is preferred.

Fig. 3.9 - The effect of tube coiling on the variance of solute distribution. Constraints (2) and (3).

σ_s^2 = variance of the straight tube

σ_c^2 = variance of the coiled tube

De = Dean's No.

Sc = Schmidt No.

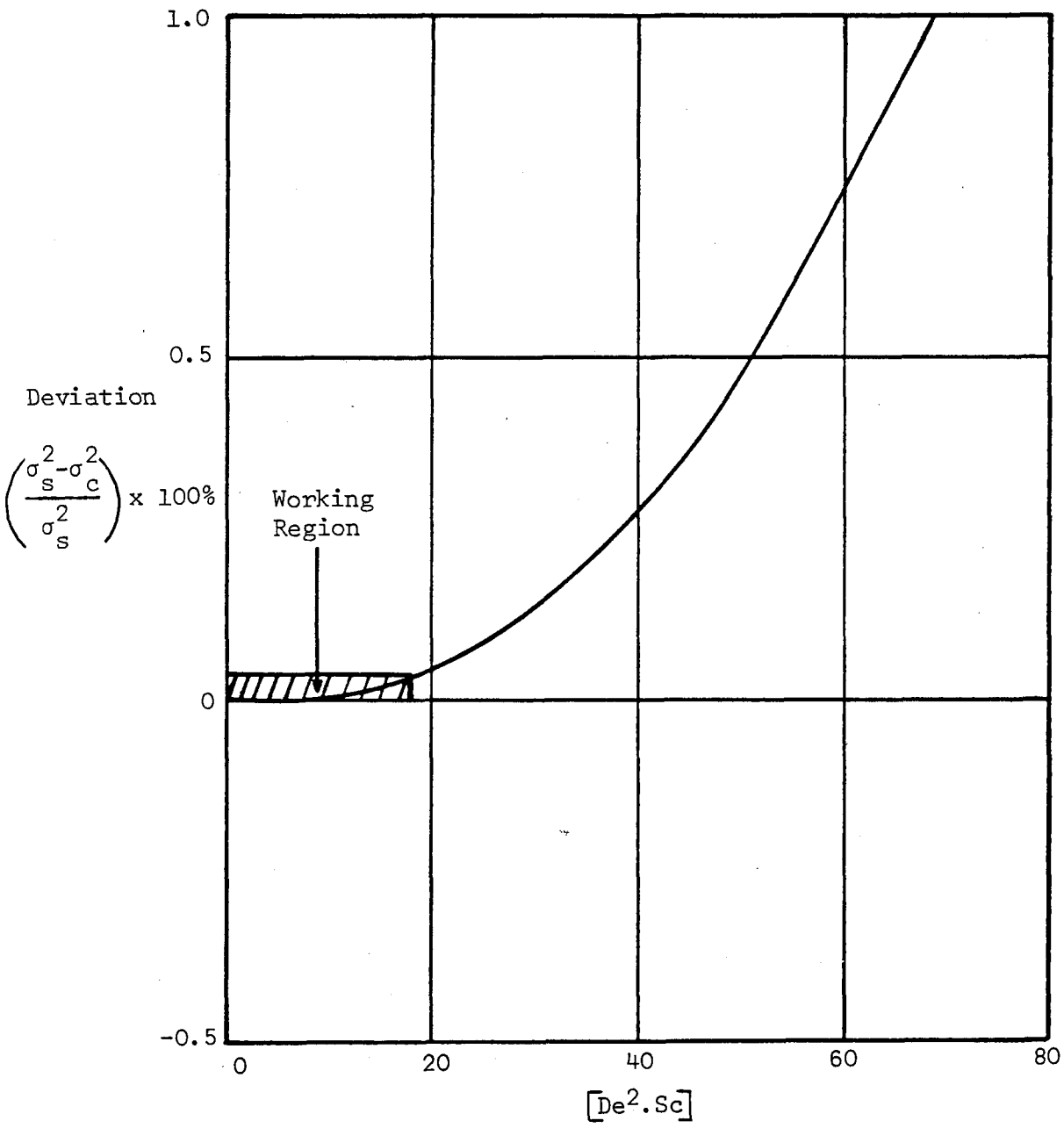

Fig. 3.10 - Reynolds No. vs Ratio $(\frac{R_c}{R_o})$

Constraints (2) and (3)

Re = Reynolds No.

$\frac{R_c}{R_o}$ = Ratio of the coil radius to tube radius

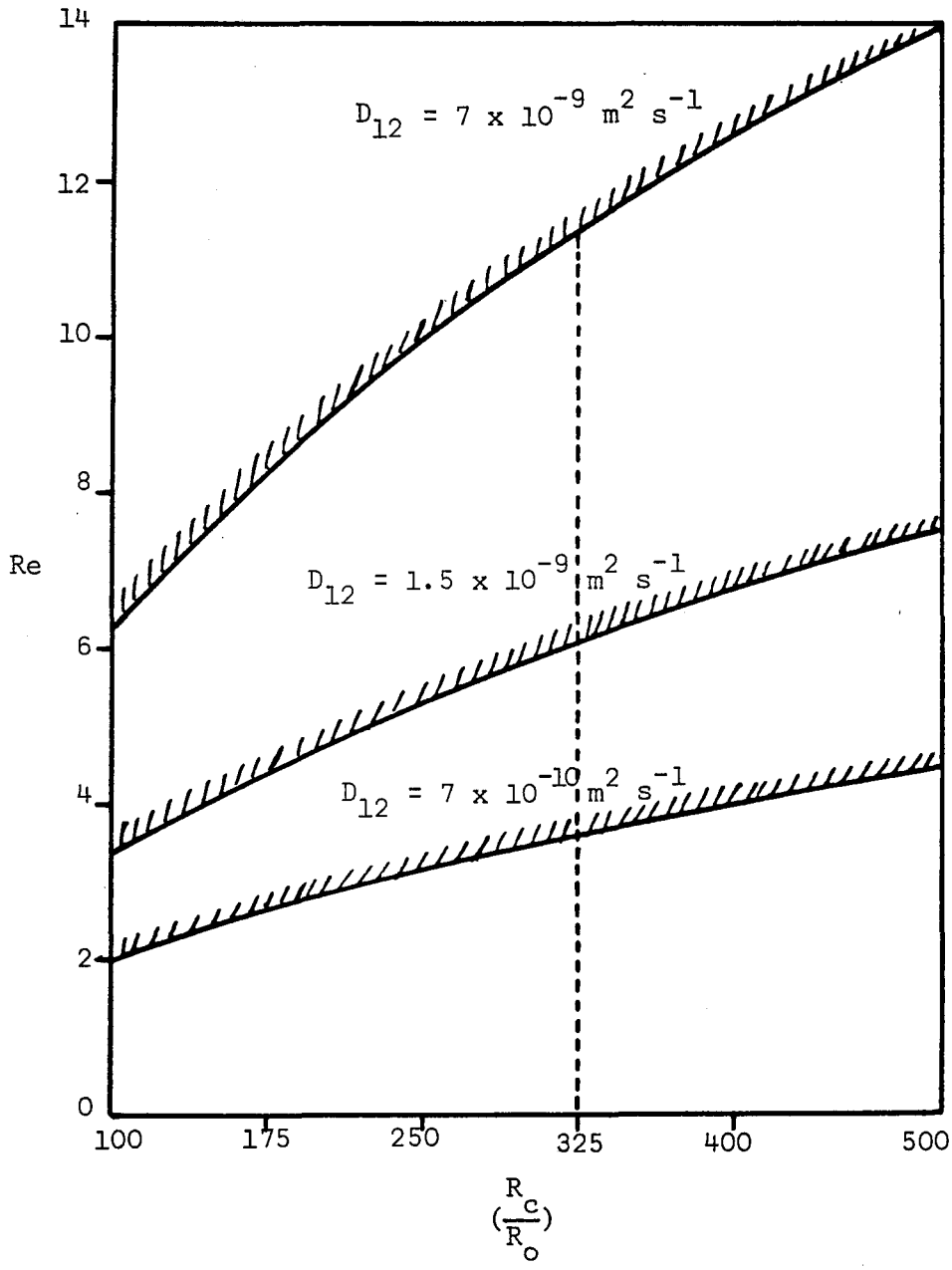

Fig. 3.11 - Taylor/Aris criterion for various tube radii and $D_{12} = 7 \times 10^{-9}$ m^2 s^{-1}. Constraint (1).

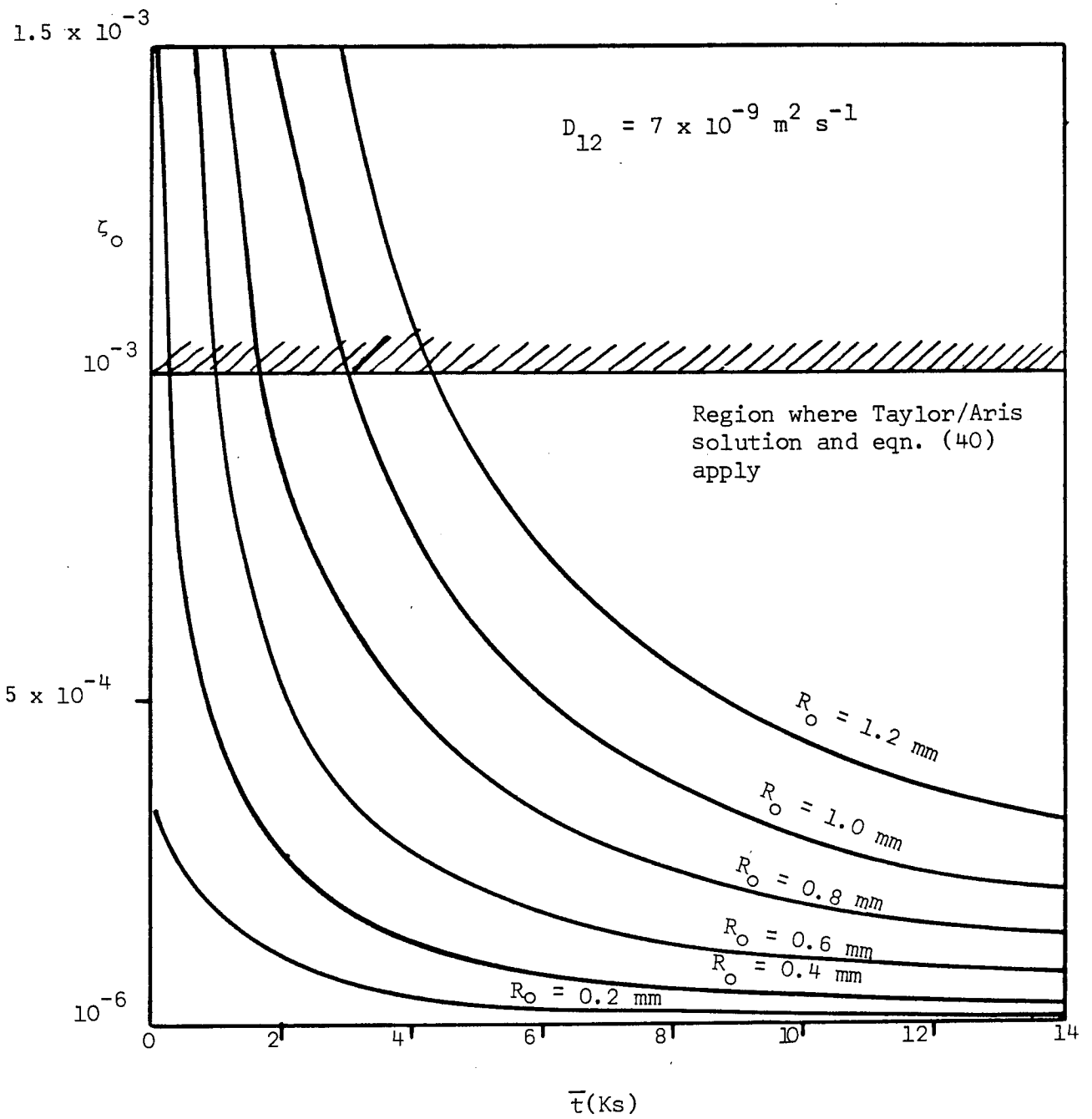

Fig. 3.12 - Taylor/Aris criterion for various tube radii and $D_{12} = 7 \times 10^{-10}$ m^2 s^{-1}. Constraint (1).

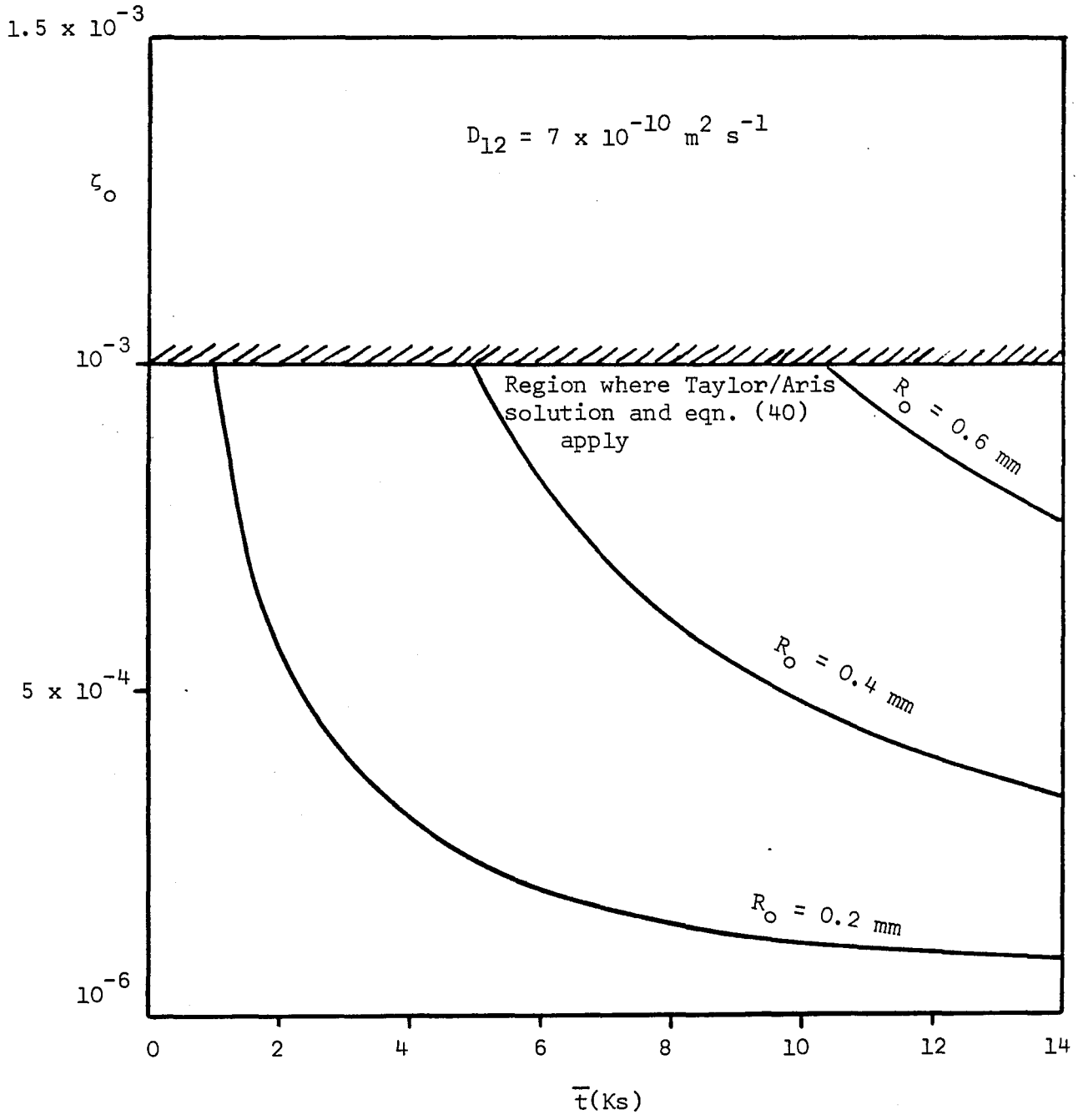

Fig. 3.13 - Taylor/Aris criterion for 0.4 mm tube and $D_{12} = 7 \times 10^{-10} - 7 \times 10^{-9}$ m^2 s^{-1}. Constraint (1)

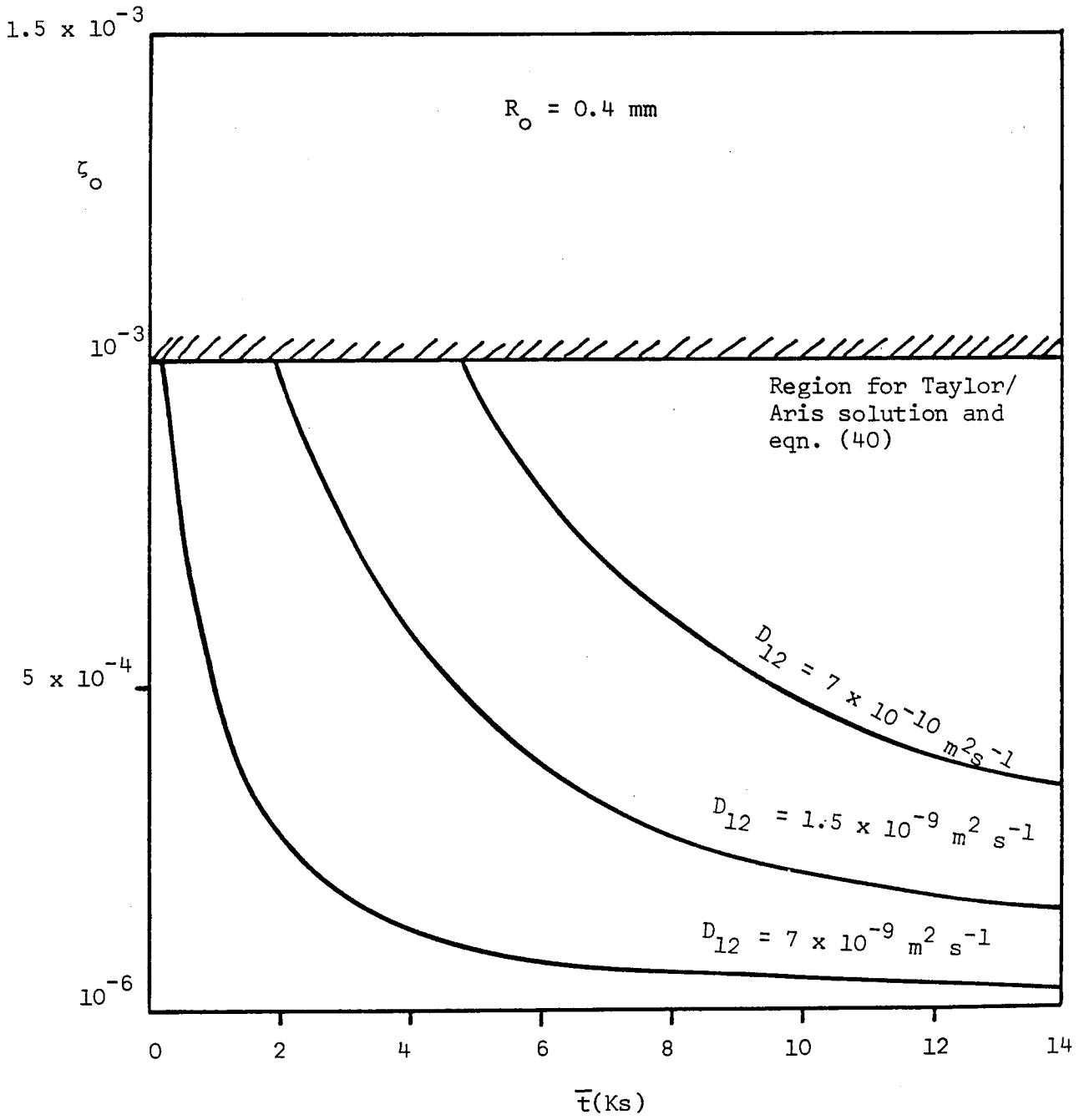

Fig. 3.14 - Minimum tube length required vs tube radius
Constraint (1)

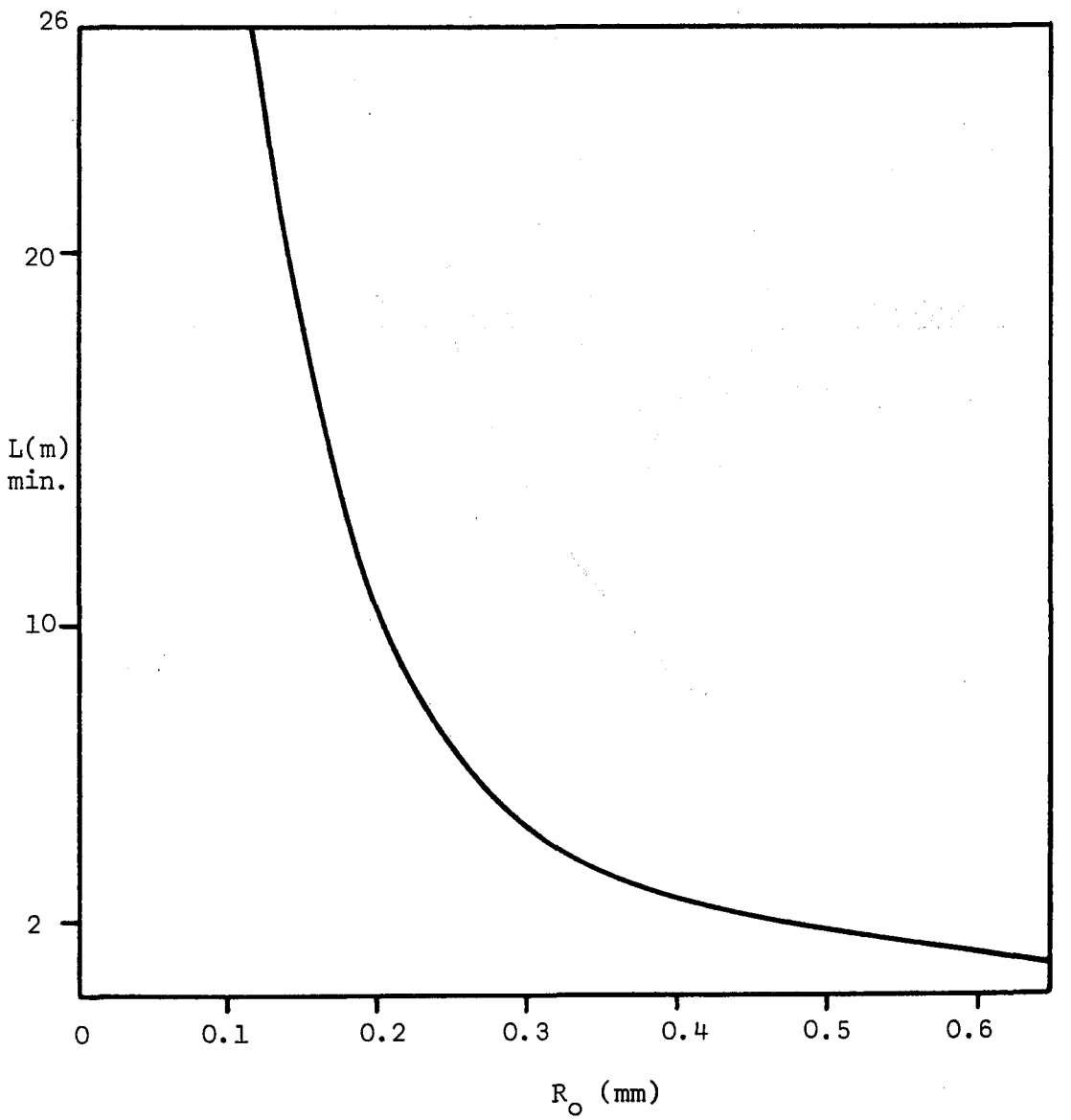

Fig. 3.15 - Total % correction for tubes of different geometry
Constraint (4)

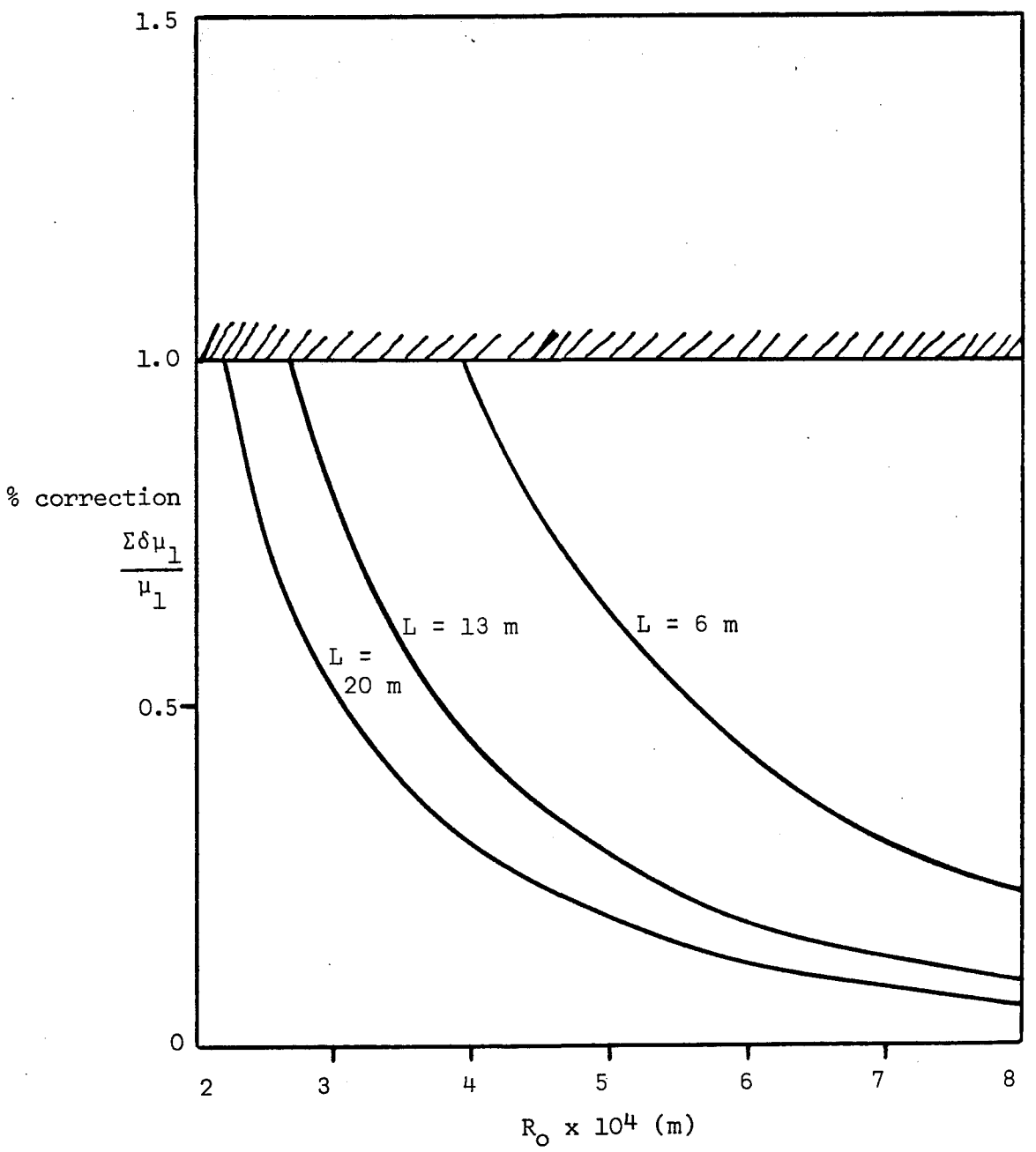

Fig. 3.16 - Pressure drop across the tube vs flow time
Constraint (6)

—·— R_o = 0.2 mm

——— R_o = 0.4 mm

----- R_o = 0.6 mm

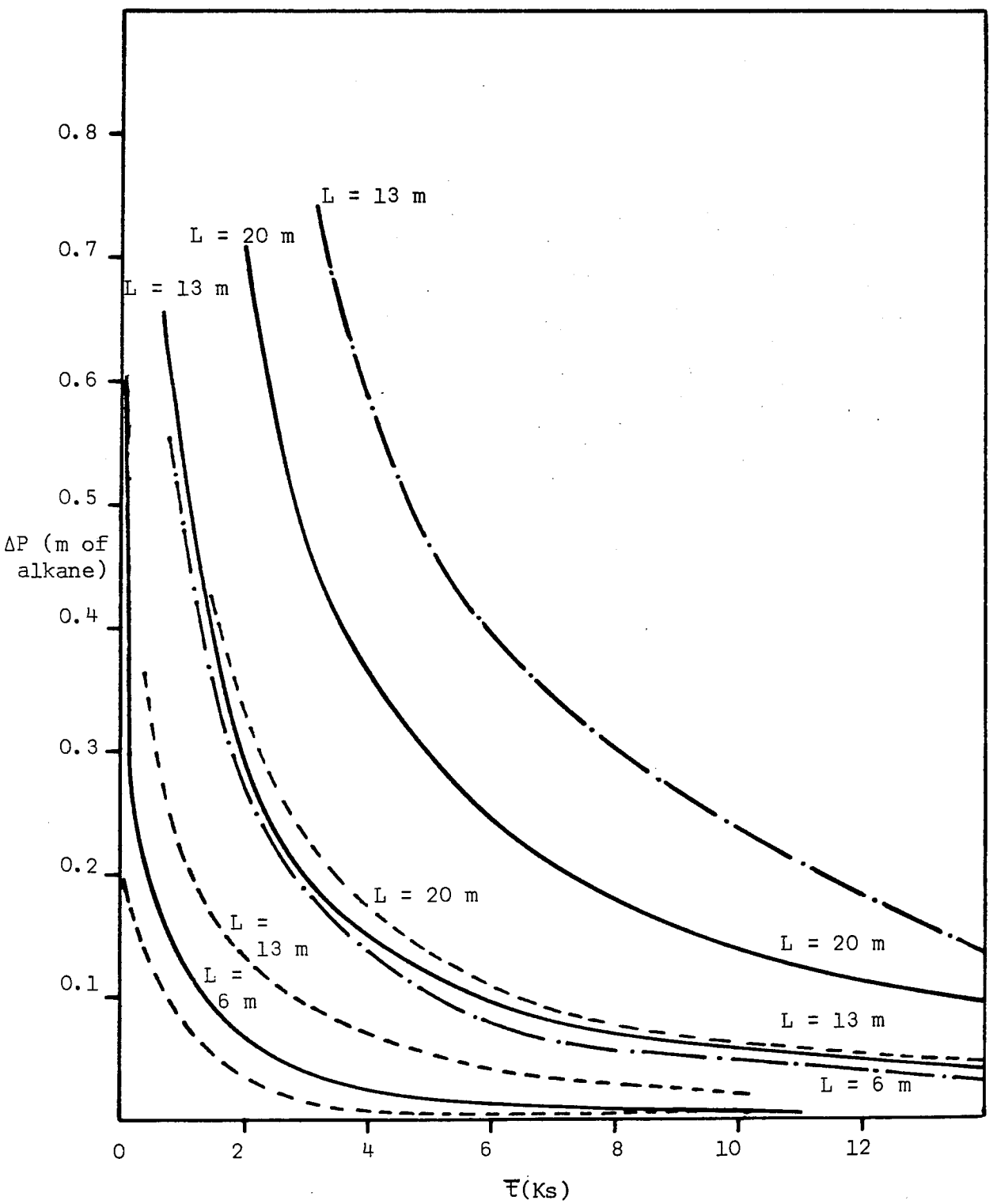

3.2.6 Conclusions of the design study

For diffusion coefficients in the range $7 \times 10^{-10} - 7 \times 10^{-9}$ m^2 s^{-1}, the optimum working design parameters for the diffusion apparatus are:

(1) Length of the diffusion tube - 13 m;

(2) Radius of the diffusion tube - 4×10^{-4} m;

(3) Injection volume - 10^{-8} m^3;

(4) Connecting tube volume - 1.43×10^{-8} m^3;

(5) Detector volume - 10^{-8} m^3;

(6) Coil radius - 0.13 m;

(7) Measurement times 3.5 - 14 Ks (1 - 4 hours).

Calculations of the effect of tube coiling have been carried out for the conditions selected above (Fig. 3.9). They indicate that for a coil radius of 0.13 m the error introduced into the diffusion coefficient is no more than ±0.05% for a diffusion coefficient of 7×10^{-10} m^2 s^{-1} with a flow time of 7 Ks. Clearly for other diffusivities a flow time can always be found for which the effect is negligible, with higher diffusion coefficients requiring shorter flow times, while still satisfying the other constraints.

3.2.7 The apparatus constants

The following Table contains the dimensions of the diffusion tube and other elements of the apparatus.

The length of the diffusion tube (316 annealed stainless steel, 1/16" nominal O.D.) employed for this work was determined in several independent measurements; it was then coiled very carefully round a copper former into a helix of known diameter. Its volume was determined gravimetrically by filling the tube with distilled water several times and weighing. The average cross-sectional area of the tube was then found from which the average tube radius was calculated. The geometry of the

diffusion tube was such that the computed errors due to non-uniformity and ellipticity (Sections 2.6.2 and 2.6.3) were found to be negligible (< ±0.01%).

Tube length L (m)	13.219 ± 0.038%
Tube radius R_o (m)	4.099×10^{-4} ± 0.24%
Cross-section area $A_o(m^2)$	5.278×10^{-3} ± 0.47%
Coil radius R_c (m)	13.175×10^{-2} ± 0.04%
Injection volume V_i (m^3)	1×10^{-8}
Detector volume V_d (m^3)	1×10^{-8}
Connecting tube volume V_c (m^3)	1.430×10^{-8} ± 0.5%

3.3 The Injection Valve

This is a six-port chromatography valve (modified P/N 30.100 - Analytical Accessories Ltd.) which is bracket-mounted to the copper former panel as shown by Fig. 3.8. It is constructed from the highest grade material for corrosion resistance and inertness. The body and connections are made from EN58J (316) stainless steel and the rotating conical insert from an inert fluoropolymer. The conical insert is spring-loaded to compensate for changes in ambient temperature. Figures 3.4 - 3.7 are diagrams of the modified value with the necessary dimensions and a schematic diagram of its operation is given by Fig. 3.3.

Although the value was recommended for operations up to 250°C at atmospheric pressure, it failed to operate satisfactorily at temperatures around 40°C. Bubbles were detected by the refractometer and shown as spikes on the chart recorder only during the elution of a peak which was thereby distorted. After a long investigation, it was found that the formation of bubbles was due to valve leakage, liquid degassing, possible

surface tension effects and temperature/pressure changes during injection. The flow is disturbed only for a few seconds when the valve is switched from fill to the inject position (Fig. 3.3). Various tests with sample loops of 10 - 500 μℓ showed that even a small change in the liquid temperature or pressure during injection was sufficient to produce bubbles particularly at elevated temperatures. Therefore the valve was modified and tested for satisfactory operation in the desired temperature range of 20 - 70°C.

The modifications made in the valve design (Figs. 3.4 - 3.7) and its operation which proved to eliminate the above effects, and hence bubble formation, are as follows:

(i) All "special" tube fittings connected to the solvent and solute ports were replaced by identical fittings with the same I.D. as the diffusion tube.

(ii) A 10 μℓ (10^{-8} m^3) sample loop made from the same tube as (i) was used.

(iii) The valve internal ports were carefully redrilled to suit the "special" tube fittings described in (i).

(iv) The normal rotating conical insert (Rulon - glass filled teflon) was replaced with a stainless steel/ceramic reinforced fluoropolymer conical insert whose liquid ports (grooves) had the same volume as before but were cut deeper into the insert (Fig. 3.7).

(v) Both the solvent and the solute were degassed, filtered and preheated before entering the valve by gravity flow.

(vi) The sample loop is filled by gravity feed supply as shown by Figs. 3.1 - 3.3, which indicate that the loop is always under the same liquid head irrespective of the valve position.

When the modified injection valve was operated in the desired temperature range, normally distributed peaks with steady lines were obtained.

3.4 The Gravity Feed Reservoir

The gravity feed reservoir is a driving head device designed to be constant to within ±0.1% in order to maintain the flow velocity constant to within this value during the course of a single measurement. It can easily be shown that a suitable cylindrical reservoir, similar to an aspirator, can be used for this purpose. The change in the driving head, δh, is then given by

$$\delta h = \left(\frac{2R_o}{d}\right)\left(\frac{L}{h}\right) \qquad (3.1)$$

where, in this work,

$R_o = 4 \times 10^{-4}$ m; L = 13 m; h = 1-2 m liquid head and $d = 12 \times 10^{-2}$ m diameter of the 2.5 litre reservoir.

Therefore the flow velocity is constant to within ±0.06% during a single measurement.

3.5 The Temperature Measuring Device

The diffusion tube temperature is measured by means of the four thermocouples described in Section 3.1. The thermocouples, with a common reference junction (the ice point), were connected through a rotary selector switch to the instrument by means of a Zone Box [180]. Each thermocouple could then be connected to the precision vernier potentiameter (type 7568 Pye & Co. Ltd.) through the rotary multi-switch (type 651858 Cambridge Instrument Co. Ltd). The potentiameter (4 V D.C., 1.01860 V standard cell), in conjunction with a D.C. power supply (Harrison 6289A, Hewlett Packard), thermal compensator and photocell amplifier (type 5214, Tinsley Co. Ltd.) and a scalamp galvanometer (Pye & Co. Ltd), was used to measure the E.M.F. values correct to ±0.5 micro-

volts. The uncertainty in the temperatures measured is therefore estimated as ±0.01 K. The diffusion tube temperature stability and uniformity was found to be approximately ±0.05 K over a period of several hours.

The thermocouples (iron/constantan) were calibrated against a standard N.P.L. calibrated platinum resistance thermometer (± 1 mK). The thermometer was shielded by a copper tube and immersed in a well-stirred thermostat bath. Each thermocouple was inserted into the copper shield and for a particular bath temperature "Θ_B" the corresponding E.M.F. generated and the resistance of the thermometer "R_θ" were recorded by means of a Smith Double Bridge (No. 3, type 41623/f1.11, Tinsley & Co. Ltd.). The bath temperature was computed from a correlation for pure platinum recommended by the International Practical Temperature Scale [181, 182] which reads

$$\Theta_B(^\circ C) = 0.42682W^3 + 8.39235W^2 + 232.7017W - 241.82095 \qquad (3.2)$$

where

$$W = \frac{R_\theta(\Omega)}{R_o(\Omega)} \qquad (3.3)$$

$$R_o(\Omega) = 25.7507$$

such that for $\Theta_B = 100^\circ C$, $R_{100}(\Omega) = 1.3927$.

The resistance of the thermometer varied from 27Ω to 39Ω for a bath temperature variation of $10^\circ C$ to $150^\circ C$, the corresponding generated E.M.F.'s being in the range 0.5 - 8 mV.

With the aid of a least square analysis, it was found that the data obtained as a result of thermocouple calibration, i.e. the E.M.F. generated at a particular temperature "Θ", fits the quadratic equation

$$\text{E.M.F.} = 2.04938005 \times 10^{-4}\Theta^2 + 5.195329338 \times 10^{-2}\Theta - 1.800460368 \times 10^{-2} \qquad (3.4)$$

with a standard deviation s.d. = ±0.001. Thus the E.M.F. of each thermocouple could be read at any time from the potentiameter and the corresponding temperature (in degrees centigrade) was easily computed from the above equation. Under isothermal conditions, the mean of the computed values (Θ_m) was taken to be the mean temperature of the liquid flowing through the diffusion tube. This procedure was repeated over different time intervals during each measurement so as to ensure the temperature stability and uniformity.

3.6 The Refractive Index Detector

Detection of the dispersed solute was achieved by means of a refractive index detector (Model R403 Waters Associates) capable of detecting refractive index changes as small as 10^{-8}. A metering piston pump (type 196-0042-055 Milton Roy) was used to provide high flow rates through the diffusion tube and the refractometer when it was necessary to clean the system. Due care was being taken to ensure the linearity of the detector which is verified later in Section 3.10. The signal from the differential refractometer (maximum 10 mV) was recorded on a variable speed chart recorder and also on a magnetic cassette tape with the aid of a digital voltmeter (DYMEC). Data recorded by the latter method was processed by a PDP11 computer for the calculation of the diffusion coefficients with a higher accuracy than their graphical values obtained by the former method [18, 27a].

3.7 Working Equations

3.7.1 Density of the liquid mixture

From the theoretical analysis in Chapter 2 it is evident that accurate calculation of the reference composition, i.e. equation (2.130) for x_{1r} composition to which a measured diffusivity refers, accurate knowledge of density of the injection sample "ρ_i" and of the flowing stream

"ρ_f" are essential. Due to the scarcity of such data, particularly in a wide temperature/composition range, densities of the binary mixtures used in this work were calculated from the literature values for the pure components [6, 22, 151] and a known correlation. It has been shown [39] that the density of a binary mixture of pure liquids 1 and 2, both under the same condition, is given by

$$\frac{1}{\rho_{1,2}} = \frac{w_1}{\rho_1} + \frac{w_2}{\rho_2} + w_1 w_2(\delta V) \tag{3.5}$$

where ρ, w and δV denote the density, weight fraction and change in volume of the liquid mixture respectively. For binary liquid mixtures of n-hexane to n-dodecane, the value of δV is relatively negligible [39] and equation (3.5) reduces to

$$\frac{1}{\rho_{1,2}} = \frac{w_1}{\rho_1} + \frac{w_2}{\rho_2} \tag{3.6}$$

Substituting for "w" in terms of mole fraction "x" and molecular weight "M", equation (3.6) becomes

$$\rho_{1,2} = \frac{\rho_1 \rho_2 (M_1 x_1 + M_2 x_2)}{\rho_1 M_2 x_2 + \rho_2 M_1 x_1} \tag{3.7}$$

Therefore the densities of the injection sample and the flowing stream, $(\rho_{1,2})_i$ and $(\rho_{1,2})_f$ respectively, may be accurately calculated [39] from equation (3.7) for known temperatures and compositions.

3.7.2 The reference composition

It can easily be shown from equations (2.130) and (3.7) that the reference composition for a diffusion coefficient is given by

$$x_{1r} = x_{1f} + V_i \left[\frac{5/16 - \frac{1}{8\sqrt{\pi}}}{\pi R_o^2 (2E_o \bar{t})^{\frac{1}{2}}}\right] \left[\left(\frac{\rho_1 M_2 x_{2f} + \rho_2 M_1 x_{1f}}{\rho_1 M_2 x_{2i} + \rho_2 M_1 x_{1i}}\right) x_{1i} - x_{1f}\right] \tag{3.8}$$

Equation (3.8) was used in order to compute the values of x_{1r} for the measured diffusivities and compare them with x_{1i}, x_{1f}, the compositions of the injection sample and flowing stream respectively (sec.3.10.3).

3.7.3 Ideal moments of the distribution and the diffusion coefficients of liquids

The results of Chapter 2 show that the moments of the observed distribution of injected solute differ from those of the ideal distribution. We can, therefore, identify the experimental moments of the distribution with the ideal values plus three correction terms, all the others being comparatively insignificant. The three correction terms arise from the non-zero volumes of the injected pulse, detector and the connecting tube. The observed experimental moments are given by

$$(\mu_1')_{expt} = \frac{\int_o^L t\, c(t)dt}{\int_o^L c(t)dt} = (\bar{t})_{expt} = \frac{L}{U_o}(2\zeta_o+1) \qquad (3.9)$$

$$(\mu_2)_{expt} = \frac{\int_o^L (t-\bar{t})^2 c(t)dt}{\int_o^L c(t)dt} = (\sigma^2)_{expt} = \left(\frac{L}{U_o}\right)^2 (8\zeta_o^2+2\zeta_o) \qquad (3.10)$$

where μ_1' and μ_2 represent the first raw moment and the second central moment of the distribution. Similarly, the higher moments can be determined from which the skewness "Sk" and kurtosis "Ku" are calculated.

$$Sk = \frac{\mu_3}{(\mu_2)^{3/2}} = \frac{\mu_3}{\sigma^3} \qquad (3.11)$$

$$Ku = \frac{\mu_4}{(\mu_2)^2} - 3 = \frac{\mu_4}{\sigma^4} - 3 \qquad (3.12)$$

Thus we can write

$$(\mu_1')_{id} = (\mu_1')_{expt} - \sum_{n=1}^{3} \delta_n(\mu_1') = \bar{t}_{id} = \bar{t}_{expt} - \sum_{n=1}^{3} \delta\, \bar{t}_n \qquad (3.13)$$

and

$$(\mu_2)_{id} = (\mu_2)_{expt} - \sum_{n=1}^{3} \delta_n(\mu_2) = \sigma^2_{id} = \sigma^2_{expt} - \sum_{n=1}^{3} \delta\, \sigma_n^2 \qquad (3.14)$$

with

$$\delta\bar{t}_1 = \delta\bar{t}_{1b} = \delta_1(\mu_1') = \frac{L}{U_o}\left(\frac{V_d}{\pi R_o^2 L} - 3\zeta_o\right) \qquad (3.15)$$

$$\delta\bar{t}_2 = \delta_2(\mu_1') = \frac{L}{U_o}\left(\frac{V_i}{2\pi R_o^2 L}\right) \qquad (3.16)$$

$$\delta\bar{t}_3 = \delta_3(\mu_1') = \frac{L}{U_o}(1+2\zeta_o)\left(\frac{r_c}{R_o}\right)^2\left[\frac{\ell}{L} + \zeta_o\left(1 + \frac{r_c^2}{R_o^2}\right)\right] \quad (3.17)$$

so that for $\zeta_o < 10^{-3}$

$$\frac{\sum_{n=1}^{3}\delta\bar{t}_n}{\bar{t}} = \frac{\sum_{n=1}^{3}\delta_n(\mu_1')}{(\mu_1')_{id}} \doteq \frac{V_i + 2(V_c+V_d)}{2\pi R_o^2 L} = \frac{t_i + 2(t_d+t_c)}{2\bar{t}} \quad (3.18)$$

where

$$t_i = \frac{V_i}{\pi R_o^2 U_o} \; ; \; t_c = \frac{\pi r_c^2 \ell}{\pi R_o^2 U_o} = \frac{V_c}{\pi R_o^2 U_o} \; ; \; t_d = \frac{V_d}{\pi R_o^2 U_o}$$

and with

$$\delta\sigma_1^2 = \delta\sigma_{1b}^2 = \delta(\mu_2) = \left(\frac{L}{U_o}\right)^2\left[\left(\frac{V_d}{\pi R_o^2 L}\right)^2 + 2\zeta_o\left(\frac{V_d}{\pi R_o^2 L}\right) - 13\zeta_o^2\right] \quad (3.19)$$

$$\delta\sigma_2^2 = \delta_2(\mu_2) = \frac{1}{12}\left(\frac{L}{U_o}\right)^2\left[\frac{V_i}{\pi R_o^2 L}\right]^2$$

$$\delta\sigma_3^2 = \delta_3(\mu_2) = \left(\frac{L}{U_o}\right)^2(2\zeta_o+8\zeta_o^2)\left(\frac{r_c}{R_o}\right)^4\left\{\frac{\ell}{L} + \frac{1}{2}\left(\frac{r_c}{R_o}\right)^2\zeta_o\left[3\left(\frac{r_c}{R_o}\right)^2 + 2\right]\right\} \quad (3.21)$$

Hence the experimental moments were corrected in this way so that the working equations for the ideal case could be used to evaluate the diffusion coefficient from equation (2.43) which reads

$$D_{12} = \frac{A_o}{24\pi\bar{t}_{id}}\left[\frac{(1+4\sigma_{id}^2/\bar{t}_{id}^2)^{\frac{1}{2}} + 3}{(1+4\sigma_{id}^2/\bar{t}_{id}^2)^{\frac{1}{2}} + 2\sigma_{id}^2/\bar{t}_{id}^2 - 1}\right]\left[\tfrac{1}{2} + \tfrac{1}{2}(1-\delta_a)^{\frac{1}{2}}\right]$$

The Reynolds number Re and the Dean's number De for the flow were computed from equations

$$Re = \frac{2\,R_o L}{\nu\,\bar{t}_{id}} \quad (3.22)$$

and

$$De = Re\left(\frac{R_c}{R_o}\right)^{-\frac{1}{2}} \quad (3.23)$$

3.8 Analysis of the Eluted Distributions

In this section, we present a concise description of analysis of the eluted distributions by outlining the problems involved and their appropriate solutions. An algorithm describing a computer program written to

carry out the analysis of the recorded experimental data (250-350 points per experimental run) is included.

3.8.1 Data analysis: problems and their solutions

(1) The recorded data from the digital voltmeter was in binary decimal code which had to be decoded, i.e. translated into its octal equivalent suitable for PDP11 FORTRAN processing.

(2) Characters including "D" for the delay time, plus or minus signs, and the signal output (1 μV - 10 mV) were considered acceptable and stored in an array of integers. The maximum of the signal was then found by the conventional method of comparing the recorded points. Hence coarse errors (e.g. an unreasonably high or low voltage value due to a momentary disturbance, the existence of more than one maximum, etc.) were detected and dealt with such that if the recorded data of an experimental run was seriously in error (e.g. more than one maximum) then that run was totally rejected for analysis.

(3) Because, in practice, it is impossible to zero the output from the refractometer exactly, the baseline of the recorded signal is not identically zero. Furthermore, it is occasionally possible for the baseline to drift slightly during the course of a measurement because of very small temperature or pressure changes. For these reasons, the raw data have been adjusted to obtain a zero baseline on either side of the eluted peak. For this purpose, the baseline has been assumed linear between arbitrary points some distance on either side of the peak, and recorded signal adjusted to zero according to the equation

$$(C_n)_{true} = (C_n)_{recorded} - \left(\frac{C_E - C_B}{t_E - t_B}\right)(t_n - t_B)$$

where C denotes the D.V.M. readings in mV at time t in seconds and $(C_E - C_B / t_E - t_B)$ is the slope of the recorded baseline deviating from the horizontal zero baseline as illustrated below.

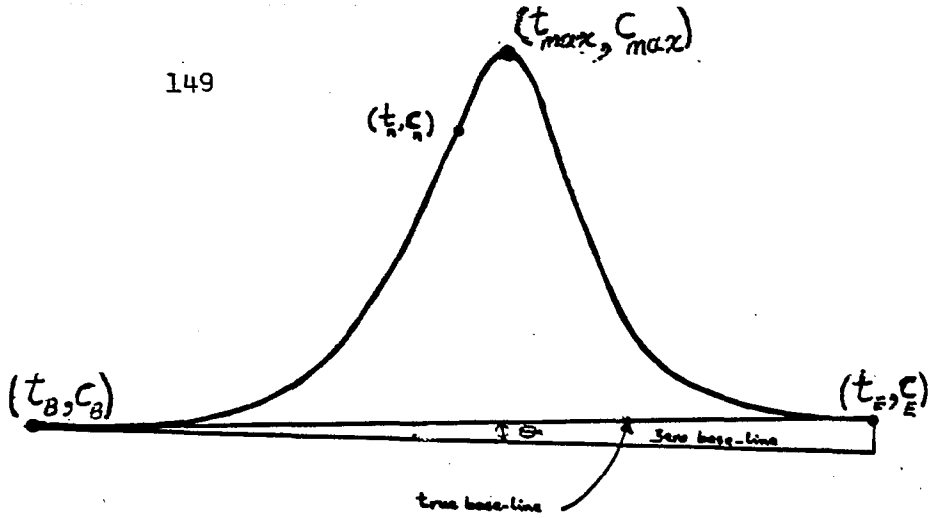

(4) The moments of the eluted distribution can be determined by numerical quadrature (e.g. Simpson's Rule) from the recorded data. However, this procedure is of only moderate accuracy ([30]; ±5% in this work) because the contributions to the integrals from the wings of the distribution are large, and the relative uncertainty in the recorded voltage is also large in these regions. Furthermore, because the integrations extend to infinity, it becomes practically necessary to introduce arbitrary finite upper and lower limits to the integration. The choice of these limits can lead to gross errors in the computed moments of the distributions. Therefore, the most crucial task in data analysis was to find a new method of calculating the variance of distributions, hence the corresponding diffusion coefficients, to a high level of accuracy ($\lesssim$ 0.5%). This was achieved by means of three subroutines contained in the main computer program.

First Subroutine: Simpson's Rule for numerical quadrature was used to compute the first four moments and hence the skewness and kurtosis of the resulting peaks from equations (3.9)-(3.12). It is worthwhile recording that the Gaussian nature of the dispersion peak is confirmed by zero skewness and the detector's linearity is assured by zero kurtosis. Thus if their computed values were close to zero (within the precision of the D.V.M.) the run was accepted and the calculated values of "$\bar{t}$" and "σ^2" were retained to be used as the initial values "$\bar{t}_1$" and (σ_1^2) in the next

routine. Otherwise the experimental run was totally rejected.

Second and Third Subroutines. The refined data was smoothed by "non-linear regression" so as to fit the normal distribution function in the following way

$$F(t) = A_1 \exp^{-\left[\frac{(t-\bar{t})^2}{2\sigma^2}\right]} = C_{calc} \qquad (3.24)$$

The distribution function F(t) is evaluated for selected values of "A_1", "$\bar{t}$" and "σ^2" and compared with the refined experimental values by calculating the deviation

$$\frac{\sum_{n=1}^{n}\left[(C_n)_{expt} - (C_n)_{calc}\right]^2}{n} = f(t) \qquad (3.25)$$

The third subroutine is called in order to minimise function f(t) by iteration, choosing new values of "A_1", "$\bar{t}$", and "σ^2". Because the procedure is iterative it requires a starting value of "C_{calc}" which is determined by taking the values of "$\bar{t}$" and "σ^2" from the first routine described above as an initial guess. Evaluations of f(t) are continued until "A_1", "$\bar{t}$" and "σ^2" are within the tolerance required. For high accuracy, many function evaluations may be required but the procedure ensures that eventual convergence is obtained. Precautions are taken to prevent convergence to a local, and therefore spurious minimum, and to prevent an excessive step being taken. Since the procedure is based on minimising the least square function f(t), dependent on three variables "A_1", "$\bar{t}$" and "σ^2" by non-linear regression, it is identical to that of determining the minimum of a curved surface. Once this minimum is found, the function evaluation is terminated and the corresponding "$\bar{t}$" and "σ^2" are the required experimental moments of the eluted distribution.

Essentially no difference was observed ($\sim \pm 0.2\%$) in the value of "$\bar{t}$", the dispersion time, when determined experimentally by volumetric flow rate measurements and computed by the "non-linear regression" method. The variances of the eluted distributions have been calculated with a reproducibility of ±0.5% leading to the experimental results given in Chapter 4. Also the result of the test measurement described in Section 3.10.4 shows that the calculated value of the diffusivity for octane-

dodecane mixture is practically identical (± 1%) to the literature value [39]. We can therefore conclude that the "non-linear regression" method is correct and very accurate as well as being fast and direct.

3.8.2 Algorithm for data analysis

In order to present a concise summary of the analysis of the experimental data, we include in this section an algorithm describing a computer program written to carry it out.

1. Decode the recorded data for FORTRAN processing.

2. Detect coarse errors. If the error is serious, reject the experimental run completely, otherwise discard and proceed to the next step.

3. Refine the recorded experimental data by carrying out the baseline correction.

4. Compute the first four moments and hence the skewness and kuortosis of the resulting distribution from equations (3.9)-(3.12) by using Simpson's Rule for numerical quadrature.

5. If the values of skewness/kuortosis are not close to zero (i.e. not within the DVM precision) reject the experimental run. Otherwise use the "non-linear regression" technique, taking $\bar{t}$ and σ^2 from step 4 as an initial guess, in order to determine the values of $(\bar{t})_{expt}$ and $(\sigma^2)_{expt}$ for the resulting distribution.

6. Calculate an approximate binary diffusion coefficient D_{12}^a of the liquid mixture by substituting $(\bar{t})_{expt}$ and $(\sigma^2)_{expt}$ for $(\bar{t})_{id}$ and $(\sigma^2)_{id}$ in equation (2.43) respectively.

7. Compute the ideal moments $(\bar{t})_{id}$ and $(\sigma^2)_{id}$ of the resulting distribution from equations (3.13)-(3.21).

8. Calculate the true binary diffusion coefficient D_{12} of the liquid mixture from equation (2.43).

9. Calculate the Reynolds number "Re" and the Dean's number "De" for the flow from equations (3.22) and (3.23) respectively.

10. Compute "θ_m", the mean temperature of the liquid mixture flowing through the diffusion tube, from equation (3.4).

3.9 Experimental Procedure

The liquids, n-hexane, n-heptane and n-octane, were supplied by BDH with a minimum purity of 99 - 99.5%. They were degassed and purified [14, 184, 185] before use, by alternate freezing and pumping to high vacuum followed by batch rectification (Fig. 3.17), until they showed a purity better than 99.9% when standardised against a reference 99.99% pure. The mixtures for the flowing stream and the samples for injection were prepared gravimetrically and the mole fractions were computed with a typical associated uncertainty of ±0.0005. The samples for injection usually differed in mole fraction from the composition of the flowing stream by 0.1. The density and viscosity of the liquids were obtained from the experimental data [22, 151, 183].

Figure 3.2 presents a flow diagram of the experimental arrangements made for the diffusion process. The temperature controller (C) which consists of a contact thermometer connected to a universal relay electronics unit, is set to the desired value. The controller is capable of maintaining the bath temperature constant to within ±0.01 K. Water bath (W) circulates the heat exchange water through the fitted copper pipes round the diffusion block (D) continuously. Thermal equilibrium was reached overnight by the water circulation which maintained the block isothermal for the whole day. The emf readings of the four thermocouples (t) inserted into the diffusion tube assembly (T) did not vary by more than ±0.1% (± 0.05 K). They were recorded continuously by means of a high precision potentiameter (M) with an accuracy of ±0.5 μV. Hence the corresponding

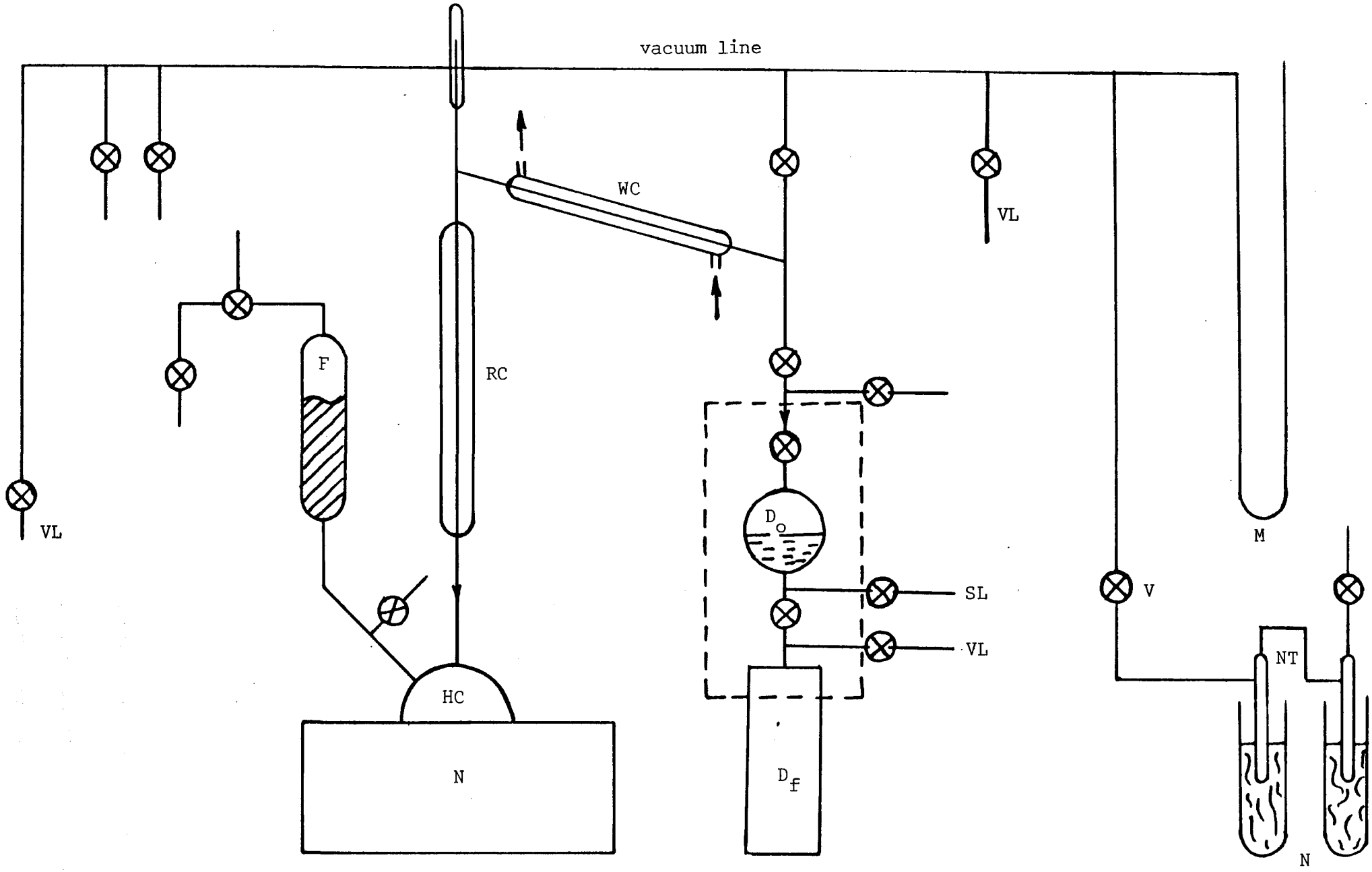

Fig. 3.17 - Vacuum degassification/distillation apparatus [184].

temperatures were computed and their mean was taken as the diffusion tube temperature with an associated uncertainty of ±0.01°C.

The system was purged thoroughly by pumping the solvent through until a steady baseline was observed on the chart recorder and the thermocouples' readings indicated the isothermal condition. At this stage, valves V_s, V_p, V_a and V_b were the only ones open. Then V_p and the reference flow control valve V_b were shut, the pump was switched off and the gravity flow control value V_g was opened. The solvent feed from a well-stirred and thermally-controlled reservoir (A) was then flowing through the diffusion tube under gravity. Pumping of the fluid was avoided during measurements since it imposes pulsations and disturbances upon the flow which make the process experimentally complicated and theoretically difficult to handle [166,167]. Any change in the concentration, flow rate or the temperature of the flowing stream was observed by a change in the position of the baseline on the chart recorder (Z) and by an offset of the zero reading of the digital voltmeter (G). Flowrate measurements at the exit of the diffusion tube ensured that the liquid was flowing through the injection valve at constant velocity (Fig. 3.18). When the system was under steady state condition, indicated by a steady baseline and zero signal on the digital voltmeter, valves V_f and V_e were opened. The solute from reservoir (B) identical to (A) was then flowing through the sample loop, the injection valve being in the fill position (Fig. 3.3). The DVM settings for the baseline zero output signal, the magnetic tape recorder switch "on", the integration time (0.1 s), the time delay (3.5 Ks) and the time intervals (5 s) were checked.

The solute was then injected into the flowing stream (i.e. by rotating the injection valve shaft through 90°) and the time delay switch on the DVM was set to the "on" position instantly. The solute flow control

Fig. 3.18 - Constant liquid flow rate through the injection valve

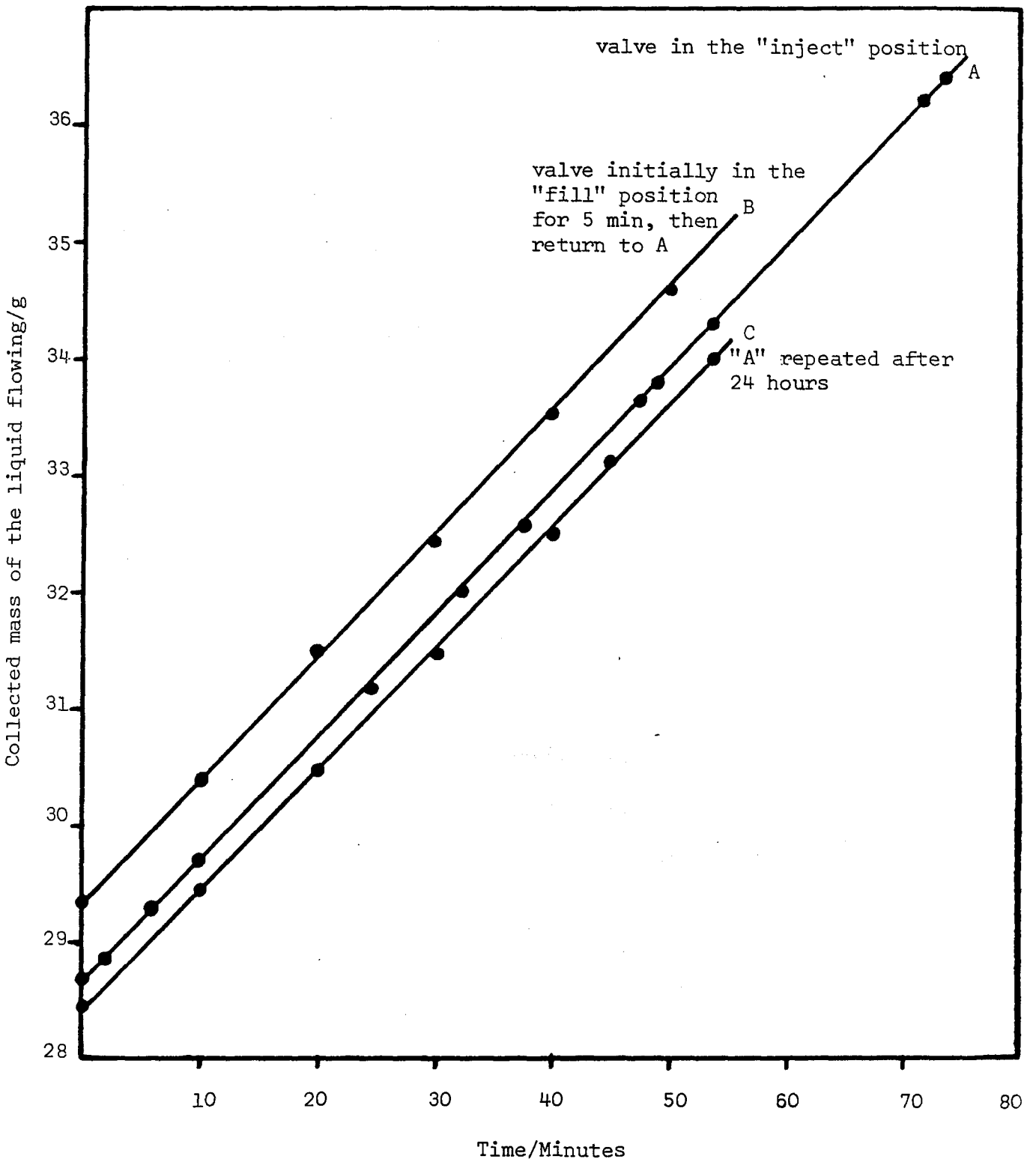

valve V_e was closed and the thermocouples' readings were recorded. The temperature of the diffusion tube was measured several times during an experimental run which usually extended over a period of at least one hour. The analog output signal of the differential refractometer was digitized by the DVM and recorded on magnetic tape at five-second intervals during the course of a single measurement. Each measurement has been repeated at least three times. The recorded data were subsequently analysed to determine the moments of the effluent distribution and hence the mean value of the diffusion coefficient.

3.10 Performance of the Equipment

3.10.1 Departures from the ideal model

The apparatus has been constructed according to the design specifications resulting from the conclusions of the design study in Section 3.2.6. Evidently, all the design criteria and constraints (Sections 3.2.2 - 3.2.6) are met so that the instrument does not depart from its ideal model significantly. Computation of the effects of these departures shows that some are negligible (i.e. less than ±0.04%) and others amount to no more than ±0.7%,

$$\text{i.e.} \quad \frac{\sum_{n=1}^{3} \delta_n(\mu_1')}{(\mu_1')_{id}} \lesssim \pm 0.45\% \quad \text{and} \quad \frac{\sum_{n=1}^{3} \delta_n(\sigma^2)}{(\sigma^2)_{id}} \lesssim \pm 0.7\%$$

Figure 3.19 contains the typical experimental results for hexane-heptane mixtures at 45.8°C (pure hexane flowing). It shows the instrument's working region where the effect of coiling the diffusion tube is negligible (less than 0.05%) for a dispersion time $\bar{t} \geq 3.3$ Ks. The figure also contains the prediction of equation (2.77) which has been calculated for our experimental arrangement, $\lambda = \frac{R_c}{R_o} = 321.4$, with the aid of the appropriate viscosity and density data [22,151,183] and the measured diffusion coefficient. The theoretical prediction is in good agreement with the

Fig. 3.19 - Experimental determination of the coil effect

● - experimental data

— - prediction by equation (2.77)

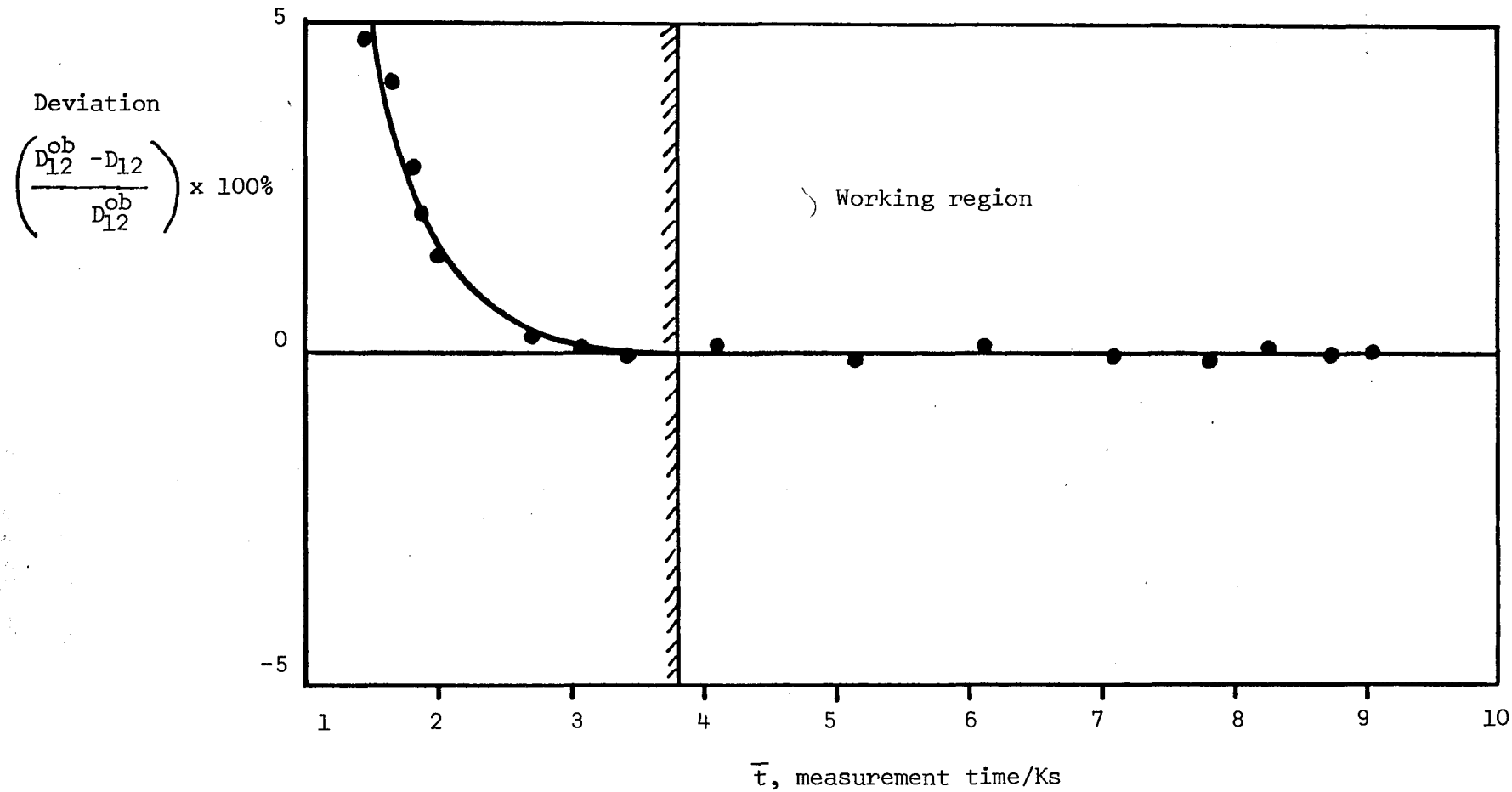

experimental observation indicating that the effect of tube curvature is negligible for $\bar{t} \geq 3.3$ Ks. The experimental results contained in Fig. 3.19 confirm the insignificance of coil effect by showing that the observed diffusion coefficients are independent of the flow velocity to within ±0.5% for such measurement times.

The agreement between the theoretical and experimental results, i.e. Figs. 3.9 and 3.19, is remarkable particularly since no adjustable parameters have been used in comparison. We can therefore use the evident agreement to support the use of Figs. 3.9 and 3.19 or equations (2.77-78) and (2.43 or 2.46) as a means of estimating the effect of tube curvature on our measured diffusion coefficient. For the conditions employed in our measurements, equations (2.77-78) and (2.43 or 2.46) and Fig. 3.9 (working regn) revealed that even in the worst case (i.e. $De^2.Sc = 18$) for hexane-octane mixtures around 70°C) the error incurred by the neglect of the effects of tube coiling amounts to less than ±0.05%.

It must be pointed out that the mole fractions of the injection and flowing stream did not differ by more than 0.1 throughout the measurements. Consequently, errors due to composition and buoyancy effects mentioned in the previous chapter were eliminated. Analysis of samples of the solvent at the entrance and exit of the diffusion tube led to the result of their compositions being identical, suggesting the absence of any adsorption. The skewness and kurtosis of all eluted peaks were found to be zero within the precision of the digital voltmeter indicating that no perturbing effects arose from non-linearity of the detector or adsorption of the injected species on the tube wall. However, the adsorption of fully-saturated n-alkanes such as hexane, heptane and octane (inert) on the stainless steel surface (inert) is highly unlikely. From the experimental results of the energetics of

adsorption of n-hexane and n-octane on solid surfaces [15a,18b] it can be deduced that their adsorption on stainless steel is negligible.

3.10.2 Linearity of the detector

The determination of the diffusion coefficient from the characteristics of the eluted distribution is dependent on the linearity of the response of the refractive index detector. That is, the signal from the refractometer should be directly proportional to the concentration difference of the eluted species between the sample and reference sides of the cell. In order to confirm this linearity for the present detector, measurements of the zeroth moment (the peak area) for various known amounts of solute injected, have been performed for the hexane-heptane mixture at 45.8°C. Provided that the detector response is linear, the zeroth moment of the eluted distribution should be directly proportional to the concentration of the injected solute. Figure 3.20 shows the experimental results of this test and indicates that only for large composition differences (i.e. large refractive index n_D differences) between the injection sample and flowing stream is the detector's response non-linear. This non-linearity was expected due to the high sensitivity of the refractometer even at extremely low composition differences ($\delta n_D \lesssim 10^{-8}$). Hence the samples for injection were made such that they always differed in mole fraction from the composition of the flowing stream by no more than 0.1 which is well within the linearity range of the detector as shown by Fig. 3.20. As mentioned earlier on, the skewness and kurtosis of all the eluted peaks were found to be zero, confirming the detector's linear response throughout this work.

3.10.3 The reference composition

Binary diffusion coefficients for the typical hexane-heptane mixture (around 30°C) measured at various compositions of the flowing stream and injection are included in Figs. 3.21 and 3.22. Also included in

these Figures are the reference compositions to which the measured diffusivities should refer according to the theoretical analysis of Chapter 2. Equation (3.8) was used to compute the reference composition for a measured diffusion coefficient. The experimental and theoretical results contained in Figs. 3.21 and 3.22 confirm the validity of equations (2.180) and (3.8), showing that under the experimental conditions employed throughout this work

$$D_{12}\ (x_{1r}) \;=\; D_{12}\ (x_{1f}) \pm 0.1\% \qquad (3.21)$$

where x_{1r} and x_{1f} are the reference and flowing stream mole fractions of species 1 respectively.

3.10.4 Reproducibility of the results and precision

Figure 3.23 plots $\frac{D_{12} - \bar{D}_{12}}{\bar{D}_{12}}$, deviations of the measured diffusion coefficients from their mean for the hexane-octane mixture ($x_{hex.f} = 0.6$, $x_{hex.i} = 0.7$) at 50°C, against the measurement times $\bar{t}$. It can be seen that for $\bar{t} \geq 3.5$ Ks the results are reproducible to within ±0.45%. Similarly for the mixture hexane-heptane ($x_{hex.f} = 0.3$, $x_{hex.i} = 0.4$) at 27.8°C, the reproducibility of six repeated experimental runs each taking around 4 Ks was found to be ±0.48% as shown by Fig. 3.24. The deviations of the eluted distributions from normality under the conditions of our experiments were insignificant as shown by Fig. 3.25, which is typical for the hexane-heptane mixture.

It is not possible to perform the conventional analysis of random experimental errors for these measurements to estimate their precision because the diffusion coefficient is determined from the entire distribution function of the eluted sample, and not a number of discrete measurements. Consequently, the alternative strategy has been adopted whereby the reproducibility of the measurements under nominally identical thermo-

dynamic conditions is taken as a measure of the precision. On this basis it is concluded that the precision of our experimental data is one of ±0.5%. The graphical method proved to have an inferior precision (2-5%) and hence it was discarded for the purpose of calculating the results.

Furthermore, the diffusion coefficient for octane-dodecane mixture ($x_{oct.f}$ = 1.0) at 24.95°C was measured and compared with its published value [39] determined at 25°C by the diaphragm cell method. It was found that the two values, 1.699 x 10^{-9} (m^2 s^{-1}) measured and 1.718 x 10^{-9} ± 1% (m^2 s^{-1}) published, differed by only 1.0%.

The above results, together with the experimental results of the proceeding chapter, present a conclusive evidence for the correct operation of our equipment.

3.10.5 Accuracy of the results

The largest single source of error in the measured diffusion coefficients arises from the determination of the variance of the dispersion peak which contributes an uncertainty of ±0.5%. The uncertainty in the determination of the diffusion time and the possible systematic errors due to the corrections discussed above amount to no more than ±0.2%. The only other source of random error is the measurement of the tube radius and this contributes ±0.24%. Thus the overall accuracy of the reported dissusion coefficient values is believed to be ±1%.

Fig. 3.20 - Linearity of the refractometer

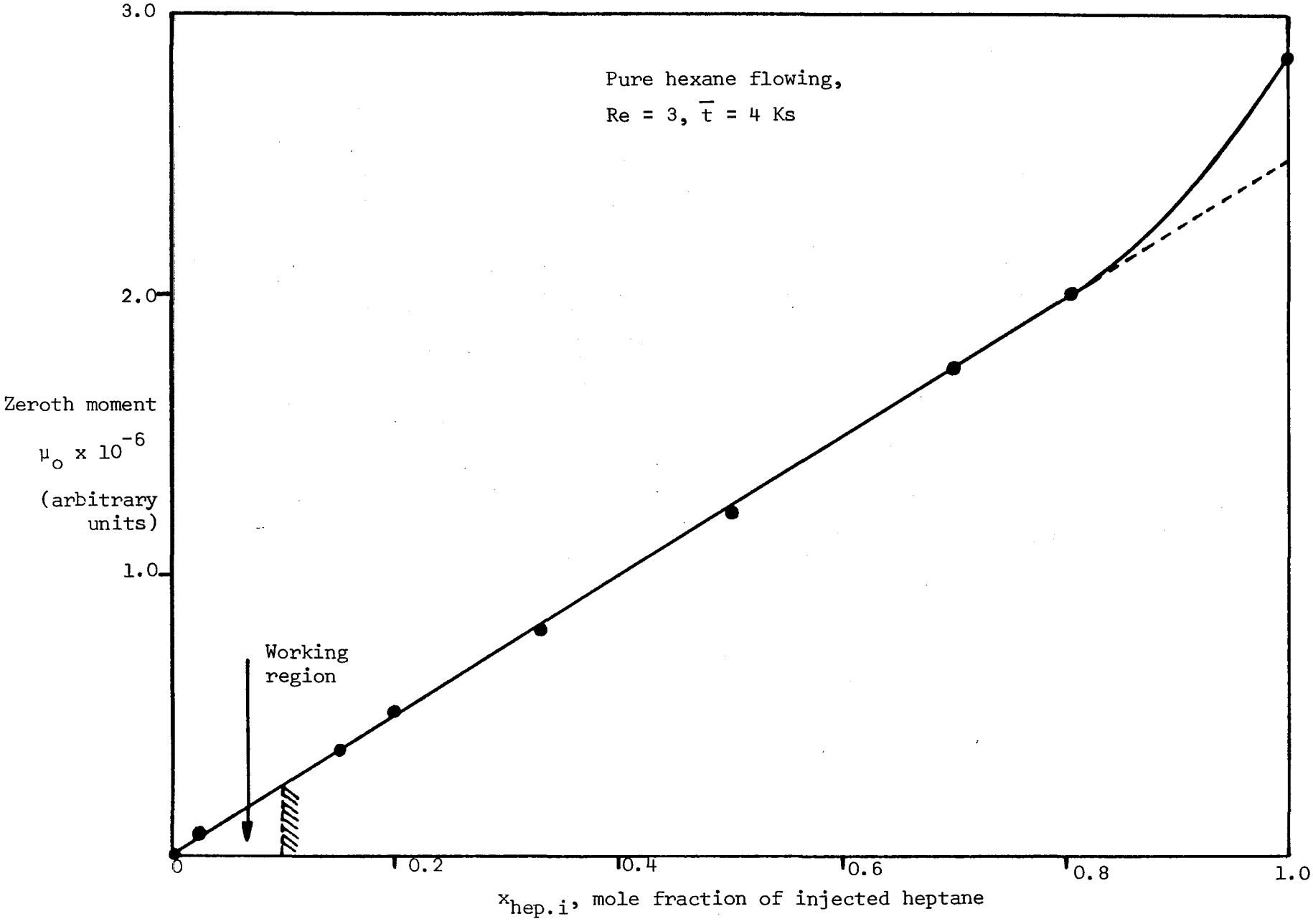

Fig. 3.21 - Diffusion coefficient vs mole fraction for hexane-heptane mixture at 30°C

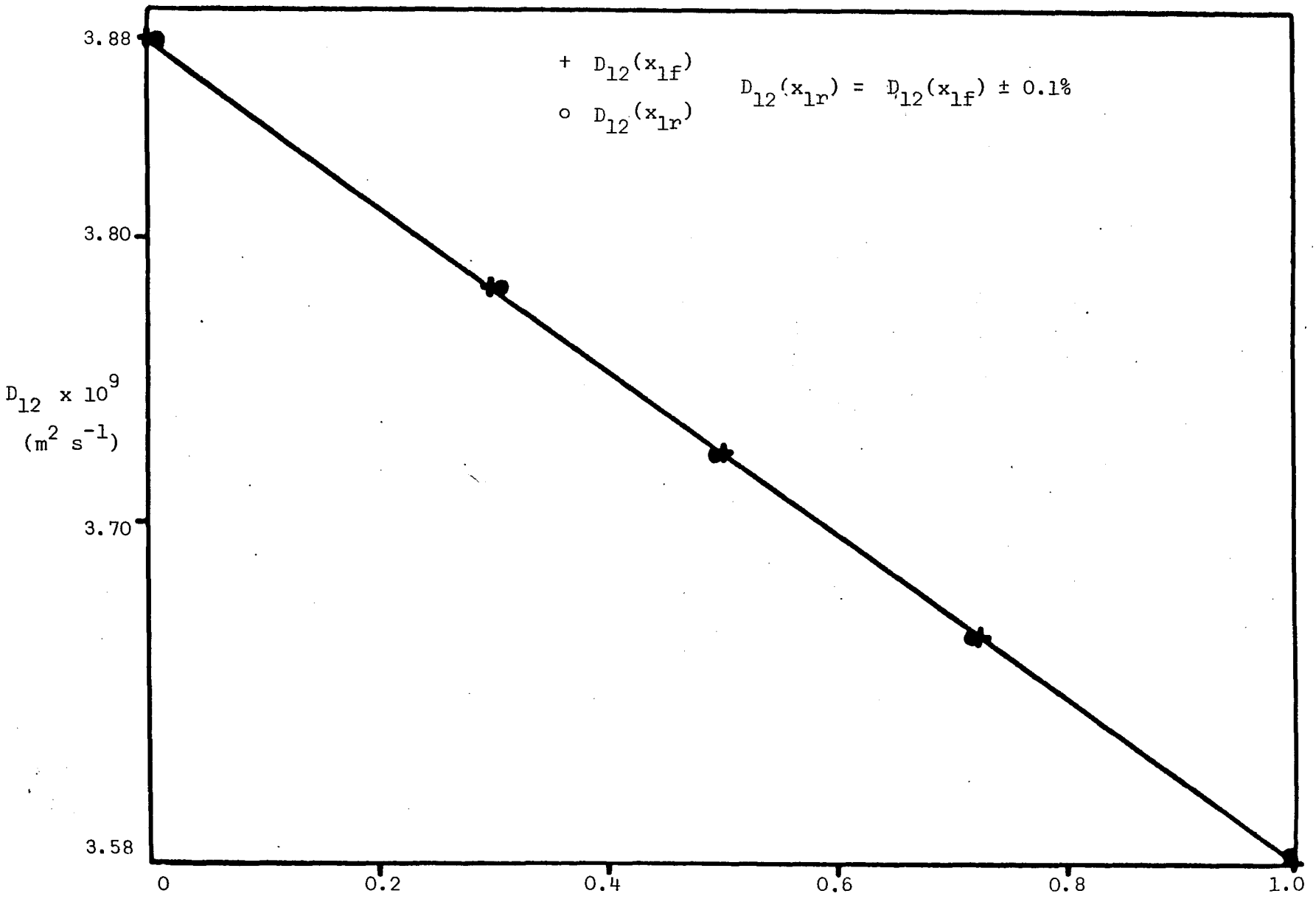

Fig. 3.22 - Hexane-Heptane mixture at 29°C, $x_{6f} = 1.0$
Measured diffusion coefficient vs mole fraction of heptane injected.

\+ $D_{12}(x_{1i})$, expt $\quad D_{12}(x_{1r}) = D_{12}(x_{1f}) \pm 0.1\%$

— $D_{12}(x_{1r})$, eqns. (3.8) and (2.43)

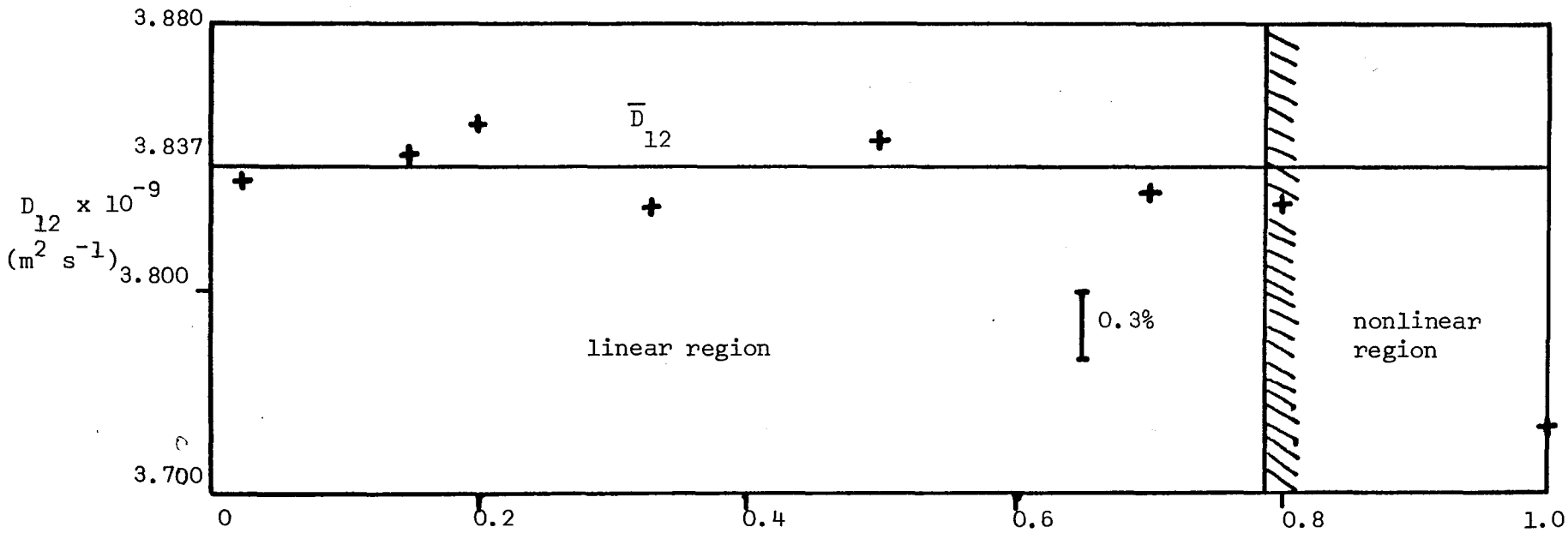

Fig. 3.23 - Reproducibility for Hexane-Octane mixtures at 50°C

$x_{hex.f} = 0.60 \qquad x_{oct.i} = 0.30$

$\overline{D}_{12} = 4.200 \times 10^{-9}\ m^2\ s^{-1}$

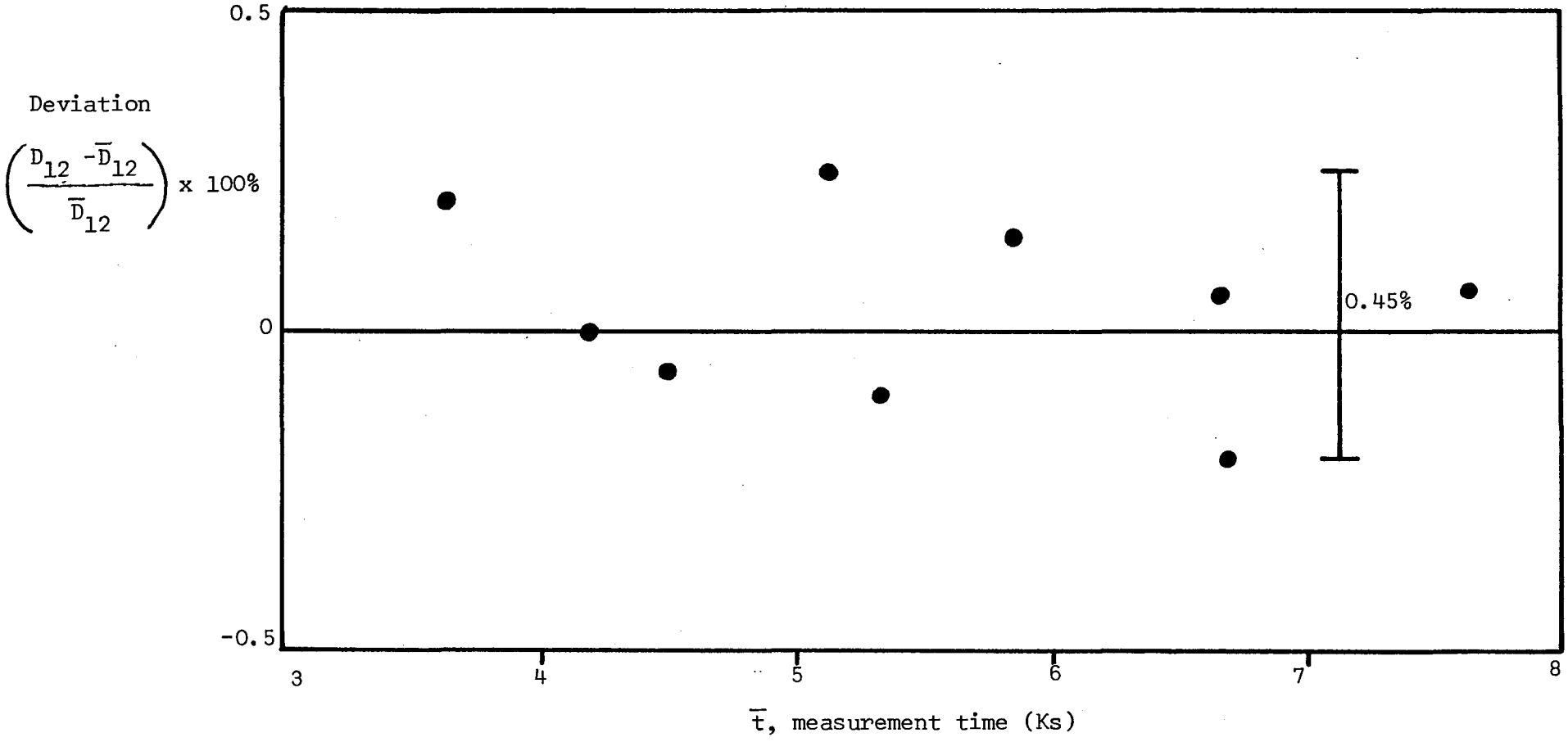

Fig. 3.24 - Reproducibility for hexane-heptane mixtures at 27.8°C

$\bar{t}$ = 4 Ks; $x_{hex.f}$ = 0.3; $x_{hex.i}$ = 0.4

$\bar{D}_{12}$ = 3.553 x 10^{-9} m^2 s^{-1}

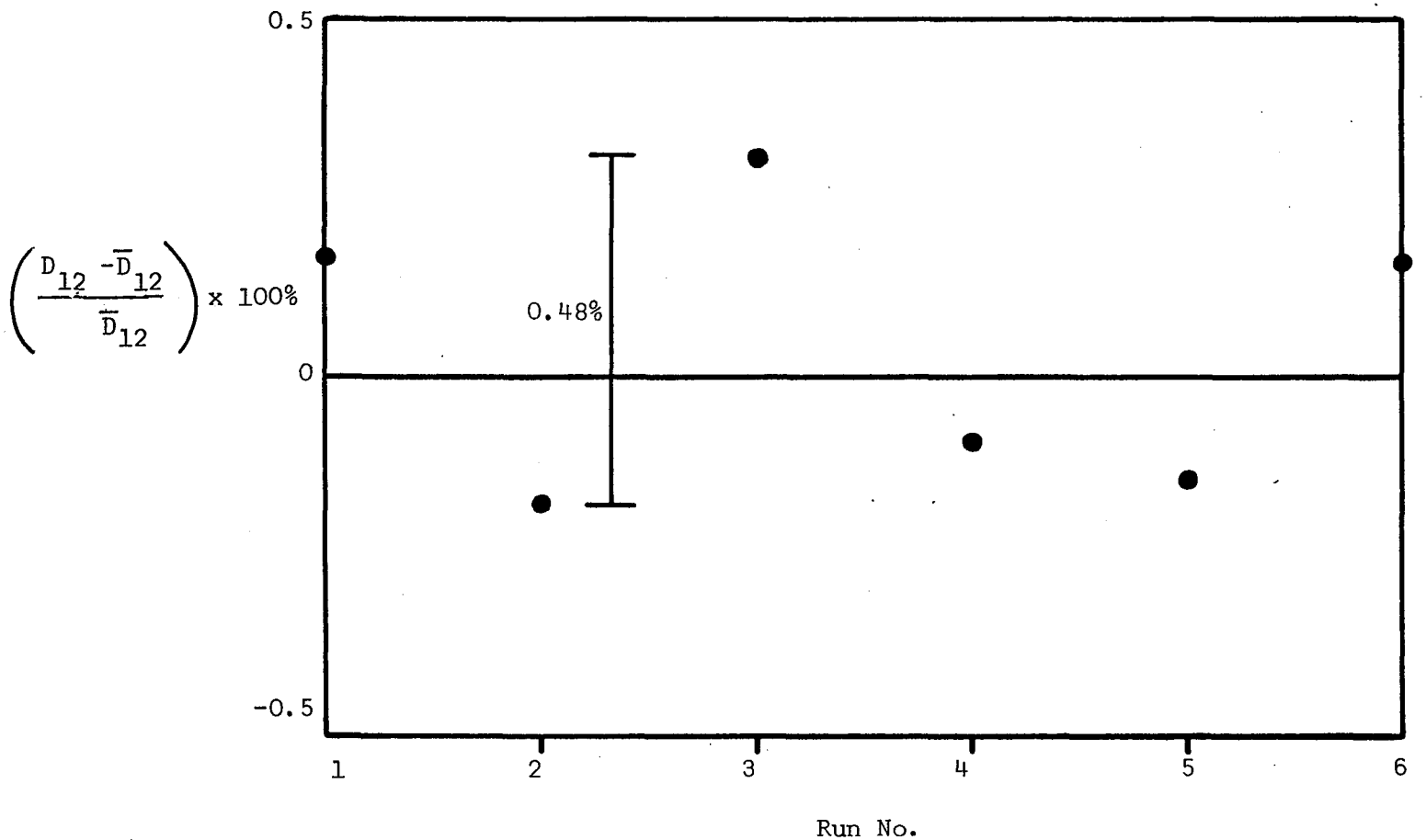

Fig. 3.25 - Recorded data (•) fitted to a Gaussian distribution (-)

$(x_{hex})_f = 1.0$; $(x_{hep})_i = 0.1$; $\bar{t} = 4$ Ks;

$\theta_m = 29^{\circ}C$; Re = 3.

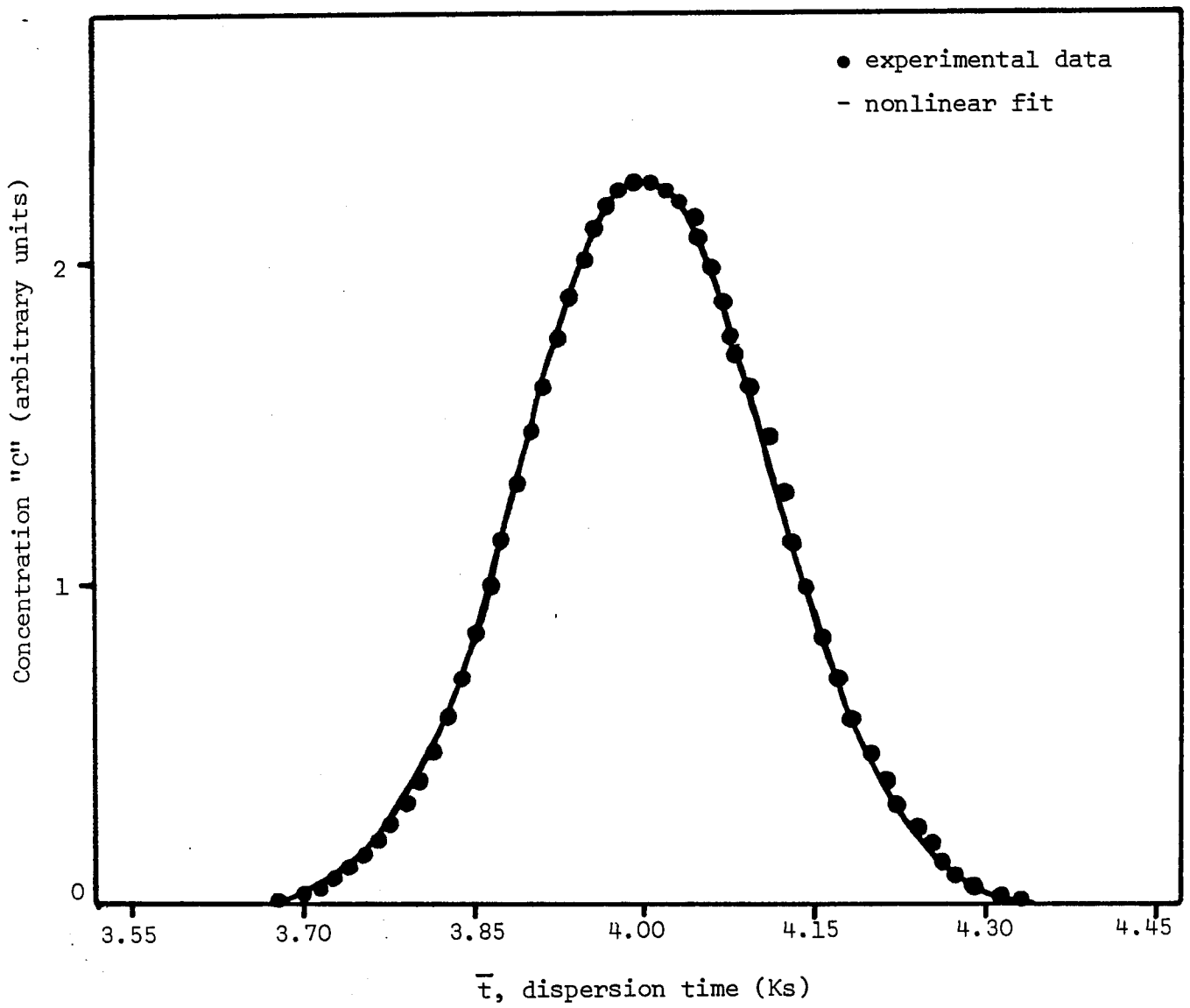

C H A P T E R 4

RESULTS

4 Introduction

The previous chapters have presented the theory behind the Taylor dispersion technique and described how the apparatus employed in this work has been designed and used to perform accurate measurements of the liquid-phase diffusion coefficients. Using this apparatus and the Taylor dispersion method, the binary diffusion coefficients for n-hexane-n-heptane, n-hexane-n-octane and n-heptane-n-octane binary mixtures of various compositions were measured within the temperature range 20-70°C and at atmospheric pressure. The time of measurements varied from about 4 Ks to 8 Ks with the Reynolds Number for the flow being in the range 3 - 6. In this chapter, we present the results of the measurements, with a reproducibility of ±0.5% and an estimated overall accuracy of ±1%, and delay the discussion and usage of these results until the next chapter.

The n-alkanes under investigation, n-C_6H_{14} (refractive index n_D = 1.3740 - 1.3760), n-C_7H_{16} (n_D = 1.3880 - 1.3885) and n-C_8H_{18} (n_D = 1.3970 - 1.3980), were each at least 99.9% pure (see Chapter 3, Section 3.9). The stated purity was supported by means of independent measurements of the refractive index of samples of the n-alkanes and through tests on a gas chromatograph. The characteristics of the diffusion tube (Section 3.2.7) and the method of evaluating the experimental results (Sections 3.5 - 3.8) included in this chapter have been previously described in Chapter 3.

Tables 4.1 - 4.15 list the entire body of our experimental results for the three n-alkane binary systems, each at five different compositions, for a pressure of 1 bar (10^5 Pa). Figures 4.1 - 4.15 display the binary diffusion coefficient, D_{12}, as a function of temperature, θ_m, at a constant

composition, x_{1r}, for several mixtures.

For the purposes of correlating the experimental results and interpolating the data within the range of measurements, the data were fitted to polynomials, of the form $Y = \sum_{n=0}^{4} A_n^j X^n$, by means of a least-squares computer program. As can be seen from Figs. 4.1 - 4.15 the data fitted the regression straight lines, of the form $[D_{12}]_{x_{1r}} = A_o^j + A_1^j \theta_m$, and the fitted data agreed with the experimental ones with a maximum deviation of less than 1%.

The values of constants A_o^j and A_1^j for the several mixtures of each binary system are contained in Table 4.16 and the corresponding lines are displayed by Figs. 4.16a - 4.16c. These Figures, which show the variation of D_{12} with θ_m along the constant composition lines, reveal that for each binary system such lines are parallel, with a maximum slope deviation of 1% (typical of the C_7-C_8 system) according to the regression results listed in Table 4.16.

In Figs. 4.17a - 4.17c the isotherms for the binary diffusion coefficient as a function of composition, for each binary system, are shown. In constructing these regression lines, of the form $[D_{12}]_{\theta_m} = A_o^k + A_1^k x_{1r}$ with constants A_o^k and A_1^k being given for each case in Table 4.17, the data has been employed at nominal temperatures computed from the earlier regression results given in Table 4.16. The data fit these lines with a maximum deviation of 0.5%.

All the isotherms of each binary system display similar behaviour and are parallel with a maximum slope deviation of 3% (typical of the C_6-C_7 and C_7-C_8 systems). Thus variations of the binary diffusion coefficient, D_{12}, with temperature and composition, within the range of measurements, are linear to within a maximum deviation of 1% and 0.5% as shown by

Figs. 4.1 - 4.16 and 4.17a - 4.17c respectively. The following equations (4.1) and (4.2) can be used in conjunction with Tables 4.16 and 4.17 to compute the binary diffusion coefficients for each liquid system as a function of temperature (θ_m = 20 - 70°C) and composition (x_{1r} = 0 - 1) respectively, with a maximum uncertainty of ±2%.

$$[D_{12}]_{x_{1r}} = A_o^j + A_1^j \theta_m \qquad (4.1)$$

(A_o^j and A_1^j values of Table 4.16); j ≡ system a, b or c.

$$[D_{12}]_{\theta_m} = A_o^k + A_1^k x_{1r} \qquad (4.2)$$

(A_o^k and A_1^k values of Table 4.17); k ≡ system a, b or c.

The binary diffusion coefficient, D_{12}, as a function of temperature, Θ_m, for the system hexane-heptane at fixed mole fractions of heptane, x_{lr}, and 1 bar pressure.

Table 4.1

Θ_m (°C)	D_{12} (m^2s^{-1}) x 10^9
26.375	3.7010
34.940	4.1180
42.751	4.5040
49.964	4.8500
50.989	4.9170
56.375	5.1710

Fig. 4.1 x_{lr} = 0.016

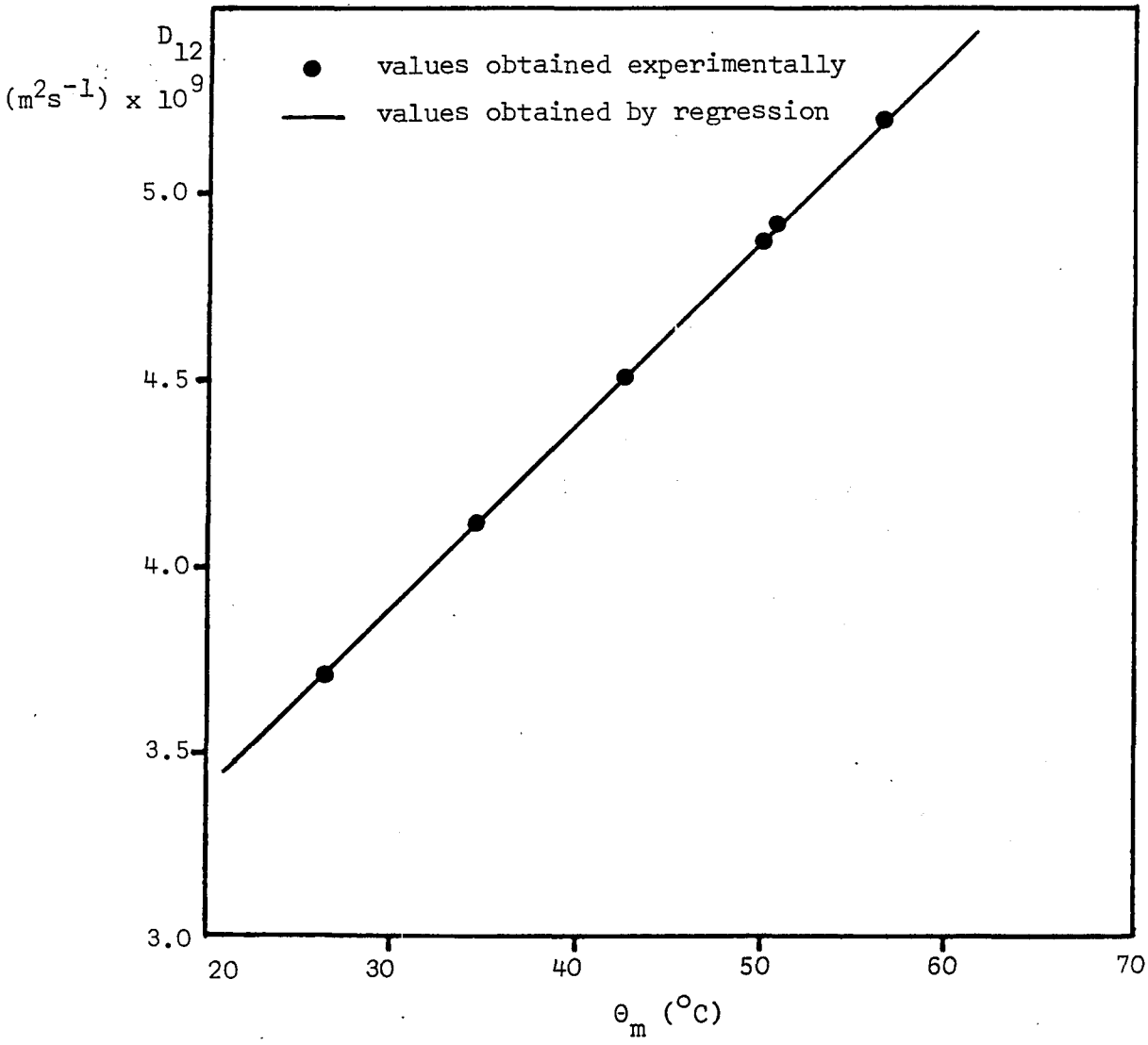

Table 4.2

θ_m (^oC)	D_{12} (m^2s^{-1}) x 10^9
27.388	3.6750
32.999	3.9370
40.375	4.3103
46.242	4.5950
55.762	5.0775

Fig. 4.2 x_{lr} = 0.3015

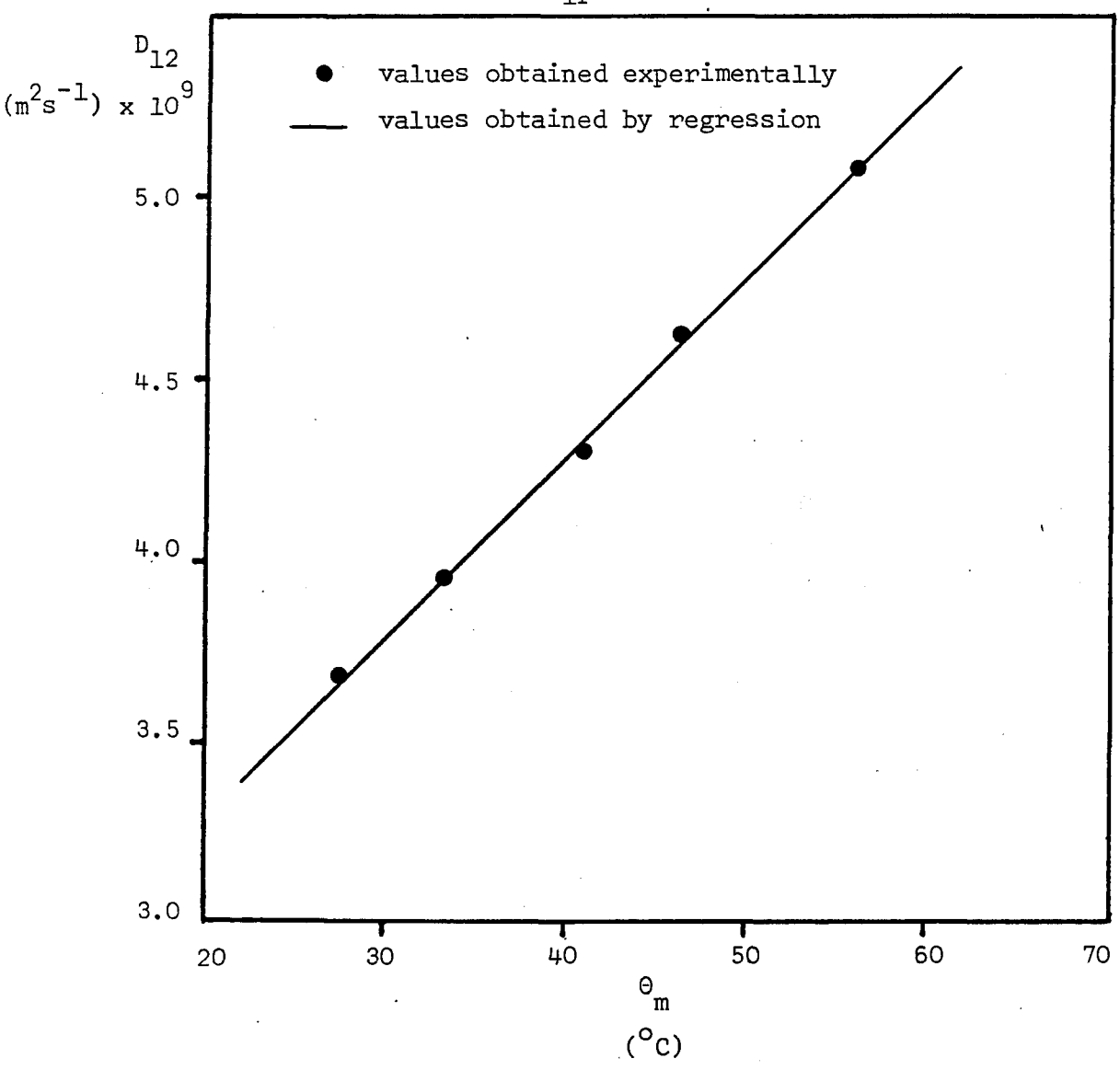

Table 4.3

Θ_m (^oC)	D_{12} (m^2s^{-1}) x 10^9
28.661	3.6440
30.338	3.7560
34.485	3.9500
40.140	4.2165
45.638	4.4925
50.816	4.7530
58.000	5.0900

Fig. 4.3 x_{1r} = 0.4985

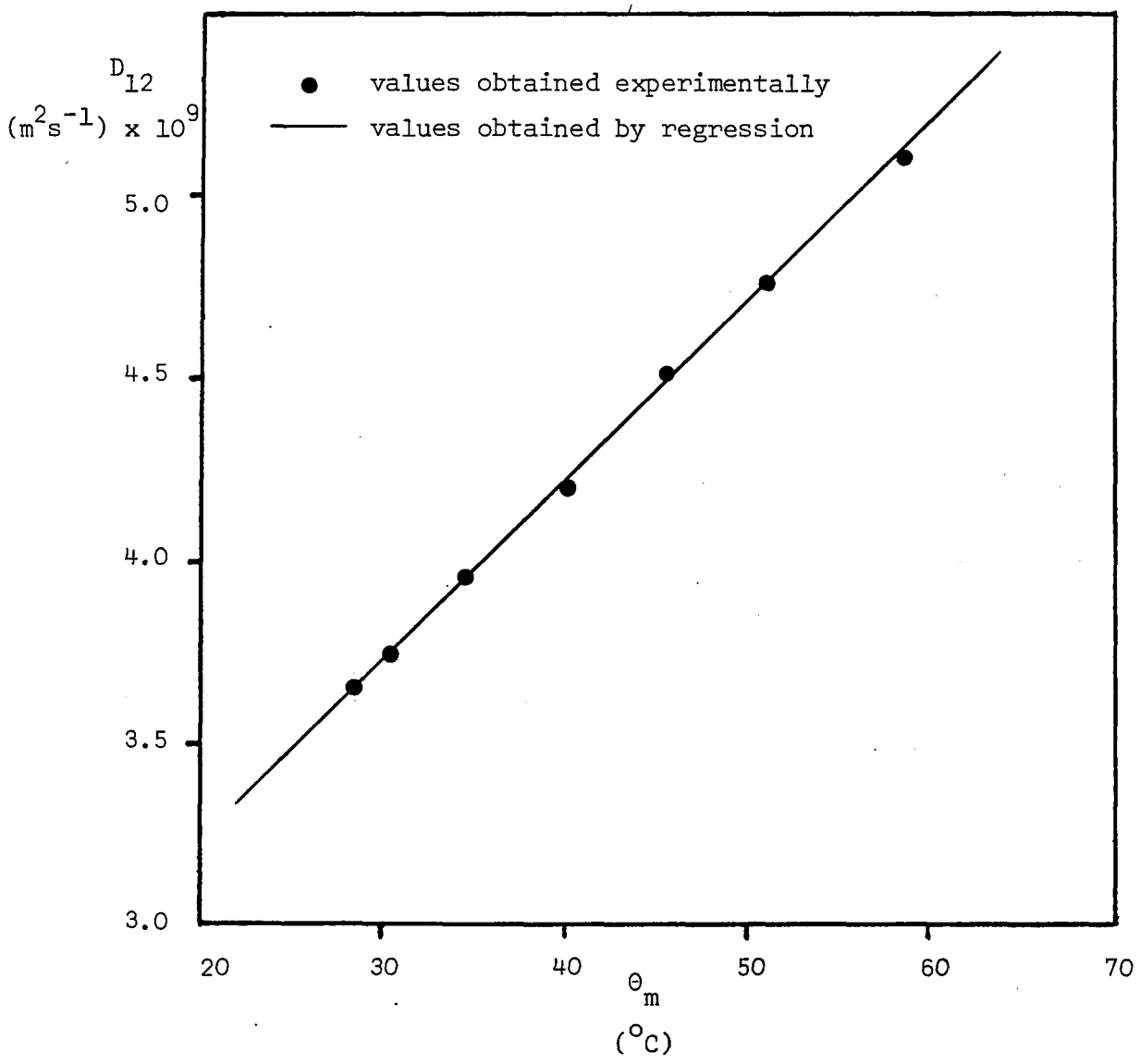

Table 4.4

θ_m (^oC)	D_{12} (m^2s^{-1}) x 10^9
25.229	3.4475
36.239	3.9633
46.488	4.4445
54.116	4.8590
59.006	5.0635

Fig. 4.4 x_{lr} = 0.6985

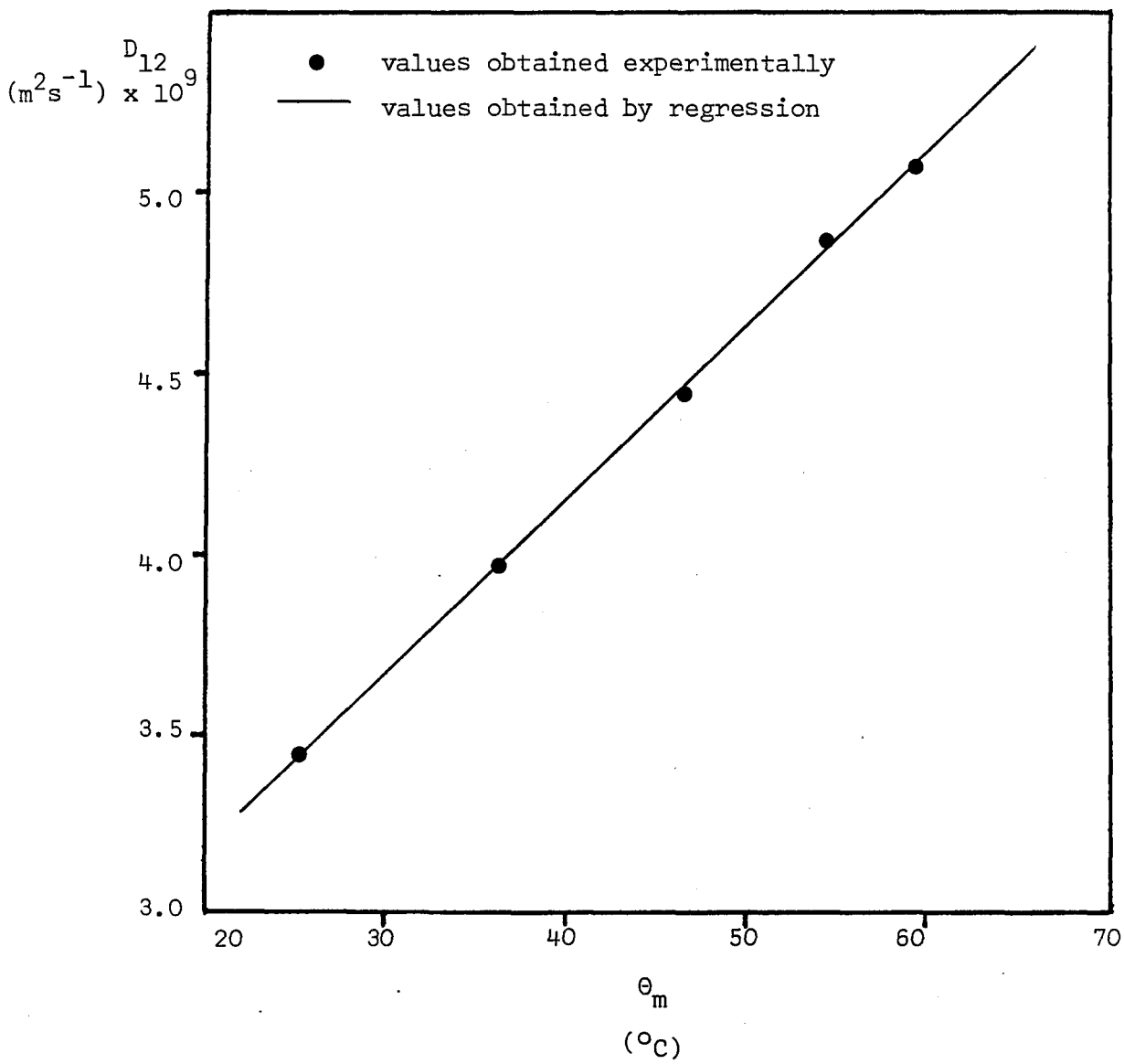

Table 4.5

θ_m (^oC)	D_{12} (m^2s^{-1}) x 10^9
20.010	3.1010
29.996	3.5685
33.253	3.7360
39.068	4.0050
41.217	4.1415
49.630	4.5500
54.817	4.8230
60.008	5.0515

Fig. 4.5 x_{1r} = 0.9985

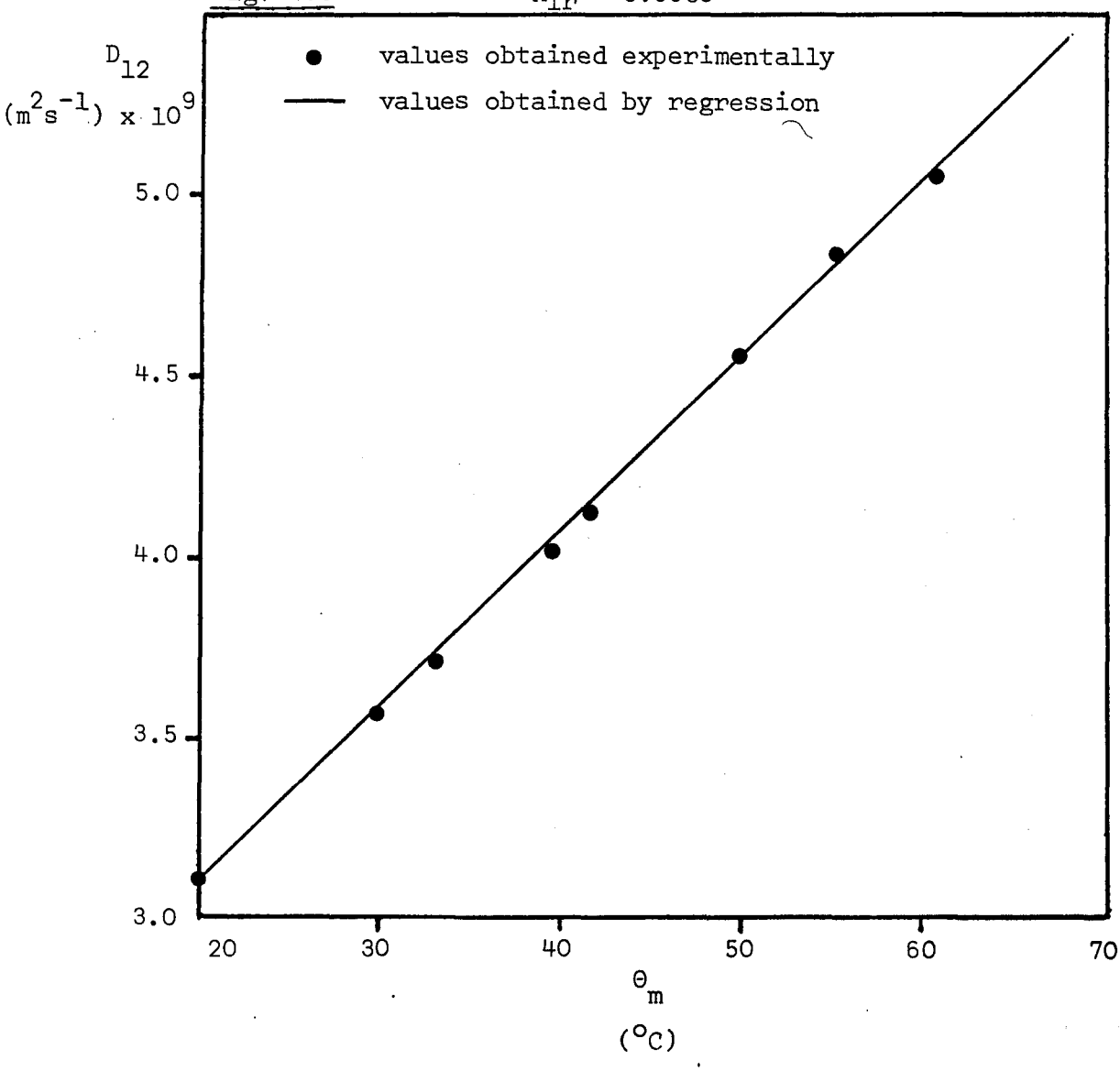

The binary diffusion coefficient, D_{12}, as a function of temperature, θ_m, for the system hexane-octane at fixed mole fractions of octane, x_{1r}, and 1 bar pressure

Table 4.6

θ_m (°C)	D_{12} ($m^2 s^{-1}$) x 10^9
23.004	3.3035
29.853	3.6203
36.110	3.9137
43.968	4.2590
47.901	4.4816
54.000	4.7500

Fig. 4.6 x_{1r} = 0.0200

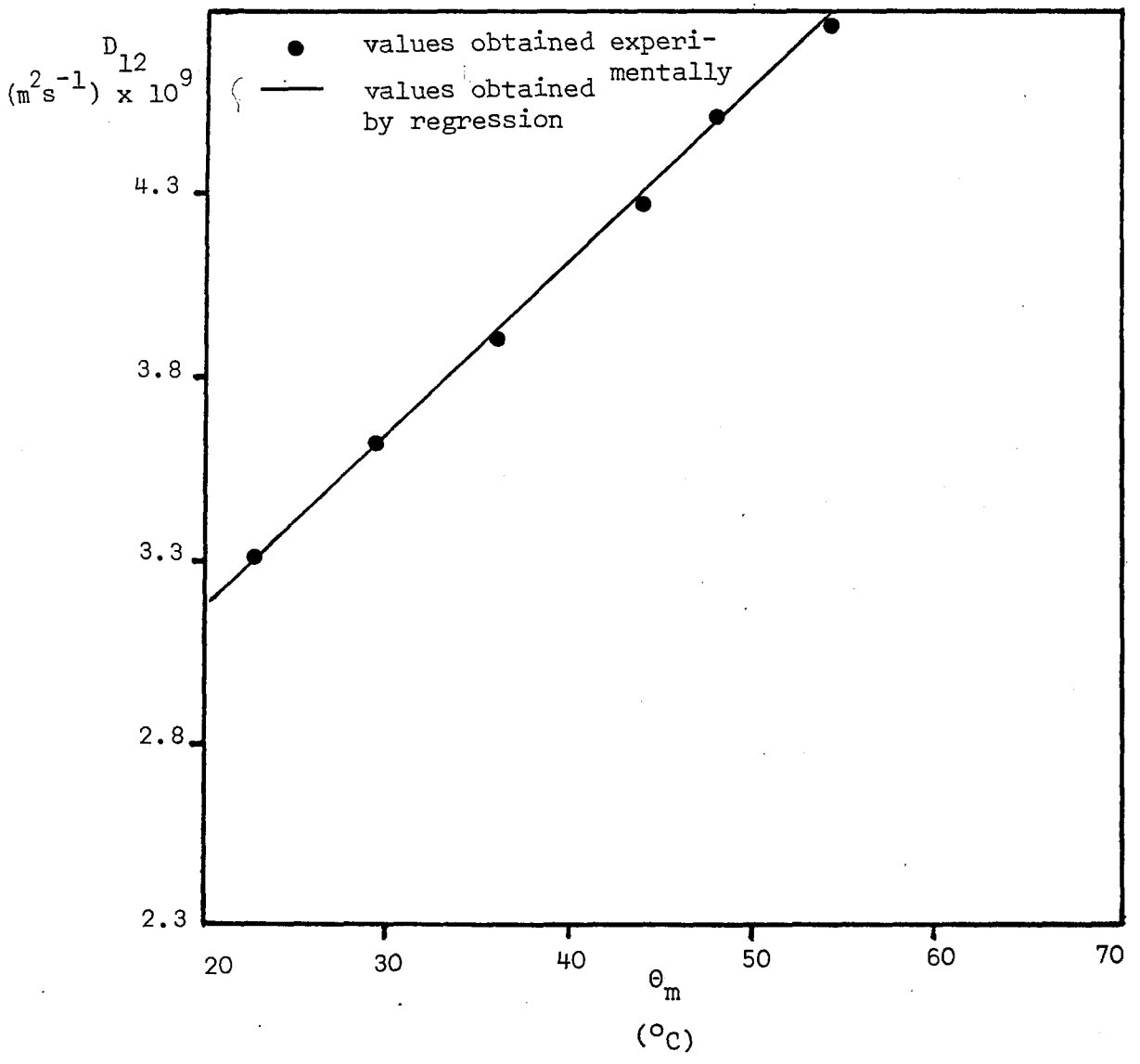

Table 4.7

θ_m (^oC)	D_{12} (m^2s^{-1}) x 10^9
25.898	3.2340
32.143	3.5260
40.344	3.9175
48.061	4.2890
56.149	4.6707

Fig. 4.7 x_{1r} = 0.2023

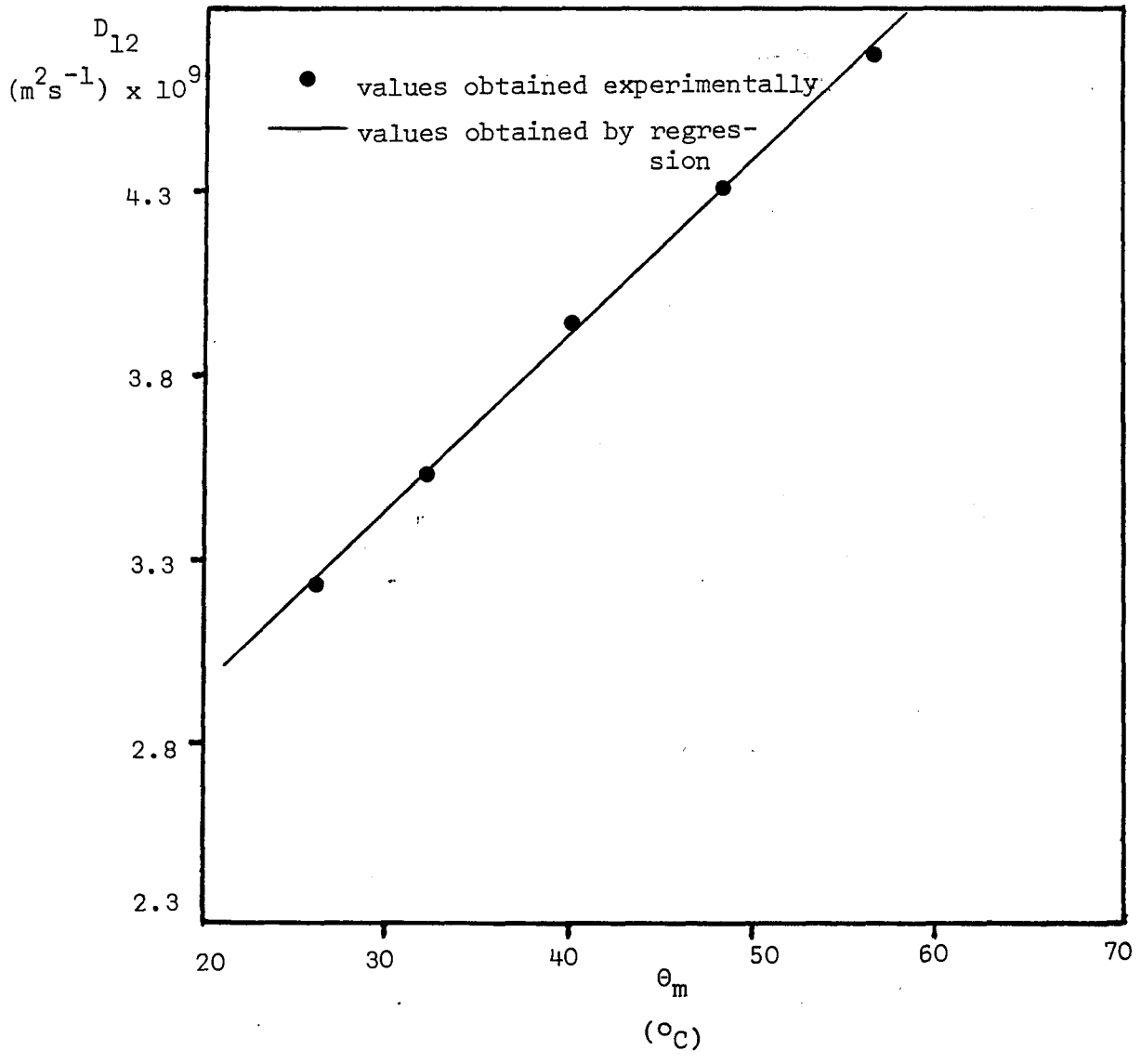

Table 4.8

θ_m (^oC)	D_{12} (m^2s^{-1}) x 10^9
25.888	2.9985
34.201	3.3740
41.673	3.7300
47.569	4.0000
54.139	4.3340

Fig. 4.8 $x_{lr} = 0.4987$

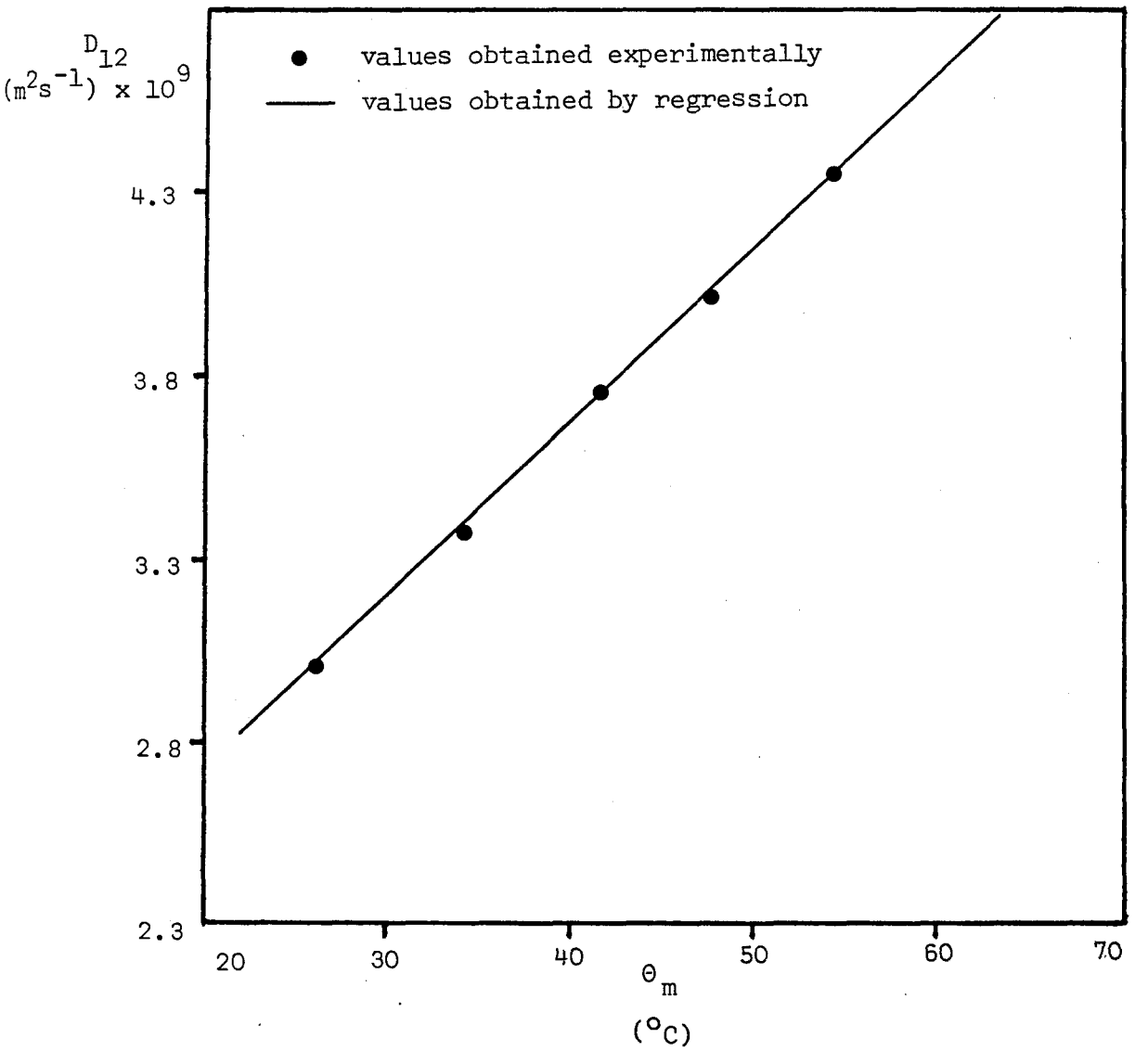

Table 4.9

θ_m (^oC)	D_{12} (m^2s^{-1}) x 10^9
23.001	2.6510
30.107	3.0010
41.619	3.5340
50.404	3.9300
60.299	4.4085

Fig. 4.9 x_{lr} = 0.7038

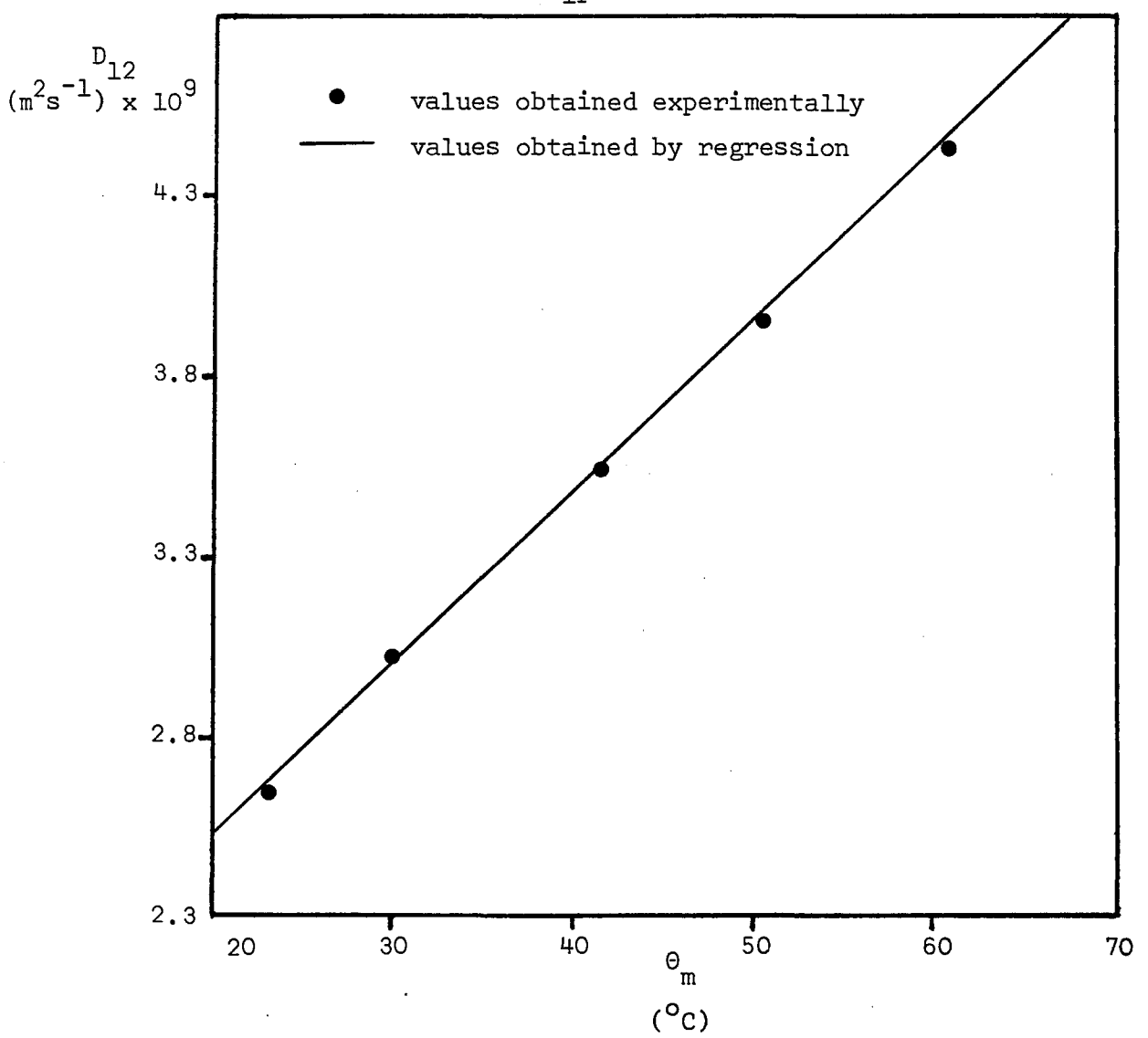

Table 4.10

Θ_m (^oC)	D_{12} (m^2s^{-1}) x 10^9
21.001	2.3002
29.301	2.6817
39.922	3.2090
48.976	3.6250
58.897	4.0890

Fig. 4.10 x_{lr} = 0.9980

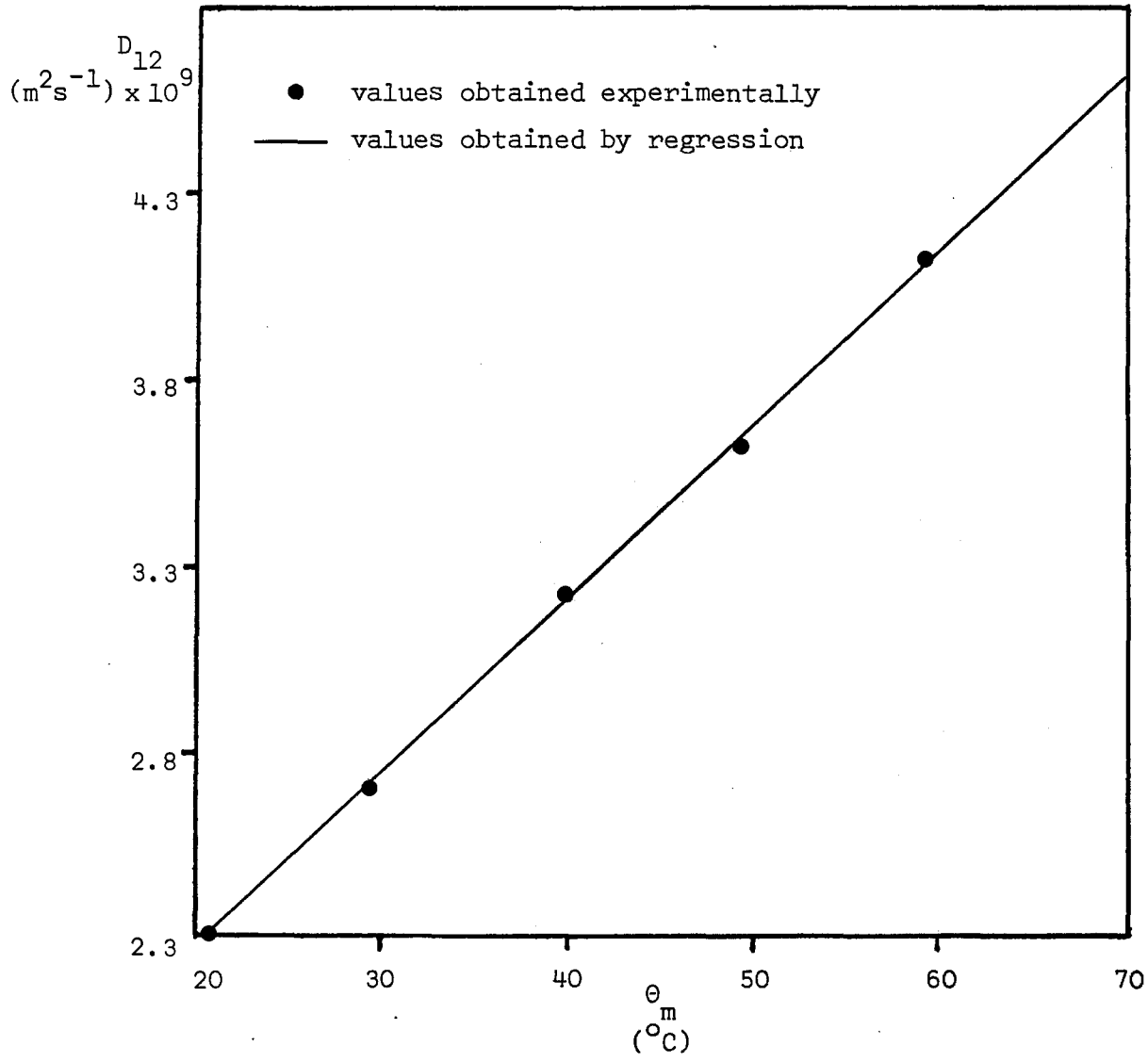

The binary diffusion coefficient, D_{12}, as a function of temperature, Θ_m, for the system heptane-octane at fixed mole fractions of octane, x_{1r}, and 1 bar pressure

Table 4.11

Θ_m (°C)	D_{12} $(m^2 s^{-1}) \times 10^9$
20.113	2.6020
35.932	3.2580
50.075	3.8330
60.152	4.2500
65.003	4.4627
70.776	4.7820

Fig. 4.11 $x_{1r} = 0.0298$

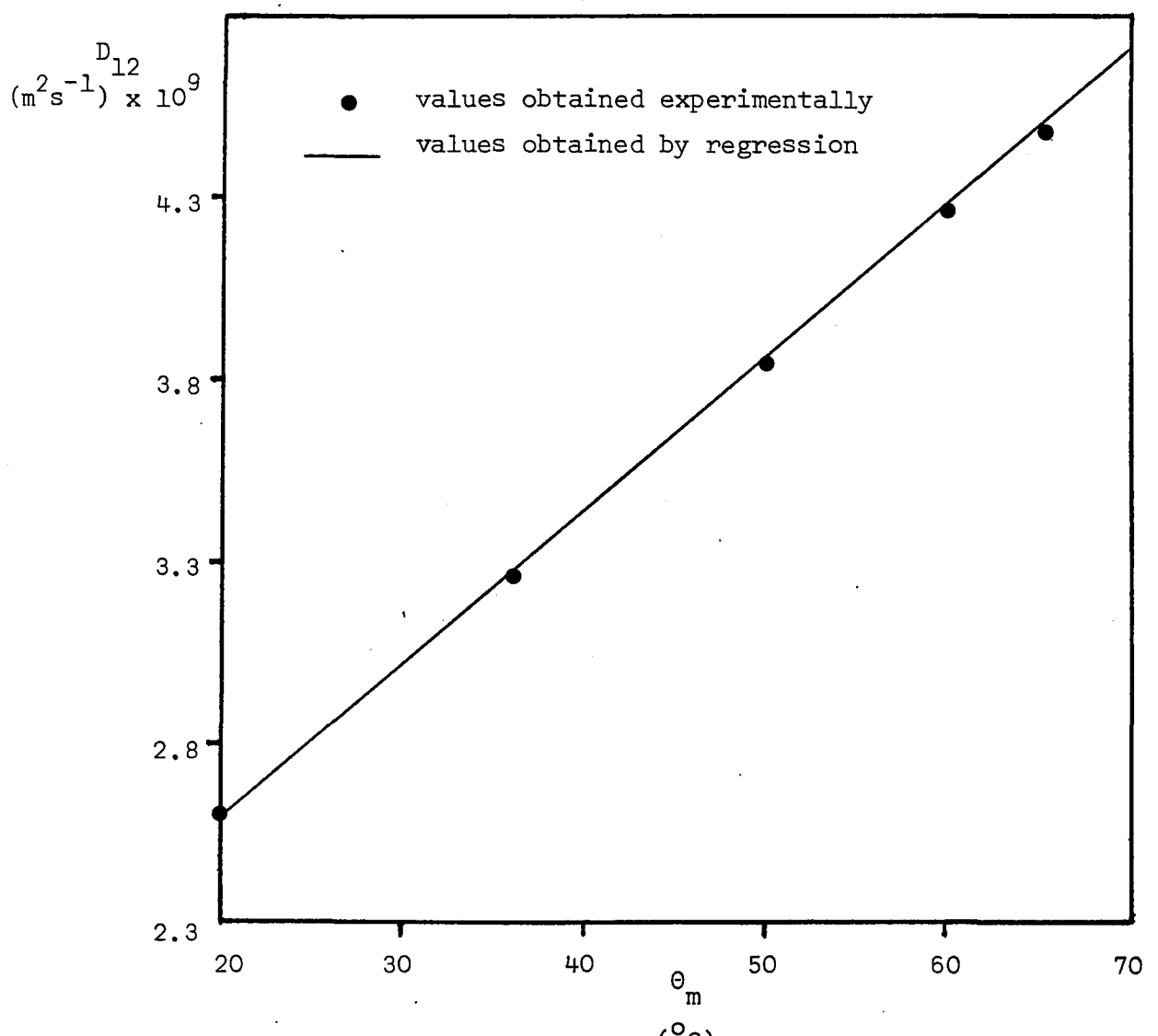

Table 4.12

Θ_m (^oC)	D_{12} (m^2s^{-1}) x 10^9
21.065	2.5490
32.211	3.0220
42.120	3.4100
59.371	4.1100
68.044	4.5220

Fig. 4.12 x_{1r} = 0.2513

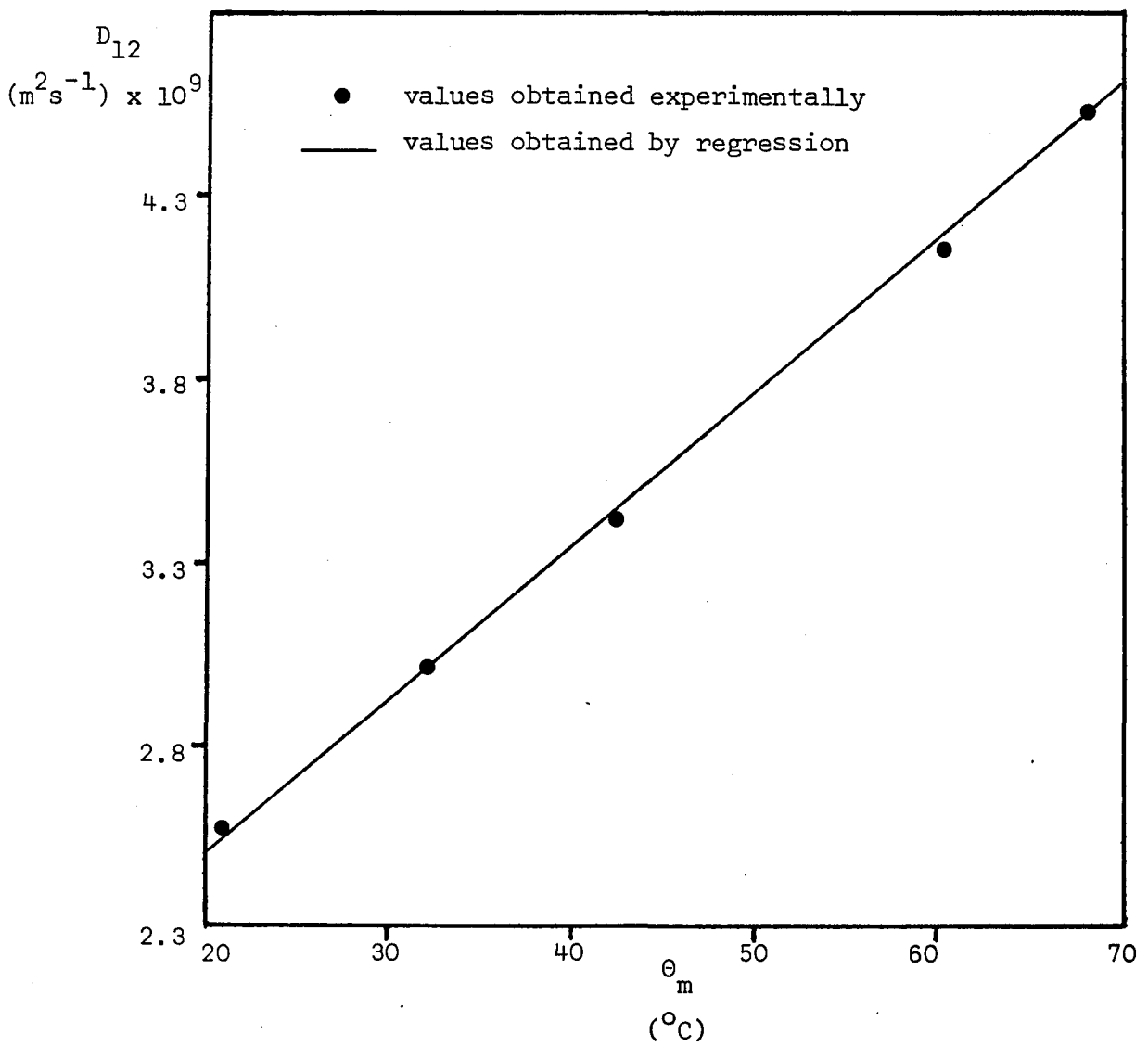

Table 4.13

θ_m (°C)	D_{12} $(m^2s^{-1}) \times 10^9$
20.403	2.4361
35.029	3.0600
50.340	3.6565
59.615	4.0600
69.921	4.5369

Fig. 4.13 $x_{1r} = 0.4988$

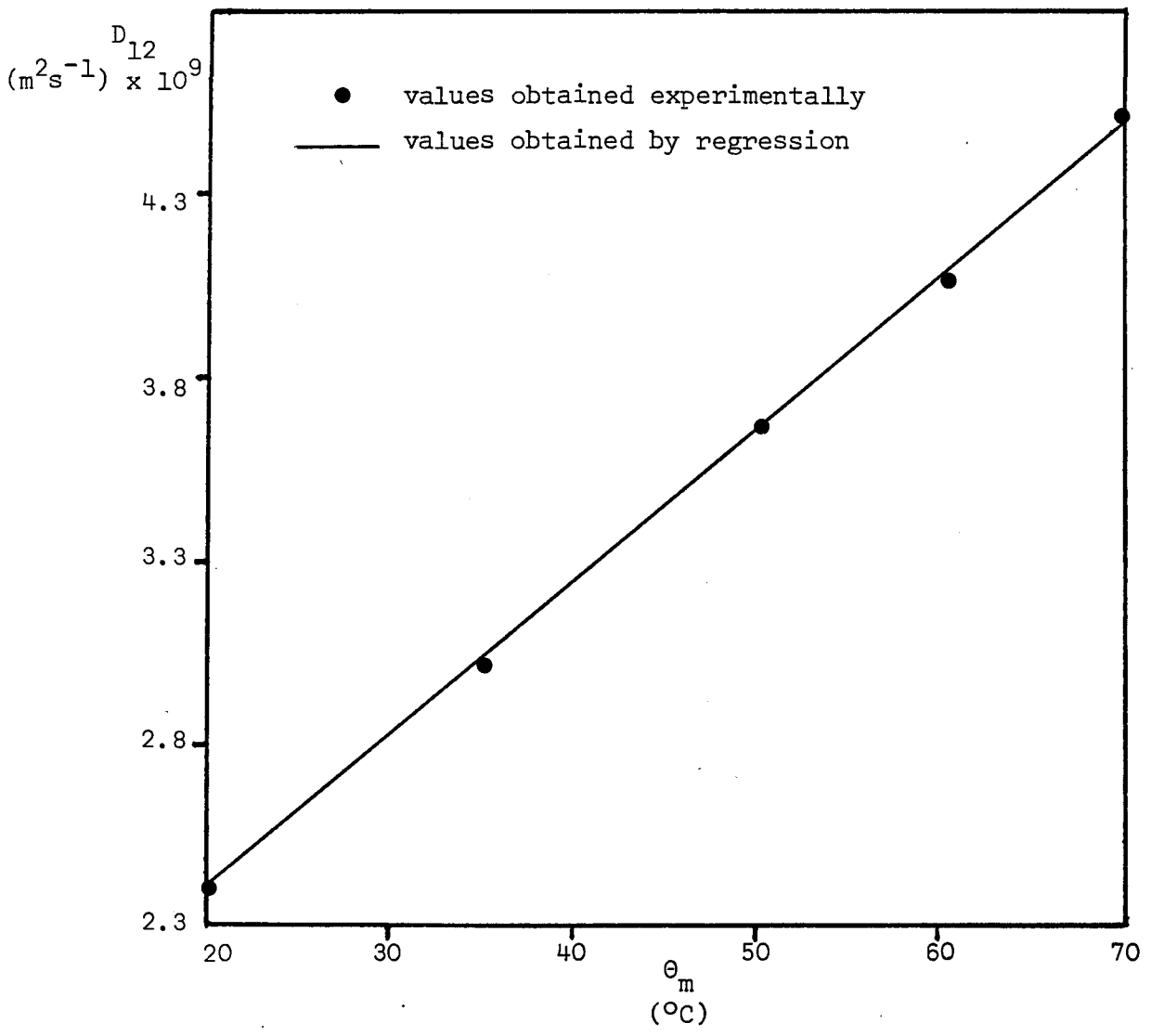

Table 4.14

θ_m (°C)	D_{12} (m^2s^{-1}) x 10^9
22.489	2.4301
32.750	2.8560
46.047	3.4210
61.250	4.0400
68.752	4.3875

Fig. 4.14 x_{lr} = 0.7488

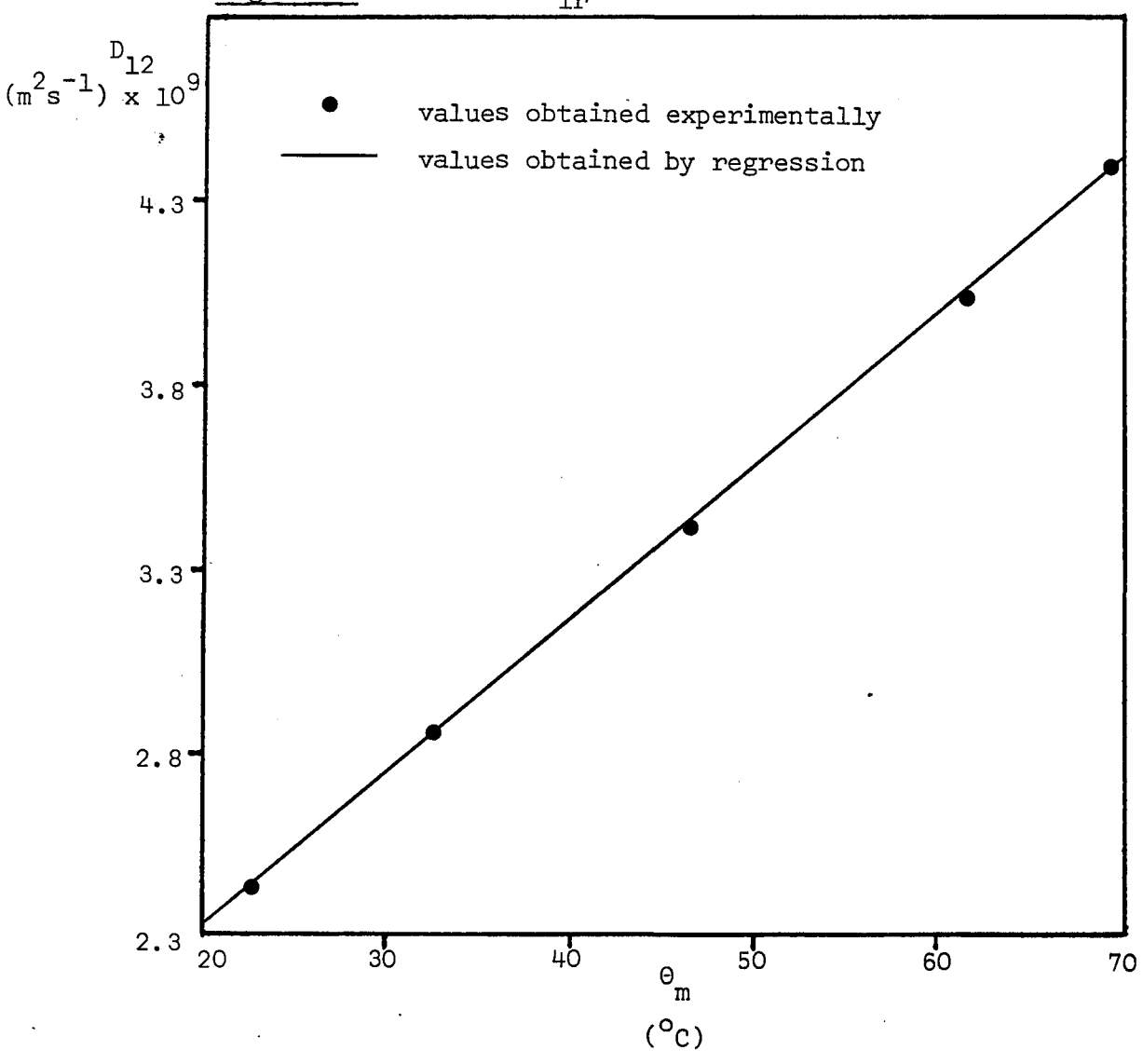

Table 4.15

Θ_m (°C)	D_{12} (m^2s^{-1}) x 10^9
21.756	2.3125
29.548	2.6500
40.012	3.0930
53.128	3.6000
58.551	3.8320
63.644	4.0535
69.769	4.3622

Fig. 4.15 $x_{lr} = 0.9990$

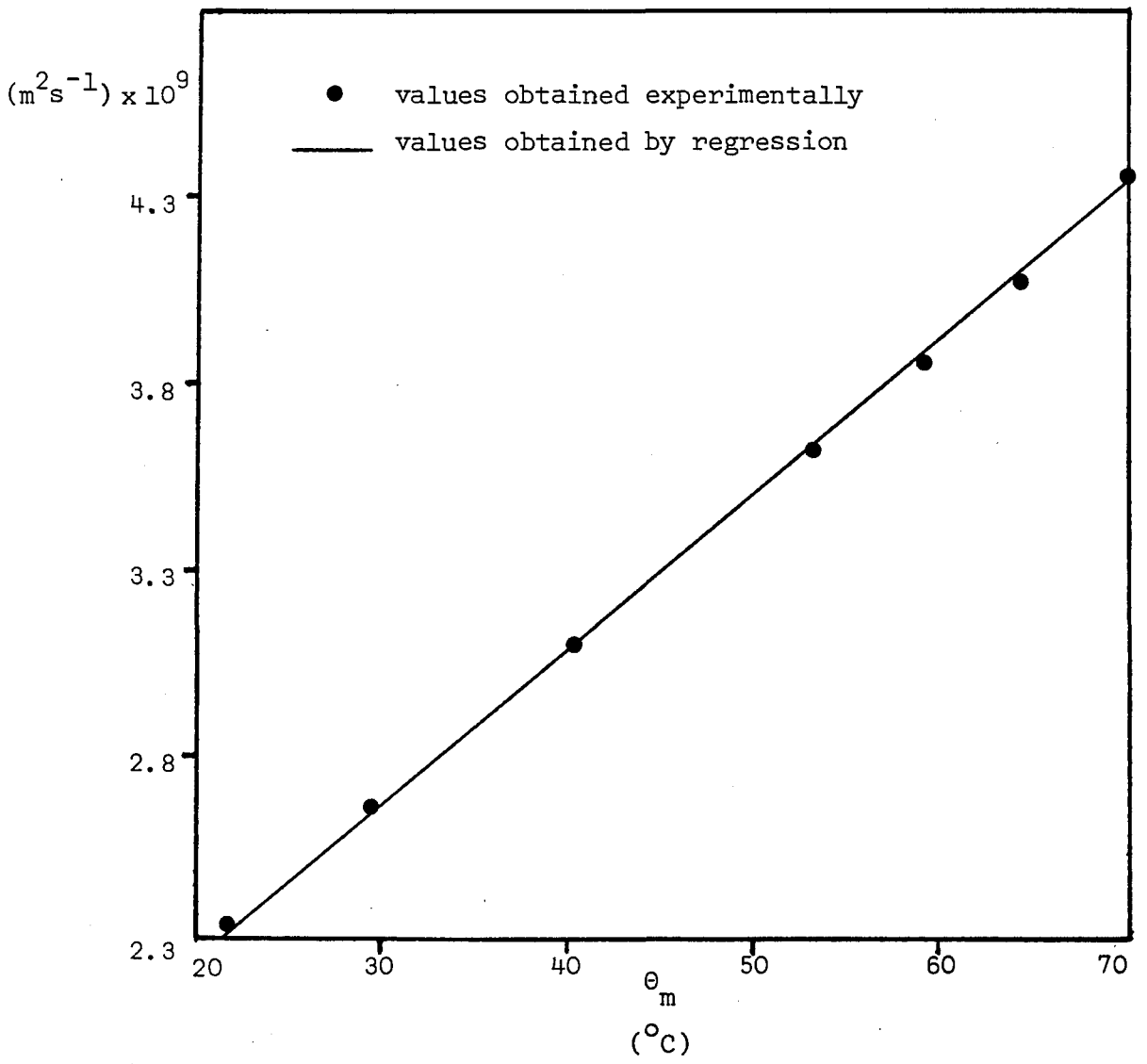

Table 4.16 - Values of the constants A_o^j and A_1^j for each of the regression lines of the form

$$[D_{12}]_{x_{1r}} = A_o^j + A_1^j \theta_m \qquad j = a, b \text{ or } c$$

for the n-alkane binary systems, at a constant composition x_{1r}, and 1 bar pressure

Binary System	x_{1r}	A_o^j $(m^2s^{-1})x10^9$	A_1^j $(m^2s^{-1}{}^oC^{-1})$ $x10^{11}$
$n\text{-}C_6H_{14}$——$n\text{-}C_7H_{16}$	0.0016	2.4501	4.9083
(a)	0.3015	2.3104	4.9528
	0.4985	2.2415	4.9262
	0.6985	2.1987	4.8803
	0.9985	2.0988	4.9347
$n\text{-}C_6H_{14}$ ——$n\text{-}C_8H_{18}$	0.0200	2.2097	4.7402
(b)	0.2023	1.9977	4.7632
	0.4987	1.7687	4.7146
	0.7038	1.5679	4.7319
	0.9980	1.3043	4.7368
$n\text{-}C_7H_{16}$——$n\text{-}C_8H_{18}$	0.0298	1.7295	4.2511
(c)	0.2513	1.6547	4.2068
	0.4988	1.5715	4.2411
	0.7488	1.4789	4.2122
	0.9990	1.3875	4.2158

Fig. 16a - The binary diffusion coefficient, D_{12}, as a function of temperature, Θ_m, for the system hexane-heptane at 5 different mole fractions of heptane, x_{lr}, and 1 bar pressure.

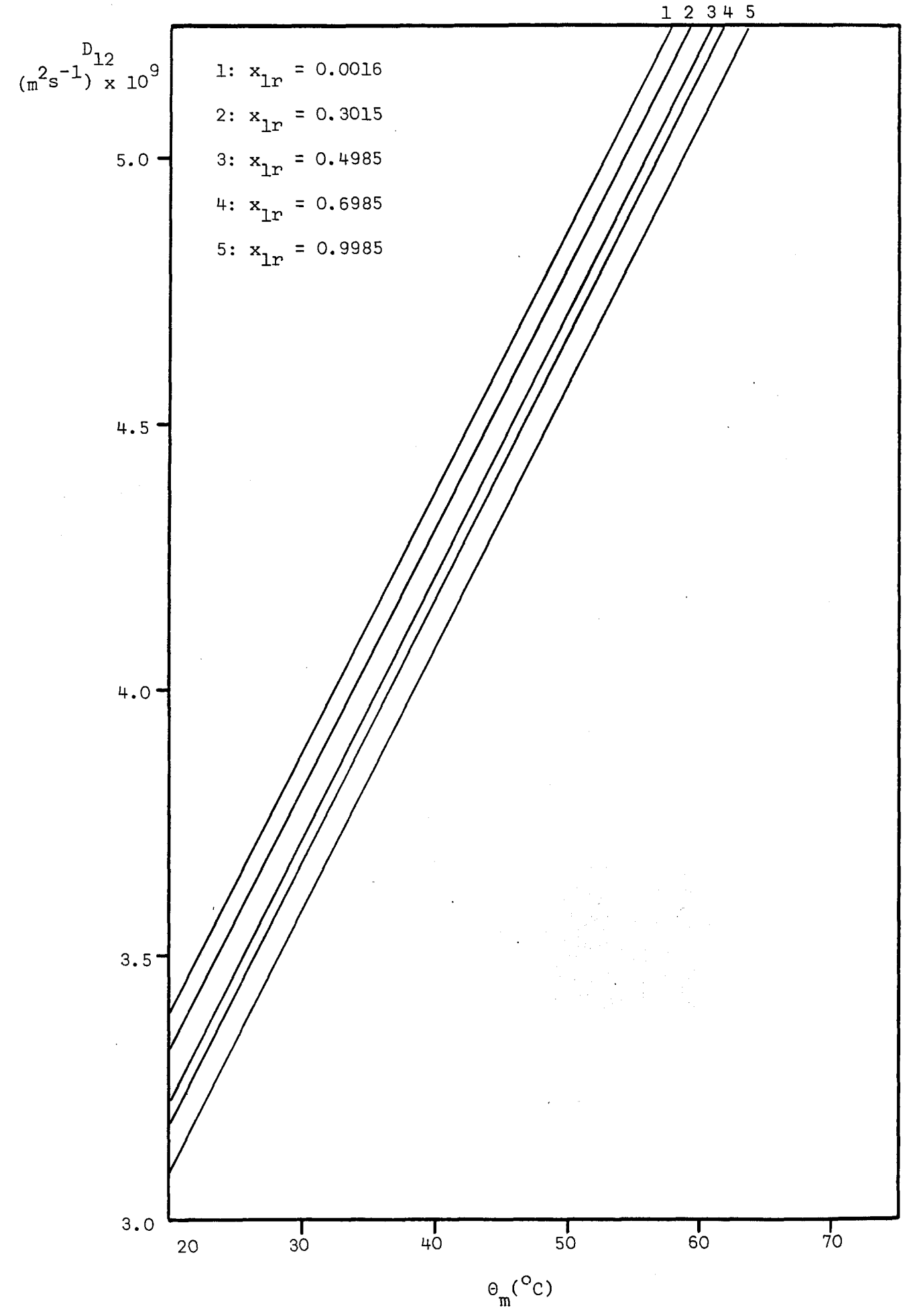

Fig. 16b - The binary diffusion coefficient, D_{12}, as a function of temperature, Θ_m, for the system hexane-octane at 5 different mole fractions of octane, x_{1r}, at 1 bar pressure

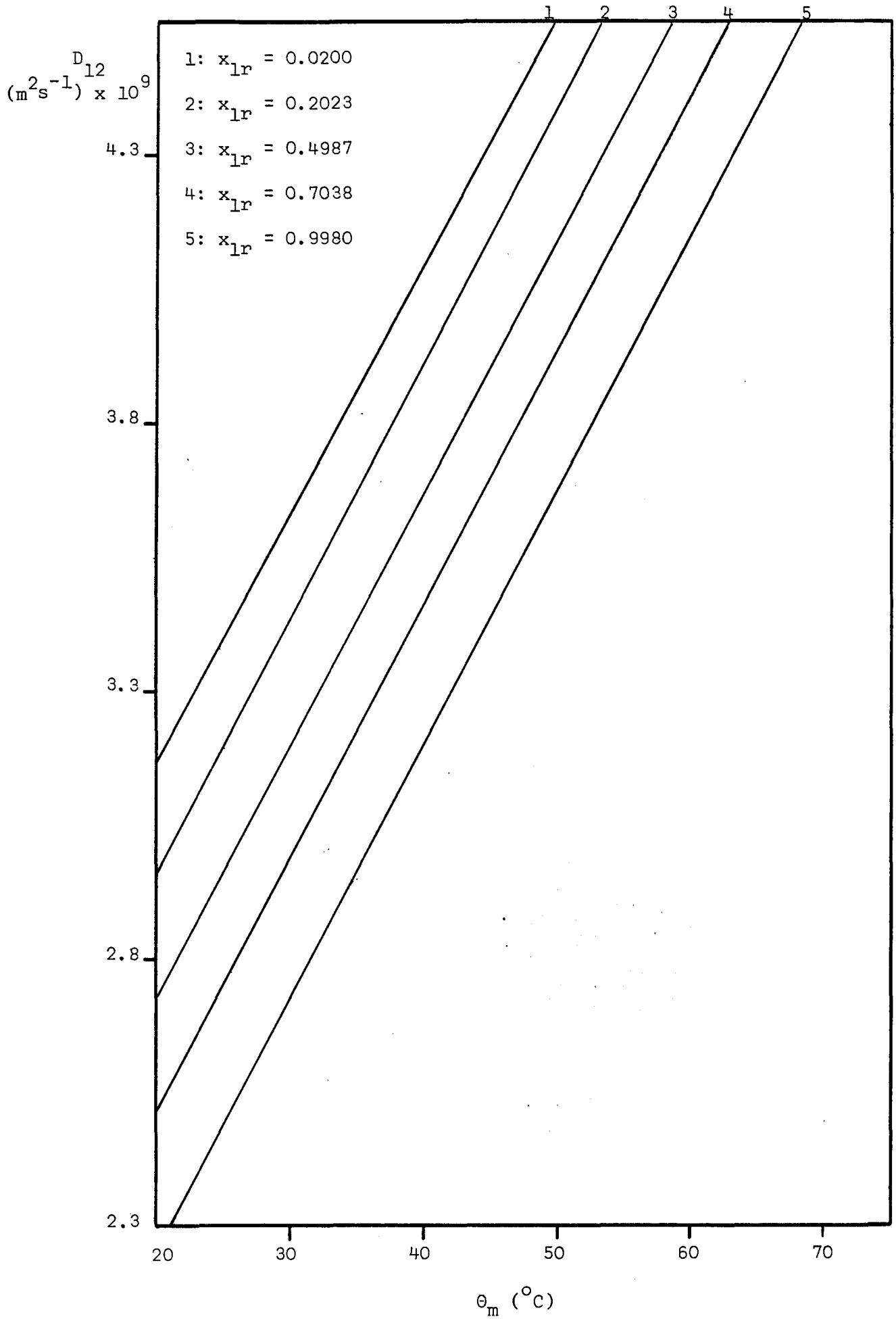

Fig. 16c - The binary diffusion coefficient, D_{12}, as a function of temperature, Θ_m, for the system heptane-octane at 5 different mole fractions of octane, x_{1r}, and 1 bar pressure.

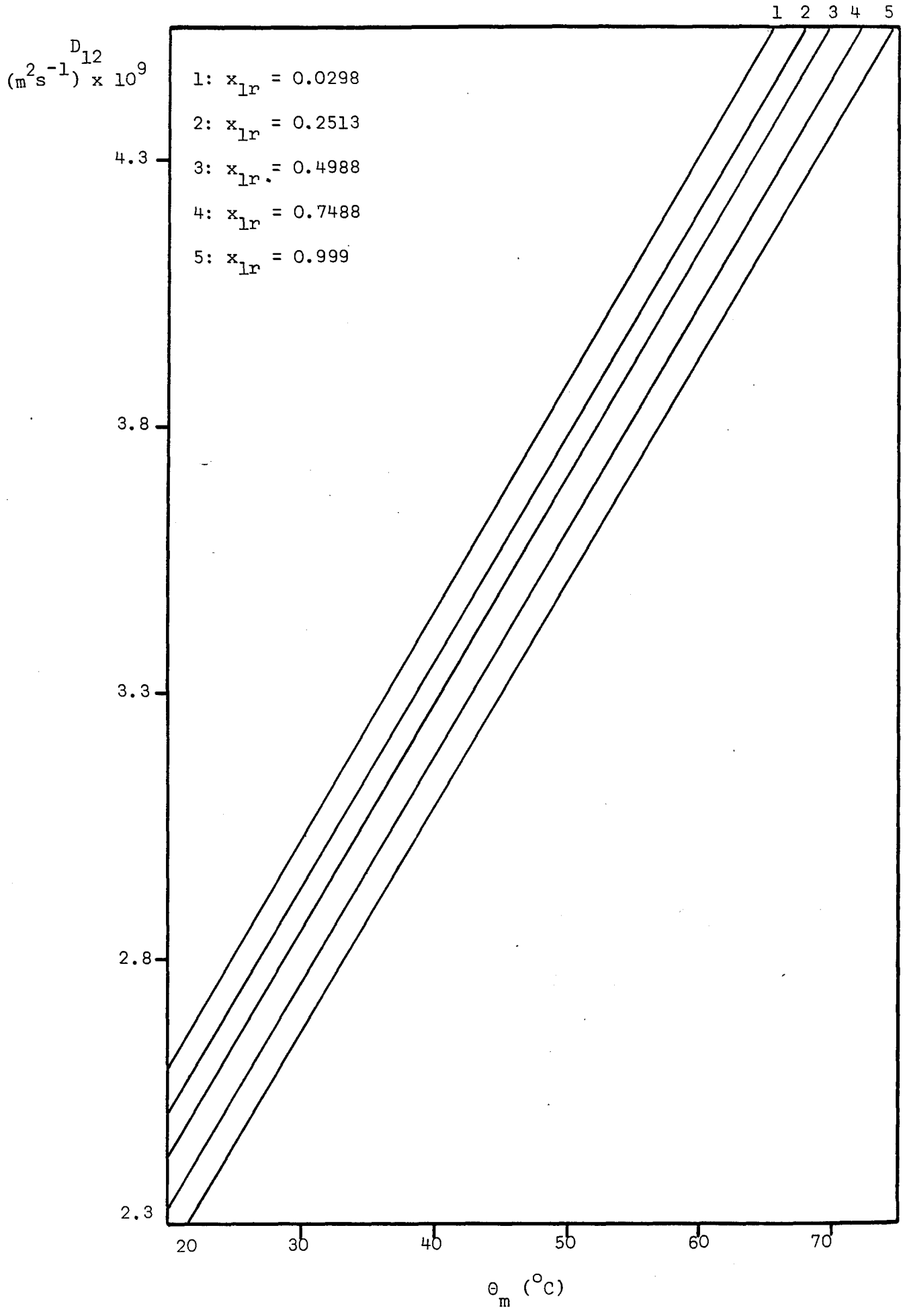

Table 4.17 - Values of the constants A_o^k and A_1^k for each of the regression isotherms of the form

$$[D_{12}]_{\Theta_m} = A_o^k + A_1^k x_{1r}$$

for the n-alkane binary systems at 1 bar pressure.

Binary System	Θ_m (°C)	A_o^k $(m^2s^{-1}) \times 10^9$	A_1^k $(m^2s^{-1}) \times 10^{10}$
$n\text{-}C_6H_{14}$——$n\text{-}C_7H_{16}$	20	3.3869	-3.0418
(a)	30	3.8804	-3.0614
	40	4.3740	-3.0832
	50	4.8676	-3.1057
	60	5.3612	-3.1259
$n\text{-}C_6H_{14}$——$n\text{-}C_8H_{18}$	20	3.1591	-9.1221
(b)	30	3.6337	-9.1388
	40	4.1083	-9.1571
	50	4.5828	-9.1738
	60	5.0574	-9.1905
$n\text{-}C_7H_{16}$——$n\text{-}C_8H_{18}$	20	2.5906	-3.5838
(c)	30	3.0145	-3.6099
	40	3.4383	-3.6356
	50	3.8622	-3.6617
	60	4.2861	-3.6878
	70	4.7100	-3.7150

Fig. 4.17a - Isotherms for the binary diffusion coefficient, D_{12}, of hexane-heptane mixtures as a function of heptane mole fraction, l_{xr}, at five different temperatures and 1 bar pressure.

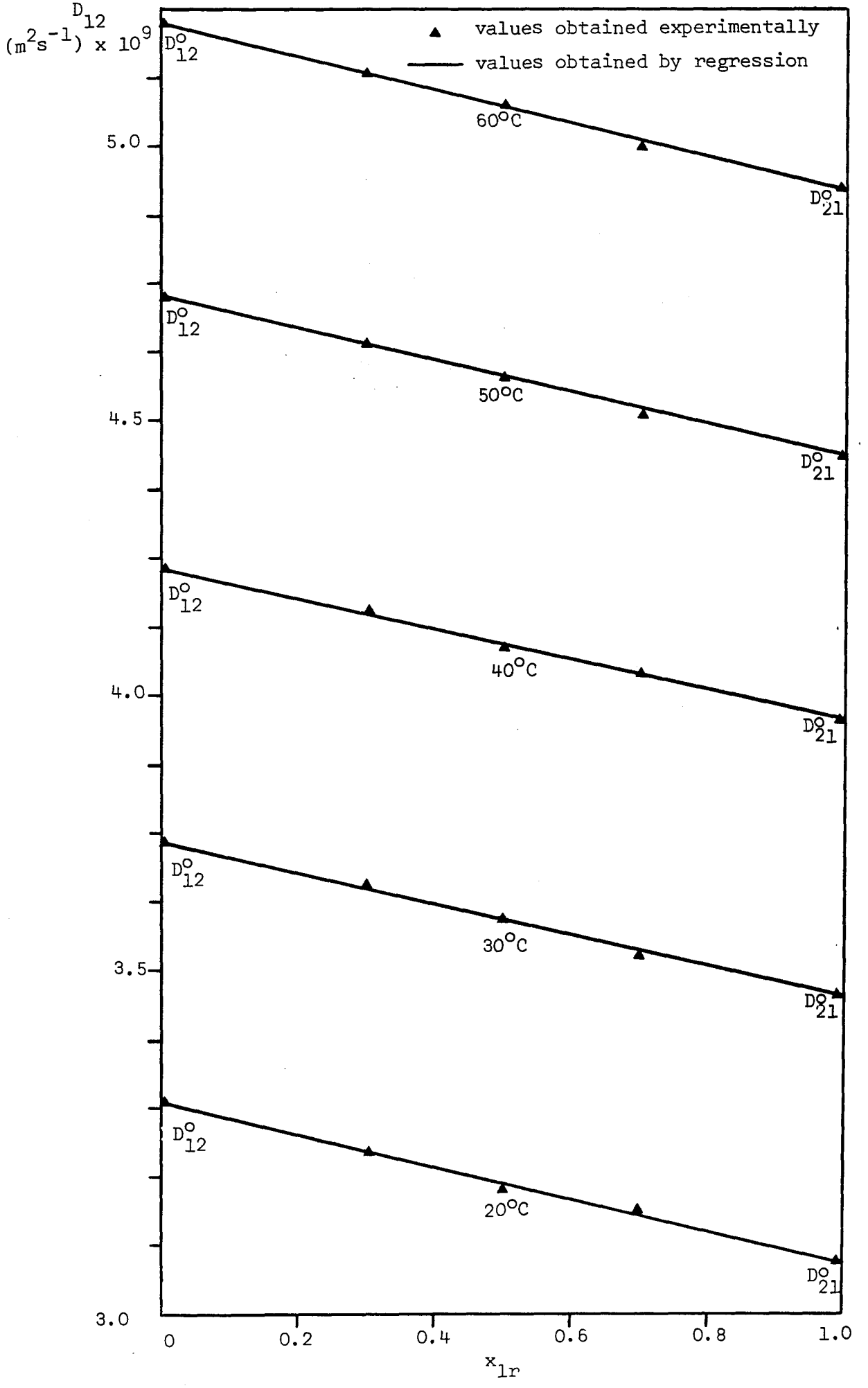

Fig. 4.17b - Isotherms for the binary diffusion coefficient, D_{12}, of hexane-octane mixtures as a function of octane mole fraction, x_{1r}, at five different temperatures and 1 bar pressure.

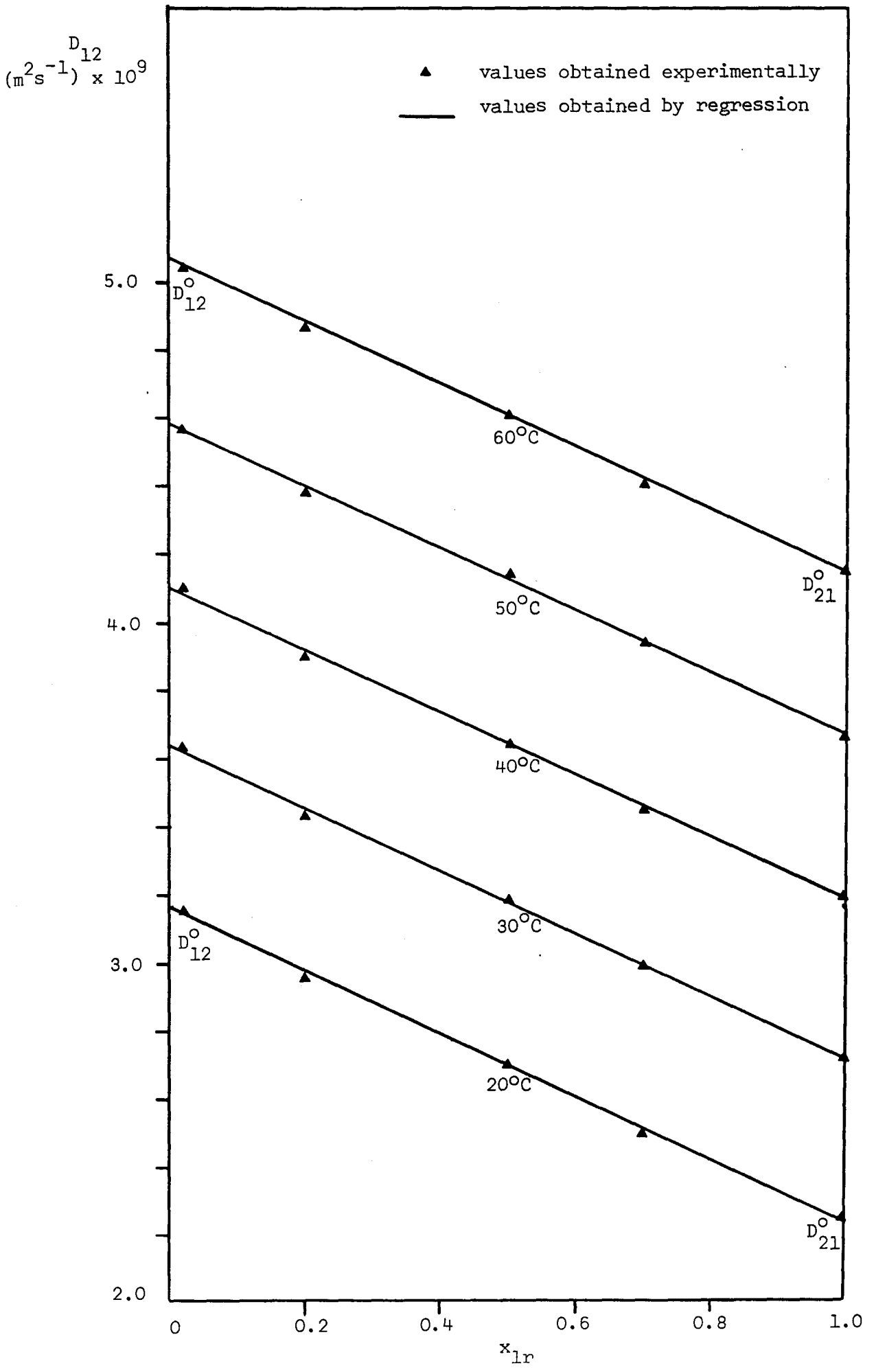

Fig. 4.17c - Isotherms for the binary diffusion coefficient, D_{12}, of heptane-octane mixtures as a function of octane mole fraction, x_{1r}, at six different temperatures and 1 bar pressure.

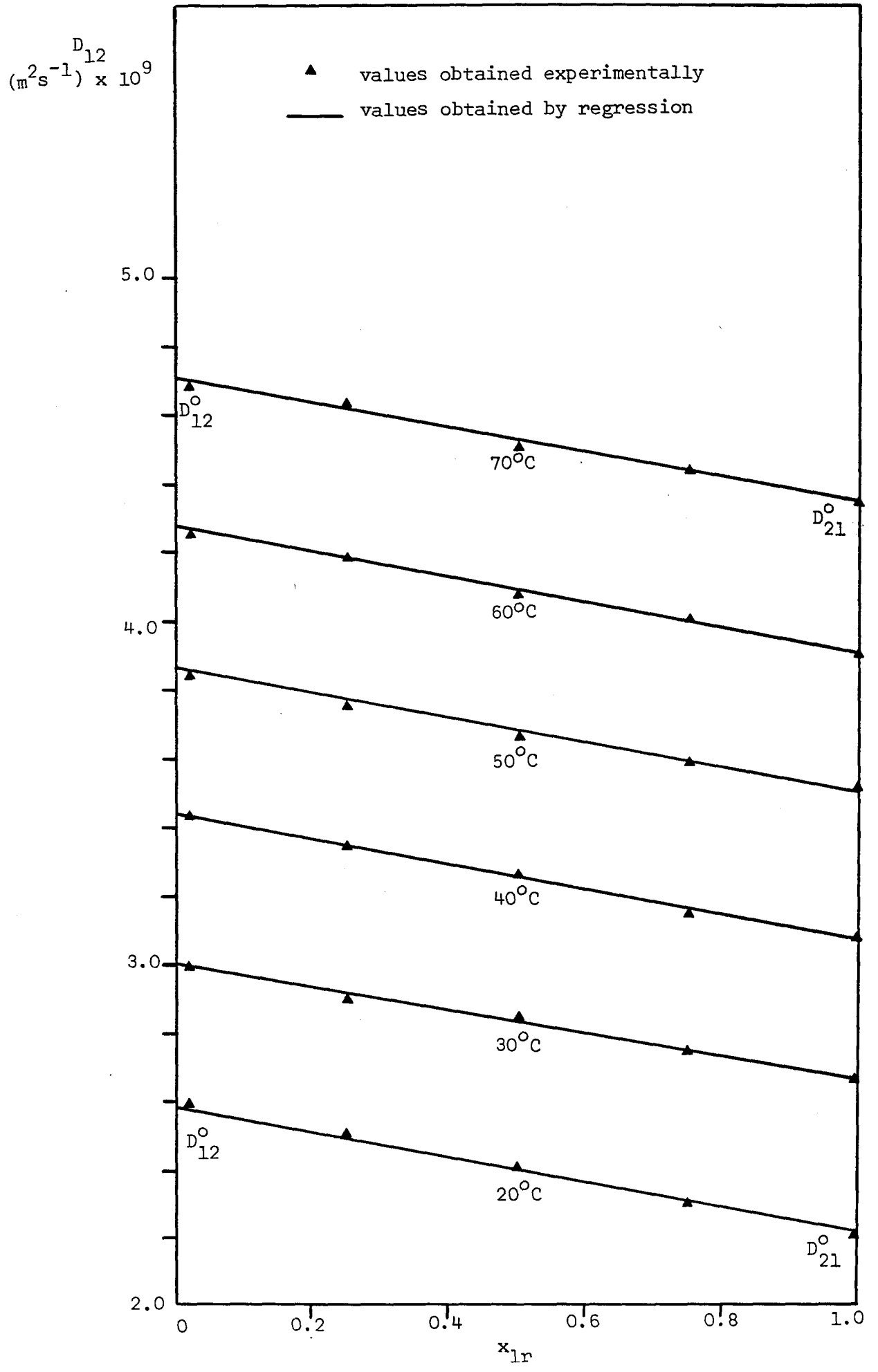

CHAPTER 5

DISCUSSION

5. Introduction

The present experimental data may be used for three purposes. First, the measurements stand alone as definitive values for binary (or mutual) diffusion coefficients for the three systems: n-hexane + n-heptane, n-hexane + n-octane, and n-heptane + n-octane. Secondly, they can be employed to assess the validity of the theoretical descriptions of diffusion processes in liquid mixtures such as those discussed in Chapter 1. Finally, they provide a test of the various empirical prediction schemes for liquid-phase diffusion coefficients. In this Chapter, we consider the last two of these uses in some detail.

5.1 Data for the properties of the pure components and their mixtures

In order to proceed with the above investigations, further relatively accurate data (around ±1%) for the n-alkane mixtures, for example, density, molecular size parameters, viscosity and other properties, are required. Surprisingly, such data for the relatively simple liquid mixtures studied here, particularly in the temperature and composition ranges needed, were difficult to find and in many cases unobtainable. However, with the aid of several publications [6, 39, 113, 151, 187, 188] and institutions [22, 177] we have managed to gather the accurate data (±3% maximum) for the pure components contained in Tables 5.1 and 5.2.

The densities of the mixtures were evaluated using equation (3.7) whilst the corresponding kinematic viscosities were obtained by analogy with the diffusivity results of Chapter 4. That is, from Figs. 4.17(a)-(c), a

TABLE 5.1 - Properties of the pure components [6, 187]

Component	Molecular Weight M	Critical Volume* $\dot{V}_c$ (ml)	Normal Boiling Point, T_b (^oK)	σ^{**} $\times 10^{10}$ (m)
n-Hexane	86.178	370	341.9	5.77 (a)
n-Heptane	100.205	432	371.6	6.05 (b)
n-Octane	114.232	492	398.8	6.28

TABLE 5.2***

θ (^oC)	η_{hex} (C.P)	η_{hep} (C.P.)	η_{oct} (C.P.)	ρ_{hex} (g/ml)	ρ_{hep} (g/ml)	ρ_{oct} (g/ml)
20 (a)	0.312	0.414	0.549	0.659	0.684	0.703
30	0.282	0.371	0.486	0.650	0.675	0.695
40	0.254	0.336	0.434	0.641	0.666	0.687
50	0.234	0.304	0.390	0.631	0.658	0.678
60 (b)	0.215	0.267	0.333	0.622	0.649	0.671
70	0.187	0.231	0.284	0.613	0.641	0.663

* Molar volume at $T_b = \dot{V}_b = 0.28\ (\dot{V}_c)^{1.048}$ [6]

** Mean molecular diameters (a) 20-60°C; (b) 20-70°C [187]

*** Data accurate to (a) ±1%; (b) ±3% [22, 177]

correlation for the present experimental diffusion coefficients (equation (4.2)) may be written in the form

$$[D^c_{12}]_\theta = x_1 D^\circ_{21} + x_2 D^\circ_{12} \tag{5.1}$$

which is identical to the empirical equation (1.52). Here,

$$D^\circ_{21} = \lim_{x_2 \to 0} D_{12} \; ; \; D^\circ_{12} = \lim_{x_1 \to 0} D_{12} \tag{5.2}$$

Thus, by analogy with equation (5.1), the kinematic viscosity, ν, is obtained from the equation

$$[\nu^c_{12}] = x_1 \nu_1 + x_2 \nu_2 \tag{5.3}$$

Since $\nu = \eta/\rho$, where η and ρ denote the dynamic viscosity and density respectively, from equations (3.7) and (5.3) and Tables 5.1 and 5.2 it is possible to write a correlating equation for the composition dependence of the dynamic viscosity in the form

$$[\eta^c_{12}]_\theta = x_1 \eta_1 + x_2 \eta_2 \tag{5.4}$$

which reproduces the available experimental data with a maximum deviation of ±0.5%. Finally, it is useful to record that the absolute viscosity data contained in Table 5.2 fitted the regression lines

$$\eta_{hex} = 0.3558 - 2.41 \times 10^{-3}\theta \quad \text{for pure n-hexane} \tag{5.5}$$
$$(\theta = 20 - 60^\circ C) \; ; \quad \text{in m Pa·s}$$

$$\eta_{hept} = 0.4845 - 3.662 \times 10^{-3}\theta \quad \text{for pure n-heptane} \tag{5.6}$$
$$(\theta = 20 - 70^\circ C)$$

and $$\eta_{oct} = (0.6495 - 5.279 \times 10^{-3}\theta \quad \text{for pure n-octane} \tag{5.7}$$
$$(\theta = 20 - 70^\circ C)$$

with a maximum deviation of ±2.5%. These equations are similar to our

general empirical equation (4.1) which gives the variation of the binary diffusion coefficients with temperature, θ, in the range 20 - 70°C.

5.2 The molecular dynamics approach to the interpretation of binary diffusion coefficients in n-alkanes

The molecular dynamics simulation based on the rough hard sphere theory (Sections 1.2.3 and 1.3.4), formerly developed by Chandler [86] and Dymond [78, 83] for pure fluids, has been extended by Czworniak, Anderson and Pecora [87] and Bertucci et al. [88] and employed to investigate the composition dependence of the binary diffusion coefficients of several two-component solutions. They arrived at the conclusion that for ideal solutions (e.g. binary solutions of n-alkanes, or benzene, chlorobenzene, bromobenzene and toluene), the calculated diffusion coefficients were in 'excellent' agreement (with a mean deviation of ±1% to ±6%) with experiment. But the recent results of Castro and Calado [89, 187] indicate that this is only true for self-diffusion coefficients and binary diffusion coefficients of n-alkanes of close carbon numbers. Nevertheless, we now employ the theoretical analysis described by Czworniak et al. [87] in order to predict the temperature and composition dependence of the binary diffusion coefficients for the n-alkane mixtures studied here and compare the results with those of the present work.

The kinetic diffusion coefficient, D_{12}^{kin}, based on the theory of irreversible thermodynamics and discussed in Chapter 1, Section 1.2.3. is, under isothermal and isobaric conditions, given by

$$D_{12}^{kin} = \frac{D_{12}^{expt}}{\beta_t} \qquad (5.8)$$

where D_{12}^{expt} is the experimental binary diffusion coefficient and β_t is the non-ideality thermodynamic factor

$$\beta_t = 1 + \frac{\partial \ln a_i}{\partial \ln x_i}$$

For the present systems [39, 145] the factor β_t may be expressed as

$$\beta_t = 1 + 0.002(n_1 - n_2)^2 x_1 x_2 \quad ,$$

so that for the present purposes, it may be taken as unity with negligible error. Czworniak et al. [87] and Bertucci et al. [88] assume that D_{12}^{kin} of a real binary fluid is equal to that of a two-component mixture of rough hard spheres at the same temperature and with the same number density and mole fraction as the real fluid, the masses of hard spheres being equal to those of the corresponding molecules. In this case, the theoretical, or kinetic, binary diffusion coefficient is given by equation (1.71) which may be rewritten as

$$\left[D_{12}^{kin}\right]_{theory} = D_E^{kin} \; A \; F\left(\phi, \frac{m_1}{m_2}, \frac{\sigma_1}{\sigma_2}, x_1\right) \tag{5.9}$$

The Enskog kinetic diffusivity, D_E^{kin} at an absolute temperature T, is obtainable from

$$D_E^{kin} = \left(\frac{3}{8n^* \sigma_{12}^2}\right)\left[\frac{KT}{2\pi}\left(\frac{m_1+m_2}{m_1 m_2}\right)\right]^{\frac{1}{2}} \left(\frac{1}{g_{12}(\sigma_{12})}\right) \tag{5.10}$$

where n^* is the total number density, defined by

$$n^* = \frac{N \rho_{12}}{x_1 M_1 + x_2 M_2} \tag{5.11}$$

so that

$$n_i^* = n^* x_i \tag{5.12}$$

and

$$\sigma_{12} = \frac{\sigma_1 + \sigma_2}{2} \quad \text{particle (or molecular) size parameter} \tag{5.13}$$

$$N = 6.022 \times 10^{23} \text{ mole}^{-1} \text{ (Avagadro's number)}$$

$$K = 1.381 \times 10^{-23} \text{ J } {}^{o}K^{-1} \text{ (Boltzman's constant)}$$

If the last bracket term of equation (5.10) is excluded, the equation becomes identical to that for a dilute, binary gas mixture. In addition,

m_1 and m_2 represent the molecular masses of the diffusing species and $g_{12}(\sigma_{12})$ the pair distribution function for unlike species at contact. The factor F accounts for the deviations of the diffusion coefficient from the Enskog value arising from molecular velocity correlations. The symbol A represents translational-rotational coupling constant introduced by Chandler [86] which is supposed to depend just upon the molecular species involved and is, in particular, independent of composition and temperature.

In the present analysis, we presume that equation (5.9) is valid and have employed our experimental data to determine the translational-rotational coupling constant A for each system at two representative temperatures 20°C and 70°C. For this purpose, we have calculated the pair distribution function $g_{12}(\sigma_{12})$ according to the method proposed by Czworniak et al. [87]. In their approach the pair distribution function is written as

$$g_{12}(\sigma_{12}) \simeq g_{py}(\sigma_{12})[Z_{cs} - 1]/[Z_{py} - 1] \tag{5.14}$$

where $g_{py}(\sigma_{12})$ is the Percus-Yevick pair distribution function for unlike hard spheres. In addition, Z_{py} is the Percus-Yevick [197] compressivity factor and Z_{cs} that for the Carnahan-Starling [85] equation of state for hard-sphere systems. All of the quantities g_{py}, Z_{cs} and Z_{py} may be expressed as analytic functions of the packing fractions of individual species, η_i, in a hard-sphere mixture,

$$\phi_i = \frac{\pi}{6} n_i^* \sigma_{pi}^3 \tag{5.15a}$$

and the total packing fraction [87]

$$\phi = \phi_1 + \phi_2 \tag{5.15b}$$

The factor F, which expresses the deviations of the diffusion coefficient of a real hard-sphere fluid mixture from that of an Enskog fluid, has been obtained from a correlation of the results of molecular dynamics simulations of self-diffusion in fluid mixtures [79, 87]. The simulations were carried out for a trace of one species in another and for mass and size ratios near unity, and so yield the factor F at limiting concentrations $F(\phi, m_1/m_2, \sigma_1/\sigma_2, 1)$ or $F(\phi, m_1/m_2, \sigma_1/\sigma_2, 0)$. Czworniak et al. [87] have suggested that the value of F appropriate to any mixture of the same two components may be obtained by a simple linear combination of these results so that

$$F(\phi, m_1/m_2, \sigma_1/\sigma_2, x_1) \simeq x_1 F(\phi, m_1/m_2, \sigma_1/\sigma_2, 1) + x_2 F(\phi, m_1/m_2, \sigma_1/\sigma_2, 0) \qquad (5.16)$$

The correlations for $F(\phi, m_1/m_2, \sigma_1/\sigma_2, 0)$ have been adapted here without change.

In order to make use of these results we have employed the rigid sphere diameters of the n-hexane, n-heptane and n-octane determined by Castro and Calado [187] which permit the evaluation of $g_{12}(\sigma_{12})$ and F for each binary system at each temperature. Subsequently, the value of the translation-rotation coupling constant A for each system has been determined by a least-square fit to the present experimental data for each temperature. It should be noted that the determination of A in this manner does not affect the composition dependence of the diffusion coefficient obtained theoretically, but merely serves to scale the results.

Figures 5.1 - 5.3 contain plots of the experimental diffusion coefficients together with the least squares representation of them according to equations (5.9) and (5.10). Table 5.1 includes the values of the rigid

FIG. 5.1 - Binary diffusion coefficient, D_{12}, of the hexane-heptane mixture as a function of composition, at 20°C and 60°C and 1 bar, determined experimentally and by Molecular Dynamics Simulation

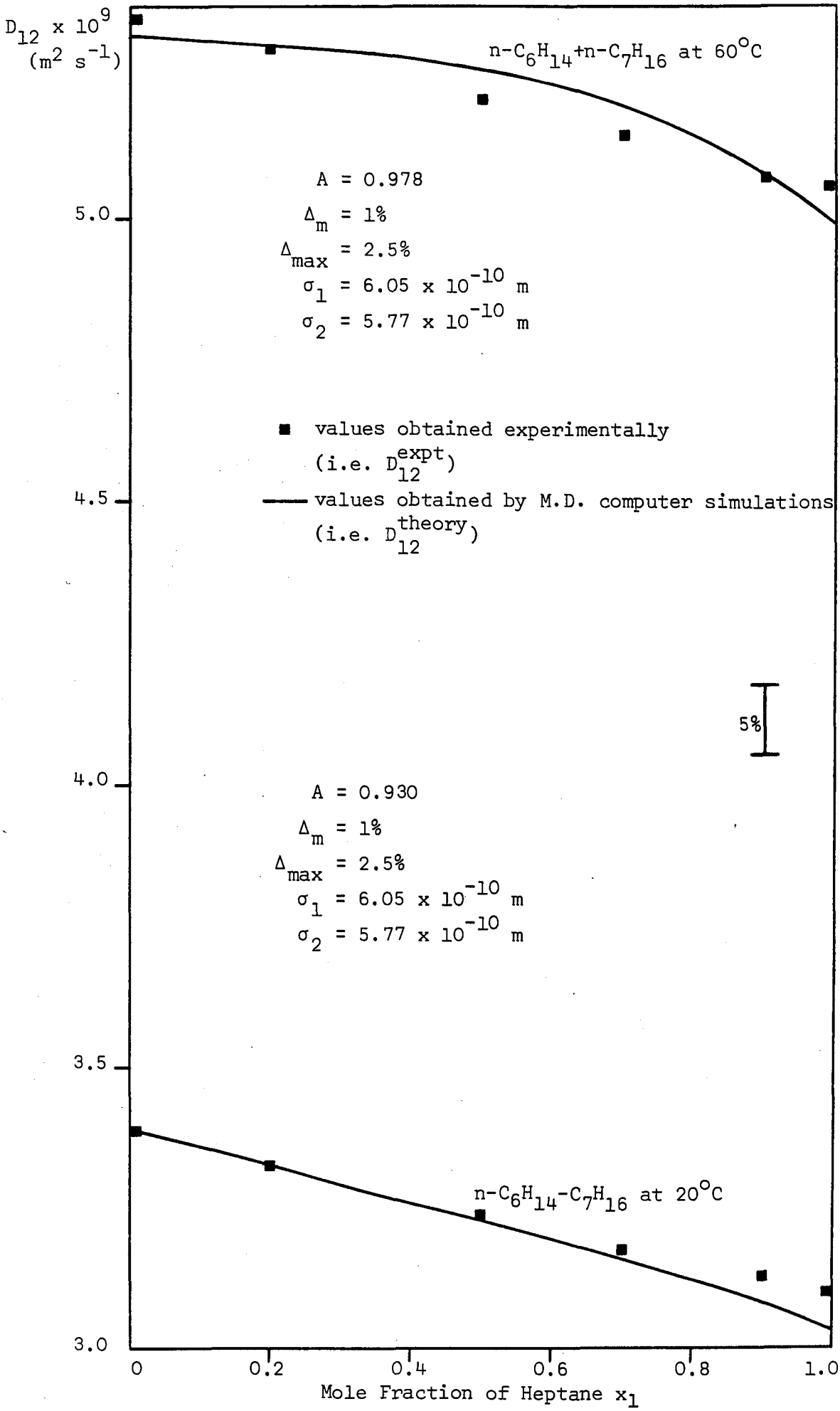

FIG. 5.2 - Binary diffusion coefficient, D_{12}, of the heptane-octane mixture as a function of composition, at 20°C and 70°C and 1 bar, determined experimentally and by Molecular Dynamics Simulation

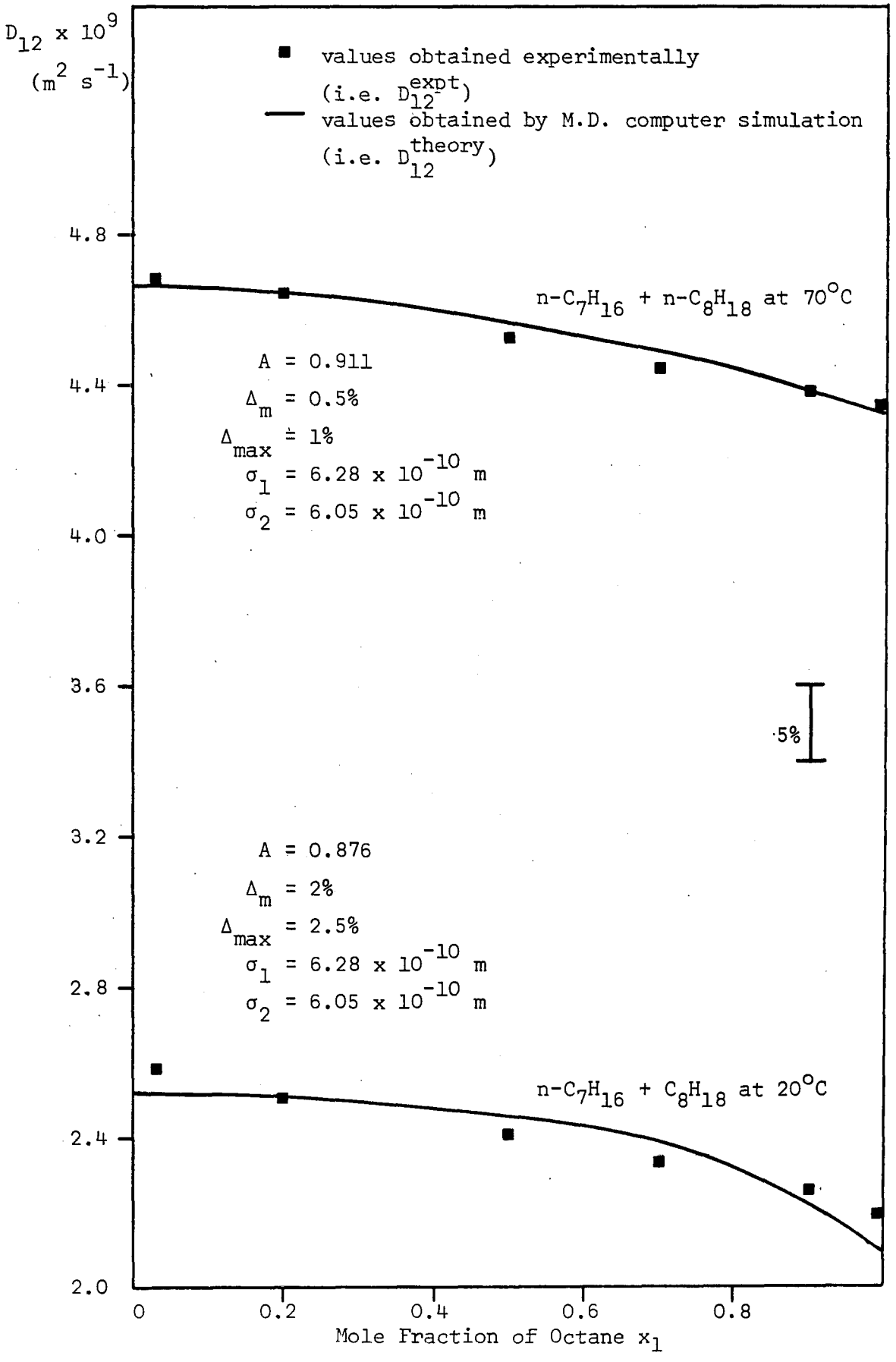

FIG. 5.3 - Binary diffusion coefficient, D_{12}, of the hexane-octane mixture as a function of composition, at 20°C and 60°C and 1 bar, determined experimentally and by Molecular Dynamics Simulation

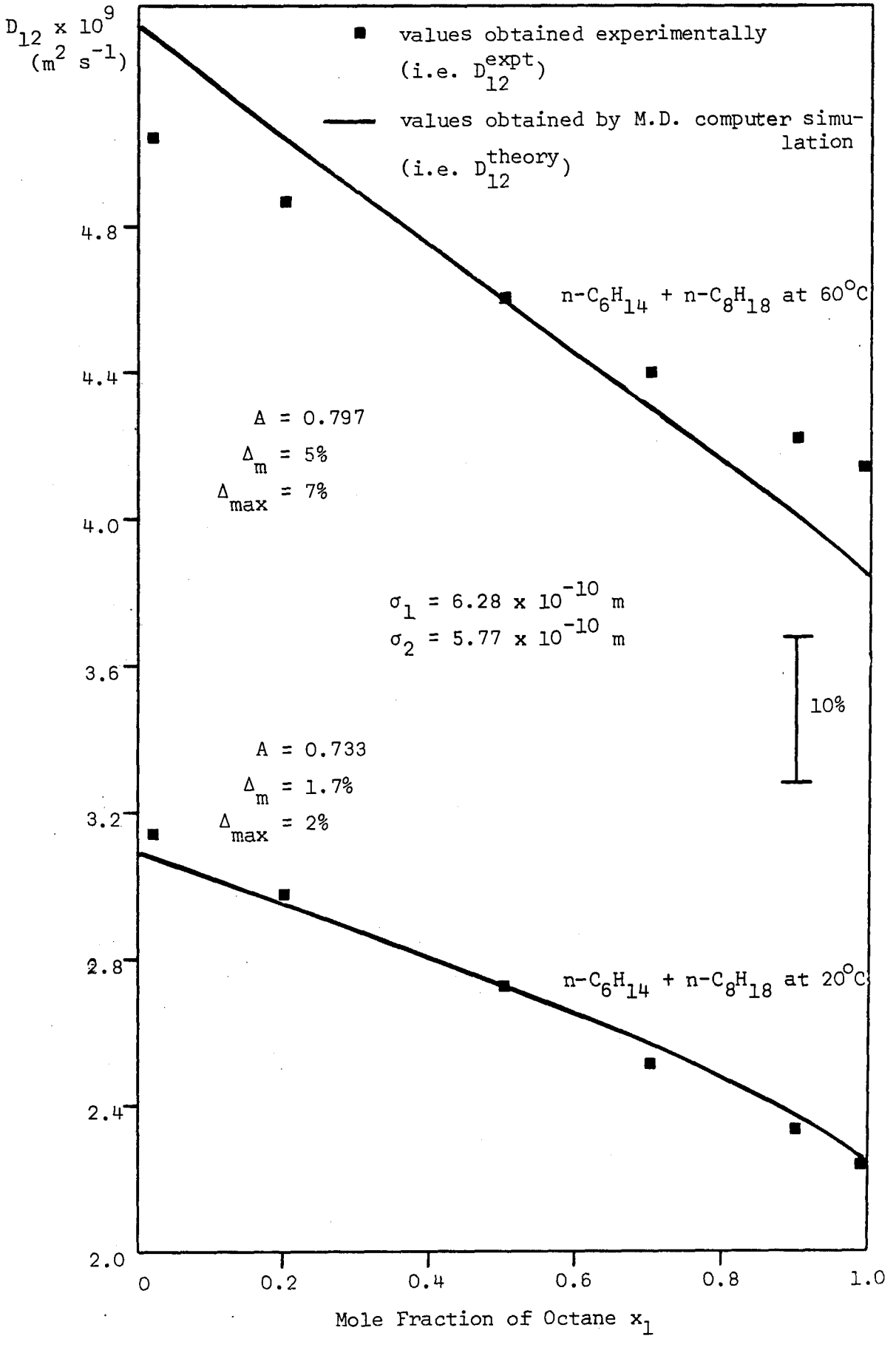

sphere diameters for each molecule, whereas Table 5.3 contains the derived values of the translation-rotation coupling constant, A. The latter Table also includes the mean and maximum deviation of the experimental data from the representation by equations (5.9) and (5.10).

TABLE 5.3

Binary System	Θ (^{o}C)	A	Δ_m (%)	Δ_{max} (%)
$C_6 + C_7$	20	0.930	1.0	2.5
	60	0.978	1.0	2.5
$C_7 + C_8$	20	0.876	2.0	2.5
	70	0.911	0.5	1.0
$C_6 + C_8$	20	0.733	1.7	2.0
	60	0.797	5.0	7.0

It can be seen that for the systems hexane-heptane and heptane-octane, the composition dependence of the diffusion coefficient obtained theoretically, which is independent of the value of A is in reasonable agreement with that observed experimentally. The maximum deviation from the present experimental data is one of ±2.5%. The derived value of A lies within the range expected and while it is not completely temperature independent is very nearly so. On the other hand, for the system hexane-octane, the composition dependence of the diffusion coefficient predicted theoretically is significantly different from that observed experimentally at the higher temperature. At this higher temperature, the deviation amounts to as much as ±7%. It is possible that this increased discrepancy is to be attributed to the fact that the mass and size ratios for this system are sufficiently different from unity that the computer simulations on which the calculations are based are no longer applicable. Nevertheless, these results confirm that the rigid sphere model of a fluid, supported by molecular dynamics simulation results can give a reasonable description of the behaviour of diffusion coefficients in relatively complicated molecular liquids.

5.3 Validity of simple models of diffusion

The simple models of diffusion discussed in Chapter 1, Section 1.2, such as Eyring's activation energy [63, 65] and Stokes-Einstein models [13, 17, 127] suggest that the group $[KT/D^{o}_{12}\eta]$ should be temperature independent. Thus the applicability of such models may be assessed by an examination of the constancy of the experimental values of the group $[KT/D^{o}_{12}\eta]$ for the liquids investigated in this work. Accordingly, Fig. 5.4 displays plots of this group as a function of absolute temperature, which have been constructed with the aid of our diffusivity data for the extremely dilute solutions (i.e. the limiting D^{o}_{12} values) and the viscosities contained in Table 5.2. It is evident that the group $[KT/D^{o}_{12}\eta]$ increases as the temperature is increased beyond 313 ^{o}K. In particular, for the hexane-heptane system, the value of the group at 333 ^{o}K lies some 8% above that at 293 ^{o}K, whereas for the heptane-octane system the discrepancy at 343 ^{o}K is 12%. Thus, on this basis, and because the mixtures considered here are very nearly ideal, we must conclude that neither the Eyring nor the Stokes-Einstein model, or other similar models, are entirely adequate to describe the diffusion processes in liquids.

5.4 Schemes for predicting the liquid-phase diffusivities

There exist a large number of empirical prediction and correlation schemes for the binary diffusion coefficient in liquid mixtures, relying to a varying extent on simplified theories (Chapter 1). Because it is impossible to carry out measurements on all possible systems over a wide range of conditions, it is certain that such schemes will continue to be used for engineering design purposes for some time to come. Now we employ the present experimental data in order to assess the validity of some of the prediction schemes in frequent use.

FIG. 5.4 - The group $[KT/D^{o}_{12}\eta]$ for two n-alkane binary systems at infinite dilution

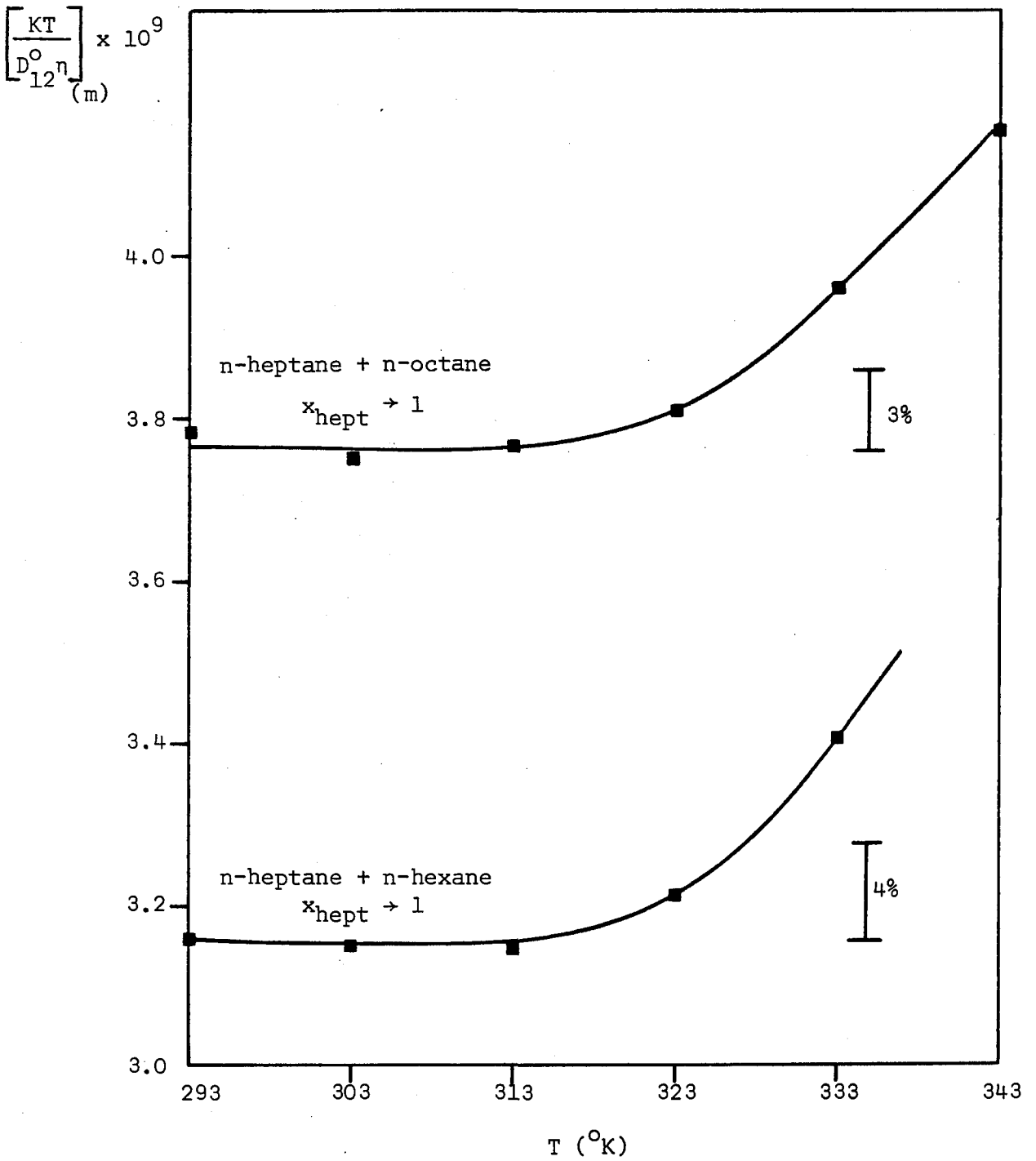

From Bearman's analysis [44, 45], based on statistical thermodynamics, Darken [195] proposed that the composition dependence of the binary diffusion coefficient of a regular solution is given by

$$D_{12}^{c} = (x_1 D_{22} + x_2 D_{11})\beta_t \qquad (5.17)$$

which for ideal solutions becomes

$$D_{12}^{c} = x_1 D_{22} + x_2 D_{11} \quad .$$

In these equations, D_{ii} represents the self-diffusion coefficient of pure liquid i. On the other hand, several investigators (e.g. Van Geet et al. [39], Sanchez et al. [90] and Babb et al. [196]) have found that an empirical equation of the form of (5.1) which involves limiting diffusion coefficients of the mixture predicts the composition dependence of the binary diffusion coefficients satisfactorily. Clearly, equation (5.1) has a great practical advantage over equation (5.17) since only two values of diffusivity are required (the mutual diffusivities D_{12}^{o} and D_{21}^{o}) which are more easily measured than the self-diffusivities (D_{11} and D_{22}). The latter are concentration dependent and have to be measured throughout the entire range of concentration. The limiting values of the binary diffusion coefficients (D_{12}^{o} and D_{21}^{o}) may themselves be calculated from several well-known empirical correlations such as that of Wilke and Chang which will be discussed later in this chapter.

The limiting mutual diffusion coefficients for the systems studied in this work have been measured on a number of occasions by different investigators. Van Geet [39], Lo [145] and Bidlack et al. [189] have employed the diaphragm cell and Table 5.4 lists their values and the deviations from those of the present work. The agreement is generally good - the deviations not exceeding ±2%. On the other hand, the results

of Moore and Wellek [151] obtained with a porous frit apparatus deviate considerably from the present data as shown in Table 5.4 and Figs. 5.5 and 5.6. In the worst case, the deviation amounts to 11%. These deviations, combined with the non-physical behaviour displayed by Moore and Wellek's results confirm that the porous frits method of measurement is not reliable [37].

A semi-empirical expression for the composition dependence of the binary diffusion coefficients of ideal liquid mixtures has been deduced by Hartley and Crank [18, 27, 59] which may be written as

$$\left[\frac{D_{12}^{c}\eta_{12}^{c}}{KT}\right] = \frac{1}{\alpha_1^{\cdot}} + \left(\frac{\alpha_1^{\cdot} - \alpha_2^{\cdot}}{\alpha_1^{\cdot}\alpha_2^{\cdot}}\right)x_1 \qquad (5.18)$$

$$= c + mx \quad \text{(Bearman [18, 27])}$$

where $\alpha_p^{\cdot}$ is a constant proportional to the molecular diameter, σ_p, of the diffusing species. It is useful to note that at either end of composition range x_1 = 0-1, this equation reduces to the familiar Stokes-Einstein relation (Chapter 1).

The present data for the diffusion coefficients, together with the available viscosity data (Table 5.2 and equation (5.4)) may be employed to test the applicability of this relationship. Figure 5.7 contains a plot of the group $[D_{12}^{c}\eta_{12}/T]$ as a function of the mole fraction for the hexane-heptane system at three temperatures - which is linear as expected on the basis of equation (5.18). This linearity allows us to determine the values of $\alpha_1^{\cdot}$ and $\alpha_2^{\cdot}$ from the intercept and slope of the line. Assuming that $\alpha_p^{\cdot} = 2\pi\sigma_p$, the values of σ_1 (for n-heptane) and σ_2 (for n-hexane) derived were σ_1 = (6.07, 6.10 and 6.30) x 10^{-10} m and (5.95, 5.88 and 6.10) x 10^{-10} m for T = 293, 313 and 333 ^{o}K respectively. The mean values for each species are therefore σ_1 = 6.16 x 10^{-10} m and

$\sigma_2 = 5.97 \times 10^{-10}$ m which are in quite good accord with those obtained in other ways (Table 5.1).

For the remaining systems, Fig. 5.8 shows that equation (5.18) is not obeyed, which casts considerable doubt on the general validity of equation (5.18).

Finally, Tables 5.4 and 5.5 compare the present results with those obtained from several commonly used correlations for predicting the limiting diffusivities of binary liquid mixtures. In particular, we include the Wilke-Chang equation [190] which requires the viscosity of the solvent and the molar volume of the solute $(V_1)_b$ at the normal boiling point of the solvent. It can be seen that this correlation leads to deviations of as much as 14% from the present results. It has been found that a modest improvement in the predictions of this scheme may be achieved if $(V_1)_b$ is replaced by $(V_1)_\theta$, the molar volume of the solute at the temperature at which the diffusion coefficient is to be calculated (see Tables 5.4 and 5.5).

The other methods of prediction which have been examined include those due to Lusis-Ratcliff [191], Otherm-Thakar [192], Scheibel [5] and Reddy-Doraiswamy [194]. Table 5.4 demonstrates that among these, only the Lusis-Ratcliff method leads to generally good results. Over the entire body of the present experimental data only the modified Wilke-Change method or the Lusis-Ratcliff scheme provide acceptable predictions of the diffusion coefficients with a maximum deviation of ±6% (Tables 5.4 and 5.5).

Thus, in conclusion, three important facts have emerged as a result of the data presented in Chapter 4. First, the simple models describing diffusion in liquid mixtures on the basis of Stokes-Einstein's or Eyring's

treatment are generally inaccurate. Secondly, the interpretation of temperature and concentration dependence of the binary diffusion coefficients by the rough hard-sphere model is in excellent agreement with our experimental results for n-hexane + n-heptane, and n-heptane + n-octane mixtures, but for the n-hexane + n-octane mixture the agreement deteriorates. This suggests that only for the binary mixtures in which molecular mass ratios of the diffusing species are close to unity is the present scheme appropriate. Finally, we have found that the concentration dependence of the binary diffusion coefficients of the n-alkanes studied here is given very accurately (±2%) by the empirical correlation

$$[D_{21}^{c}]_{\Theta} = x_1 D_{21}^{o} + x_2 D_{12}^{o}$$

TABLE 5.4 - Comparison of the literature values of the limiting diffusion coefficient D_{12}^{o} with those obtained in this work, for three different binary mixtures at 25°C and 1 bar.

Solute 1	Solvent 2	D_{12}^{o} $(m^2 s^{-1}) \times 10^9$	Data Reference	% Deviation* From Present Work
$n\text{-}C_7H_{16}$	$n\text{-}C_6H_{14}$	3.71	(1) Present work	0
		3.75	(2) Lo [145] (Diaphragm cell)	-1
		3.78	(3) Bidlack et al. [189] (Diaphragm cell)	-2
		3.27	(4) Wilke-Chang [190] (original; at $(V_1)_b$)	12
		3.74	(5) Wilke-Chang (modified in this work; at $(V_1)_\theta$)	-1
		3.63	(6) Lusis-Ratcliff [191]	2
		3.64	(7) Othmer-Thakar [192]	2
		3.58	(8) Scheibel [193]	3.5
		3.32	(9) Reddy-Doraiswamy [194]	10
$n\text{-}C_8H_{18}$	$n\text{-}C_6H_{14}$	3.46	(1)	0
		3.46	(2)	0
		3.47	(3)	-0.3
		2.98	(4)	14
		3.25	(5)	6
		3.32	(6)	4
		3.56	(7)	-3
		3.34	(8)	3.5
		3.17	(9)	8
$n\text{-}C_8H_{18}$	$n\text{-}C_7H_{16}$	2.85	(1)	0
		2.84	(2)	0.3
		2.88	(3)	-1
		2.45	(4)	14
		2.70	(5)	5
		2.70	(6)	5
		2.26	(7)	20
		3.16	(8)	-10
		2.61	(9)	8

TABLE 5.5 - Comparison of D°_{12} values of three different binary mixtures in the range 20 - 60°C and 1 bar, obtained by the empirical correlation, with those of present work.

* % deviation = $\frac{(D^{\circ}_{12})_{Aliz} - (D^{\circ}_{12})_{ref}}{(D^{\circ}_{12})_{Aliz}} \times 100$

Solute 1	Solvent 2	θ (°C)	D°_{12} $(m^2 s^{-1})_{x\ 10^9}$	Data Reference	% Deviation From Present Work*
$n\text{-}C_7H_{16}$	$n\text{-}C_6H_{14}$	20	3.38	(1) Present work	0
			3.05	(2) Wilke-Chang [190] (original)	10
			3.24	(3) Wilke-Chang (modified in this work)	4
			3.37	(4) Lusis-Ratcliff [191]	0.3
		40	4.37	(1)	0
			4.00	(2)	8.5
			4.24	(3)	3
			4.25	(4)	4
		60	5.35	(1)	0
			5.03	(2)	6
			5.19	(3)	3
			5.38	(4)	0.6
$n\text{-}C_8H_{18}$	$n\text{-}C_6H_{14}$	20	3.15	(1)	0
			2.81	(2)	11
			3.06	(3)	3
			3.17	(4)	-0.6
		40	4.10	(1)	0
			3.69	(2)	10
			4.00	(3)	2
			3.92	(4)	4
		60	5.05	(1)	0
			4.64	(2)	8
			4.88	(3)	3
			4.94	(4)	2
$n\text{-}C_8H_{18}$	$n\text{-}C_7H_{16}$	20	2.58	(1)	0
			2.28	(2)	12
			2.47	(3)	4
			2.45	(4)	5
		40	3.43	(1)	0
			3.03	(2)	12
			3.32	(3)	3
			3.28	(4)	4
		60	4.28	(1)	0
			4.02	(2)	6
			4.23	(3)	1
			4.19	(4)	2

FIG. 5.5 - Comparison of the limiting diffusion coefficients for the heptane-octane mixtures at different temperatures and 1 bar, obtained by Moore and Wellek [151], with those determined in the present work.

$D^{\circ}_{12} = \lim_{x_1 \to 0} (D_{12})$; x_1 = heptane mole fraction

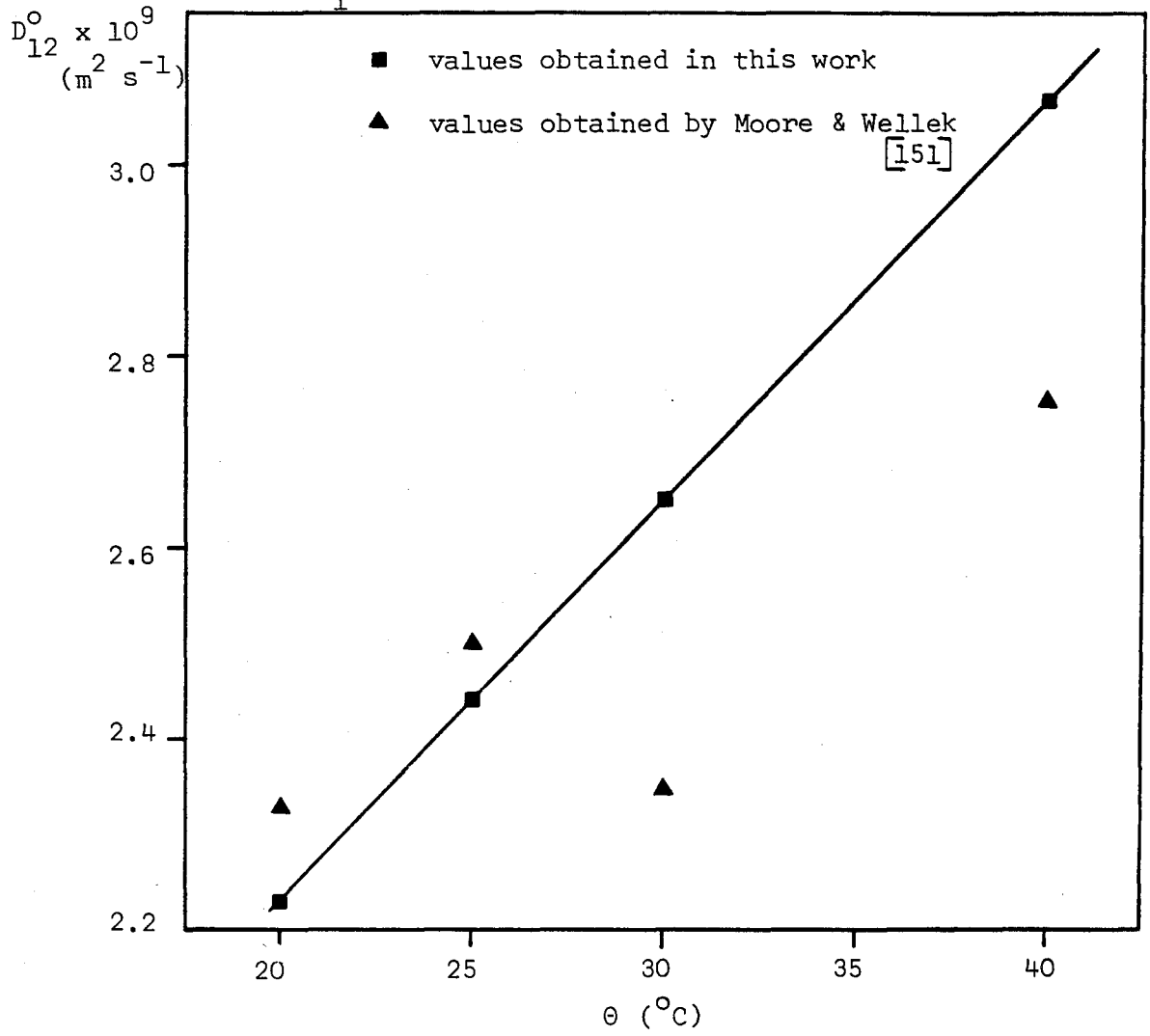

FIG. 5.6 - Percentage deviation of the values obtained by Moore and Wellek, $(D^{\circ}_{12})_{MW}$ from those obtained in this work, $(D^{\circ}_{12})_{Aliz}$

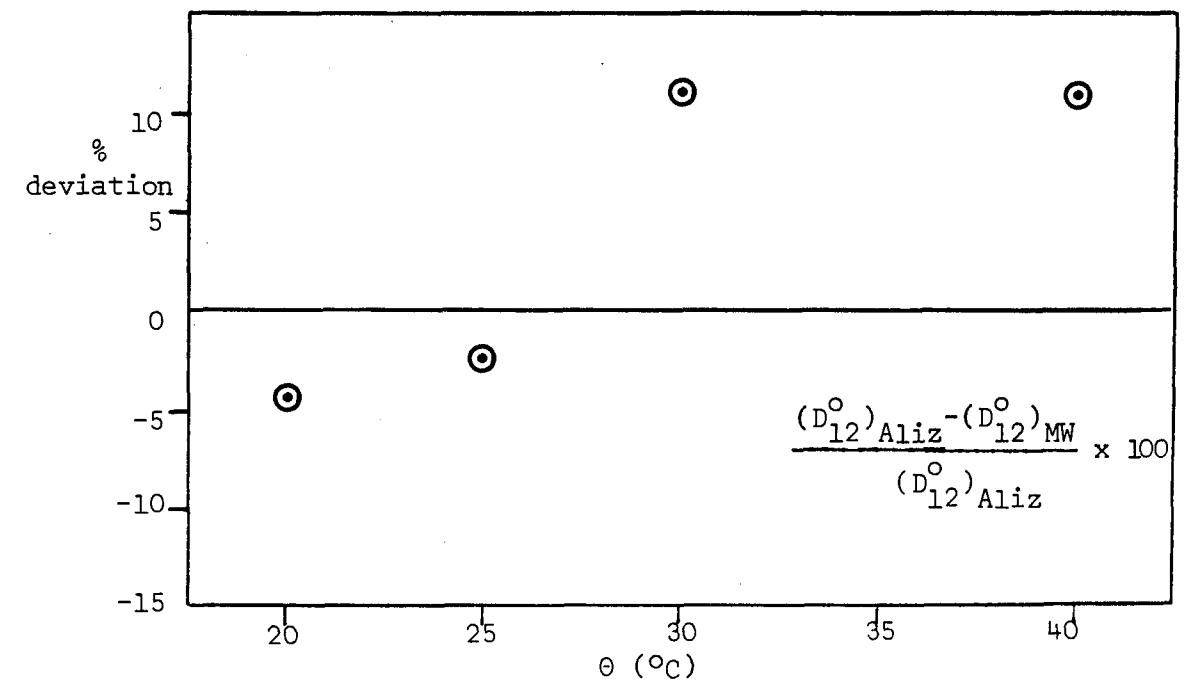

FIG. 5.7 - Stokes-Einstin group, $[D^c_{12}\eta_{12}/T]$, for the hexane-heptane mixture at 1 bar, against heptane mole fraction x_1

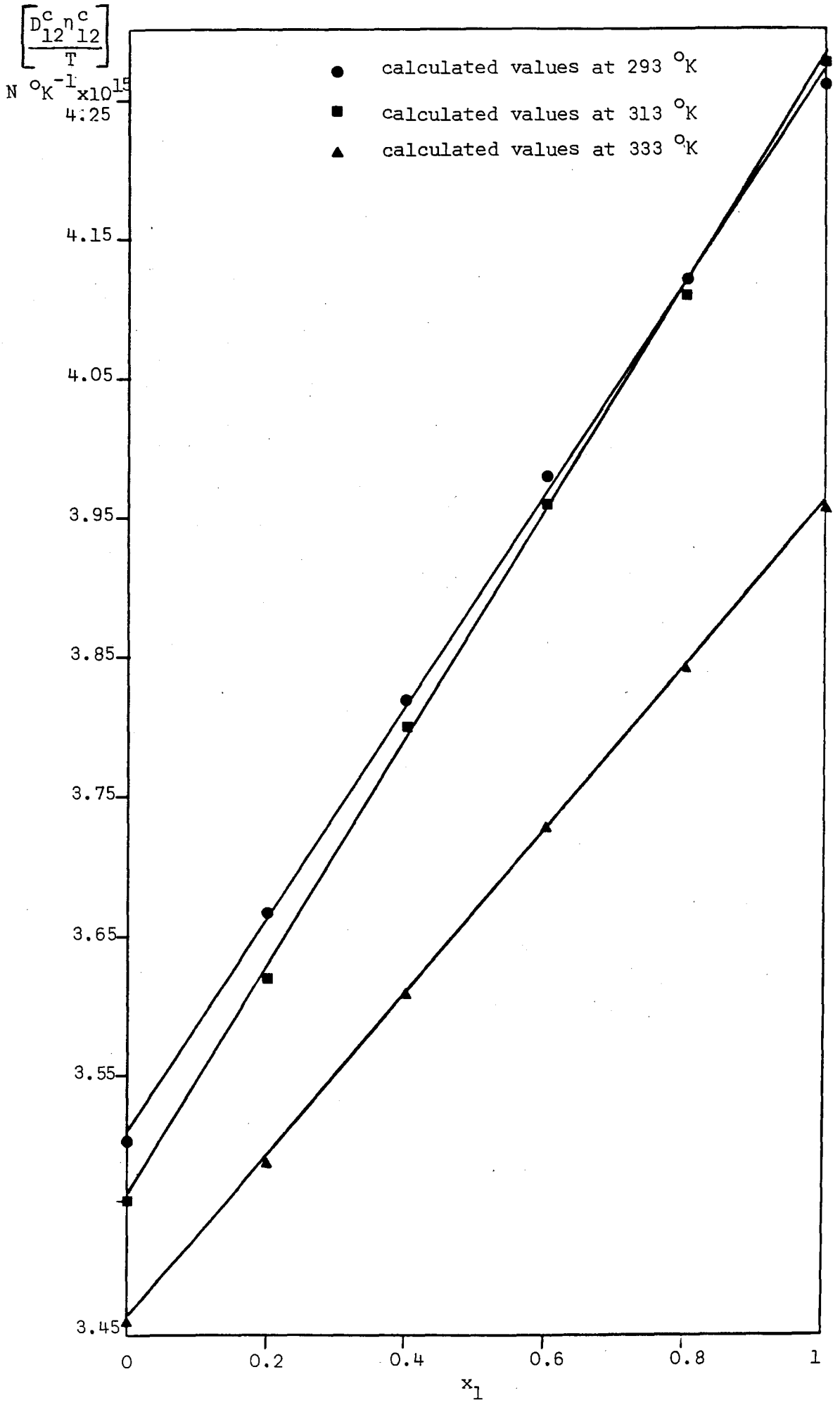

FIG. 5.8 - Stokes-Einstein group, $[D_{12}\eta_{12}/T]$ for hexane-octane and heptane-octane binary mixtures at 293 °K and 333 °K and 1 bar, against octane mole fraction x_1.

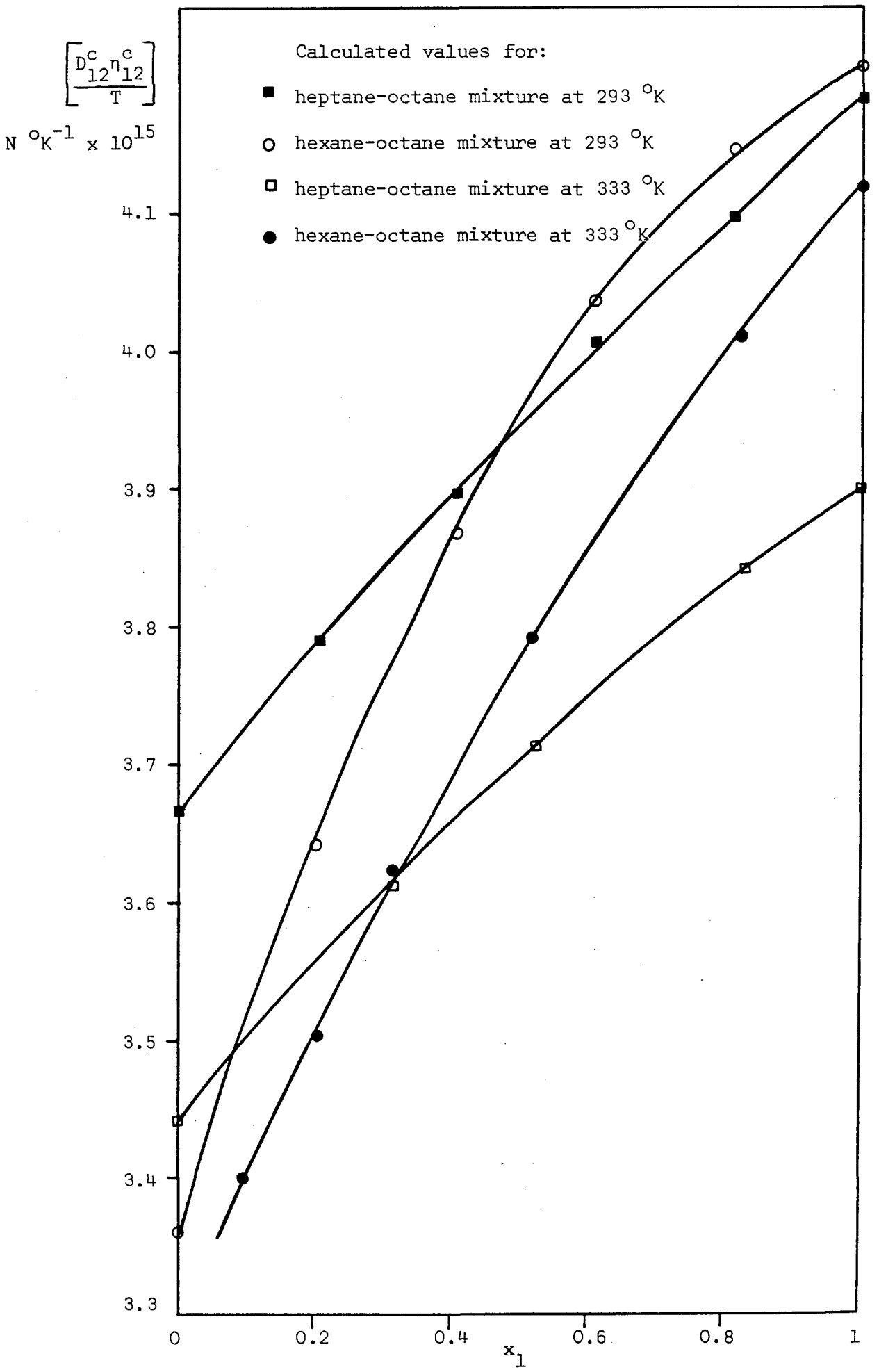

CONCLUSIONS

The work described in this thesis has demonstrated that the Taylor Dispersion Technique has now been developed to a point where it permits accurate measurements of diffusion coefficients of liquid mixtures over a moderate range of temperatures. Because the technique is rapid and simple it is now possible to use the technique to accumulate a large body of data on a wide variety of well-chosen systems in the same temperature range. The technique also lends itself to operation at elevated pressures and over a wider range of temperatures. It is therefore suggested that these are two directions for future work.

The experimental data obtained in this work are of sufficient accuracy that they provide a stringent test of available molecular theories and prediction procedures. Although none of the theories examined is capable of describing the experimental data within their uncertainty, the rough hard-sphere theory which makes use of molecular dynamics simulation results is the most promising. Nevertheless, it seems that molecular dynamics simulation of diffusion for molecular models more similar to the alkanes such as spherocylinders would be useful.

REFERENCES

[1] (a) R.K. Ghai, H. Ertl and F.A.L. Dullien, AIChE J. 19, 881 (1973); 20, 1 (1974).

(b) I.R. McDonald and J.P. Hansen, "Theory of Simple Liquids", Academic Press, 1976.

(c) J.A. Pryde, "The Liquid State", Hutchinson Pub., 1966.

(d) H.N.V. Temperley and D.H. Trevena, "Liquids and Their Properties", Ellis Harwood, 1978.

(e) J.O. Hirschfelder, C.F. Curtiss and R.B. Bird, "Molecular Theory of Gases and Liquids", John Wiley & Sons, N.Y., 1954.

[2] S.A. Rice and J.P. Boon, "Comments on the experimental and theoretical study of transport properties in simple liquids", a review prepared exclusively for the Chemistry Department of ISM of Chicago University, Chicago, Illinois (1980).

[3] U.S. Department of Commerce and National Bureau of Standards, "The Technological Importance of Accurate Thermophysical Property Information", N.B.S. Special Publication No. 590, Washington (Oct. 1980).

[4] M. Assael, C.A. Nieto de Castro and W.A. Wakeham, Proc. of Chempor 78, Braga, Portugal, 1978.

[5] E.G. Scheibel, J. Ind. Eng. Chem. 46, No. 8, 1569 (1954).

[6] R.C. Reid, T.K. Sherwood and J.M. Prausznitz, "The Properties of Gases and Liquids", 3rd ed., McGraw Hill, 435-469, 566-601 (1977).

[7] D.M. Himmelblau, Chem. Rev. 64, 527 (1964).

[8] J.F. Davidson and E.J. Cullen, Trans. Inst. Chem. Engrs. 35, 51 (1957).

[9] A. Alizadeh, C.A. Nieto de Castro and W.A. Wakeham, 3rd Nat. Meeting on Chemistry, Portugal, Centro de Quimica Estrutural, IST, Lisbon, 1980.

[10] J.W. Williams and L.C. Cady, Chem. Rev. 14, 171 (1934).

[11] (a) L.G. Longsworth, Annals. New York Acad. Sci. 46, 211; (b) L. Onsager, 241 (1945).

[12] (a) E.A. Mason and T.R. Merrero, "Advances in Atomic and Molecular Physics", Bates and Eastermann Eds., 155, Academic Press, N.Y., 1970; (b) J. Phys. Chem. Ref. Data 1, 3 (1972).

[13] (a) H.J.V. Tyrrell, "Diffusion and Heat Flow in Liquids", Butterworth, London, 1961; (b) "Diffusion Processes", J.N. Sherwood et al., eds., 1, Ch. 2, Gordon and Breach, N.Y., 1971.

[14] R.F. Treyball, "Mass Transfer Operations", 2nd ed., McGraw-Hill, 1968.

[15] (a) J.M. Thomas and W.J. Thomas, "Principles of Heterogeneous Catalysis", Academic Press, 1967; (b) J.J. Carberry, "Chemical Catalytic Reaction" 9, McGraw-Hill, 1976.

[16] H.J.V. Tyrrell and M. Mitchell, J. Chem. Soc. Faraday Trans. II, 358 (1971).

[17] R.B. Bird, W.E. Stewart andE.N. Lightfoot, "Transport Phenomena", Wiley Intn. Ed., Chs. 16-19, 1960.

[18] K.C. Pratt and W.A. Wakeham, Proc. Roy. Soc. Lond. A336, 393 (1974).

[19] A.C. Ouano, Ind. Eng. Fundam. 11, No. 2, 268 (1972).

[20] A.C. Ouano and J.A. Crothers, J. Phys. Chem. 79, No. 13, 1314 (1975).

[21] A. Alizadeh, C.A. Nieto de Castro and W.A. Wakeham, Int. J. Thermophys. 1, 243 (1980).

[22] Amer. Petrol. Inst. Petrol. Refin. Tech. Data Book Nos. A4220-B4220 (1964-72); National Engineering Laboratory, Glasgow - private communication through Dr. Isdale.

[23] (a) K.C. Pratt and W.A. Wakeham, Proc. Roy. Soc. Lond. A342, 401 (1975); (b) J. Chem. Soc. Faraday Trans. II, 73, 977 (1977).

[24] H.J.V. Tyrrell and P.J. Watkiss, Ann. Rep. Chem. Soc. A 35 (1976).

[25] E.R. Pike, "Photon Correlation Light Beating Spectroscopy". H.Z. Cummins and E.R. Pike, eds., NATO Adv. Study Institute Series, Plenum, London, 5 (1974).

[26] H.J.V. Tyrrell and A.W. Ellis, Symp. on Transport Props. Fluids, N.E.L., Glasgow, April 1979.

[27] (a) W.A. Wakeham and D.H. Slater, J. Phys. B: Atom. Mol. Phys. 6, 886 (1973); (b) ibid. 7, 297 (1974).

[28] Confidential Report on "The Chloride Ion Diffusivities", prepared at Imperial College by W.A. Wakeham et al. for the ICI Mond Division (1979).

[29] B. Anderson and T. Berglin, Proc. Roy. Soc. Lond. A377, 251 (1981).

[30] V. Hancil, V. Rod and M. Rosenbaum, Chem. Eng. Commun. 3, 155 (1979).

[31] K.G. Denbigh, "The Principles of Chemical Equilibrium", 2nd ed., Cambridge University Press, 86 (1968).

[32] T.E. Gruz, "Transport Phenomena in Aqueous Solutions", Ch. 3, Adam Hilger , 1974.

[33] H.J.V. Tyrrell, J. Chem. Educ. 41, 397 (1964).

[34] A. Fick, Pogg. Annalen 94, 59 (1855).

[35] J. Crank, "The Mathematics of Diffsuion", 2nd ed. Oxford University Press, 1975.

[36] J.G. Kirkwood, P.J. Dunlop, R.L. Bladwin, L.J. Gosting and G. Kegeles, J. Chem. Phys. 33, 1505 (1960).

[37] P.J. Dunlop, B.J. Steel and J.E. Lane, "Physical Methods of Chemistry", A. Weissberger and B.W. Rossiter, ed., 1, Part IV, 205, Interscience, 1972.

[38] P.J. Dunlop, K.R. Harris and C.K.N. Pua, J. Phys. Chem. 74, 3518 (1970).

[39] A.L. Van Geet and A.W. Adamson, J. Phys. Chem. 68, 238 (1964); A.L. Van Geet, PhD Thesis, University of Southern California, Los Angeles, 1961.

[40] M.J. Pikal, J. Phys. Chem. 76, 3038 (1972).

[41] A. Gassman and J. Sedlacek, Z. Phys. Chem. 240, 26 (1969).

[42] P.J. Dunlop and I.R. Shankland, J. Phys. Chem. 79, 1319 (1975).

[43] (a) S.R. de Groot, "The Thermodynamics of Irreversible Processes", Amsterdam, 1963; (b) I. Prigogine, "Introduction to the Thermodynamics of Irreversible Processes", Oxford University Press, 1968.

[44] T. Loflin and E. McLaughlin, J. Phys. Chem. 73, 186 (1969).

[45] R.J. Bearman and J.G. Kirkwood, J. Chem. Phys. 28, 136 (1958).

[46] A.S. Cukrowsky and B. Baranowski, Z. Phys. Chem. 240, 167, 253 (1969).

[47] S.A. Rice and P. Gray, "The Statistical Mechanics of Simple Liquids", Interscience, N.Y., 1965.

[48] J.H. Dymond and T.A. Brawn, Sump. on Transp. Props. Fluids, No. 3.4, N.E.L., Glasgow, 1979.

[49] W. Southerland, Phil. Mag. 9, 781 (1905).

[50] A. Einstein, Ann. Phys. 19, 289 (1906); 34, 591 (1911).

[51] F. Perrin, J. Phys. Radium, 7, 1 (1936).

[52] R.O. Herzog, R. Illig and H. Kudar, Z. Phys. Chem. 167, 329 (1933).

[53] R.J. Bearman, J. Chem. Phys. 32, 1308 (1960).

[54] P. Walden, Z. Electrokem. 12, 77 (1906).

[55] L.G. Longsworth, J. Amer. Chem. Soc. 75, 5705 (1953).

[56] A. Polson, J. Phys. Chem. 54, 649 (1950).

[57] A.R. Gordon, J. Chem. Phys. 5, 522 (1937).

[58] J.H. Wang, J. Phys. Chem. 58, 686 (1954).

[59] G.S. Hartley and J. Crank, Trans. Faraday Soc. 45, 801 (1949).

[60] C. Carman and L.S. Stein, Trans. Faraday Soc. 52, 619 (1956).

[61] H.S. Harned, Disc. Faraday Soc. 24, 7 (1957).

[62] C.J. King and C.H. Byers, J. Phys. Chem. 70, 2499 (1966).

[63] H. Eyring, S. Glasstone and K.J. Laidler, "The Theory of Rate Processes", McGraw-Hill, 1941.

[64] H. Eyring, J.F. Kincaid and A.E. Stearn, Chem. Rev. 28, 301 (1941).

[65] J. Frenkel, "Kinetic Theory of Liquids", Dover, N.Y., 1955.

[66] T. Einwohner and B.J. Alder, J. Chem. Phys. 49, 1458 (1968).

[67] S. Nir and W.D. Stein, J. Chem. Phys. 55, 1958 (1971).

[68] J. Hirschfelder and H. Eyring, J. Phys. Chem. 41, 249 (1937).

[69] J.C.M. Li and P. Chang, J. Chem. Phys. 23, 518 (1955).

[70] I. Ruff and V. Friedrich, J. Phys. Chem. 75, 3297 (1971).

[71] G.M. Panchenkov, Zh. Fiz. Khim. 24, 1390 (1950).

[72] D. Frenkel, G.H. Wegdam and J. Van der Elsken, J. Chem. Phys. 57, 2691 (1972).

[73] S.J.K. Jensen, D. Kivelson and M.K. Ahn, J. Phys. Chem. 57, 2940 (1972).

[74] J.H. Dymond and B.J. Alder, J. Chem. Phys. 45, 2061 (1966).

[75] D. Tabor, "Gases, Liquids and Solids", Penguin, 1970.

[76] P.C. Hemmer, M. Kac and G.E. Uhlenbeck, J. Math. Phys. 5, 60 (1964).

[77] E.B. Smith and B.J. Alder, J. Chem. Phys. 30, 1190 (1959).

[78] J.H. Dymond, Physica 75, 100 (1974).

[79] B.J. Alder, D.M. Gass and T.E. Wainwright, J. Chem. Phys. 53, 3813 (1970).

[80] S. Chapman and T.G. Cowling, "The Mathematical Theory of Non-Uniform Gases", Camb. Univ. Press, 1939.

[81] B.J. Alder, "Prediction of Transport Properties of Dense Gases and Liquids", UCRL 14891 T, Univ. Calif. Berkeley, U.S.A. (1966).

[82] B.J. Alder and J.H. Dymond, "Van der Waals' Theory of Transport in Dense Fluids", UCRL 14870 T, Univ. Calif. Berkeley, U.S.A. (1966).

[83] (a) J.H. Dymond, J. Chem. Soc. Faraday Trans. II, 1789 (1972); (b) J. Chem. Phys. 60, 969 (1974); (c) 17, 101, 175 (1976); (d) Proc. 6th Symp. Thermophys. Props. ASME 143, New York (1973).

[84] J.H. Dymond and T. Brown, Proc. 7th Symp. Thermophys. Props. ASME 660, New York, (1977).

[85] N.F. Carnahan and K.E. Starling, J. Chem. Phys. 51, 635 (1969).

[86] (a) D. Chandler, J. Chem. Phys. 60, 3500, 3508 (1974); (b) 62, 1358 (1975).

[87] K.J. Czworniak, H.C. Anderson and R. Pecora, Chem. Phys. 11, 451 (1975).

[88] J.J. Bertucci and W.H. Flygare, J. Chem. Phys. 63, 1 (1975).

[89] C.A. Nieto de Castro and J.C.G. Calado, Chem. Soc. Symp. Transport Props. Polyatom. Fluids, Statistical Mechanics & Thermodynamics Group, Imperial College, London (April 1980).

[90] V. Sanchez and M. Clifton, Ind. Eng. Chem. Fundam. 16, 318 (1977).

[91] S.A. Rice and P. Gray, "The Statistical Mechanics of Simple Liquids", Interscience, N.Y., 1965.

[92] (a) P. Gray; (b) B.J. Alder and W.G. Hoover; (c) W.W. Wood, "Physics of Simple Liquids", H.N.V. Temperley, J.S. Rowlinson and G.S. Rushbrook eds., North Holland, Amsterdam, 1968.

[93] S.A. Rice, J.P. Boon and H.T. Davis, "Simple Dense Fluids", Academic Press, N.Y., 1968.

[94] G.H.A. Cole, "The Statistical Theory of Simple Dense Fluids", Pergamon Press, Oxford, 1967.

[95] J. Jeans, "An Introduction to the Kinetic Theory of Gases", Camb. Univ. Press, 1967.

[96] F.C. Collins and M. Raffel, J. Chem. Phys. 29, 699 (1958).

[97] B.J. Alder and T.E. Wainwright, Phys. Rev. Lett. 18, 988 (1967).

[98] B.J. Alder, AIP Conf. Proc. 11, 1 (1973).

[99] W.A. Steel, "Transport Phenomena in Fluids", Marcel Dekker, N.Y., 1969.

[100] B.J. Alder and T.E. Wainwright, "Transport Processes in Statistical Mechanics", Interscience, 1958.

[101] (a) W.W. Wood and J.E. Erpenbeck; (b) J.R. Dorfman et al., "Statistical Mechanics" B: Time Dependent Processes (Plenum, N.Y., 1977).

[102] W.G. Hoover and M. Ross, Contemp. Phys. 12, 339 (1971).

[103] W.W. Wood and F.R. Park,er J. Chem. Phys. 27, 720 (1957).

[104] B.J. Alder and T. Einwohner, J. Chem. Phys. 43, 3399 (1965).

[105] S.A. Rice and A.R. Allnatt, J. Chem. Phys. 34, 409 (1961).

[106] G.L. Gouy, Compt. Rend. Acad. Sci. Paris 90, 307 (1880).

[107] L.G. Longsworth, J. Amer. Chem. Soc. 69, 2516 (1947).

[108] G. Kegeles and L.J. Gosting, J. Amer. Chem. Soc. 69, 2516 (1947).

[109] L.J. Gosting,, E.M. Hanson, G. Kegeles and M.S. Morris, Rev. Sci. Instr. 20, 209 (1949).

[110] L.J. Gosting and M.S. Morris, J. Amer. Chem. Soc. 71, 1998 (1949).

[111] L.J. Gosting and L. Onsager, J. Amer. Chem. Soc. 74, 6066 (1952).

[112] L.J. Gosting and H. Fugita, J. Amer. Chem. Soc. 79, 1359 (1957).

[113] J.C. Shieh and P.A. Lyons, J. PHys. Chem. 73, 3258 (1969).

[114] H.J.V. Tyrrell and G.J. Dudley, J. Chem. Soc. Faraday Trans. I. 69, 2200 (1973).

[115] T.A. Renner and P.A. Lyons, J. Phys. Chem. 78, 2050 (1974).

[116] J.M. Creeth, J. Amer. Chem. Soc. 77, 6428 (1955).

[117] A.L. Babb, J.R. Hall and C.S. Caldwell, Rev. Sci. Instr. 28, 816 (1957).

[118] L.J. Gosting and H. Kim et al., Rev. Sci. Instr. 44, 1602 (1973).

[119] (a) O. Bryngdahl, Acta. Chemica. Scand. 11, 1017 (1957); (b) 12, 684 (1958).

[120] T.C. Amu, Doctoral Thesis, Faculty of Science, Upsala Univ. Sweden, 1978.

[121] J.G. Albright and D.G. Miller, J. Phys. Chem. 76, 1853 (1972).

[122] K.W. Beach, R.H. Muller and C.W. Tobias, Rev. Sci. Instr. 40, 1248 (1969).

[123] F.R. McLarnon, R.H. Muller and C.W. Tobias, Applied Optics 14, 2468 (1975).

[124] D. Gabor, Proc. Roy. Soc. A197, 545 (1949).

[125] L.O. Sundelöf, Arkiv för Kemi 25, 1 (1965); idem. Chem. Scripta. 6, 55 (1974).

[126] J.N. Northrop and M.L. Anson, J. Gen. Physiol. 12, 543 (1928).

[127] R.H. Stokes, J. Amer. Chem. Soc. 72, 763, 2243 (1950).

[128] R. Mills and L.A. Woolf, "The Diaphragm Cell", Austral. Nat. Univ. Press, Camberra, 1968.

[129] H.J.V. Tyrrell and G.J. Dudley, J. Chem. Soc. Faraday Trans. I 69, 2188 (1973).

[130] G. Wedlake and F.A.L. Dullien, J. Chem. Eng. Data 19, 230 (1974).

[131] C. Barnas, J. Appl. Phys. 5, 4 (1934).

[132] A.R. Gordon, Ann. N.Y. Acad. Sci. 46, 285 (1945).

[133] J.B. Lewiss, J. Appl. Chem. 5, 228 (1955).

[134] R.D. Walker, K.E. Gubbins and R.N. Bhatia, Trans. Faraday Soc. 64, 2091 (1968).

[135] W.H. Hayduk and S.I. Oakimidis, J. Chem. Eng. Data 21, 255 (1976).

[136] J.T. Holms. Rev. Sci. Instr. 36, 831 (1965); Holms et al., J. Phys. Chem. 67, 1409 (1963).

[137] J.O.L. Wendt and G.C. Fraizer, Ind. Eng. Fundam. 12, 239 (1973).

[138] M.T. Tyn and W.F. Calus, J. Chem. Eng. Data 20, 310 (1975).

[139] C.J.D. Fell and H.P. Hutchinson, Ind. Eng. Chem. Fundam. 10, 303 (1971).

[140] R.W. Laity and M.P. Miller, J. Phys. Chem. 68, 2145 (1964).

[141] A.F. Collings, D.C. Hall, R. Mills and L.A. Woolf, J. Phys. E. 4, 425 (1971).

[142] R.R. Irani and A.W. Adamson, J. Phys. Chem. 62, 1517 (1958).

[143] R.L. Robinson, W.C. Edmister and F.A.L. Dullein, J. Phys. Chem. 69, 258 (1965).

[144] S.A. Sanni, C.J.D. Fell and H.P. Hutchinson, J. Chem. Eng. Data 16, 424 (1971).

[145] H.Y. Lo, J. Chem. Eng. Data 19, 236 (1974).

[146] H.S. Carslaw and J.C. Jaeger, "Conduction of Heat in Solids", 2nd edn., Oxford Univ. Press, 1959; J. Crank, "The Mathematics of Diffusion", 2nd edn., Oxford Univ. Press, 1975.

[147] (a) H.S. Harned and D.F. French, Ann. N.Y. Acad. Sci. 46, 267 (1945); (b) H.S. Harned and R.M. Hudson, J. Amer. Chem. Soc. 73, 5880 (1951).

[148] G.I. Taylor, Proc. Roy. Soc. London A219, 186 (1953); A223, 446; A225, 473 (1954).

[149] A.R. Aris, Proc. Roy. Soc. London A235, 67 (1956); F.R. Tillman, PhD Thesis, Texas University, U.S.A., 9, 108 (1966).

[150] W.A. Wakeham and C.A. Nieto de Castro, Symp. 2nd Encontro Nat. de Quimica OPORTO, Portugal, January 1979.

[151] J.W. Moore and R.M. Wellek, J. Chem. Eng. Data 19, 136 (1974).

[152] D.W. McCall and D.C. Douglass, J. Phys. Chem. 71, 987 (1967).

[153] K.J. Packer, C. Rees and D.J. Tomlinson, Mol. Phys. 18, 421 (1970); R.J. Hyward and K.J. Packer, ibid. 23, 1083 (1972); ibid. 26, 1533 (1973).

[154] T. Uano and T. Aratani, Seigyo Kogaku, 12, 18 (1968).

[155] O. Levenspiel and K.B. Bischoff, Adv. Chem. Eng. 4, 105 (1963); O. Levenspiel and W.K. Smith, Chem. Eng. Sci. 6, 227 (1957).

[156] C.Y. Wen and L.T. Fan, "Models for Flow Systems and Chemical Reactors", Marcel Dekker, N.Y., 1975).

[157] S. Goldstein, "Modern Developments in Fluids Dynamics" 1, 313, Dover, N.Y., 1965.

[158] M.E. Erdogan and P.C. Chatwin, J. Fluid Mech. 29, 465 (1967).

[159] D.J. McConalogue, Proc. Roy. Soc. London A315, 99 (1970).

[160] R.J. Nunge, T.S. Lin and W.N. Gill, J. Fluid Mech. 51, 363 (1972).

[161] L.A.M. Janssen, Chem. Eng. Sci. 31, 215 (1976).

[162] W.R. Dean, Phil. Mag. 5, 673 (1928).

[163] H.C. Topakoglue, J. Math. Mech. 16, 1321 (1969).

[164] D.J. McConalogue and R.S. Srivastava, Proc. Roy. Soc. London A307, 37 (1968).

[165] J.S. Ultman and H.S. Blatman, AIChE J 23, 169 (1977).

[166] R.N. Trivedi and K. Vasudeva, Chem. Eng. Sci. 29, 2291 (1974).

[167] K.D.P. Nigam and K. Vasudeva, Chem. Eng. Sci. 31, 835 (1976).

[168] E. Th. Van der Laan, Chem. Eng. Sci. 7, 187 (1958).

[169] H. Schlichting, "Boundary Layer Theory", 6th edn., McGraw-Hill, N.Y., 1968.

[170] C.B. Thorsness, PhD Thesis, Illinois University, Urbana, USA, 1975.

[171] M.R. Hopkins, Proc. Phys. Soc. 50, 703 (1938).

[172] N.G. Barton, J. Fluid Mech. 74, 81 96 (1976).

[173] R. Smith, J. Fluid Mech. 88, 323 (1978).

[174] R.D. Patel, J.J. McFeeley and K.R. Jolls, AIChE J. 21, 259 (1975); B.N. Wood, A.W. Seed and M.R. Nerem, J. Fluid Mech. 52, 137 (1972).

[175] J.M. Kay, "An Introduction to Heat Transfer", 2nd edn., 6.2, 66, Cambridge Univ. Press, 1968.

[176] D.L. Bidlack and D.K. Anderson, J. Phys. Chem. 68, 206, 3790 (1964).

[177] Engineering and Science Data Unit London - Private communication and item no. 79027, viscosity (alkanes).

[178] P. Eisenklam and L.F. Flint, Cand. J. Chem. Eng. 47, 101 (1969).

[179] P. Eisenklam and L.F. Flint, Proc. Roy. Soc. London A315, 519 (1970); "Oil Recovery", Private communication with Dr. P. Eisenklam, Chem. Eng. Dept., Imperial College, London.

[180] Amer. Inst. Phys., "Temperature and Its Measurements in Science and Industry", 199 (1945).

[181] International Practical Temperature Scale of 1976, N.P.L., Revised edn., H.M.S.O., London (1976).

[182] M. Assael, PhD Thesis, Imperial College, London, (1980).

[183] B.D.H. Chemicals Laboratory (Middx), Private communication.

[184] C.A. Nieto de Castro, PhD Thesis, Instituto Superior Tecnico, Lisboa (1977).

[185] H.C. Van Ness and M.M. Abbott, Ind. Eng. Chem. Fundam. 17, 66 (1978).

[186] A.V. Kiselev, Q. Rev. XV. 99 (1961).

[187] J.C.J. Calado and C.A. Nieto de Castro, J. Chem. Soc. Faraday Trans. (to be published).

[188] E.L. Heric and J.G. Brewer, J. Chem. Eng. Data 12, 574 (1967).

[189] D.L. Bidlack, T.K. Kett, C.M. Kelly and D.K. Anderson, J. Chem. Eng. Data 14, 342 (1969).

[190] C.R. Wilke and P. Chang, AIChE J. 1, 264 (1955).

[191] M.A. Lusis and G.A. Ratcliff, Can. J. Chem. Eng. 40, 385 (1968).

[192] P.F. Othmer and M.S. Thakar, Ind. Eng. Chem. 45, 589 (1953).

[193] E.G. Scheibel, Ind. Eng. Chem. 40, 2007 (1954).

[194] K.A. Reddy and L.K. Doraiswamy, Ind. Eng. Chem. Fundam. 6, 77 (1967).

[195] L.S. Darken, Trans. Amer. Inst. Mining Met. Eng. 175, 184 (1948).

[196] A.L. Babb and C.S. Caldwell, J. Phys. Chem. 60, 51 (1956).

[197] G.A. Mansoori, N.F. Carnahan, K.E. Starling and T.W. Leland, Jr., J. Chem. Phys. 54, 1523 (1971).

LIST OF SYMBOLS

A Translational-rotational coupling constant

A_o Cross-sectional area of the diffusion tube

A_e Elliptical cross-section area

A_n^m Constants ($n = 0, 1, 2 \ldots$, $m = i, j, k \ldots$)

A_p Effective cross-sectional area of the pores

a_1, a_2 Major and minor axes of the elliptical cross-section of the non-uniform tube

a_i The activity of species i

a' Cell thickness

B_n, B_n^m Constants ($n = 0, 1, 2 \ldots$, $m = i, j, k \ldots$)

B_1^c The thermodynamic factor for solute "1" $= 1 + \dfrac{\partial \ln \gamma_1^*}{\partial \ln c_1}$

b The co-volume $= \dfrac{2\pi n^*}{3} \sigma_p^3$

b' The optical lever arm for the convergent light in the diffusiometer

C, C^o Fluid concentrations, in general and (molar) in the uniform tube respectively

C_T^o, C_B^o, C_T^t, C_B^t Top and bottom cells concentrations at times zero and t respectively

C_{1f}, C_{1i}, C_{1r} Molar concentrations of species 1 in the flowing and injection streams and that of the reference respectively

C_1, C_{1m}, C_1^o Perturbation to the flowing stream composition, its mean and that of the uniform tube

$\overline{\Delta C_1}$ Average concentration perturbation

ΔC_d Perturbation to the concentration in the detector

δC_1 Correction to the flowing stream concentration

C_n, C_E, C_B Recorded concentrations (end and beginning)

c, c_i, c_T Molar concentrations in general, that of species i and the total respectively

c' Perturbation to the concentration distribution

c_i^* Concentration of the labelled species i

c_p The p^{th} spatial moments of the concentration distribution (p = 0-4)

D_i, D_i^v Diffusivities of species i in general and based on volume frame of reference respectively.

D_{ij}, D_{ii}, D_i^* Binary-, self-, and Tracer-Diffusion coefficients of the species (i = integer, j = integer; $i \neq j$)

D, D^+, D^x, D_E, D_o, D_{MD} Diffusion coefficients, general, hard-sphere fluid, dense gas, due to Dymond and Enskog at high and low densities and that calculated by molecular dynamics simulations respectively

D_{12}^c Concentration dependent binary diffusion coefficient

D_{12}^o, D_{21}^o The limiting values of D_{12} at $x_1 \to 0$ and $x_2 \to 0$ respectively

$\overline{D}(t)$, $\overline{D}$ Integral diffusion coefficient and its average respectively

D_{12}^{ob}, D_{12}^e Binary diffusivities of a coiled and elliptical cross-section tube respectively

D_{12}^f Binary diffusion coefficient at the flowing stream composition tubes respectively

$D_{12}^{\cdot}$, $(D_{12}^a)_\rho$ Concentration and density dependent binary diffusivities,

D_{SH}, D_{RH} Diffusivities derived by the smooth-, and rough-hard sphere models respectively

D_{12}^{kin}, D_E^{kin} Kinetic binary diffusiviity and thatof Enskog respectively

D_{12}^{expt}, $[D_{12}^{kin}]_{theory}$ Experimental (= D_{12} values in Chapter 4 Tables) and theoretical binary diffusion coefficients

$\mathfrak{D}_{12}$ Activity dependent binary diffusion coefficient = $\dfrac{D_{12}}{\partial \ell n a_1 / \partial \ell n x_1}$

De Dean's number = $Re.(\dfrac{R_o}{R_c})^{\frac{1}{2}}$

d Diameter of the liquid reservoir

E or E_D, E_c Effective diffusivities of the diffusion $\left(= \dfrac{R_o^2 U_o^2}{48 D_{12}}\right)$ and connecting $\left(\dfrac{r_c^2 u_o^2}{48 D_{12}}\right)$ tubes respectively

E^o E at the flowing stream composition

e Eccentricity $\left[= (1-(\dfrac{a_2}{a_1})^2)^{\frac{1}{2}}\right]$

F Correction due to the correlated motion of the particles

$\tilde{f}_{N_p}$ N_p-particle distribution function

f_B, f_H Effective friction coefficients for the Brownian and the hard-sphere motions respectively

f_s, f_i Frictional force of resistance of each spherical and non-spherical solute molecule

f_e Empirical values of f_s

$g(\sigma_p)$ The radial distribution function at contact for two like spheres

$g_{12}(\sigma_{12})$ The radial distribution function at contact for two unlike spheres

$H(s)$ Transfer function

ΔH_{evap} The latent heat of evaporation

h The driving head for the liquid flow

δh Change in h

$\vec{J}_i$ Molar flux of species i with respect to stationary coordinates

$\vec{J}_{ir}$ $\vec{J}_i$ relative to molar average velocity

$\vec{J}_m$, $\vec{J}_h$ Mass and heat fluxes in general

$\vec{J}_i^v$ $\vec{J}_i$ with respect to the volume frame of reference

J_o Bessel function - zeroth order of the first kind

$\vec{j}_i$, $\vec{j}_{ir}$ Mass fluxes of species i relative to stationary or moving coordinates respectively

j Total number of fringes

K Boltzmann's constant = 1.381×10^{-23} J $^oK^{-1}$

K_c Constant = $2.1701 \ldots \times 10^{-5}$ (eqn. (2.23))

K_U Kurtosis = $(\frac{\mu_4}{\sigma^4}) - 3$

k_b, k_f Rate constants for the backward and forward reactions respectively

k_n Number of any fringe maximum

L Length of the diffusion tube

δL Small length of the tube

L_i^* Phenomenological coefficients

L_{mm}^*, L_{hh}^* L_i^* corresponding to the effects of $\nabla\dot{\mu}$ and $\nabla\theta_i$ on mass and heat transport of species i respectively

L_{mh}^*, L_{hm}^* The cross coefficients, i.e. effects of $\nabla\dot{\mu}$ and $\nabla\theta_i$ on heat and mass transport respectively

ℓ Length of the connecting tube

ℓ_i, ℓ Distances - axial (optics) and vertical (diaphragm cell) respectively

M_i Molecular weight of species i

$\mathcal{M}$ Mobility - velocity gradient as a result of unit force

m_i Mass of a sphere or particle (molecular atom) i (i = integer)

m Reduced mass = $\frac{m_1 m_2}{m_1+m_2}$

m_p Cross-section averaged c_p

N Avagadro's number = 6.022×10^{23} (mol^{-1})

$\vec{N}_{ir}$ Molar flux of species i relative to the mass average velocity

N_1 Number of moles of species i (in the injection) in excess of those having an equal volume in the flowing stream

$N_{i\beta}$ Number of moles of species i in phase β

$dN_{i\beta}$ Number of moles of species i leaving phase β

N_p Number of particles (atoms, spheres, molecules, etc.)

n, n_i Number of molecules, and that of species i

n_D, n_{Di} Refractive index, and that of species i

n^* Number density of a fluid system (pure or binary mixture)

n_i^* Number density of the n-alkane i = $n^* x_i$

n_o^* Number density for a dilute gas

$\vec{n}_{ir}$ Mass flux of species i relative to the mass average velocity

P, p Pressures - in general and that of the fluids in the tube

Pe Peclet number $\left(\frac{R_o U_o}{D_{12}}\right)$

ΔP Pressure drop across the diffusion tube

Q Volumetric flowrate

Q_2 Quantity defined by equation (2.135); f(Pe, Sc)

Q_{ra} Reduced height-area ratio

R The universal gas constant = 8.314 J mol^{-1} $^oK^{-1}$

R_o Internal radius of the diffusion tube

R_c Coil radius

$R(z)$ Internal radius of the non-uniform tube

Re Reynolds number = $\frac{2R_o U_o}{\nu}$

$R_\theta(\Omega)$, $R_o(\Omega)$ Resistances of the iron-constantan thermocouples (latter = 25.7507Ω)

r_c Internal radius of the connecting tube

r Radial distance (polar coordinate)

r_i, r_{pi} Radii of spheres and particles i

Sc Schmidt number = $\frac{\nu}{D_{12}}$

S_i Entropy of the system i

Sk Skewness of the eluted distribution = $\frac{\mu_3}{\mu_2^{3/2}}$ or $\frac{\mu^*_3}{\mu^{*3/2}_2}$

s Laplace transform variable

T Absolute temperature

T_b, T_c Boiling and critical temperatures respectively

t Time in general

$\bar{t}$ Measurement time = $\frac{L}{U_o}$

$\bar{t}_a$ Taylor-Aris minimum time criterion

t_c, t_d Correction times contributed by the connection tube and detector respectively

$\delta\bar{t}_n$ The small correction to $\bar{t}$ detector respectively due to the non-idealities (n = 0, 1, 2, ...)

U_o Mean velocity of the flow through the diffusion tube

U_z, U_r Axial and radial velocity components

U'_z, u'_r Velocity perturbation components (non-uniform tube)

u_o Mean velocity of the flow through the connecting tube

V Volume in general

V_t, V_c, V_d, V_i Volumes of the diffusion tube, connecting tube, detector and the injected sample respectively

V^*_i Molar volume of hard-sphere i

V^*_{ip} Molar volume of the particles i in a binary liquid mixture

V^*_c, V^*_b Molar volumes of the n-alkanes at T_c and T_b respectively

$(V^*_1)_b$, $(V^*_1)_\theta$ Molar volumes of the solute at the boiling point of solvent and at the solution temperature

V^*, V^*_o High and low density molar volumes respectively

δV A small or negligible change in volume

v_f Free volume of the liquid

$\underline{v}_i$, v_i Molecular velocity of i^{th} component (the former is time-dependent)

v^*_i, v^{*}_i Mass and molar relative velocities of component i respectively

$\overline{\overline{v_i}}$, $\overline{v}$, $\overline{\overline{v}}^*$ Molar average velocities defined by equations (1.8)-(1.11) and (1.54)

W The ratio $R_\theta(\Omega)/R_o(\Omega)$

W_i, w_i Weight fractions of the i^{th} component and that of the n-alkane (i = 1, 2, 3 ...)

X_i Generalized driving forces to transport species i

X_θ X_i due to temperature gradient

x_i Mole fraction of species i

x_{1f}, x_{ii}, x_{ir} Mole fractions of i in the flowing and injection streams and that of reference respectively (i = 1, 2, 3 ...)

Y Distance through which light rays are deflected

Z_{cs} Carnahan-Starling compressibility factor

Z_{py} Percus-Yevick compressibility factor

z Axial distance (Cartesian coordinate)

z^* The quantity defined by equation (1.88); $= \dfrac{z}{2\sqrt{Dt_{12}}}$

∇ The vector differential operator

∇^2 Laplace operator

α Constant $= \dfrac{V_d}{V_t}$

$\tilde{\alpha}$, $\tilde{\alpha}(\Gamma_{N_p})$ A macroscopic quantity and its corresponding microscopic value

α_{on} The n^{th} zero of d $J_o(z)/dz$

α', α_{ip} Spherical particle size parameters

β Parameter $= \left[1 + \dfrac{4\zeta_o Ls}{U_o}\right]^{\frac{1}{2}}$

β' The sliding frictional coefficient

β_c Diaphragm cell constant

γ Density coefficient

γ_i^* Activity coefficient of species i (i = 1, 2, 3, ...)

Δ Finite difference - % deviation $= \dfrac{\sigma_s^2 - \sigma_c^2}{\sigma_s^2} \times 100$ (in practice)

Δ_{max}, Δ_{ones} Maximum and mean deviations of theoretical data from experimetal

$\delta(z)$ Delta function (pulse)

δ A small or infinitesimal change

δ_a Constant = $(768)^2 K_c \zeta_o$

ε Amplitude of oscillations

η Dynamic viscosity

η_i Dynamic viscosity of pure i^{th} component (i = 1, 2)

η_{12}^c Concentration dependent dynamic viscosity of the binary mixture

θ Temperature (^oC)

θ_m Mean temperature of the fluid (measured ^oC)

θ_B Bath temperature (^oC)

θ Angular polar coordinate

λ Wave length (e.g. that of wavy surface; light)

λ^* Distance between two equilibrium positions or potential barriers

$\mu_{i\alpha}$, $\mu_{i\beta}$ Chemical potentials of species i in phases α and β respectively

$\Delta\mu_i$ Chemical potential driving force to transport i

μ_p, μ_p^* p^{th} temporal and spatial central moments respectively (p = 0, 1, 2..)

μ_p', $\mu_p'^*$ p^{th} temporal and spatial raw moments respectively

μ_p^*, μ_{ps}^* p^{th} normalized moment ($= \frac{m_p}{m_o}$) and μ_p^* under conditions (2.21) and (2.24)

$(\mu_1')_{id}$, $(\mu_1')_{exp}$ The ideal and experimental ($= \frac{L}{U_o}$) first raw moments

μ_{1e}' The first moments of the non-uniform (elliptical cross-section) tube

$(\mu_p')_{nu}$, $(\mu_p)_{nu}$ The moments of the non-uniform cross-section tube

μ_n^{*c}, $\mu^{*\rho}$ The n^{th} moments of the perturbed distributions due to concentration and density dependence of D_{12} respectively (n = 0, 1, 2 ...)

$\delta\mu_n'$, $\delta_n(\mu_n')$ Small corrections to the n^{th} raw moments

$\delta\mu_{nm}'$ The m^{th} correction to the n^{th} moment

ν_i Kinematic viscosity of pure species i = $\frac{\eta_i}{\rho_i}$

ν_{12}^c Concentration dependent kinematic viscosity of the binary mixtures

ζ, ζ_o Dimensionless groups = $\frac{R_o}{48D_{12}t}$ and $\frac{R_o}{48D_{12}\bar{t}}$ respectively

ξ Dimensionless axial distance with respect to the moving origin = $\frac{(z-U_o t)}{R_o}$

Γ_{N_p} A point in 6N-dimensional phase space

ρ Composition dependent density = $\rho_f (1 + \gamma \Delta C_1)$

ρ_f Density at the flowing stream composition

ρ_i Density of the pure component i (i = 1, 2)

ρ_{12} Density of the binary mixture

$\sigma 2$ Temporal variance (2nd central moment) of the eluted

σ^{*2} The spatial variance

σ^2_{id}, σ^2_{expt} Ideal and experimental σ^2

σ^2_{IT} Variance at the end of a transient period

σ^2_e, $(\sigma^2)_{nu}$ Variances of the elliptical and variable cross-section tubes respectively

σ^2_s, σ^2_c Variances of the straight and coiled tubes respectively

$\delta\sigma^2_n$, $\delta_n(\sigma^2)$ The n^{th} small corrections to σ^2

σ_i, σ_{pi}, σ_{ij} Molecular diameters for the hard spheres and the effective binary one $(= \sigma_1 + \sigma_2/2)$ respectively

τ Dimensionless time = $\frac{U_o t}{L}$; also time referring to $\underline{v}_i$

ϕ The dissipation function $(= T \frac{dS_i}{dT})$

ϕ_i Packing fraction of hard spheres i = $\frac{1}{6} \pi n^* x_i \sigma_i^3$

ϕ_{12} The effective binary packing fraction = $\frac{\pi n^*}{6} (x_1\sigma_1^3 + x_2\sigma_2^3)$

ϕ' Parameter defined by equation (2.136)

$\tilde{\phi}$ The probability integral

ψ Parameter = $\frac{b}{4V_i'}$

χ Coefficient for the composition dependence of D_{12}

ω The ratio $\frac{R_c}{R_o}$